

Runyan

TEXAS INSTRUMENTS INCORPORATED
Semiconductor-Components Division



TEXAS
INSTRUMENTS
INCORPORATED

Silicon Semiconductor Technology

Silicon Semiconductor Technology

W. R. Runyan

Texas Instruments Electronics Series
McGraw-Hill Book Company

McGraw-Hill
54276

Silicon Semiconductor Technology

RUNYAN

Silicon Semiconductor Technology



TEXAS INSTRUMENTS ELECTRONICS SERIES

**Texas
Instruments
Incorporated**

**McGRAW-
HILL**

**Silicon
Semiconductor
Technology**

TEXAS INSTRUMENTS ELECTRONICS SERIES

The Engineering Staff of

Texas Instruments Incorporated ■ TRANSISTOR CIRCUIT DESIGN

Runyan ■ SILICON SEMICONDUCTOR TECHNOLOGY

Sevin ■ FIELD-EFFECT TRANSISTORS

Silicon Semiconductor Technology

W. R. Runyan

*Semiconductor Research and Development Laboratory
Texas Instruments Incorporated*

M c G R A W - H I L L B O O K C O M P A N Y

New York San Francisco Toronto London Sydney



SILICON SEMICONDUCTOR TECHNOLOGY

Copyright © 1965 by Texas Instruments Incorporated. All Rights Reserved. Printed in the United States of America. This book, or parts thereof, may not be reproduced in any form without permission of Texas Instruments Incorporated. *Library of Congress Catalog Card Number 64-24607.*

Information contained in this book is believed to be accurate and reliable. However, responsibility is assumed neither for its use nor for any infringement of patents or rights of others which may result from its use. No license is granted by implication or otherwise under any patent or patent right of Texas Instruments or others.

54276

3 4 5 6 7 8 9 - M P - 9 8 7 6

Preface

The purposes of this book are to provide in a single reference the properties of silicon important to those who would use it as a semiconductor and to discuss at length several of the more important semiconductor technologies, such as crystal growing and diffusion. It had its beginning in a set of notes I began compiling shortly after starting work in the semiconductor industry. Since most of my activities were with silicon, these notes were restricted to information pertaining to that material. A few years later, while teaching a graduate course in semiconductor technology at Southern Methodist University, the notes were expanded from a collection of data to a unified coverage of topics relating to semiconductor material technology and were used as an adjunct to a general text. However, because of my interest in silicon, after the semiconductor material technology was presented in some depth it was then applied specifically to silicon. This in no sense restricts the book's use to those interested only in silicon since the majority of each of those chapters not relating to specific silicon properties discusses each technology independent of the material.

While this book will be of most interest to device designers and those working as semiconductor technologists, it should also prove of considerable interest to those using devices, both circuit designers and systems engineers, in that it will supply background information and material properties helpful in understanding device performance.

An attempt was made to cover all aspects of the technology except those relating to the surface itself. The complexity of surface behavior would warrant a separate volume and is beyond the scope of this book. In addition, where there are books covering some phase of the technology in great detail, e.g., Pfann's "Zone Melting," only a cursory treatment is given.

The author would like to thank Harry L. Owens for his continued interest and support, Dr. Lyndon Taylor of the University of Texas and Dr. W. E. Phillips of Texas Technology College for a critical reading of the manuscript, John R. Miller for editorial advice, Virginia Belshaw for typing, Stacy B. Watelski for the photomicrographs, Earl W. Scott of Scott's Studio for the crystal photographs of Chap. 4, and the photographic staff of Texas Instruments Incorporated for all other photography. In addition, the help of the many other members of the Semiconductor Research and Development Laboratory of Texas Instruments Incorporated is gratefully acknowledged.

W. R. Runyan

Foreword

It is particularly timely for a book to appear on the subject of silicon semiconductor technology. Until the past few years the semiconductor device industry was based largely on germanium technology, with silicon being restricted chiefly to military and power applications.

During recent years silicon technology has been developed so that silicon now promises, along with germanium, to have broad usage. Integrated circuits have been developed almost exclusively around silicon technology. While these were developed first for military applications, they will be applied broadly to industrial and consumer markets. It is also evident that future generations of devices will be far more sophisticated than those now in use, and that a much better understanding and blending of material properties with device functions will be required.

Dr. Runyan has written a book which should prove to be a useful addition to the literature on semiconductor technology and an aid in this blending process. He is especially well qualified to author such a book since much of his professional career has been devoted to research and development on silicon materials and devices. At present he leads the materials research program in the Semiconductor Research and Development Laboratory at Texas Instruments.

This book is a part of the new Texas Instruments Electronics Series, through which we hope to make readily available to the technical community important research findings which will further the progress of the electronics industry.

Richard L. Petritz, DIRECTOR
SEMICONDUCTOR RESEARCH AND
DEVELOPMENT LABORATORY

Contents

<i>Preface</i>	v
<i>Foreword</i>	vi
Chapter 1. An Historical Note	1
REFERENCES	3
Chapter 2. Silicon-manufacturing Processes	5
2.1 Early Methods of Manufacture	5
2.2 Summary of Applicable Methods	7
2.3 Zinc-Silicon Tetrachloride	7
2.4 Silane Decomposition	9
2.5 Iodide Process	10
2.6 Silicon Tetrachloride and Trichlorosilane Processes	12
REFERENCES	14
Chapter 3. Silicon-casting Processes	17
3.1 Melting in Mold	17
3.2 Pouring into Mold	22
3.3 Ambient Casting	24
REFERENCES	27
Chapter 4. Crystal Growth	29
4.1 Crystal-growing Environment	29
4.2 Types of Crystal Growth	30
4.3 Crystallization from a One-component System	32
4.4 Growth from Multicomponent Systems	36
4.5 Teal-Little	38
4.6 Behavior of Impurities During Growth from the Melt	49
4.7 Miscellaneous Techniques	60
4.8 Growth from Low-temperature Melts	63
4.9 Vapor-Liquid-Solid (VLS) Method of Crystal Growth	65
4.10 Growth from the Vapor	65
REFERENCES	78

○ Chapter 5. Crystal Habit and Orientation	84
5.1 Crystal Systems	84
5.2 Silicon Structure	88
5.3 Crystal Habit	89
5.4 Rough Orientation	93
5.5 X-ray Orientation	94
5.6 Optical Orientation	97
5.7 Twinning	98
5.8 Detection of Twinning	101
5.9 Grain Boundaries	101
5.10 Lineage	102
REFERENCES	102
Chapter 6. Doping Procedures	104
6.1 Effects of Impurities on Resistivity	104
6.2 Effect of Segregation Coefficient on Resistivity	107
6.3 Methods of Doping	110
6.4 Discussion of Crystal Yields	114
REFERENCES	116
Chapter 7. Diffusion	117
7.1 Elementary Theory	117
7.2 Diffusion Along a Grain Boundary	133
7.3 Field-aided Diffusion	136
7.4 Numerical Calculations	137
7.5 Diffusion Processes	141
7.6 Diffusion Coefficients	151
REFERENCES	159
Chapter 8. Electrical Properties	164
8.1 Resistivity	164
8.2 Mobility	166
8.3 Drift Mobility	168
8.4 Hall Coefficient and Hall Mobility	169
8.5 Effects of High Field on Resistivity	172
8.6 Width of Space-charge Region in p-n Junctions	174
8.7 Effects of Pressure	176
8.8 Energy Bands	182
8.9 Effective Masses for Electron and Holes	183
8.10 Miscellaneous Effects	185
REFERENCES	185

Chapter 9. Optical Properties	187
9.1 Absorption Coefficients	187
9.2 Photoconductivity	197
9.3 Reflection Coefficient	198
9.4 Index of Refraction	198
9.5 Emissivity	200
9.6 Light Emission	200
9.7 Tyndall Effect	203
9.8 Birefringence	203
9.9 Optical Elements	204
9.10 Optical Coatings	205
9.11 Optical Grinding and Polishing Procedures	210
REFERENCES	210
Chapter 10. Miscellaneous Physical Properties and Processes	213
10.1 Elastic Constants	214
10.2 Some Tensile Testing Definitions	221
10.3 Plastic Flow	222
10.4 Distribution of Breaking Strengths	223
10.5 Impact Testing	224
10.6 Hardness	225
10.7 Thermal Expansion Coefficient	225
10.8 Thermal Conductivity	228
10.9 Surface Energy	229
10.10 Hot Forming	229
10.11 Sawing and Lapping	231
REFERENCES	233
Chapter 11. Metallurgy	236
11.1 Review of Binary Phase Systems	236
11.2 Phase Diagrams	241
11.3 Limits of Solubility	241
11.4 Segregation Coefficient	242
11.5 Silicon-Germanium Alloys	247
11.6 Solubilities and Formation of Precipitates	248
11.7 Effect of High-impurity Concentration	259
11.8 Copper Decorations	261
11.9 Gettering Techniques	262
REFERENCES	267
<i>Author Index</i>	269
<i>Subject Index</i>	273

An Historical Note

Silicon, from the Latin *silex*, meaning flint,^{1,*} is the second most abundant element and comprises over 20 per cent of the earth's crust. It occurs in nature never as the element, but chiefly as silica (SiO_2) and silicates. Silica forms beautiful crystals of clear quartz[†] (rock crystal), amethyst (blue, due to manganese), rose quartz (colored by the presence of small quantities of titanium), and smoky quartz (organics). Occasionally crystals of tridymite and cristobalite, which are the high-temperature modifications of silicas, may be found in volcanic deposits. SiO_2 abounds in massive form as quartzite, agate, jasper, carnelian, opal, and flint. The worldwide use of flint for the first-formed tools of man (Paleolithic Age) was probably the result of its abundance, hardness, and relative ease of working. Flint again figured in the development of civilization when it was used as a spark generator for firing gunpowder and thus made lightweight, portable firearms practical. Silica is a constituent of igneous rocks such as granite, syenite, and rhyolite and occasionally is found in basalt and diorite. In addition, it is present in nearly all metamorphic rocks and is the major component of sandstone.

The silicates are exceedingly common and include such minerals as the micas, feldspars, zeolites, and garnets. Clay is primarily a collection of silicates and has been used in pottery construction since time immemorial. Likewise, the silicates are a major constituent of glass. It is not clear just when or how "glass" first came to be made, but it was probably somewhere in Asia Minor, before 12,000 B.C.²

Compounds of silicon are found in all natural waters, in the atmosphere as dust, in many plants, and in the skeletons and tissues of animals. Diatomaceous earth, sometimes called kieselguhr, is an opal composed of the siliceous shells of diatoms (unicelled aquatic plants) and is found in thick beds resembling chalk.

Until 1787 it was assumed that silica was an element, but in that year Lavoisier suggested that it was the oxide of some unknown element. Apparently, Gay-Lussac and Thénard first produced silicon in 1811 by reducing silicon fluoride with potassium, but did not recognize it as such. Berzelius reported evidence of the new element as a precipitate in cast iron in 1817. He succeeded in isolating it in

* Superscript numbers indicate items listed in References at the end of the chapter.

† The word "quartz" appears to have originated in provincial Germany sometime in the Middle Ages.³

1823 by reacting potassium fluosilicate with metallic potassium. Silicon was obtained in reproducible form in 1854 by Sainte-Claire Deville, who crystallized it from an electrolyzed melt of mixed chlorides.^{4,23} It was originally thought that there were two varieties of amorphous silicon. One, quite active chemically, was called silicon α , while the other, relatively inert, was silicon β . Likewise, there have been occasional reports of both a cubic and a graphitic or hexagonal form.⁵ Apparently, the active amorphous silicon was caused by impurities remaining after manufacture. The early reference to hexagonal silicon arose from a misinterpretation of the hexagonal platelets that sometimes occur. The more recent work describing a high-temperature hexagonal modification has not been substantiated.

The early findings notwithstanding, silicon is indeed a very inert material, so efforts were made around the turn of the century to use it for chemical ware.⁶ These were never very successful because of its brittleness and the difficulties associated with working it. Several years ago there was some hope that high-purity silicon would be ductile at room temperature, but there is now no evidence that this is to be expected.

Silicon is widely used in the steel industry to combine with and remove iron carbide and dissolved oxygen. Added in larger quantities (≈ 15 per cent), a steel is produced which is hard and corrosion-resistant. The total quantity of silicon involved is quite large since it is estimated that 1 lb of silicon is needed for every 350 lb of steel produced. For this purpose ferrosilicon, a low-purity iron-silicon alloy, is used because it can be relatively cheaply prepared by the reaction of iron or iron oxide, silicon dioxide, and coke.⁵ The aluminum industry consumes large quantities of low-grade silicon in the making of aluminum-silicon alloys. Within recent years, the expanding silicone industry has also become a major user of silicon compounds.

→ Silicon has the highest latent heat of fusion of any element, and for this reason has been suggested as a storage element for heat energy in solar-energy-conversion systems which use heat engines.

The infrared transmissivity of silicon is very high in the 1 to 8 micron range.⁷ This, coupled with its hardness, chemical inertness, and ability to take an optical finish, has contributed to its wide usage in infrared optical elements. Originally it was believed that single crystals were required for optical components, so silicon crystal-growing capabilities were extended to diameters of several inches.⁸ Later work, however, showed that the optical-image quality of polycrystalline silicon was quite satisfactory and allowed casting techniques to supplant crystal growing.

Because of the fine polish possible, both silicon and high-silicon-content iron-silicon alloys have been suggested as a material for jewelry and sculpture. Unfortunately, however, the hardness of silicon is close to that of sand particles, so its abrasion resistance is fairly low.

In 1901, 11 years after the invention of the coherer, a patent was filed by J. C. Bose for a detector using galena.⁹ By 1906, both Pickard^{10,11} and Austin¹² had described detectors using a silicon-metal point contact, and Dunwoody¹³ had proposed a carbon-silicon combination for the same purpose. By the mid-thirties, silicon was being widely used in the laboratory as a microwave detector. During World War II great advances were made in the purification and handling of silicon

and in diode-fabrication techniques. The original diodes used a very low-purity commercial-grade silicon with no intentional doping. In the early forties, the situation was improved by powdering the silicon, leaching it with various acids, and then casting it into an ingot. This increased purity allowed deliberate doping, e.g., the addition of aluminum and beryllium* as used by the General Electric Co., Ltd. Shortly thereafter Du Pont developed a method of making semiconductor-grade silicon by the zinc reduction of silicon tetrachloride, which decreased the impurity concentration by orders of magnitude. Simultaneously with this work, Scaff and Theuerer at Bell Telephone Laboratories were using gradient freezing to segregate the impurities in one end of an ingot.^{14,15}

In 1950 an experimental silicon transistor was announced,¹⁶ but it was not until 1954 that they were available in any quantity.¹⁷ All the silicon diodes and early transistors were made on either polycrystalline chips or small pieces of single crystal cut from polycrystalline ingots. However, in 1952 Teal and Buehler¹⁸ grew single crystals of silicon from a melt in an apparatus previously developed by Teal and Little for germanium crystal growing. Still further purification of silicon became possible with the introduction of float zoning, which was developed independently by Keck, Theuerer, and Emeis.¹⁹ In 1957 a vapor-phase method of growing silicon single crystals was proposed by Sangster,²⁰ although it was 1960 before such a technique was used in device construction. At that time Bell Telephone Laboratories announced a method of transistor fabrication that started with single-crystal slices that were partially grown epitaxially† from a vapor.²²

In 1955 the Bureau of Mines began separating the production figures of semiconductor-grade silicon from lesser purity forms, and gave the total U.S. usage for the year as 35,000 lb. The estimated number of silicon transistors produced that year was about 93,000. In 1964, when silicon production had only increased to about 90,000 lb, approximately 400 million silicon devices were manufactured.

REFERENCES

1. Colliers Encyclopedia, vol. 17, 1957.
2. Phillips, C. J.: "Glass: The Miracle Maker," Pitman Publishing Corporation, New York, 1941.
3. Sosman, Robert B.: "The Properties of Quartz," ACS Monograph Series, no. 37, Chemical Catalog Company, Inc., New York, 1927.
4. Encyclopaedia Britannica, vol. 20, 1961.
5. Bereznoi, A. S.: "Silicon and Its Binary Systems," translated from Russian, Consultants Bureau, New York, 1960.

* The beryllium was presumably electrically inactive, but reduced the tendency of the cast ingots to crack during cooling.

† The term "epitaxie" was apparently first used by Royer and was applied to the orientation of crystal layers by a substrate of different material and structure. (See for example M. L. Royer, *Recherches expérimentales sur l'épitaxie ou orientation mutuelle de cristaux d'espèces différentes*, *Bull. Soc. Franc. Mineral.*, vol. 51, pp. 7-159, 1928.) It has continued to be used in that sense, but has been extended to cover, for example, the fresh-silicon-silicon-seed bond in crystals grown from the melt.²¹

4 Silicon Semiconductor Technology

6. Allen, T. B.: Silicon Articles, U.S. Patent 1,073,560, 1913.
7. Fan, H. Y., and M. Becker: Infrared Optical Properties of Silicon and Germanium, "Semiconducting Materials," Butterworth & Co., Ltd., London, 1951.
8. Runyan, W. R.: Growth of Large Diameter Silicon and Germanium Crystals by the Teal-Little Method, *Rev. Sci. Instr.*, vol. 30, pp. 535-540, 1959.
9. Bose, J. C.: U.S. Patent 755,840, 1904.
10. Pickard, G. W.: Thermo-electric Wave Detectors, *Electrical World*, vol. 48, p. 1003 (L), Nov. 24, 1906.
11. Pickard, G. W.: Means of Receiving Intelligence Communicated by Electric Waves, U.S. Patent 836,531, 1906.
12. Austin, L. W.: The High Resistance Contact Thermo-electric Detector for Electrical Waves, *Phys. Rev.*, vol. 24, pp. 508-510, 1907.
13. Dunwoody, H. H. C.: Wireless-telegraph System, U.S. Patent 837,616, 1906.
14. Torrey, Henry C., and Charles A. Whitmer: "Crystal Rectifiers," McGraw-Hill Book Company, New York, 1948.
15. Pearson, G. L., and W. H. Brattain: History of Semiconductor Research, *Proc. IRE*, vol. 43, pp. 1794-1806, 1955.
16. Pietenpol, W. J., and R. S. Ohl: "Characteristics of Silicon Transistors," paper presented at the Conference on Electron Devices, University of Michigan, Ann Arbor, June 22, 1950.
17. Teal, G. K.: "Some Recent Developments in Silicon and Germanium Materials and Devices," paper presented at the National Conference on Airborne Electronics, Dayton, Ohio, May 10, 1954.
18. Teal, G. K., and E. Buehler: Growth of Silicon Single Crystals and of Single Crystal Silicon p-n junctions, *Phy. Rev.*, vol. 87, p. 190 (A), 1952.
19. Petritz, Richard L.: Contributions of Materials Technology to Semiconductor Devices, *Proc. IRE*, vol. 50, pp. 1025-1038, 1962.
20. Sangster, R. C., E. F. Maverick, and M. L. Crouch: Growth of Silicon Crystals by a Vapor Phase Pyrolytic Deposition Method, *J. Electrochem. Soc.*, vol. 104, pp. 317-319, 1957.
21. Dash, William C.: The Growth of Silicon Crystals Free from Dislocations: Growth and Perfection of Crystals, pp. 361-385, John Wiley & Sons, Inc., New York, 1958.
22. Theuerer, H. C., J. J. Kleimack, H. H. Loar, and H. Christensen: Epitaxial Diffused Transistor, *Proc. IRE*, vol. 48, pp. 1642-1643 (L), 1960.
23. Mellor, J. W.: "A Comprehensive Treatise on Inorganic and Theoretical Chemistry," vol. VI. Longmans, Green & Co., New York, 1957.

Silicon-manufacturing Processes

Silicon is a very abundant element of the earth's crust, but always occurs as a compound, and almost exclusively either as the oxide or as a silicate. Because of its availability, most large-scale silicon-manufacturing processes start with the oxide. The order of steps determines the final purity, not only by determining the ease with which impurities in the original silica can be separated, but also by the available quality of chemicals used in the various stages.

The actual level of allowable purities varies somewhat with the devices to be made from the silicon and also with the specific impurity. It is important to have the normal doping elements (Groups IIIA and VA) reduced to the parts-per-billion range, and, similarly, such elements as gold, copper, and iron. The roles of others, such as sodium, calcium, zinc, tin, and lead, are not well understood and apparently can be tolerated in somewhat higher levels in the manufactured silicon. However, because of their very low segregation coefficients, the final concentrations of these elements in the grown crystal are probably comparable to those of the IIIA's and VA's. The discussion of the probable impurity concentrations leads to the realization that the ranges involved are almost always below the limits of detectability of standard analytical methods, and that the electrical behavior of either the bulk silicon, or devices made from it, are the primary ways by which impurity content is estimated. Some of these latter methods are considered in Chap. 8, but no attempt will be made to discuss the various chemical, spectrographic, and neutron activation procedures which are used during the various stages of semiconductor-grade silicon manufacturing.

2-1. EARLY METHODS OF MANUFACTURE^{1,*}

About 1808 Berzelius heated a mixture of silica, carbon, and iron and obtained what he called "silicon," though it was apparently an iron silicide, or what would now be called "ferrosilicon." Soon after, Gay-Lussac and Thénard reduced silicon tetrafluoride with potassium and formed "amorphous" silicon. In the following years a variety of other reactions were studied. Sodium and magnesium were used

* Superscript numbers indicate items listed in References at the end of the chapter.

to reduce silicon tetrafluoride. Silicon tetrachloride was reduced with the potassium, sodium, magnesium, beryllium, aluminum, zinc, and sodium amide. It was suggested that hydrogen would reduce silica and was shown that magnesium, calcium, and aluminum certainly would. In 1880 silicon was obtained by an electric discharge in silane. Shortly thereafter, the thermal decomposition of silane and trichlorosilane was observed. The hydrolysis of silicon sulfide was reported to yield silicon. Silicon has been prepared by the electrolysis of a molten mixture of potassium fluosilicate and potassium fluoride, and can apparently be similarly prepared from other alkali fluorides. Likewise, silicon may be obtained from the reduction of silicofluorides by sodium² or aluminum.³

Copper has also been used to obtain silicon from silica, but in this case it is a two-stage process. First, SiO_2 and copper react to form some free silicon, but predominantly Cu_2Si . The latter is then heated with sulfur to form CuS and silicon.⁴

The most common method of producing silicon is very similar to the first one used, i.e., by the reduction of silica with carbon, though it is now usually done in an electric furnace.⁵⁻¹⁰

In an effort to increase the yield of silicon by preventing its vaporization and by minimizing the formation of silicon carbide, several per cent of various silicates have been added to the silica carbon charge.¹¹

Assuming that the rapid formation of CO carried away excessive amounts of the vaporized silicon, another approach to yield improvement involved first partially reducing the silica, then adding an excess of silica, and heating further.¹²

In order to remove carbon from low-grade silicon, one suggestion was to melt it in a crucible which had a layer of alkaline earth carbonate on the bottom. The carbonate decomposed, the CO_2 bubbled up through the silicon and reacted with carbon to form CO . With this process, silicon with resistivities of the order of $\frac{1}{2}$ ohm-cm were reported (1909).¹³

Another procedure involved remelting the silicon under a layer of fused silicate.¹⁴ The molten glass protects the silicon from oxidation and getters various impurities as is evidenced by the gradual darkening of the glass.

Rather than starting with silica, several processes started with silicates, which are also readily available, and used carbon or aluminum to reduce them.^{15,16} Unfortunately, most of these methods as originally conceived gave a very impure grade of silicon, so a variety of leaching systems were used for several years in an effort to upgrade it.

One such process used in the early forties to prepare silicon suitable for microwave diodes consisted in crushing the silicon to about 200 mesh; letting it soak in a water-HCl- HNO_3 mixture for several hours; washing with distilled water; adding H_2SO_4 and HF; boiling, washing, and treating with an HF-water mixture; and then giving a final washing.¹⁷ A similar system, adapted to larger-scale operation, has been described in a recent U.S. patent.¹⁸ In 1905 the reduction of silicon monoxide with silicon carbide was proposed,¹⁹ and in 1961 a more sophisticated system using hydrogen as the reducing agent was patented.²⁰ The latter claimed to obtain high purity by distilling the silicon monoxide prior to reduction.

It has been proposed to make semiconductor-grade silicon by reducing the silicates in low-temperature glasses with molten aluminum, and then precipitating the silicon from the excess aluminum.²¹ The silicon, thus prepared, is saturated with

aluminum, but presumably the majority of other impurities are separable by leaching processes. Another approach using aluminum is to first react SiO_2 with aluminum to form $\text{Si} + \text{Al}_2\text{O}_3$. After all free aluminum is removed by an HCl leach, the silicon is dissolved by molten tin. Since tin is much less soluble in silicon than is aluminum, a higher-purity silicon is then obtained after precipitating it from the tin.²² In addition, this process is said to be very efficient (up to 90 per cent) and could be of use, for example, in reducing isotope-enriched silica where the starting material costs are extremely high.

2-2. SUMMARY OF APPLICABLE METHODS

The processes successfully used include the reduction of silicon tetrachloride with zinc, cadmium, or hydrogen;²³ the reduction of trichlorosilane (SiHCl_3) with hydrogen;²⁴ the pyrolytic decomposition of silane (SiH_4);^{25,26} and the reduction of silicon tetraiodide²⁷ and silicon tetrabromide with hydrogen.²⁸ In each case, the starting materials must be carefully purified and great care exercised in the selection of storage and reaction-chamber materials. For detailed discussion of silicon chemistry the reader is referred to Refs. 1, 25, and 26.

The usual sequence is to make a low-grade silicon or ferrosilicon, chlorinate the impure silicon, carefully purify the resulting halogen, and then reduce it. If some silicon compound other than silicon tetrachloride is to be used, it may also be prepared directly, e.g., the bromide, or by further reactions involving the tetrachloride. Huge quantities of silicon tetrachloride and trichlorosilane are produced for use in silicone manufacture so a ready source of feedstock for the semiconductor industry is available.

Halides are most often purified by direct distillation, but occasionally other methods are used with, or in addition to, the distillation. If purities in the range of 50 to 100 ohm-cm are desired, pyrex or steel columns are adequate, and indeed high-purity silicon tetrachloride and trichlorosilane are normally shipped in steel tanks. However, for higher purity it appears advantageous to use quartz columns. There is considerable difficulty in separating some of the Group IIIA and VA halides from those of silicon, so the addition of complexing agents prior to distillation has sometimes been used. One group of compounds suggested for this purpose is some of the aliphatic and aromatic dinitriles such as succinonitrile, adiponitrile and acetonitrile.²⁹ Liquid-extraction systems using some of these same compounds have also been proposed.²⁹ Likewise, liquid- and gas-absorption columns have been used. One of these contained activated alumina,³⁰ while another used a column containing an absorbent, e.g., activated charcoal, charged with compounds such as CNBr or $\text{C}_2\text{H}_5\text{CN}$.³¹ A process has also been reported in which electrodes were immersed in a halide-methyl alcohol mixture, and various impurities deposited at the electrodes.³²

2-3. ZINC-SILICON TETRACHLORIDE

The first commercial process for the production of semiconductor-grade silicon used zinc to reduce silicon tetrachloride.^{23,33} Zinc is an acceptable reducer since it is available in reasonable purity, does not form a silicide, is relatively noncorro-

sive, and is not explosive in the presence of air. Since the solubility of zinc in silicon is quite low, and the reaction produces zinc chloride, and since zinc itself is quite soluble in many solvents which do not attack silicon, contamination by zinc or zinc compounds is minimal. A sketch of early equipment is shown in Fig. 2-1. In this process, the zinc and silicon tetrachloride are separately vaporized and metered and are then introduced into the reaction chamber in approximately stoichiometric proportions. Because silicon tetrachloride is liquid at room temperature, the flow rates can be monitored and controlled by standard flowmeters and valves. Zinc with its much higher melting point poses more problems. One solution, described in U.S. Patent 2,912,313,³⁴ consists in melting the zinc in one container, then feeding the liquid to a flash evaporator. The reaction-chamber temperatures are kept high enough for the reduction to be reasonably efficient, and yet low enough to minimize side reactions with the container. Temperatures of 900 to 1100°C are satisfactory, with 950 to 1000°C being preferred. The reactor and associated plumbing are of fused silica. The silicon grows out in dendrites, or needles, from the walls of the container. The reaction products and unreacted components are condensed and the zinc reclaimed. The silicon needles can be leached with HCl to remove any zinc which might remain.

Some operating numbers given in Ref. 33 are as follows: (1) reaction-chamber diameter, 8 in.; (2) reaction-chamber length, 6 ft; (3) reaction-chamber temperature, $\approx 950^\circ\text{C}$; (4) temperature of incoming SiCl_4 and zinc, $\approx 950^\circ\text{C}$; (5) length of run, 40 hr; (6) amount of zinc used, 147 lb; (7) amount of SiCl_4 used, 285 lb; and (8) amount of silicon produced, 15.5 lb. When the run is to end, the boilers and lines can be freed of zinc by purging with nitrogen. Since the silicon thus produced is needlelike and has a high volume-to-weight ratio, some form of densification must be used prior to charging into a crystal puller.

It has also been suggested that one contributor to low-process yields is the reduction which may take place in the gas stream and not on the furnace walls. When this occurs, the silicon is finely divided and is carried out with the exit gases and is

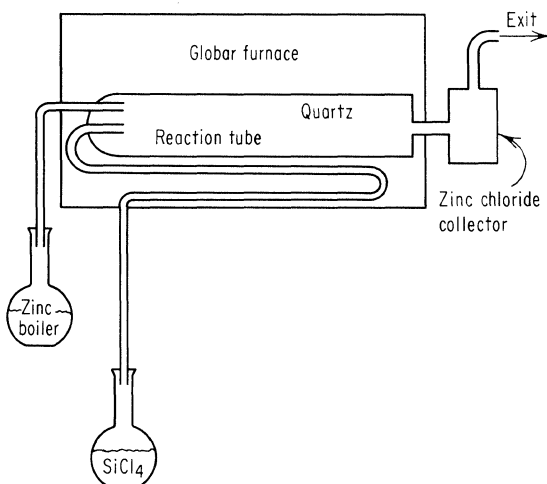


Fig. 2-1. Early high-purity silicon-manufacturing process.

lost. One solution to this problem is to introduce the two reactants in such a manner that there is a minimum of turbulence, and so that they are initially directed toward the hot walls.³⁵

Even though the starting materials are carefully purified before feeding into the reactor, trace impurities still remain and appear in the deposited silicon. However, by making use of the fact that many of the chlorides either can be reduced or thermally decompose at lower temperatures than the silicon, various predeposition furnace arrangements have been proposed.

In one of these, the deposition furnace is simply separated into two furnaces, with the geometries and temperatures being such that about 10 per cent of the silicon deposits in the first chamber. As a variation, the reactants can first be fed into two parallel predeposition furnaces in which there is a stoichiometric excess of zinc in one and of silicon tetrachloride in the other.³⁶ Other suggestions include passing the silicon tetrachloride over hot silicon³⁷ and over a pool of molten zinc.³⁸

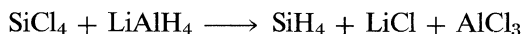
The zinc process has apparently been completely supplanted in the United States by various hydrogen-reduction methods.

2-4. SILANE DECOMPOSITION

This process, in principle is very simple, involving only the pyrolytic decomposition of silane. It has not been widely used, however, because of the difficulty of making silane, and because of its instability. Silane will ignite and explode in air and is decomposed by water containing traces of alkali. Also, it reacts explosively with halogens to give silicon halides, and in the absence of air it decomposes to silicon and hydrogen at 400°C.^{26,39} Two variations have been used: (1) the silane is made and then decomposed in the next step; (2) the silane is prepared separately and stored in cylinders until needed.

Silane (SiH₄) can be prepared by the reaction of a metal hydride with some silicon compound containing silicon bound to fluorine, chlorine, bromine, iodine, cyanide, oxygen, sulfur, or nitrogen. The hydride (most commonly lithium aluminum hydride) is dissolved in an ether and the silicon compound bubbled through the solution.⁴⁰

One specific choice is⁴¹



with the ether being tetraethylene glycol dimethyl ether. Another combination uses silicon tetrachloride plus a mixture of sodium aluminum hydride and calcium aluminum hydride in tetrahydrofuran to generate the silane.⁴² The addition of the calcium aluminum hydride in very small amounts presumably reduces the amount of boron appearing after reduction of the silane. Possible contaminants to the silane leaving the system are solvent vapor, unreduced silicon tetrachloride or some intermediates such as SiHCl₃, and impurities in the original silicon tetrachloride which also form volatile hydrides. Synthetic zeolite beds at -78°C have been used to remove any arsenic and phosphorus compounds which may be present at this point.⁴³ Figure 2-2 shows a sketch of the equipment.

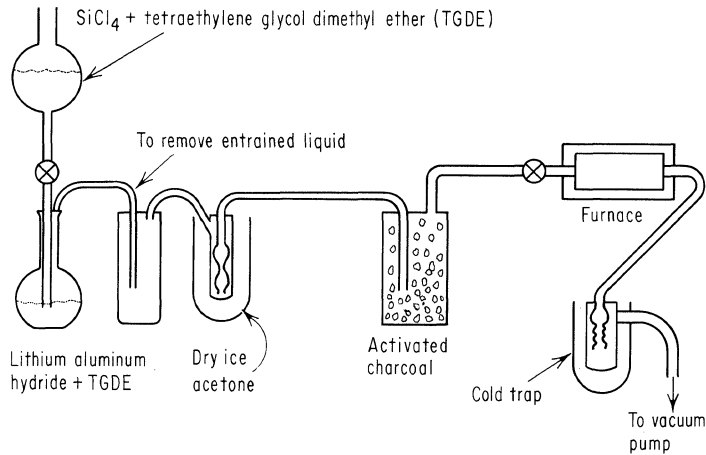


Fig. 2-2. Silane-generation and decomposition apparatus.

Silane begins to decompose at about 400°C . The reaction products may include appreciable quantities of higher silanes, as well as silicon and hydrogen. As might be expected, low pressure favors decomposition, and most processes operate at a few torrs. Likewise, the decomposition efficiency increases with increasing temperature. It has been reported⁴¹ that at pressures less than 8 torrs, 100 per cent decomposition occurs from 777°C up to at least the melting point of silicon. While deposition can occur on the walls of a hot tube, it is preferable to use a heated silicon seed or filament and deposit directly on it. This prevents contamination from the tube, as well as eliminating the necessity for leaching away or otherwise separating the tube from the silicon. One method of accomplishing this is to heat the tip of a silicon bar inductively and then, as deposition occurs, to keep the growing ingot moving so that the tip remains in the r-f field.^{44,45} Another variation^{45,46} is to keep the silicon tip molten, and again, as the silicon forms and enters the molten pool, to continuously lower the seed. In order to speed up the deposition process, a number of systems using high-frequency radio waves to assist in decomposition have been proposed.⁴⁷⁻⁴⁹ This process can produce a very high-grade silicon, but has not been widely used commercially.

2-5. IODIDE PROCESS

The decomposition of silicon tetraiodide to form silicon is a straightforward process, and apparently because of the ease of purification, the iodide has been used to produce extremely high-purity silicon.^{27,50,51} Because of the high cost of iodine, a recovery process is necessary. In order to obtain reasonable deposition rates, low pressures are required, so that a combination of vacuum pumps and iodine traps is required. It is presumably because of these additional requirements that the process has thus far not proved commercially feasible, even though some companies have operated iodide plants on a limited basis. One process^{49,52,53} consisted of these five operations.

1. Reaction of iodine with commercial-grade silicon.
2. Filtration of the silicon tetraiodide.
3. Distillation of the iodide.
4. Decomposition to form silicon and iodine.
5. Iodine recovery.

This is illustrated schematically in Fig. 2-3. A somewhat more elaborate process has been described;⁵⁴ it employs an additional purification step consisting of zone refining the silicon-tetraiodide before distillation.

The SiI_4 is formed by reacting commercial silicon with iodine at about 600°C ; this may be done in either a fixed or a fluid bed. The reaction is exothermic and requires no additional external heat once the bed is brought to operating temperature. In order to remove any unreacted silicon dust that comes from the reaction bed, the iodide can be filtered before distillation. Since SiI_4 freezes at 124°C , all transfer lines must be kept heated. Both quartz and tantalum have been used for the distillation unit, with quartz being preferred. Forecuts of 10 to 30 per cent, and pot residues of from 10 to 30 per cent of the total charge have been used. The deposition surface may be a quartz tube, tantalum rod, or silicon rod. The temperature of the surface should be in the order of 1000°C for good decomposition efficiency, and the pressure in the deposition chamber should be in the order of 1 torr or less.

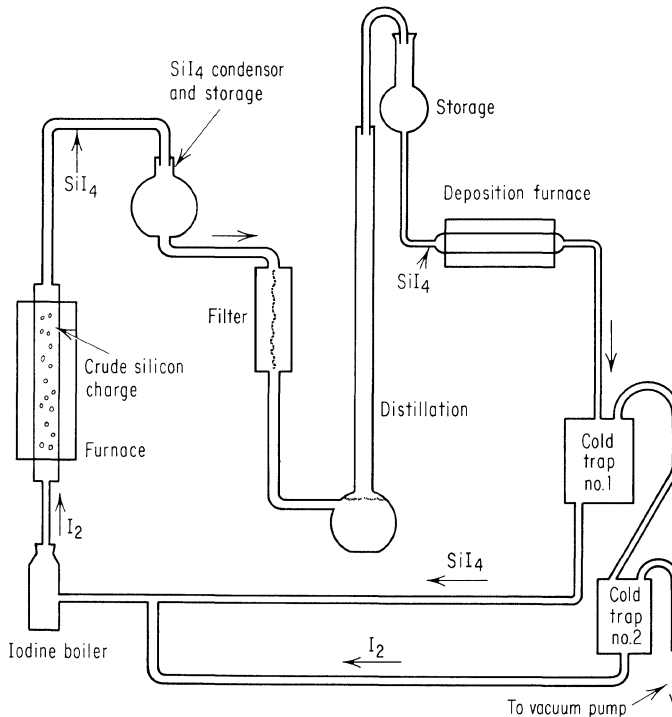


Fig. 2-3. The iodide process.

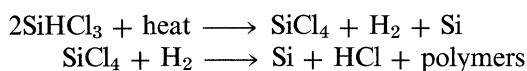
Another process has been developed which makes use of a film-boiling technique to simultaneously maintain high efficiency and deposition rate.⁵⁵ The heated wire vaporizes the liquid in the vicinity and supplies heat for decomposition so that silicon is deposited on it. An arc has also been used for supplying the heat for decomposition,⁵⁶ but does not appear applicable for high-purity silicon.

2-6. SILICON TETRACHLORIDE AND TRICHLOROSILANE PROCESSES

Both SiCl_4 and trichlorosilane (SiHCl_3) are now used in the manufacturing of silicon. Trichlorosilane will thermally decompose at a slow rate to give silicon. Silicon tetrachloride is apparently stable up to at least 1200°C . With hydrogen, however, either of them react and produce silicon with reasonable efficiencies and rates. While the overall reactions can be written as



these are gross simplifications. For example, in reaction (1) considerable SiHCl_3 , SiCl_2 and long chain polymers occur as well as HCl and silicon, and reaction (2) probably proceeds as



In either the hydrogen-reduction or thermal-decomposition process, lower temperatures favor the production of very small, brownish particles. For example, at 800°C most of the SiCl_4 reduction output will be powder. SiHCl_3 decomposition at 830°C gives aggregates of fine powder. At 1230°C the silicon begins to have a nodular appearance.⁵⁷ Hydrogen reduction of either SiCl_4 or SiHCl_3 above the 1000°C range produces a distinctly crystalline looking deposit which may vary from dendrites to large, well-defined crystals such as shown in Fig. 2-4.

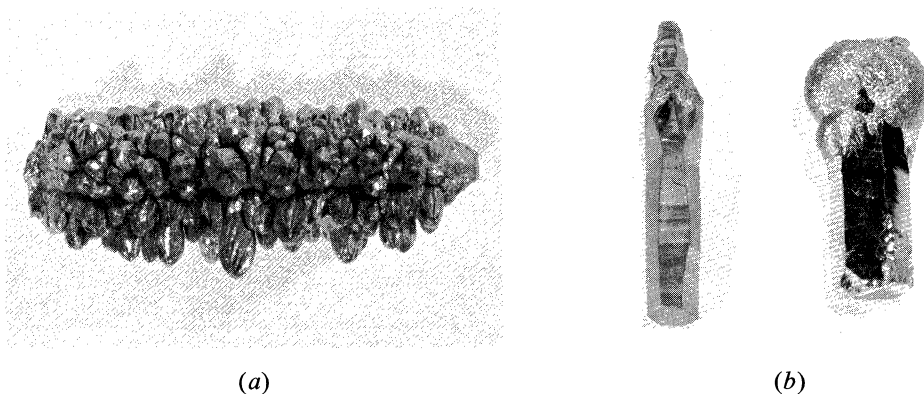
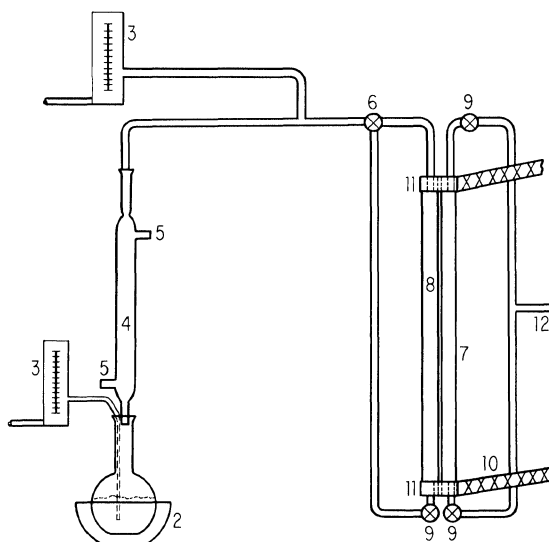


Fig. 2-4. Photograph of different forms of silicon from trichlorosilane deposition (each piece approximately 1.5 in. long).

Fig. 2-5. The silicontetrachloride reduction process.



The use of trichlorosilane is favored over silicon tetrachloride because of faster deposition rates and because it is apparently easier to remove phosphorus and boron compounds from it. Figure 2-5 is a schematic of a typical SiCl_4 or SiHCl_3 silicon-production process. Numbers given in Ref. 58 for trichlorosilane are: (1) temperature of main deposition zone, 950°C ; (2) initial hydrogen rate, 100 liters/hr; (3) final hydrogen rate; 300 liters/hr; (4) all hydrogen bubbled through SiHCl_3 initially at -9°C ; (5) as hydrogen rate is raised to 300 liters/hr, SiHCl_3 temperature is raised to -5°C ; (6) length of run, 100 hr; (7) amount of silicon, ≈ 1000 g.

As might be expected, there have been almost as many reactors designed as there are investigators; these reactors vary from a simple heated quartz tube, through silicon-particle fluid beds⁵⁹ and hot tantalum wires upon which deposition occurs, to deposition on high-purity silicon rods (for the highest-purity silicon). The quartz tube is very simple, may be resistance-heated, and produces predominantly dense silicon with some protuberances on the inside. The silicon bonds to the quartz, which must be removed by leaching in hydrofluoric acid. The loss of a quartz tube each run raises the processing costs, and the etching usually introduces contamination, as does the quartz tube itself. Various methods of preventing sticking and contamination have been proposed. One of these deposited a thin layer of carbon on the inside of the tube by the thermal decomposition of CH_4 .⁶⁰ A better scheme consists of depositing an additional layer of SiO_2 on the tube by the reaction of SiCl_4 or SiHCl_3 with high-purity water,⁶¹ or by the burning of SiI_4 and hydrogen in very pure air.⁶² The use of a tantalum tube for a combination heater and support for deposition reduces quartz costs and contamination, but still requires removal of the tantalum. Silicon-rod heaters eliminate these difficulties but do require a source of long, high-purity silicon rods.^{63,64} A photograph of a section of 4-ft by 4-in.-diameter silicon rod deposited in this fashion may be seen in Fig. 2-6.

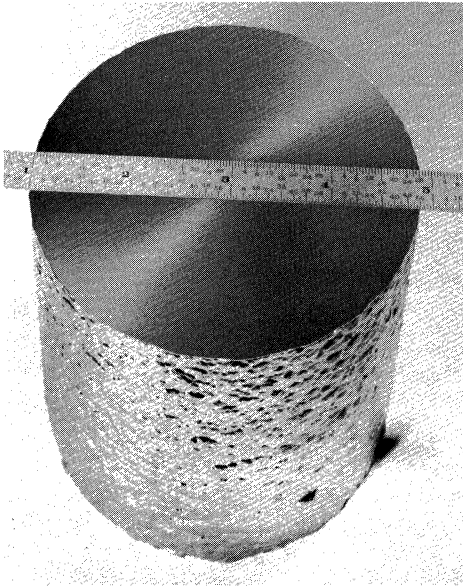


Fig. 2-6. Section of a 4-in.-diameter deposited silicon rod.

Various other gas-decomposition or reduction processes using SiBr_4 ,^{27,65} and SiCl_2 ⁶⁶ have been used, but apparently none of them have ever passed the laboratory stage, probably for economic reasons.

REFERENCES

1. Mellor, J. W.: "A Comprehensive Treatise on Inorganic and Theoretical Chemistry," vol. IV, Longmans, Green & Co., Inc., New York, 1957.
2. Eringer, Josef: Process for Obtaining Silicon from Its Compounds, U.S. Patent 2,172,969, Sept. 12, 1939.
3. Schmidt, Werner: Process of Reacting Sodium Silicofluoride with Aluminum, U.S. Patent 2,857,252, Oct. 21, 1958.
4. De Chalmot, Guillaume: Method of Obtaining Free Amorphous Silicon, U.S. Patent 602,632, Apr. 19, 1898.
5. Franchot, R.: Producing Silicon and Alloys, U.S. Patent 2,261,516, Nov. 4, 1941.
6. Tone, F. J.: Method of Reducing Metallic Compounds, U.S. Patent 937,120, Oct. 19, 1909.
7. Tone, F. J.: Process of Reducing Ores, U.S. Patent 921,183, May 11, 1909.
8. Potter, H. N.: Method of Producing Silicon, U.S. Patent 908,130, Dec. 29, 1908.
9. Udy, M. J.: Process for the Production of Metallic Silicon, U.S. Patent 2,823,983, Feb. 18, 1958.
10. Tone, F. J.: Reduction of Metals and Alloys, U.S. Patent 745,122, Nov. 24, 1903.
11. Scheid, Bernhard: Process of Manufacturing Metallic Silicum, U.S. Patent 662,548, Nov. 27, 1900.
12. Tone, Frank J.: Process of Reducing Compounds with Electrically Developed Heat, U.S. Patent 869,276, Oct. 29, 1907.
13. Dempster, John T. H.: Decarburized Silicon and Method for Making the Same, U.S. Patent 1,019,431, Mar. 5, 1912.

14. Brockbank, Clarence J.: Process for Purifying Silicon, U.S. Patent 1,180,968, Apr. 25, 1916.
15. Homan, C. H.: Manufacture of Silicon and Aluminum from Silicates of Alumina, U.S. Patent 732,410, June 30, 1903.
16. MacHalske, Forentine J.: Process of Producing Elementary Silicon and By-products, U.S. Patent 1,062,982, May 27, 1913.
17. Torrey, Henry C., and Charles A. Whitmer: "Crystal Rectifiers," McGraw-Hill Book Company, New York, 1948.
18. Voos, Walter: Production of Pure Silicon, U.S. Patent 2,972,521, Feb. 21, 1961.
19. Potter, Henry Noel: Method of Making Silicon, U.S. Patent 875,672, Dec. 31, 1907.
20. Aries, R. S.: High Purity Elemental Silicon, U.S. Patent 3,010,797, Nov. 28, 1961.
21. Smith, William E.: Process for Making Purified Silicon from Silicon-containing Substances, U.S. Patent 2,955,024, Oct. 4, 1960.
22. Thurmond, C. D.: Recovery of Silicon from Silicon Dioxide, U.S. Patent 2,904,405, Sept. 15, 1959.
23. Lyon, D. W., C. M. Olson, and E. D. Lewis: Preparation of Hyper-pure Silicon, *J. Electrochem. Soc.*, vol. 96, pp. 359–363, 1949.
24. Smotko, J. S.: "Experiments to Produce Ductile Silicon," FIAT, Final Report 789, 1946.
25. Stock, Alfred E.: "Hydrides of Boron and Silicon," Cornell University Press, Ithaca, N.Y., 1933.
26. Ebsworth, E. A. V.: "Volatile Silicon Compounds," The Macmillian Company, New York, 1963.
27. Litton, Felix B., and Holger C. Anderson: High Purity Silicon, *J. Electrochem. Soc.*, vol. 101, pp. 287–292, 1954.
28. Sangster, Ray C., E. F. Maverick, and M. L. Croutch: Growth of Silicon Crystals by a Vapor Phase Pyrolytic Deposition Method, *J. Electrochem. Soc.*, vol. 104, pp. 317–319, 1957.
29. Conn, John B.: Purification of Silicon Halides, U.S. Patent 2,970,040, Jan. 31, 1961.
30. Theuerer, H. C.: Purification of SiCl_4 by Adsorption Techniques, *J. Electrochem. Soc.*, vol. 107, pp. 29–32, 1960.
31. Pohl, Franz Arthur, and Toni Hauskrecht: Process of Purifying Silane or Chlorinated Silicones, German Patent 1,073,460, Jan. 21, 1958.
32. Rosenberger, George: Process for the Production of Pure Germanium or Silicon Halides, German Patent 1,021,838, Jan. 2, 1958.
33. Butler, Keith H., and Carl M. Olson: Process for the Production of Pure Silicon in a Coarse Crystalline Form, U.S. Patent 2,773,745, Dec. 11, 1956.
34. Mason, Robert W., and Anthony W. Yodis: Apparatus for Production of High Purity Elemental Silicon, U.S. Patent 2,912,311, Nov. 10, 1959.
35. Macphee, Malcolm, and Derek Edwin Bolger: Improvements in the Manufacture of Pure Silicon, British Patent 833,621, Apr. 27, 1960.
36. Krchma, I. J., and Carl M. Olson: Production of Elemental Silicon, U.S. Patent 2,883,269, Apr. 21, 1959.
37. Olson, Carl M.: Preparation of Pure Silicon, U.S. Patent 2,805,133, Sept. 3, 1957.
38. Krchma, I. J.: Production of Silicon, U.S. Patent 2,909,411, Oct. 20, 1959.
39. Bereznoi, A. S.: "Silicon and Its Binary Systems," translated from Russian, Consultants Bureau, New York, 1960.
40. Scott, Thomas Robertson, George King, and Jack McCreath Wilson: Improvements in or Relating to the Production of Semiconductor Material for Rectifiers, Australian Patent 200,917, Feb. 16, 1956.

41. Lewis, Charles H., Mario B. Giusto, and Sidney Johnson: "The Preparation of Transistor Grade Silicon from Silane or Analogous Compounds," Metal Hydrides Incorporated, Final Report, Contract AF19(604)-3463, 1959.
42. Pure Silane and Silicon, British Patent 851,962 Oct. 19, 1960.
43. Caswell, Earl G.: Purifying Silane, U.S. Patent 2,971,607, Feb. 14, 1961.
44. Sterling, Henley Frank, and Eric Langley Bush: Pure Silicon Semiconductor Rods, British Patent 829,421, Mar. 2, 1960.
45. Sterling, Henley Frank, and Eric Langley Bush: Methods of Producing Silicon of High Purity, U.S. Patent 2,993,762, July 25, 1961.
46. Cowland, F. C., and Leighton G. Penhale: Process for Preparing Pure Silicon, U.S. Patent 3,006,734, Oct. 31, 1961.
47. Process for the Fabrication of Metals of High Purity, French Patent 1,150,562, Jan. 15, 1958.
48. Sterling, H. F.: Manufacture of Semiconductor Material, U.S. Patent 2,955,966, Oct. 11, 1960.
49. Okura, Kirokuro, Hiroshi Arayama, and Jun Minamiya: Preparation of High Purity Silicon. I. The Reduction of SiCl_4 with Hydrogen in the Electric Field, *Nippon Kogyo Kaishi*, vol. 77, pp. 573-578, 1961.
50. General Electric Company: Final Engineering Report, Contract AF33(600)-28956, 1959.
51. Szekely, Gustav: Preparation of Pure Silicon by the Hydrogen Reduction of Silicon Tetraiodide, *J. Electrochem. Soc.*, vol. 104, pp. 663-667, 1957.
52. Herrick, C. S.: Production of Silicon of Improved Purity, U.S. Patent 3,020,129, Feb. 6, 1962.
53. Herrick, Carlyle S., and James G. Kriebel: High-purity Silicon from an Iodide Process Pilot Plant, *J. Electrochem. Soc.*, vol. 107, pp. 111-117, 1960.
54. Moats, Guy H., Bernard Rubin, and Walter B. Jackson: Apparatus for Continuous Preparation of Ultrapure Silicon, U.S. Patent 3,006,737, Oct. 31, 1961.
55. Irvine, John W., Jr.: Preparation of Silicon, U.S. Patent 2,944,874, July 12, 1960.
56. Stauffer, R. A.: Method of Producing Metals by Decomposition of Halides, U.S. Patent Reissue 24,821, May 3, 1960.
57. Eagle-Picher Research Laboratories: "Fourth Quarterly Report: Industrial Preparedness Study on High Purity Silicon," Contract DA36-039-SC66042, July 1, 1956.
58. Pauls, G.: Process for Manufacturing Dense, Extra Pure Silicon, U.S. Patent 2,943,918, July 5, 1960.
59. Bertrand, L., North Star, and Carl Marcus Olson: Silicon Production, U.S. Patent 3,012,862, Dec. 12, 1961.
60. Yodis, Anthony W.: Pure Silicon from Silanes, German Patent 1,050,321, Feb. 12, 1959.
61. Marcel, Paul: Extrapure Silicon, French Patent 1,217,812, May 5, 1960.
62. Herrick, Carlyle S.: Coating of Bodies on Which Pure Silicon Is to Be Deposited, U.S. Patent 2,967,115, Jan. 3, 1961.
63. Process for Producing Extremely Pure Silicon for Semiconductors, German Patent 1,066,564; translated by Research Information Services, New York.
64. Rummel, T.: Method of and Apparatus for Producing Highly Pure Rod-like Semiconductor Bodies, U.S. Patent 2,981,605, Apr. 25, 1961.
65. Sangster, Ray C.: Method of Producing Semiconductor Crystal Bodies, U.S. Patent 2,895,858, July 21, 1959.
66. Schaefer, H.: Method of Producing Pure Silicon, U.S. Patent 2,989,376, June 20, 1961.

Silicon-casting Processes

Several methods for the casting of silicon have been used in the past 60 years, and the articles cast have covered the range from dental mirrors^{1,*} to pipes for highly reactive chemicals² to precision infrared optics.^{3,4} The need for the latter put more emphasis on the perfection of casting techniques than any other application, but casting can also be used for silicon lot homogenization, preparation of rods for float zoning and the making of individual charges for crystal growing. Most of the work to date has been directed toward massive castings (optical-quality castings up to 30 lb in weight have been made)⁵ but in the future, emphasis will probably shift to methods of producing thin sheets for device fabrication. The requirements for various end uses are somewhat different, so rather than consider processes for a specific application, the processes will be considered separately and their limitations discussed.

3-1. MELTING IN MOLD

In principle, melting the silicon directly in a mold should be the simplest method of all. There are, however, some fundamental difficulties. The mold material is usually slightly soluble in molten silicon and thus introduces unwanted impurities. The silicon bonds to many mold materials as it cools so that differential thermal contraction causes the silicon to shatter. It is also inconvenient to heat a mold for some shapes, e.g., a rod $\frac{1}{2}$ in. in diameter by 3 ft long.

Casting Perfection. The formation of sound castings must also be considered. This problem is, unfortunately, not independent of the mold material, since whether or not the silicon adheres to the container has a great influence on the casting integrity. However, for the present assume that the mold has been chosen so that either the silicon does not stick, the coefficient of expansion of the container and silicon are well matched, or that the container is weak enough to fracture before the silicon. The methods of attaining these conditions will be discussed later.

If the free surface of the silicon is allowed to freeze first, the expansion of the

* Superscript numbers indicate items listed in References at the end of the chapters.

remainder as it freezes will cause the ingot to crack. To prevent this, cooling must begin at the bottom and move upward so that the last liquid to freeze is at the gas interface. A heater over the top of the mold may be used, or the mold may be moved slowly downward out of the hot zone, somewhat in the manner of a Bridgeman furnace. Care must be taken not to cool the ingot so fast that the thermal gradient between the center of the casting and the outside causes the breaking stress to be reached.

Another type of flaw encountered is voids in the interior of the casting. These can be eliminated by casting in a vacuum; but, again, if freezing is allowed to progress in one direction only, any bubbles in the liquid will be moved along by the solid-liquid interface to the surface.

A similar type of void can occur if high-temperature liquid is trapped and cooled (see Sec. 3-2) since it can occupy a greater volume at high temperatures than it does after freezing, even though there is a volume increase on freezing. Freezing to a free surface will also eliminate this difficulty.

If the container has an expansion coefficient less than that of silicon, the silicon, after it is cooled, will have contracted more than the mold and, if it has not bonded to the container, will release. Likewise, if a plug were to be put into the mold, e.g., to cast a hollow dome, then the plug should have a higher coefficient so it can in turn shrink away from the silicon. In principle, this inner plug could be dispensed with entirely if the outer mold were rotated. Centrifugal force would then force the silicon to pile up on the outer walls of the mold and would produce a parabolic inner cross section.

Fused Silica. Molten silicon reacts with fused silica to form silicon monoxide (which vaporizes) and oxygen.⁶ If the reaction progresses long enough, the molten silicon becomes saturated with oxygen (about 3×10^{18} atoms/cm³ of melt),* and then only silicon monoxide is liberated, but with no apparent change in reaction rate. In addition, since the fused silica is being dissolved, any impurities in it are also being added to the melt along with the oxygen. For optical castings, the impurities added from the container are insignificant, but if the goal is to densify, or homogenize, a silicon lot, then the contaminants can downgrade the silicon quality. Boron is the worst offender (1 to 2 ppb can easily be added to the melt) though aluminum is apparently present in many cases.† In any event, the quantities are so small that they are detectable only by the more sophisticated

* This number is based on Kaiser and Keck's (*J. Appl. Phys.*, vol. 28, pp. 882-887, 1959) value of approximately 2×10^{18} atoms/cm³ of oxygen in the crystal, and a segregation coefficient of somewhere between 1, as they estimated, and 0.5 as given by F. A. Trumbore (*Bell System Tech. J.*, vol. 39, pp. 205-231, 1960).

† It is known that aluminum can be incorporated into a growing quartz crystal in appreciable quantities. Most fused silica is made from natural quartz, so it is quite possible that aluminum would be found in some or all such fused-silica ware. It has also been observed that fused silica made from the reaction of oxygen with very pure silicon tetrachloride softens at a somewhat lower temperature than that made from natural quartz. This has led to the speculation that the increased softening point of the natural fused silica is due to the inclusion of aluminum. Experiments have shown that the addition of a fraction of a per cent of aluminum to the chemically prepared fused silica does indeed increase the softening point to a value close to that of the natural product.

analytical methods such as neutron activation analysis or solids mass spectrometry. Since the amount of silica dissolved is a function of exposed surface, then in principle larger-diameter containers, preferably spherical, would reduce the melt volume-to-surface ratio and reduce overall contamination. The larger the diameter, the hotter the outside must be in order to melt-in in a reasonable time, and if the silicon-fused silica reaction rate increases with the temperature, it is quite possible to introduce more impurities by this method. If the melt-in temperature is kept lower, then the reaction rate is slowed down, but it also takes longer to completely melt the charge, so that again the final impurities level could be higher than that produced in a smaller container.

Molten silicon apparently does not wet clean fused silica since the silicon will not leak out through small holes in the silica liners. However, as silicon freezes it bonds to fused silica and, because of the great difference in thermal expansion coefficients, both silicon and container usually fracture during cooling. This occurs only below about 650°C. Above that temperature the silicon will flow plastically enough to strain relieve itself. Breaking occurs, not because of thermal shock, but because of the stress between the silica and the silicon so that slow cooling will not prevent it. One method which will prevent breakage is to use such a thin-walled fused-silica container that it will stretch elastically enough to prevent the breaking strength of the silicon from being reached.⁷ The thickness varies somewhat with the ingot cross section, but for 1-in. diameter, the maximum wall thickness is about 0.004 in. Such thin-walled containers are very fragile and this process is not recommended although it was used for silicon zone-refining experiments before the advent of the float-zone technique. If a mechanically sound ingot is not required, then the above method is very convenient. Such a use would be the densification of silicon from needles to chunks.

Fused silica gradually devitrifies and becomes structurally quite weak as thermal cycling proceeds. It has been suggested to make use of this weakened form as a casting container so that it, rather than the silicon, would shatter during cooling.⁸ The devitrification product is cristobolite, which has an expansion coefficient much closer to silicon than has the original fused silica. This process is difficult but was used extensively during World War II for producing material to be used in micro-wave diodes.

The possibility of making containers of pressed or lightly sintered fused-silica powder presents itself, but the temperatures required to melt silicon causes the powder to fuse together.

A possible method of obtaining large ingots of simple shape is the "ice cube" procedure.^{9,10} In this method the silicon is melted in the fused-silica container, and allowed to cool until the ingot and container are only slightly above the temperature at which cracking occurs. Then high-intensity heating is used to raise the temperature of the container walls sufficiently fast to melt the ingot free; thus it will slide from the container much in the manner an ice cube is removed from its freezing compartment. Such a process has been demonstrated to be feasible on a small scale (buttons remaining in the bottom of a 2-in.-diameter container after a normal crystal-growing operation can be easily melted free) but presumably has not been scaled up any larger. Another method of eliminating cracking is to use

an additive to prevent the silicon from bonding to the fused silica. For example, 1 per cent gold in the silicon will prevent sticking, although the ingot itself will usually crack. The beryllium added to silicon used for microwave diodes in the early 1940s apparently performed a similar function.

Other Oxides. Other refractory oxides have been studied, but it has been shown that theoretically they are all somewhat soluble in molten silicon.¹¹ In spite of these predictions, beryllium oxide and aluminum oxide have been tried and, as expected, were soluble enough to raise the impurity content above that which could be tolerated for optical use ($>2 \times 10^{14}/\text{cm}^3$ of Group IIIA or VA). It has been suggested that single-crystal aluminum oxide (sapphire) might be more slowly attacked than the sintered variety,¹² but its inability to withstand appreciable thermal shock has hampered experiments.

Metals. All metals on which there are data dissolve in molten silicon, and a great number of them form eutectics at a much lower temperature. They are, therefore, useful only if kept cool.

Silicon Carbide. Silicon carbide is wet by molten silicon and is also slightly soluble in it. This solubility is determined by the carbon solubility in silicon, which is shown in Fig. 3-1 as a function of temperature.¹³

If a silicon-carbide crucible containing silicon is heated well above the melting point of silicon and then cooled, the excess carbon dissolved at higher temperatures precipitates on the crucible wall in the form of small, yellow, β silicon-carbide crystals as cooling occurs. The segregation coefficient of carbon in silicon is probably less than 10^{-4} ,* so, if casting is done in such a container, most of the carbon will

* Based on a radioactive carbon analysis done by Graydon Larrabee, private communication.

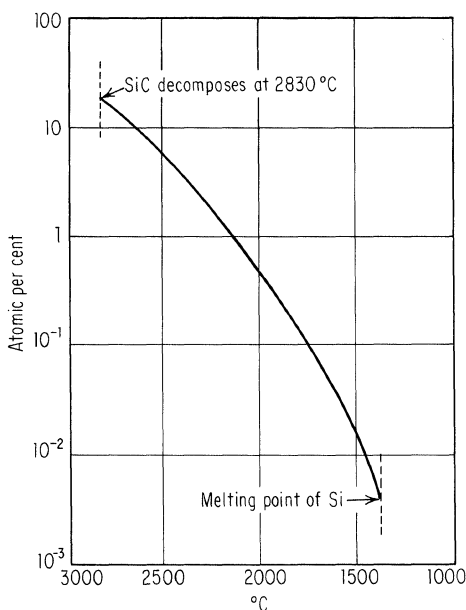


Fig. 3-1. Solubility of carbon in molten silicon. (After Seace and Slack.¹³)

be rejected by the freezing silicon, and there will be little contamination of the silicon unless it were to precipitate along grain boundaries.

The problem of obtaining a silicon-carbide crucible is a little involved. The usual variety of sintered silicon carbide is too porous; in addition, since appreciable silicon and carbon is removed from the container, any included impurities will be added to the melt. Probably most of the offenders come from the commercial-grade silicon (98 per cent silicon) used to make the silicon carbide.

It is possible to start with a graphite crucible and let the molten silicon react with it to form a silicon-carbide layer. Though not interpreted in this manner, apparently such a process was used as early as 1911 since mention is made in a patent of melting silicon in a graphite crucible.¹⁴

Unfortunately, the majority of the high-purity graphite available today is somewhat porous, so the silicon will penetrate the cracks and form silicon carbide there, as well as on the surface. There is a volume increase during the silicon-carbide formation so that the cracks expand and extend until catastrophic failure occurs. Some graphites are suitably dense to be usable, although it has been reported that if the melt is taken up to 1900°C all available grades fail.¹⁵ Rather than make the whole crucible of a dense graphite, it is possible to use any convenient variety and deposit an impervious pyrolytic graphite coating over the surface. Thin layers of nonporous high-purity silicon carbide can be vapor-deposited directly on graphite and eliminate most of the problems just mentioned.

The expansion coefficient of graphite is similar to that of silicon; in addition graphite is relatively weak in tension (approximately 1,000 psi) so that a silicon ingot should not be broken during cooling. As far as is known, 2-in.-diameter castings are the largest that have been made by this process, but there seems to be no reason why diameters could not be scaled up at least one order of magnitude.

Silicon Nitride. Silicon nitride makes an acceptable mold for silicon and is sometimes used in the casting of optical components.¹⁶ Usually any of the silicon nitride which adheres to the silicon will flake away from the body of the mold to affect release. It is possible that the bonding that does occur is due not to the silicon adhering to silicon nitride, but rather to the thin layer of silicon dioxide which is quite often present on the surface of the silicon nitride. If some of the nitride dissolves, the only impurity (other than those in the silicon nitride) would be nitrogen, which is either electrically inactive in silicon or else has an extremely low segregation coefficient.

Silicon nitride molds are normally made by slip-casting powdered silicon and then nitriding in either a nitrogen or an ammonia atmosphere at about 1300°C.¹⁷ Containers lined with a thin layer of silicon nitride are also used and are made by coating the inside of a fused-silica or graphite crucible with a thin slurry of high-purity semiconductor-quality silicon and then nitriding.¹⁸

Boron Nitride. Silicon ingots do not stick to boron-nitride molds,¹⁹ but p-type contamination invariably occurs.

Liquid Molds. Another unique method of mold construction consists in confining the molten silicon in another liquid which does not react with it.²⁰ This can be accomplished by floating the silicon on top of a liquid of higher density. Sur-

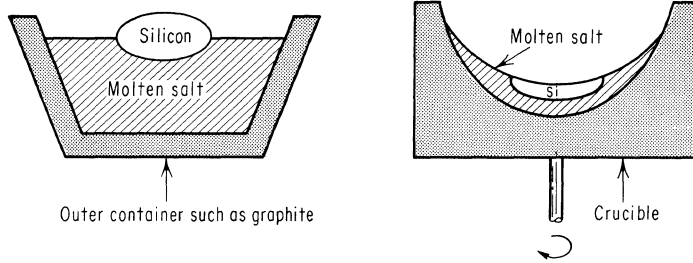


Fig. 3-2. Liquid mold for molten silicon.

face tension will keep it intact if there is only a small quantity of silicon, or the assembly may be rotated so that centrifugal force keeps the two liquids separate and forces the silicon to the center of the container. The first method would be appropriate for long, small cross-section rods being zone-refined, the latter for larger quantities such as required for crystal growing. These methods are illustrated in cross section in Fig. 3-2.

The containing liquid, besides having a higher density than silicon, must melt at a lower temperature, not react with it, be virtually insoluble in it, and boil at a temperature considerably above 1400°C . Likewise, when the containing liquid does freeze, it must not bond so tightly to the silicon that differential contraction breaks the whole assembly, and it must be readily soluble in something that does not attack silicon.

Strontium chloride has been suggested as a suitable material, though it is not clear how much strontium and chlorine can be dissolved in silicon nor what effect these have on the electrical properties of silicon.

This process was described only shortly before the advent of the float-zone method of refining silicon, so there has apparently been little effort spent searching for liquids that will meet all the requirements just listed.

Cold Molds. By heating the silicon inductively and using a water-cooled work coil to contain it and act as a mold, melting and subsequent cooling can be affected.²¹⁻²³ Both silver and copper have been successfully used. It is not clear whether levitation lifts the molten silicon free of the container or whether the high thermal gradient across normally present oxides keeps the metal surface at a low enough temperature to prevent alloying. This process has been used for both zone-refining silicon and casting into ingots.

3-2. POURING INTO MOLD

One of the first molds suggested for silicon was dry sand coated with talc to discourage sticking.¹⁴ For chemical ware, where high purity is not required, this is acceptable, but not for the majority of present day usage.

If a hot mold is used, sound castings are more easily obtained, but because of the high reactivity of silicon, mold contamination can be quite severe. If a cold mold is used, so that the silicon freezes on contact, the contamination can be vir-

tually eliminated, but crack-free castings are difficult to achieve. The problems associated with hot-mold casting differ little from those of melting in mold, so the remainder of this section will be devoted to cold molds.

Recent cold-mold castings have been used primarily for small sizes, in applications where cracks or bubbles are not necessarily detrimental, and where the utmost in purity is desired.

Rods ½ in. and larger in diameter are used as starting material for float zoning, and are often cast (though more often the silicon is manufactured directly in rod form). This casting is usually done by transferring molten silicon to a fused-silica tube surrounded by a water-jacketed metal tube. The fused silica is then kept cold enough to immediately freeze the silicon that comes in contact with it, so that little contamination or sticking occurs. There are, however, other problems to be considered.

1. Fused-silica tubing is of nonuniform bore, so that the cast rod is pinned in position. The tube must be broken to free the rod, and this broken tube represents an appreciable portion of the casting cost.
2. Because of volume changes associated with cooling silicon, it is difficult to obtain sound casting. This change of volume is depicted schematically in Fig. 3-3.

If the temperature of the melt, just before pouring into mold, were T_1 , then immediately after freezing it would occupy the same volume it did when poured and there would be no voids or excess. Deviations in temperature would then either produce a casting with holes or else one that would break the mold and possibly itself as well. Normally, one or the other of these two undesirable circumstances happens, so the temperature is usually deliberately chosen to give voids, but nevertheless the rods are intact and can thus be readily used in the zone refiner.

3. With the larger cross sections, the thermal gradients are very severe and usually cause casting failure, even if all other conditions are optimum.

The tubes may be filled either by direct pouring or by pumping a vacuum on the tube and sucking in the molten silicon.²⁴

For silicon lot homogenization, and dope and charge making, similar techniques can be used, though the tube diameters are usually larger. Here the voids are detrimental because saw debris collects in them and is virtually impossible to completely remove. A more satisfactory method is to substitute a long trough for the tube so that again, as was described in Sec. 3-1, the freezing interface can move in the direction of a free surface.

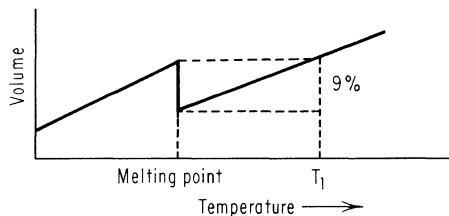


Fig. 3-3. Silicon change in volume versus temperature.

Well-cooled metal tubes may be substituted for the fused silica, but care must be taken to insure that no hot spots occur (such as localized boiling of the coolant) which will allow the metal to reach a temperature high enough to react with the silicon.

Cool fused-silica molds have been investigated for use in casting optical-quality ingots. In this application, the mold temperature needs to be high in order to reduce the likelihood of breaking the ingot due to thermal shock, and yet must not be hot enough for the silicon to stick to the fused silica. Limited success has been reported when the mold was held at about 1050°C.²⁵

3-3. AMBIT CASTING

The better parts of the cold-mold and the casting-in-mold techniques have been combined in ambit casting.^{4,5,26} In this process a cold plug (corresponding to the cold mold) is immersed in a container of molten silicon. The first silicon in contact with the plug will freeze around it and prevent melt contamination. Further freezing will progress outward from the plug so that there is always an unconfined liquid-solid interface. This process is illustrated in Fig. 3-4. The freezing rate can be controlled by the melt and plug temperature so that thermal shock will not be severe enough to cause cracking. Ideally, the plug material should have a thermal expansion coefficient greater than that of silicon so that as the assembly cools, the silicon shell will drop off. Figure 3-5 is a graph of temperature versus time for the plug and casting.

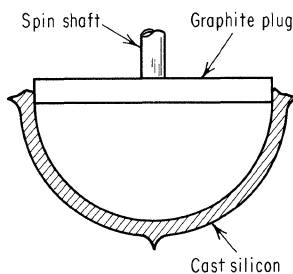
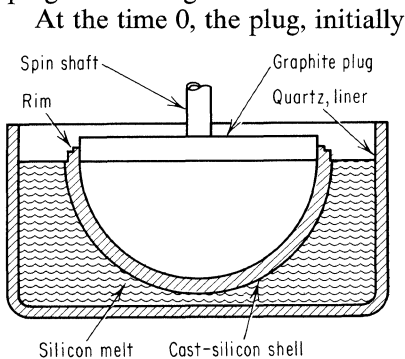


Fig. 3-4. Ambit casting.

At the time 0, the plug, initially at some temperature below the melting point of silicon, is plunged into the melt. From then until the time for removal from the melt, the freezing silicon will cool slowly while the average plug temperature goes up. During this time the silicon will be contracting and the plug expanding. If the silicon temperature is above that at which plastic flow occurs, and if the rate of strain is not enough to cause work hardening, no failure of the shell will occur. When removed from the melt, both the silicon and plug start cooling, but at different rates. The silicon, being on the outside, will cool much more rapidly than the plug. Unless the thermal expansion coefficient is much larger for the plug than for the silicon, the silicon must strain relieve itself by plastic flow. When the silicon temperature drops below its plastic region, no more strain relief can occur. However, as the temperature gets lower, the cooling rate decreases since cooling is primarily by radiation, which varies as the fourth power of temperature. The plug is still at a

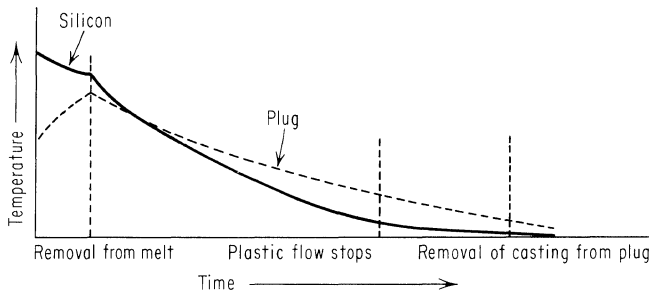


Fig. 3-5. Cooling curves for silicon and plug.

higher temperature and may now be cooling at a much higher rate than the silicon. Thus in the region between the cessation of plastic flow and the removal of the casting from the plug, it is possible for the plug volume to reduce more than the shell volume even if its coefficient of expansion is considerably less than that of silicon.

It is then, in principle, possible to choose a temperature cycle so that crack-free castings can still be produced even if the thermal expansion of the plug is less than that of the silicon. It is also possible to choose plugs and cycles that will cause the silicon shells to break quite violently.

Graphite has been found to work very well as a plug material, though some care must be taken in the cycle since the total expansion of graphite is somewhat less over the temperature range below plastic flow than the expansion of silicon.



Fig. 3-6. Ambit-cast silicon domes.

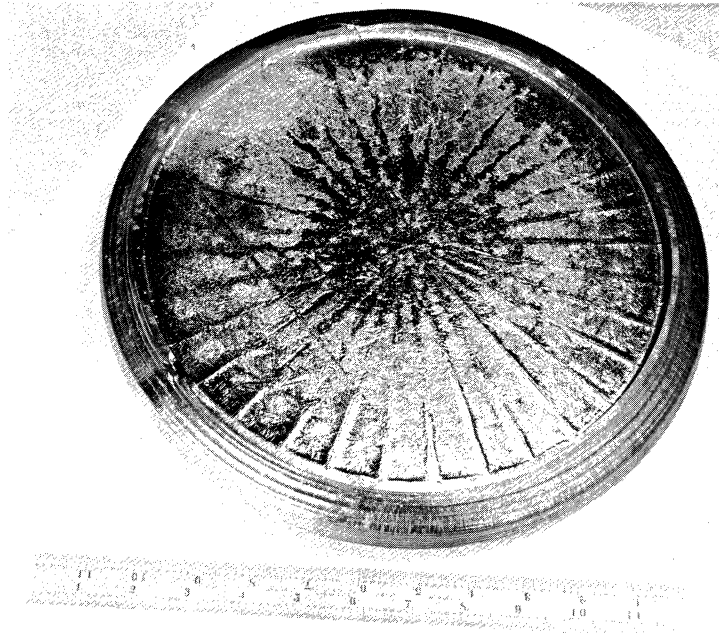


Fig. 3-7. Ambit-cast silicon plate 13 in. in diameter.

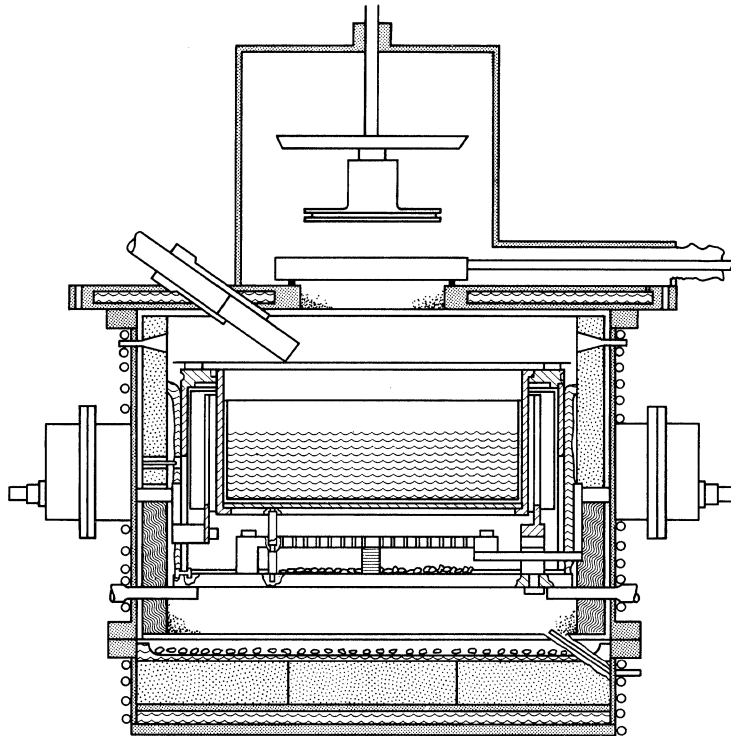


Fig. 3-8. Silicon-casting machine which has provisions for intermittent feed and a lock for the removal of cast plates.

This process was originally conceived to manufacture domes, though, by using flat-faced plugs, plates can also be produced. Domes up to 8 in. in diameter and plates 13 in. in diameter and 2 in. thick have been made in this fashion. Figures 3-6 and 3-7 are photographs of such items. Figure 3-8 is a sketch of the machine. This version is capable of continuous operation since silicon can be added through a tube at the side, and the domes or plates can be removed through a lock on top of the chamber without disturbing the melt.

REFERENCES

1. Hampel, C. A. (ed.): "Rare Metals Handbook," Reinhold Publishing Corporation, New York, 1954.
2. Allen, T. B.: Silicon Articles, U.S. Patent 1,073,560, 1913.
3. Stello, P., and R. H. Griest: Optical Properties of Cast Polycrystalline Silicon, *Proc. IRIS*, vol. 4, pp. 101-107, 1959.
4. Runyan, W. R.: Use of Cast Silicon for Optics, *IRIS Late Development Paper*, April, 1959.
5. Cole, R. L., G. Mitchell, and J. Hicks: "Development of Infrared Optical Components," Texas Instruments Incorporated, Final Report, Contract AF33(600)38085, 1960.
6. Kaiser, W., P. Keck, and L. F. Lange: Infrared Absorption and Oxygen Content in Silicon and Germanium, *Phys. Rev.*, vol. 101, p. 1264, 1956.
7. Hino, J., and H. E. Strauss: Melting of Undoped Silicon Ingots, *J. Metals*, vol. 4, p. 656, 1952.
8. Theurer, H. C.: Preparation of Silicon Material, U.S. Patent 2,475,810, 1949.
9. Cole, R. L.: "Development of Silicon Infrared Components," Texas Instruments Incorporated, Quarterly Report No. 1, Contract AF33(600)38085, 1959.
10. Stockbarger, Donald C.: Improved Crystallization of Lithium Fluoride of Optical Quality, *Discussions Faraday Soc.*, no. 5, 1949, Butterworth Scientific Publications, London, 1959.
11. Shockley, W.: "Preparation of Semiconductor Materials," Shockley Semiconductor Laboratory, Quarterly Report No. 2, Contract NObsr-72706.
12. Linde Company: Personal communication.
13. Scace, R. I., and G. A. Slack: The Si-C and Ge-C Phase Diagrams, *Proceedings of the Conference on Silicon Carbide, Boston, April, 1959*, Pergamon Press, New York, 1960.
14. Allen, T. B.: Method of Making Silicon Articles, U.S. Patent 1,037,713, Sept. 3, 1912.
15. Ellis, R. C.: Growth of Silicon Carbide from Solution, *Proceedings of the Conference on Silicon Carbide, Boston, April, 1959*, Pergamon Press, New York, 1960.
16. Mytton, Robert W., and Phyllis E. Stello: Processing Semiconductor Material, U.S. Patent 3,041,690, July 3, 1962.
17. Nicholson, K. C.: Manufacture of Silicon Nitride-bonded Articles, U.S. Patent 2,618,565, Nov. 18, 1952.
18. Bradshaw and Sargeant: Improvements in or Relating to the Processing of Silicon, Australian Patent 200,405.
19. Selker, M. L., and J. F. Cerness: Method of Producing Single Crystals of Silicon, U.S. Patent 2,823,102, Feb. 11, 1958.
20. Celmer, P. R., and R. V. Jensen: Preparation of Reactive Materials in a Molten Non-reactive Lined Crucible, U.S. Patent 2,872,299, Feb. 3, 1959.
21. Shepherd, W. H.: New Method of Cold Hearth Melting, *J. Sci. Instr.*, vol. 37, p. 177, 1960.
22. Ware, R. M.: Cold Hearth Zone Refining, *J. Sci. Instr.*, vol. 38, p. 166, 1961.

28 Silicon Semiconductor Technology

23. Sterling, H. F., and R. W. Warren: A Cold Crucible for High Temperature Melting Processes, *Nature*, p. 745, Nov. 25, 1961.
24. Buehler, E.: Contribution to the Floating Zone Refining of Silicon, *Rev. Sci. Instr.*, vol. 28, pp. 453-460, 1957.
25. Cole, R. L., C. M. Oualline, and G. A. Mitchell: "Development of Silicon Infrared Optical Components," Texas Instruments Incorporated, Quarterly Progress Report No. 3, Contract AF33(600)38085, 1959.
26. Runyan, W. R.: Method of Growing Shaped Crystals, U.S. Patent 3,025,146, Mar. 13, 1962.

Crystal Growth

Since most semiconductor devices require single-crystal material, a vast amount of effort has been spent over the past several years in perfecting growing techniques. Just the growing of crystals has not been enough, however, because in general, a specific doping level within the crystal is desired. Therefore, not only the conditions for proper crystal growth, but also the behavior of small amounts of impurity atoms originally distributed in the melt must be understood.

4-1. CRYSTAL-GROWING ENVIRONMENT

Crystal growth can be divided into four broad categories,^{1,*} each of which has several subdivisions.

1. Crystallization from a one-component system. (Note that small amounts of impurity may shift growth from this type to growth from a multicomponent system.)
 - a. Crystallization from liquid of same composition.
 - b. Crystallization from a vapor of the same composition. Evaporation and subsequent regrowth in a vacuum is an example of this.
 - c. Crystallization in the solid state from other crystals. This could include growth of larger crystallites from small ones during heat treatment (applicable to silicon), and polymorphic transitions such as that of gray to white tin.
2. Crystallization from a multicomponent system in which the material to be grown is already present. This one can be divided into the same three subdivisions as the one-component system, but in addition, each of those can be further divided into two more subdivisions.
 - a. The “solvent” is only slightly soluble in the solidifying component. An example of this would be a silicon crystal grown from a silicon-gold mixture. The growth of crystals from aqueous solutions would likewise be included. It should also be noted that the lion’s share of literature on crystal growing deals with crystallization from water.

* Superscript numbers indicate items listed in References at the end of the chapter.

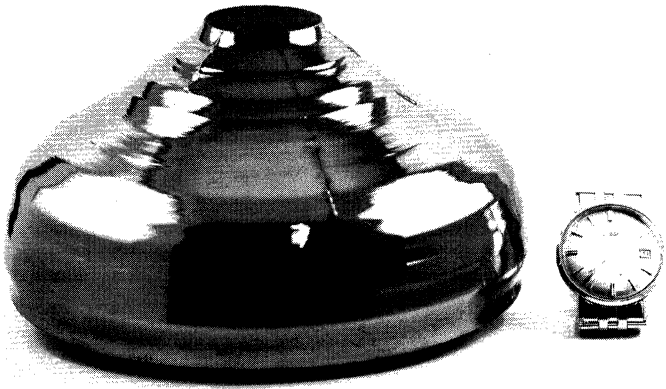


Fig. 4-2. Six-inch-diameter silicon crystal grown by the Teal-Little method.

Dendrites* are very rapidly growing crystals containing a series of twin planes which make nucleation easiest in one particular direction ($[211]$ for silicon).³ Such growths are often observed shooting across the otherwise molten surface of silicon immediately after reducing power in a crystal puller. Figure 4-3 is a photograph of a maze of dendrites pulled from a supercooled melt. Figure 4-4 shows a single dendrite deliberately grown under more controlled conditions.

Blade growth, first observed at Bell Telephone Laboratories,⁴ appears to be the vapor-phase analog of dendrite growth in a melt. These crystals are normally very small (a few millimeters long, a few hundred angstroms thick) and again grown very rapidly in the $[211]$ direction. Apparently however, only one twin plane is present in them, compared to two or more in the dendrites.

* Treelike structure.

Fig. 4-3. Silicon dendrite maze pulled from the melt. The overall length is 4-in.



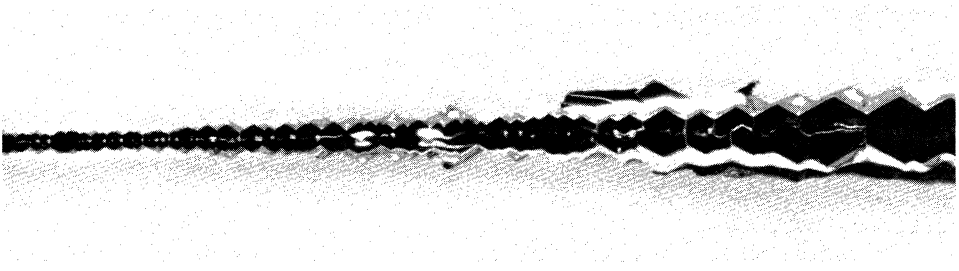


Fig. 4-4. Silicon dendrite.

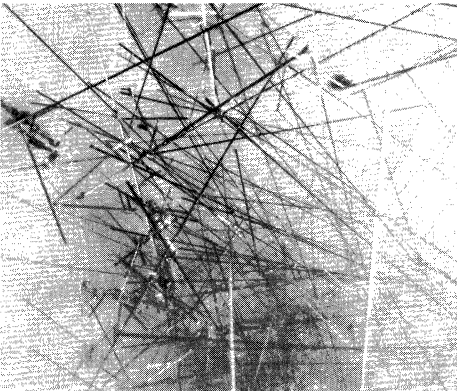


Fig. 4-5. Mass of silicon whiskers grown from the vapor.

Whiskers of silicon are also grown from the vapor. They grow rapidly in the [111] direction, are hexagonal in cross section, and have a screw dislocation running lengthwise. Figure 4-5 is a photograph of a mass of silicon whiskers.

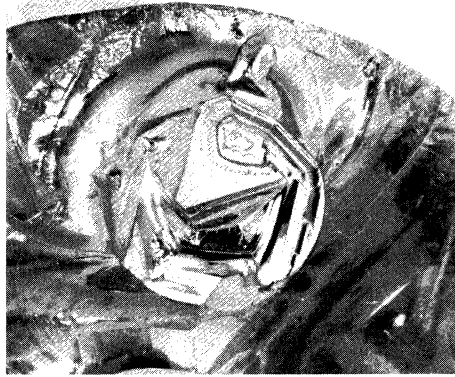
4-3. CRYSTALLIZATION FROM A ONE-COMPONENT SYSTEM

The simplest form of crystal growing from a single-component system consists merely of melting and subsequent uncontrolled freezing. This gives rise to the familiar "cast structure" which consists of myriads of randomly oriented single-



Fig. 4-6. Silicon crystal which grew in "spill-over" of a casting.

Fig. 4-7. Top of a silicon-cast ingot showing well-developed octahedral crystal faces.



crystal grains. The size of the grains depends on the rate of cooling and may range from microscopic for a rapid quench, to quite large crystals if the cooling is slow. Silicon expands when it freezes, so instead of there being voids in the casting, there will usually be some spillover. Often this final bit of molten silicon freezing will generate single crystals which have well-defined faces. Figure 4-6 shows one such crystal chipped from the top of a silicon casting. Figure 4-7 is a photograph of a complete ingot with some faces defined in the spillover.

Because trusting to luck usually does yield small crystals of random orientation, numerous methods have been devised to weight the odds in favor of given orientations and predetermined sizes of crystals.

Tammann⁵ discovered that if a molten metal is confined in a capillary tube, and allowed to slowly freeze from one end, only a few crystallites would form, and that since there is usually some preferred growth direction, if the tube were long enough, a single crystal would survive. This concept was next extended to a larger tube pointed on one end so that by the time freezing had proceeded to the main body of the container, only a single crystal remained. Refinements of this process, such as those by Bridgeman and Stockbarger, have led to the equipment illustrated in Fig. 4-8. In this arrangement, a two-zone furnace is normally used. The bottom part of the furnace is held just below the freezing point of the material to be crystallized. Thus, when a crucible containing the material is gradually lowered through the furnace, freezing occurs selectively from the bottom. An additional refinement can be obtained by placing a single-crystal seed in the bottom of the container, and never allowing it to become completely melted. In this manner preoriented crystals may be grown. Such methods are widely used to grow crystals of metals and alkali halides.⁶ They are particularly applicable where inert container tubes can be found, and where the material to be grown contracts upon freezing, or at least does not stick to the crucible walls. Unfortunately, silicon falls in neither category and so has not been successfully grown by this relatively simple process.

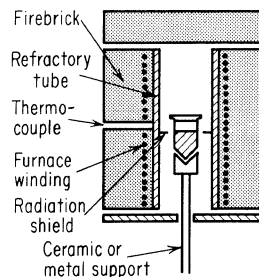


Fig. 4-8. Bridgeman crystal-growing apparatus.

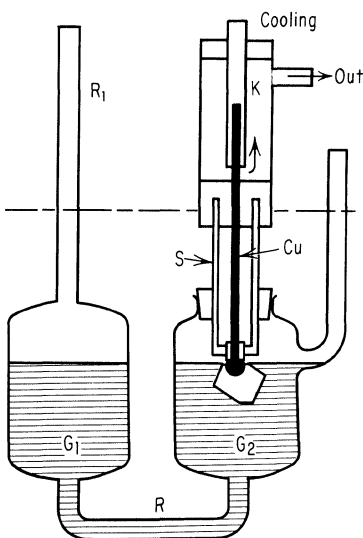


Fig. 4-9. Nacken's method of growing crystals from the melt.

ing the seed from the melt. A sketch of such equipment is shown in Fig. 4-11. Teal and others⁷ have applied this system very effectively to the growing of silicon and germanium, and indeed, most of the discussion concerning silicon crystal growth from a melt will revolve about the Teal-Little modification of the Czochralski method.

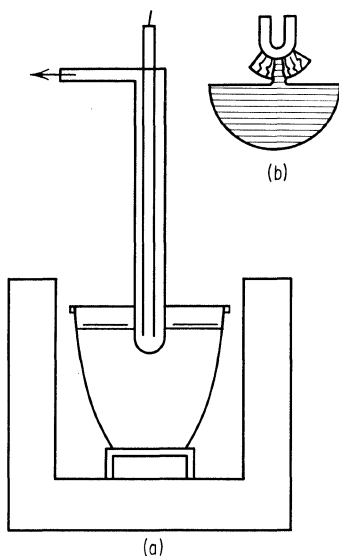


Fig. 4-10. The Kyropoulas crystal-growing method. Insert (b) shows the method of seeding a single crystal from a polycrystalline growth.

Nacken⁵ conceived the idea of causing freezing, not by changing the heat input to the melt, but by heat flow to a continuously cooled seed. His equipment was somewhat complicated and is shown in Fig. 4-9.

Kyropoulas⁵ simplified the process to that shown in Fig. 4-10. In its original form, a metal plug was first plunged into the melt, and then, after some suitable size polycrystalline boule had frozen onto it, was withdrawn until only a small area of the frozen mass touched the melt. In principle only one or two crystals would then be in contact with the surface and could serve as seeds as the remainder of the melt froze. This method was later modified to allow a single-crystal seed to be substituted for the metal plug, and thus one step in the process was eliminated. Then, except for the simplicity, it is essentially that of Nacken.

Czochralski⁵ further improved on the system by making provisions for continuously withdrawing the seed from the melt. A sketch of such equipment is shown in Fig. 4-11. Teal and others⁷ have applied this system very effectively to the growing of silicon and germanium, and indeed, most of the discussion concerning silicon crystal growth from a melt will revolve about the Teal-Little modification of the Czochralski method. Verneuil,⁵ in the 1890s, originated a system for growing single crystals of refractory oxides. In this system, shown in Fig. 4-12, the top of a seed is heated to somewhat above the melting point and then powdered feedstock slowly added. Simultaneously with the addition of material to the melt, the seed is lowered so that there is continuous freezing, and so that the level of the top of the seed remains fixed. The original version of this process used an oxyhydrogen torch to melt the seed; this would not be applicable to silicon since even with a reducing flame there would be enough oxygen present to form an oxide layer and prevent single-crystal growth. A modern version of this process which used electron beam heating has been tried however, but was not particularly successful.⁸

In 1952 Pfann originated a combination purification, crystal-growing process in which a charge placed in a horizontal boat has a narrow zone melted in it by localized heaters surrounding the boat.⁹ The molten zone is then slowly moved from one end of the boat to the other so that, as melting occurs on the forward end of the zone,

freezing takes place at the trailing end. This is illustrated in Fig. 4-13. If the original zone is allowed to partially melt a single-crystal seed, as the zone moves the single crystal will propagate down the boat. Such an arrangement works very well for semiconductors like germanium and indium antimonide, but as described in Chap. 2, all presently known crucible materials stick to the silicon and cause cracking.

Keck and others¹⁰ took the zone-leveling process, turned it on end, threw away the boat, and used surface tension to hold the molten zone in place. This is shown in Fig. 4-14. It is referred to as the "float-zone method" and is very well suited for growing single crystals of highly reactive materials like silicon.

All the systems described thus far are predicated on no phase change between the melting point and room temperature and on no decomposition of the melt. In the case of silicon, both these requirements are met. In the event that they are not fulfilled, then growing from a multicomponent system may be appropriate, or in the case of possible decomposition, growing under pressure may suffice. For example, good crystals of cadmium sulfide can be grown by the Stockbarger process if the container atmosphere is maintained at about 100 atm.¹¹

Crystals may also be grown from a vapor-phase single-component system. The most common of these is shown in Fig. 4-15. In this method polycrystalline material is placed at one end of an evacuated tube which is in turn placed in a temperature gradient. If the feedstock is in the hot end, then it will be slowly transported to the cold end and may grow large single crystals. Silicon may be grown in this fashion, but its low vapor pressure combined with the inability to properly contain itself at high temperatures limits the growth rate. On the other hand, elements like zinc which have a high vapor pressure can be successfully grown by this method.¹²

The limitation of a low source temperature may be removed by having a larger vacuum chamber in which the feed material can be isolated and heated to any desired temperature by induction, radiation, or an electron beam. This system then becomes essentially that of a standard vacuum metallizer. Single-crystal silicon has been grown

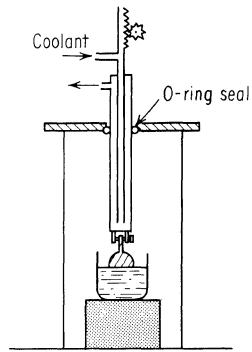


Fig. 4-11. Czochralski crystal-growing equipment.

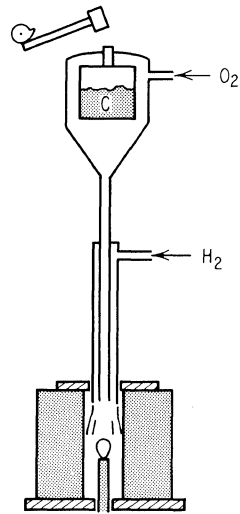
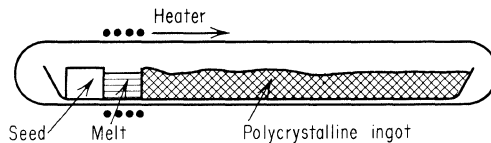


Fig. 4-12. Verneuil crystal-growing equipment.

Fig. 4-13. Zone-leveling apparatus of Pfann.



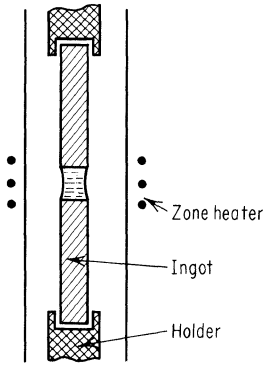


Fig. 4-14. Float-zone method.

in this fashion,^{13,14} but the crystal perfection has in general been poor. The reasons for this are not clear, but it is possibly because of the inability to maintain a good enough vacuum to have essentially a one-component system.

When strained polycrystalline materials are heat-treated there will usually be some grains that will grow at the expense of others.⁵ This process was first described by Sauveur in 1912 as a method of deliberately growing large single crystals. It has been used successfully on metals such as aluminum, iron, and tungsten, and for many organics.

It is apparently this sort of mechanism that allows mechanically polished silicon to be used as seed stock for growing crystals from the vapor phase. That is, when the silicon is heated, the smeared outer surface regrows as a continuation of the underlying single-crystal substrate.

4-4. GROWTH FROM MULTICOMPONENT SYSTEMS

Crystal growth from a liquid multicomponent system is of course somewhat more complicated than that from a single-component system, but in return it usually allows growth at considerably reduced temperatures. The most widely discussed of all crystal-growing methods, i.e., growth from aqueous solutions, comes under this category. This process may be described as follows: Consider that at some temperature and volume a suitable solvent is saturated with the material to be grown; then, if the temperature is reduced, or the volume of solvent decreased by evaporation, the solution will become supersaturated; and finally a precipitate will form. If the change in temperature or volume is slow enough, well-developed single crystals can be grown. Thus silicon may be dissolved in some low-melting-point metal such as indium or gallium and then regrown at temperatures considerably below the melting point of silicon itself. Indeed, it is this type of crystal growing that is used to produce the familiar alloy junctions found in many transistors and diodes.

Likewise, the addition of doping agents to a silicon melt changes it to a multicomponent system, but in general the growing procedures for this specific case are very similar to those for growth from a single component since the dope is usually a very small fraction of the total material supply. Conversely, as may be seen by reference to the appropriate phase diagrams, when silicon crystallizes from most metal solutions there is little of the solvent dissolved in the silicon. There are a

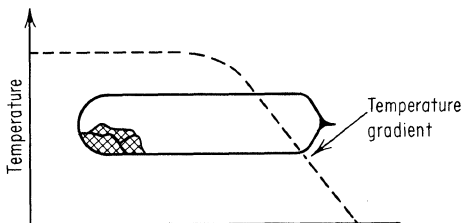


Fig. 4-15. Procedure for growing crystals from their vapor.

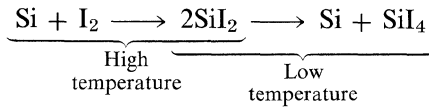
few instances however where this is not the case. For example, silicon and germanium form alloys with a continuous range of composition from 100 per cent silicon to 100 per cent germanium.

Single crystals of many materials can be grown by electrolytic deposition from a suitable bath.⁵ Usually the baths are aqueous, but may be organic or even of fused salts. There has been limited success in depositing single-crystal silicon from low-temperature organic baths.

The vapor-phase growth of single crystals of metals dates back at least to 1923 when Van Arkel described a method of reducing a halide of tungsten with hydrogen on a hot single-crystal tungsten filament and continuing single-crystal growth.¹⁵ Polycrystalline silicon was being deposited in 1943¹⁶ and single-crystal germanium by 1951.¹⁷

Two multicomponent vapor-growth systems are now in use for silicon.^{18,19}

1. A closed tube in which the silicon is transported from a source to substrate by a disproportionating reaction of



2. Reduction or pyrolytic decomposition, wherein the material is deposited on a heated substrate by chemical reduction, e.g.,

- a. $\text{SiH}_4 \longrightarrow \text{Si} + 2\text{H}_2$
- b. $\text{SiCl}_4 + 2\text{H}_2 \longrightarrow \text{Si} + 4\text{HCl}$
- c. $\text{SiHCl}_3 + \text{H}_2 \longrightarrow \text{Si} + 3\text{HCl}$

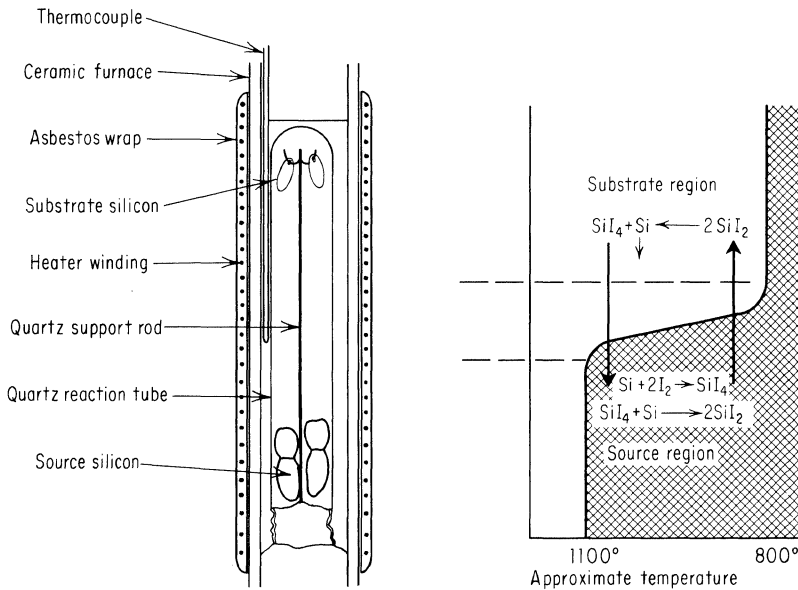


Fig. 4-16. Closed-tube silicon epitaxial deposition using the iodide disproportionation process. (Wajda and Glang.¹⁸)

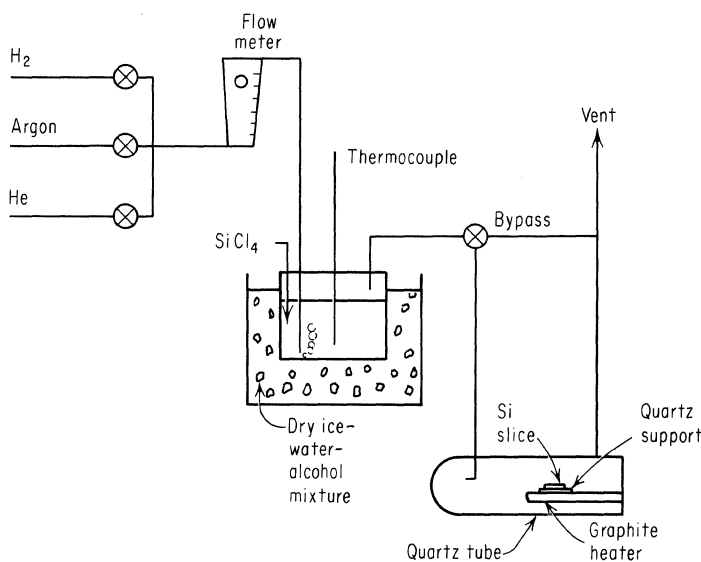


Fig. 4-17. Dynamic silicon epitaxial deposition system using the hydrogen reduction of silicon tetrachloride.

Simultaneously with the silicon deposition, appropriate dopants may be codeposited by similar reactions. These two processes are shown schematically in Figs. 4-16 and 4-17.

Of all these methods, the Teal-Little and float-zone methods, growth from low-melting-point metals, and vapor-phase deposition are the ones most widely used for silicon. Accordingly, each of these, except float zoning which is fully described in Pfann's book "Zone Refining,"⁹ will now be examined in considerable detail.

4-5. TEAL-LITTLE

The normal crystal-growing procedure is to dip a seed into the melt, wait for thermal equilibrium, slowly reduce the power input at the edge of the crucible until the proper crystal diameter has been reached, and then slowly withdraw the crystal from the melt. The radial temperature gradient along the surface of the melt must then be large enough to prevent the usual random temperature fluctuations (due to less than perfect temperature control) from causing the outer edge of the melt to freeze while leaving the middle too hot to allow crystal growth.

A rough sketch of the equipment was shown in Fig. 4-11. However, Fig. 4-18 is a much more detailed view of a "typical" crystal puller. There have been approximately as many modifications of the mechanical details as there have been investigators, but they all incorporate a method of carefully controlling the temperature of the silicon container and of smoothly withdrawing the crystal from the melt. In addition, most designs have means of spinning the crystal as it grows, and many also rotate the crucible.

A crystal-puller operator then has at his disposal during the growing operation, the ability to change the temperature of the crucible, the amount of stirring of the melt (by speed of rotation of seed and/or crucible), and the rate of withdrawal of the crystal. In addition, indirectly through the equipment designer, some control may be exercised over thermal gradients within the melt-crystal system.

In growth from the melt there are two possible rate limiting steps. One is the time required for atoms within the liquid to diffuse to an appropriate crystal site. This time is usually very short, and in most systems will not be the mechanism limiting growth rate, though it does have a considerable influence on impurity distribution. It will be discussed at some length a little later. The second rate limiter, and the one normally of most importance, is the requirement that the latent heat of fusion be removed from the crystal-melt system. There are in principle two ways by which this heat may be removed: (1) It may be removed through the body of the crystal itself as shown in Fig. 4-19a; (2) the liquid near the liquid-solid interface may be supercooled by a heat sink other than the crystal. This possibility is shown in Fig. 4-19b. Because of the high probability of spurious nucleation at the highly supercooled liquid-container boundary, the geometry of Fig. 4-19b is seldom used. (It is, however, a requirement for high-speed dendrite growth.)

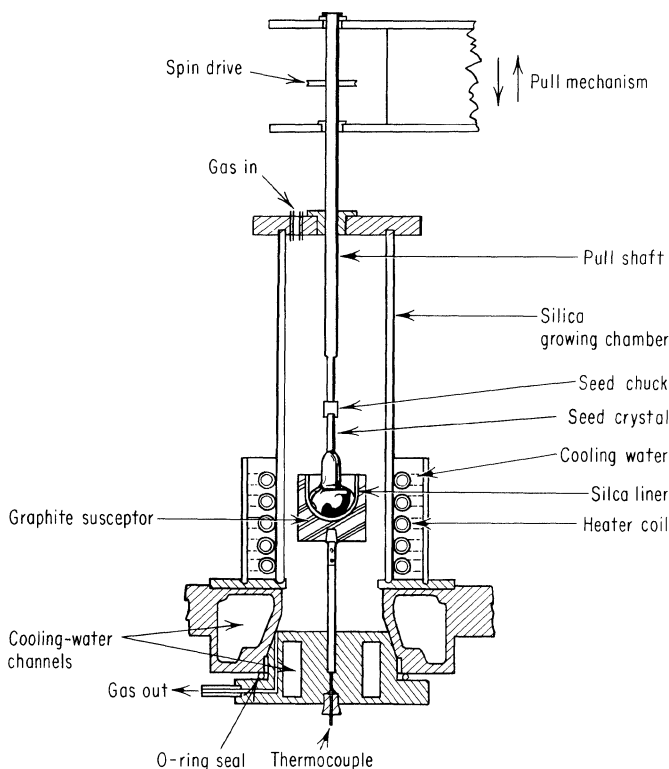


Fig. 4-18. "Typical" crystal puller.

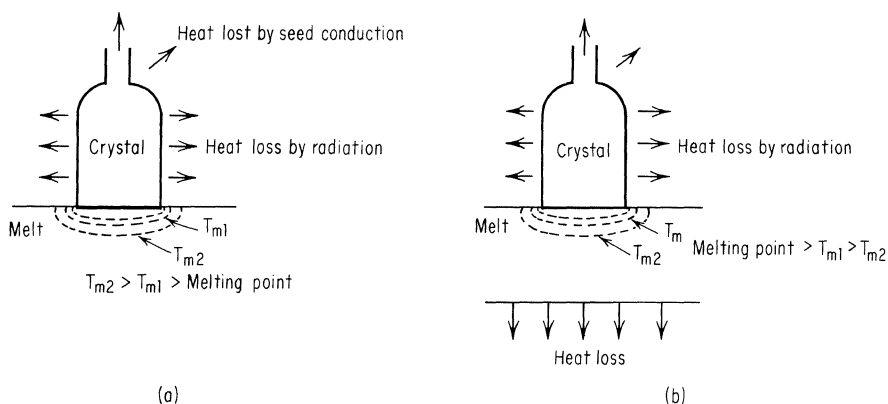


Fig. 4-19. (a) Temperature gradients near crystal for normal crystal growing. (b) Temperature gradients near crystal for supercooled melt.

For the case of Fig. 4-19a, the heat balance equation can be written as follows:

$$\text{Latent heat} + \text{heat transferred to crystal from melt} = \text{heat conducted away from the interface by the crystal} \quad (4-1)$$

$$L \frac{dm}{dt} + k_1 \frac{dT}{dx_1} A_1 = k_s \frac{dT}{dx_2} A_2 \quad (4-2)$$

where L = latent heat of fusion

dm/dt = amount freezing per unit time

T = temperature

k_1 = thermal conductivity of the liquid

dT/dx_1 = thermal gradient in the liquid at some point x_1 close to the interface

A_1 = area of the isotherm which goes through x_1

k_s = thermal conductivity of the solid

dT/dx_2 = thermal gradient in the solid near the interface

A_2 = area of the isotherm through x_2 , which will be approximately the area of the crystal (exactly, if the isotherm is planar and perpendicular to the growth direction)

$$\frac{dm}{dt} = vA_c\delta = (V_p + V_d)A_c \quad (4-3)$$

where v is the growth velocity and is equal to the pull rate V_p plus the rate of drop of the liquid surface V_d , and A_c is the area of the crystal at the liquid-solid interface. If the interface is nearly flat, then $A_c \approx \pi r^2$, where r is the radius of the crystal at the interface. V_d arises because as material is removed from the crucible, the level will drop unless the crucible is deliberately raised. The rate of fall is given by $V_d = V_p A_c / A'$ where A' is the area of the liquid surface. Normally A_c / A' is considerably less than 1, so that $v \approx V_p$, but there are circumstances where this is not true, and V_d becomes an appreciable correction term. It is also possible to

deliberately raise the level of the crucible at a rate equal to the calculated V_d and keep $v = V_p$.

Since very close to the interface, $A_1 \approx A_c$, Eq. (4-2) can be written approximately as

$$LV_p \delta A_c + k_1 \frac{dT}{dx_1} A_c = k_s \frac{dT}{dx_2} A_c \tag{4-4}$$

Thus, if there were no interaction between A_c , dT/dx_1 , and dT/dx_2 , there would be no dependence of growth rate on diameter. There usually are some very drastic interactions, however, and they are the things that must now be examined.

Effect of Crystal Radius on Growth Rate. The term $k_s(dT/dx_2)A_c$ in Eq. (4-4) represents the amount of heat transferred into the crystal, so this must be balanced by the heat lost from the crystal. These losses are illustrated in Fig. 4-20. The seed is usually of very small cross section, and after the crystal has grown awhile Q_s normally becomes considerably less than Q_r . Both Q_r and Q_c are proportional to surface area which is in turn proportional to the radius of crystal r , so as an approximation

$$k_s \frac{dT}{dx_2} A_c = Q_r + Q_c = Q' r \tag{4-5}$$

where Q' is a constant.

Thus Eq. (4-4) can be written as

$$LV_p \delta \pi r^2 + k_1 \frac{dT}{dx_1} \pi r^2 = Q' r \tag{4-6}$$

or
$$V_p + \alpha_1 = \frac{\alpha_2}{r} \tag{4-7}$$

where $\alpha_1 = \frac{k_1}{L\delta} \frac{dT}{dx_1}$ and α_2 is a constant.

From this it is concluded that if the latent heat term is large compared to the heat conduction from the melt, the growth rate is inversely proportional to the crystal diameter. On the other hand if the term $k_1 dT/dx$ is considerably larger than the latent heat term, then the crystal diameter will be small and quite independent of pull rate. This condition is only rarely found experimentally. Usually it is observed that an increase in growth rate causes the crystal diameter to reduce.

Maximum Growth Rate.²⁰ Again referring to Eq. (4-4), it can be seen that the maximum growth velocity is obtained when the thermal gradients are arranged in the crucible so that $dT/dx_1 = 0$, for which

$$L\delta v_{\max} = k_s \frac{dT}{dx_2} \tag{4-8}$$

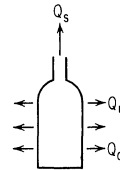


Fig. 4-20. Crystal heat losses. Q_s = heat conducted up seed to chuck, Q_r = heat lost by radiation, Q_c = heat transferred by conduction to atmosphere.

If the only loss from the crystal is assumed to be that due to radiation, the loss per length of crystal dx is given by

$$dQ = 2\pi\sigma\epsilon T^4 r dx \quad (4-9)$$

where ϵ is the emissivity and σ is Stefan-Boltzmann's constant. Heat transfer up the crystal is given by

$$Q = k_s \pi r^2 \frac{dT}{dx} \quad (4-10)$$

so that

$$\frac{dQ}{dx} = k_s \pi r^2 \frac{d^2T}{dx^2} + \pi r^2 \frac{dT}{dx} \frac{dk_s}{dx} \quad (4-11)$$

Assuming the last term to be negligible, substituting Eq. (4-11) into Eq. (4-9) gives

$$\frac{d^2T}{dx^2} - \frac{2\sigma\epsilon}{k_s r} T^4 = 0 \quad (4-12)$$

For silicon k_s varies approximately inversely with temperatures up to about 1000°K, above which it is nearly temperature-independent.²¹ For purposes of solving Eq. (4-12), assume it to vary as $1/T$ over the whole range and to be given as $k_s = k_m T_m / T$, where k_m is the thermal conductivity at the melting point, and T_m is the melting temperature. Equation (4-12) becomes

$$\frac{d^2T}{dx^2} - \alpha T^5 = 0 \quad (4-13)$$

where

$$\alpha = \frac{2\sigma\epsilon}{k_m r T_m}$$

The boundary conditions are

$$\begin{aligned} \text{at } x = \infty, T &= 0 \\ \text{at } x = 0, T &= T_m \end{aligned}$$

The solution of Eq. (4-13) is

$$T = \left(\frac{3}{4\alpha}\right)^{1/4} (X + \phi)^{-1/2} \quad (4-14)$$

where

$$\phi = \left(\frac{3}{\alpha}\right)^{1/2} \frac{1}{2T_m^2}$$

From this

$$\frac{dT}{dx_2} = \left(\frac{2\sigma\epsilon T_m^5}{3rk_m}\right)^{1/2} \quad (4-15)$$

Substitution of the value for dT/dx_2 from Eq. (4-15) into Eq. (4-8) gives

$$v_{\max} = \frac{1}{\delta L} \sqrt{\frac{2\sigma\epsilon k_m T_m^5}{3r}} \quad (4-16)$$

Substitution of appropriate numbers for silicon into Eq. (4-16) gives a maximum

rate for a ¼-in.-diameter silicon rod of 70 in./hr. About the highest rate observed is 60 in./hr.

Effect of Temperature Change on Crystal Diameter. Equation (4-7) can also be used to get a crude idea of the temperature control required to maintain a given diameter variation. Assume that the latent heat term is comparable to the conduction from the liquid term. Then

$$\frac{dr}{r} = \frac{d\alpha_1}{2\alpha_1} = \frac{d(dT/dx_1)}{2(dT/dx_1)} \quad (4-17)$$

Further assume that dT/dx_1 is proportional to the difference in temperature between the edge of the crucible (where the temperature is normally sensed) and the melting point. From this assumption and Eq. (4-17)

$$\frac{dr}{r} = -\frac{dT_c}{2(T_c - T_m)} \quad (4-18)$$

where T_c is the crucible temperature.

If it is desired to grow a 1-in.-diameter crystal, controlled to within 0.05 in., and if T_c is normally 50° above the melting point, then the variation in T_c can be no more than 5°. Normally, attempts are made to control short-term fluctuation to about 2°.

Effect of Radiation on Top Growth.²² From the previous discussions concerning the relation between growth rate and crystal diameter it might be assumed that if after equilibrium is reached and the rate is reduced, the crystal diameter would quickly increase to a new value determined by Eq. (4-4). Actually, however, it is observed that in some instances the growth continues beyond that expected and at a rate that increases as the diameter of the crystal increases. That this is reasonable during top growth can be seen from the following analysis. Rewrite Eq. (4-2) as

$$L \frac{dm}{dt} = K_1 r^2 + q_0 - K_2 r^2 \frac{dT}{dx} \quad (4-19)$$

where $K_1 r^2$ is the heat lost from a thin planar crystal of radius r by radiation from its surface, q_0 is the heat conducted up the seed, and $K_2 r^2 dT/dx$ is the amount of heat transported from the melt into the growing crystal due to a temperature gradient dT/dx .

In order to derive an expression for dm/dt , consider first a crystal growing with no pull. The crystal will grow primarily along the surface. The melt-liquid interface will usually be somewhat curved, but for simplicity assume that the portion of the crystal beneath the surface of the melt can be described as a right circular cylinder having radius r (crystal radius), and length \bar{x} . Assume that \bar{x} is independent of time. Then

$$\frac{dm}{dt} = 2\pi\delta\bar{x}r \frac{dr}{dt} \quad (4-20)$$

where δ is the density of the solid.

Now, assume that over reasonable limits, \bar{x} is independent of any pull rate that

might be applied. Then, since only that portion of the crystal beneath the surface can grow,

$$\frac{dm}{dt} = 2\pi\delta xr \frac{dr}{dt} + \delta\pi r^2 v \quad (4-21)$$

where $v = dx/dt =$ pull rate $=$ a constant. Combining Eq. (4-19) and (4-21) gives

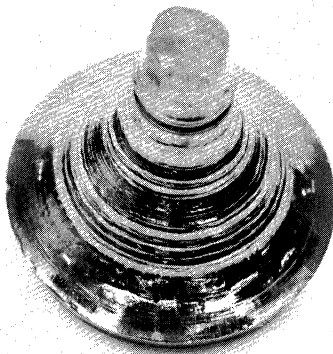
$$r \frac{dr}{dt} - C_1 r^2 = C_2 \quad (4-22)$$

where C_1 and C_2 are constants. Solving Eq. (4-22) gives

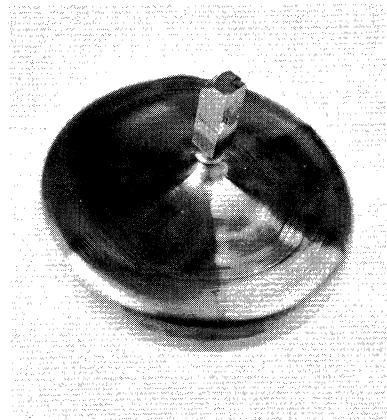
$$r^2 = C_3 \exp 2C_1 t - \frac{C_2}{C_1} \quad (4-23)$$

where C_3 is a constant. This equation says that the top area can increase exponentially with time.

Figure 4-21a is a photograph of a 4-in.-diameter crystal grown for several minutes at constant pull rates and with the temperature of the melt surface stabilized only 1 or 2° above the point where it began to freeze. This illustrates the exponential character of the diameter increase. It is usually observed that the crystal will grow very slowly until it is perhaps 1.5 in. in diameter and will then grow very rapidly. Figure 4-21b is a photograph of such a crystal grown with the same pull rate as before (0.1 mil/sec), but with the amount of heat transferred up the seed increased and the furnace changed somewhat to allow greater cooling of the crystal by radiation. The latter is accomplished by having a minimum of heat shielding and crucible above the surface of the melt at the beginning of the growing operation. Considerable adjustment of the temperature gradients can also be accomplished by changing the position of the crucible with respect to its heat shield and to the work coil (or heater element).



(a)



(b)

Fig. 4-21. Two crystals grown under similar spin and pull rates but under different conditions of heat transfer.

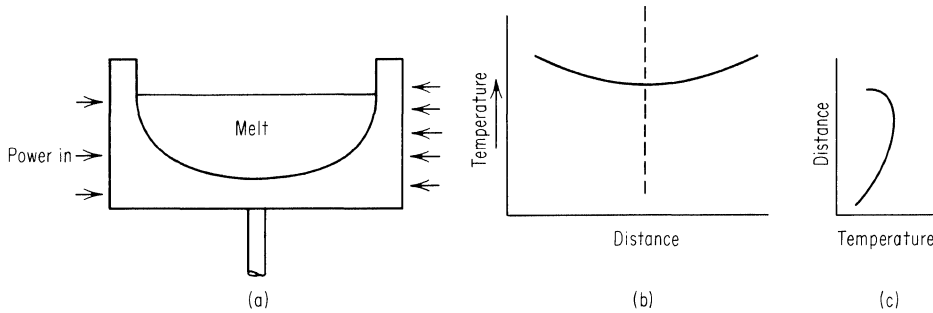


Fig. 4-22. Thermal gradients in a melt. The shape may be changed by changing the relative amount of heat lost through the crucible support and by radiation.

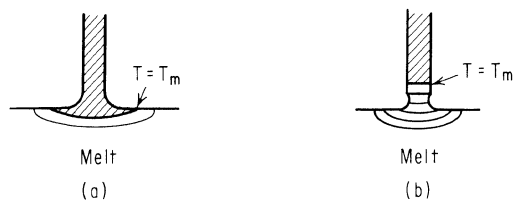
Actually, the increased rate of growth as the crystal size increases is undoubtedly due to both the radiation losses and the stirring effect, since cases have been observed where the crystal would not grow until the spin was increased, and likewise, there have been crucible designs that would not allow crystal growth, irrespective of spin rate.

Shape and Position of the Melt-Solid Interface. During the growing operation the melt-solid interface is seldom planar and in general will vary in curvature along the length of the crystal. The problem now becomes one of determining the shape and position of the $T = T_m$ isotherm as a function of crystal spin, diameter, length, and growth rate; of crucible design; of input power level; and of upper-chamber design (which affects the amount of radiation from the crystal).

Consider a crucible, such as shown in Fig. 4-22a, without any crystal in it. The radial temperature gradient in the melt will be approximately as shown in Fig. 4-22b, while the axial gradient will be of the form shown in Fig. 4-22c. If the melt temperature is just above the melting point, then the immersion of a seed with a suitable heat sink may extract enough heat to cause the melting isotherm to take up the position shown in Fig. 4-23a. On the other hand, if the melt temperature is considerably higher, a portion of the seed itself may melt and be held in place by surface tension as shown in Fig. 4-23b. If the melt temperature is too high, then the T_m isotherm will be so far up the seed that surface tension cannot support the molten column and the seed will separate from the melt. The position of the freezing interface may be lowered by increasing the heat conduction up the seed, increasing the heat loss down the crucible support, or by reducing the power input.

If the only source of heat input is the edge of the crucible, then the freezing interface will always be cupped downward. However, as soon as growing commences,

Fig. 4-23. Position of freezing isotherm for two different melt temperatures.



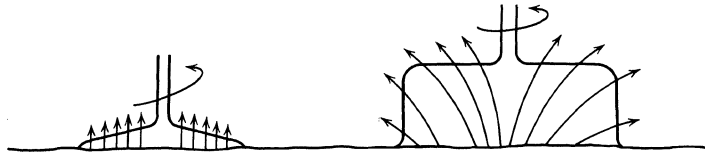


Fig. 4-24. Heat-flow pattern for two crystals of different thickness.

there is an additional source $L dm/dt$ distributed over the interface. This, in conjunction with varying fractions of heat lost by radiation and by conduction up the seed can change the shape to planar, and finally to one cupped upward. Without attempting to mathematically solve the thermal problem it can be seen qualitatively from Fig. 4-24 that the change in the nature of the heat-flow pattern from a thin flat crystal to a very long one could produce such an effect because of the increased heat-flow path in the latter case.

Figure 4-25 shows two crystals, each approximately 4 in. in diameter, grown under as nearly identical conditions as possible except that one was grown considerably longer than the other. The gradual decrease in bottom curvature is very noticeable. If, however, the growing is continued until the melt is very shallow, the relatively large radial thermal gradient of the bottom of the crucible may cause sufficient cooling to again increase the bottom curvature.

Effect of Spin.²² As a crystal rotates, it causes the melt to circulate not only around the crucible in the direction of rotation, but also with a component normal to the surface. The greater the speed of rotation, the larger the diameter, or the sharper the points on the growing crystal, the greater will be the circulation.

One of the most important advantages of stirring the melt by crystal spinning is that it minimizes the radial gradients and also allows symmetrical crystals to be grown even if there are severe asymmetric gradients in the melt. Figure 4-26a illustrates the fashion in which a silicon crystal can grow if only pulled and not rotated. Figure 4-26b shows the effect of rotation. The crystal has a "threaded" look, but does not continue to grow toward the cooler portion of the crucible. Nonsymmetric radial gradients can also be minimized by rotating the crucible, but this complicates the heat sensing equipment. The latter method requires slip rings

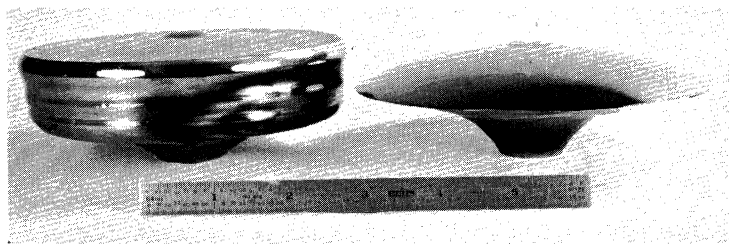


Fig. 4-25. Two 4-in.-diameter crystals grown under as nearly identical conditions as possible and illustrating the effect of radiation on bottom curvature as the crystal length increases. (Runyan.²²)

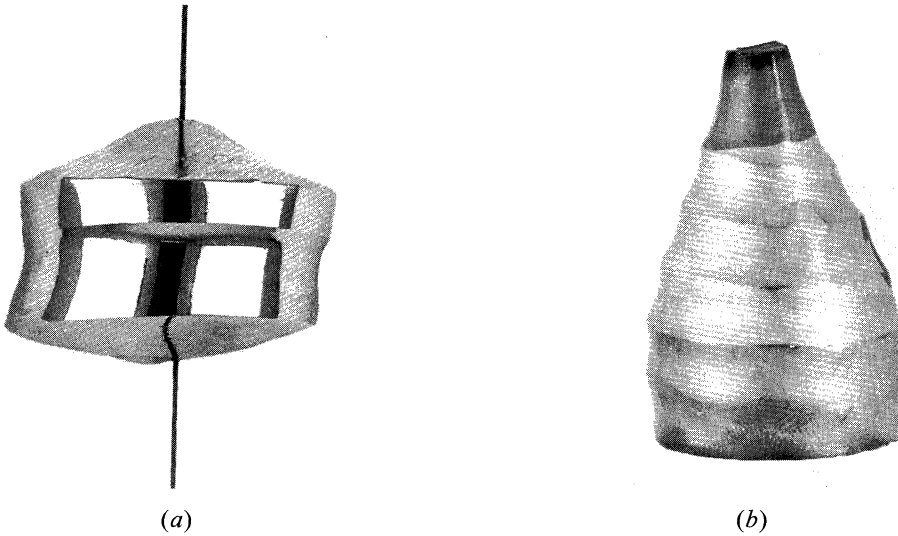


Fig. 4-26. (a) Silicon crystal grown without rotation in an asymmetric temperature gradient. (b) Silicon crystal grown with rotation in an asymmetric temperature gradient.

which may inject excessive noise into the control system. A radiation detector and light pipe are sometimes used to circumvent these difficulties, but continually sense temperatures from different portions of the crucible.

Spinning also causes cooler liquid from the bottom of the container to sweep by the crystal and enhance the growth rate. Meanwhile, an adequate surface temperature can be maintained to prevent such things as circulating gas currents from causing spurious surface freezing.

Experimental verification of the cooling effect of spinning can be observed by arranging the temperature so that a straight-sided crystal is being grown at some given spin rate. If the spin is stopped, the crystal diameter will start decreasing. By suddenly increasing the temperature of the melt so that a growing crystal top which had well-defined points is melted back just enough to make the crystal round again (and thereby reduce the stirring action) and then quickly reducing the temperature to its original value, top growth will proceed much slower than before. This effect is particularly noticeable during the transition from a spreading top growth to straight-side body growth. Stirring also tends to keep the temperature more uniform along the bottom of the crystal and consequently will reduce the curvature of the crystal-melt interface. Figure 4-27 shows the effect of spin on the curvature of the interface of crystals about 1.2 in. in diameter which were grown from 2-in.-diameter hemispherical liners.

In the case of small crystals (1 to 1½ in. in diameter), it is possible to combine the stirring effect with a crucible designed to enhance radiation and produce a perfectly straight interface at any desired time in the growth of the crystal.

Effect of Growth Rate on Interface Shape. Consider a crystal of diameter r_0 being grown at a velocity v and with a curved crystal front such as shown in

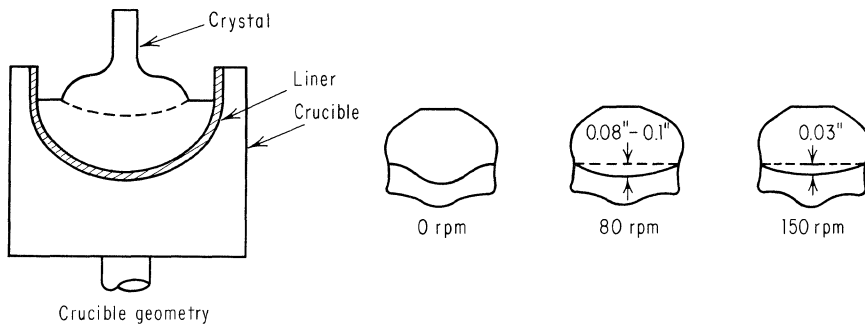


Fig. 4-27. Effect of spin stirring on crystal-melt interface curvature.

Fig. 4-28. As long as the diameter remains the same, one would expect the amount of heat being conducted up the crystal to be independent of growth rate. Thus if the growth rate (via pull rate) is increased and the dT/dx_1 of Eq. (4-4) adjusted so that the diameter remains fixed at the original r_0 , relatively more heat is being generated at the surface and less conducted up from the melt. To analytically determine the effect of this change on the crystallization front would be quite difficult, but as a rough approximation it has been assumed that if $L dm/dt$ were increased by an amount required to melt in unit time the shaded volume of the crystal in Fig. 4-28, then the crystal would grow with a flat interface.²³ Likewise, if the interface were cupped upward, as shown by the dotted line, then the growth velocity should be decreased in a similar fashion. It is then possible to grow a fixed diameter crystal at some constant growth rate, determine the curvature profile as a function of length, and calculate a new variable growth rate that will maintain a flat interface throughout the crystal length.

Effect of Surface Tension. If the $T = T_m$ isotherm is located as shown in Fig. 4-23a, surface tension has little effect on the growing crystal. However, if it is located so far above the main surface of the liquid that the melt is drawn in, as shown in Fig. 4-29a, then the diameter of the crystal will continually decrease as it is withdrawn because of the decreasing diameter of liquid available. Ideally if a constant diameter is desired, the interface should be low enough that the contact angle is essentially vertical, such as Fig. 4-29b.²⁴ Similarly, if an expanding crystal is to be grown, the interface must be even lower.

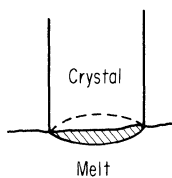


Fig. 4-28. Crystal with a curved melt-solid interface. More rapid growth can produce the shape indicated by the dashed line.

Effect of Gas Conduction on Growth. As indicated in Fig. 4-20, both radiation and gas conduction can aid in the transport of heat from the crystal. Usually the conduction term is small, e.g., some crystals are grown in a vacuum; most other systems have very low flow rates and large distances between the crystal and the chamber walls. It is possible in principle to enhance the gas cooling, however, and grow crystals at higher growth rates than otherwise possible. Consider an arrangement such as shown in Fig. 4-30. Gas forced through the orifice can contribute heavily to heat

Fig. 4-29. Dependence of the melt-solid contact angle on melt temperature.

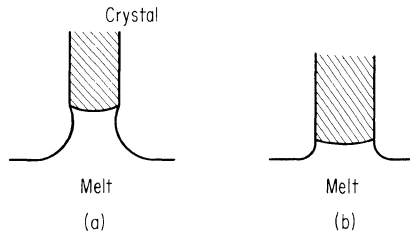
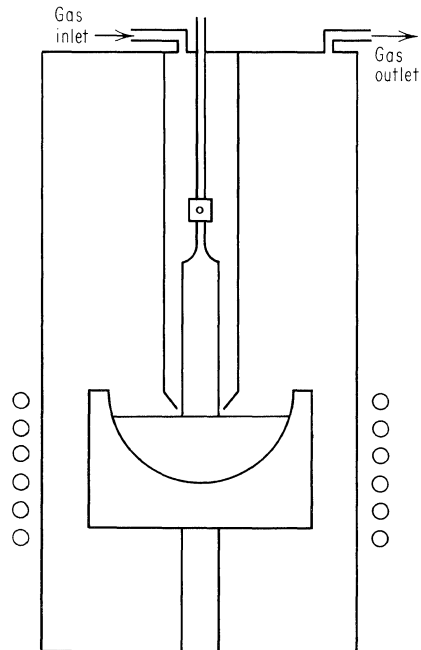


Fig. 4-30. Crystal growing with gas cooling to help control the crystal diameter.



conduction. In the event that the crystal diameter increases, the gas flow, and accordingly the amount of heat removed by the gas, decreases so that the diameter will decrease and thus impart some measure of diameter control to the system.²⁵

4-6. BEHAVIOR OF IMPURITIES DURING GROWTH FROM THE MELT

When small amounts of impurities are present during the crystal-growing operation, two things are of interest: how the impurities affect crystal growth and their final distribution in the crystal after it is grown. The latter is of particular importance since most impurities deliberately introduced are for the purpose of controlling resistivity, and usually there are fairly narrow limits imposed on tolerable resistivity variations within the crystals. (The correlation between resistivity and impurity concentration, along with other information necessary to dope silicon crystals, is given in Chap. 6.)

Distribution of Impurities in Grown Crystals.²⁶ As a material freezes, the concentration of impurities incorporated into the solid is usually different from the concentration in the liquid at the interface. The ratio of these two concentrations is defined as the equilibrium segregation coefficient k_0 , i.e.,

$$N_s = k_0 N_l \quad \text{or} \quad k_0 = \frac{N_s}{N_l} \quad (4-24)$$

where N_s is the concentration in the solid and N_l is the concentration in the liquid.

Consider a crystal being grown by the Teal-Little process at a time when some fraction l of the original melt has solidified.* Let

V_0 = initial volume of melt

V = volume frozen

$l = \frac{V}{V_0}$, fraction frozen

I_0 = total number of impurities in original melt

I = number of impurities remaining in unfrozen portion (4-25)

$\frac{I_0}{V_0} = N_0$, the initial impurity concentration

$$N_l = \frac{I}{V_0 - V}$$

If a small additional volume dv freezes, then it will remove from the melt an amount of impurity

$$dI = k_0 N_l dv = -k_0 \frac{I}{V_0 - V} dv \quad (4-26)$$

$$\frac{dI}{I} = -k_0 \frac{dv}{V_0 - V} \quad \text{or} \quad \int_{I_0}^I \frac{dI}{I} = -k_0 \int_0^V \frac{dv}{V_0 - V} \quad (4-27)$$

Integrating and substituting in limits gives

$$\log \frac{I}{I_0} = \log \left(1 - \frac{V}{V_0} \right)^{k_0} \quad (4-28)$$

so that

$$I = I_0 \left(1 - \frac{V}{V_0} \right)^{k_0} \quad (4-29)$$

but the concentration N_s in any incremental volume frozen is just the ratio of the amount of impurity dI removed from the melt when the volume dv froze, divided by the volume dv . This is found by differentiating Eq. (4-29).

$$-\frac{dI}{dv} = N_s = k_0 \frac{I_0}{V_0} \left(1 - \frac{V}{V_0} \right)^{k_0-1} = N_0 k (1 - l)^{k_0-1} \quad (4-30)$$

* The type of distribution to be discussed is referred to as normal freezing distribution and is applicable in any type of crystal growth in which all of the material is initially melted and then allowed to uniformly freeze from one direction.

N_s calculated from Eq. (4-30) is plotted in Fig. 4-31 for various values of k appropriate for silicon. In the event that k is very small, Eq. (4-30) reduces to

$$N_s = \frac{N_0 k_0}{1 - l} \tag{4-31}$$

so that the variation of concentration with length becomes independent of k_0 (the absolute magnitude, however, is still in direct proportion to k_0).

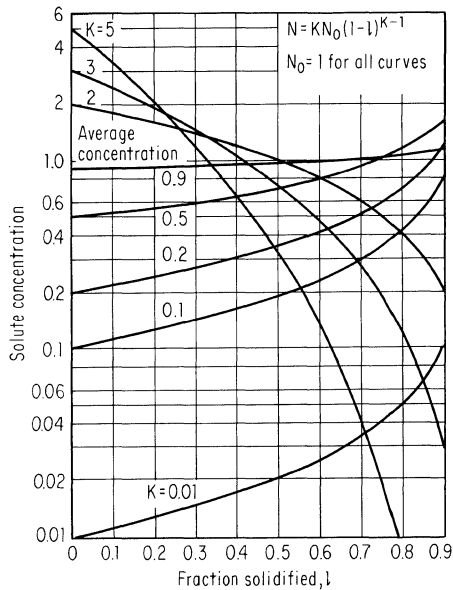
The process described by Eq. (4-30) represents a purification of the material being grown, so that if the last portion of the melt is discarded and another crystal grown from the reduced amount of material remaining, the concentration $N_{0,2}$ for the second growing is less than the initial N_0 and is given by

$$N_{0,2} = N_0 k_0 \int_0^{l'} (1 - l)^{k_0-1} dl = [1 - (1 - l')^{k_0}] \frac{N_0 k_0}{l'} \tag{4-32}$$

where l' is the fraction of the original volume used in the second growing operation. In the early years of silicon-device manufacture it was quite common to resort to a “double pulling” operation to upgrade the available silicon, but the combination of better manufacturing methods and the use of float zoning, if required, has made such an operation unnecessary.

Distribution of Impurities during Zone Melting.^{26,9} If instead of initially melting the whole charge, only a narrow zone is melted and then swept through the charge, a distribution somewhat different from that of Eq. (4-30) is obtained. Assume a rod of unit cross section and length x_0 has a molten zone of length L . If the rod has an original concentration N_0 , the melting of an additional length dx on one end of the zone adds $N_0 dx$ impurities to the melt. The freezing of an additional length dx on the other end removes $k_0 N_l dx$ from the melt.

Fig. 4-31. Curves for normal freezing, showing solute concentration in solid as a function of l , the fraction solidified. (Pfann.²⁶)



Let $I =$ the number of impurities in the zone
 $dI = (N_0 - k_0 N_i) dx$ (4-33)

$$N_i = \frac{I}{L} \quad (4-34)$$

so that $dI = \left(N_0 - \frac{k_0 I}{L}\right) dx$ (4-35)

$$\int_0^x dx = \int_{I_0}^I \frac{dI}{N_0 - k_0 I/L} \quad (4-36)$$

where I_0 is the number of impurities in the zone when it was first formed at the front end of the rod.

$$x = \frac{L}{k_0} \log \frac{N_0 - (k_0/L)I_0}{N_0 - (k_0/L)I} \quad (4-37)$$

$$\exp \frac{k_0 x}{L} = \frac{N_0 - k_0 I_0/L}{N_0 - k_0 I/L} \quad (4-38)$$

Substituting $I_0 = N_0 L$ and $N_s = k_0 I/L$ into Eq. (4-38) gives

$$\frac{N_s(x)}{N_0} = 1 - (1 - k_0) \exp \frac{-k_0 x}{L} \quad (4-39)$$

This equation for various values of k_0 is plotted in Fig. 4-32. A comparison with Fig. 4-31 shows that a single pass does not produce as much purification as a crystal can be grown, cropped, and regrown, as was described in the previous section.

The distribution after an arbitrary number of passes is given by

$$dx = \int \frac{dN}{N - k_0 I/L} \quad (4-40)$$

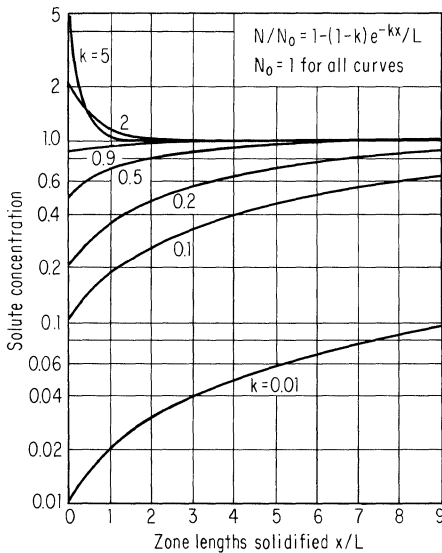


Fig. 4-32. Curves for zone melting, showing solute concentration in solid as a function of x/L . (Pfann.²⁶)

where $N(x)$ is determined by the previous passes. The solution is somewhat involved and the reader is referred to Pfann.⁹ After repeated passes, the number depending on such things as the segregation coefficient and the ratio of L to x_0 , the purification or redistribution of impurity, reaches a limiting value. For this case assume that the final concentration is $N_s \equiv F(x)$. The concentration in the molten zone is given by

$$N = \frac{1}{L} \int_x^{x+L} N_s(x) dx \quad (4-41)$$

The part that freezes has a concentration

$$N_s = k_0 N_l = F(x) \quad (4-42)$$

Substituting Eq. (4-42) into Eq. (4-41) gives

$$F(x) = \frac{k_0}{L} \int_x^{x+L} F(x) dx \quad (4-43)$$

Equation (4-43) has as its solution

$$N_s(x) = A e^{Bx} \quad (4-44)$$

where

$$k = \frac{BL}{e^{BL} - 1}$$

$$A = \frac{N_0 B x_0}{e^{Bx_0} - 1}$$

In the event that it is desired to dope the rod rather than purify it, consider the case in which all the dope (I_d) is introduced in the first zone and the initial bar impurity concentration N_0 is much less than $k_0 I_1/L$. Equation (4-38) gives

$$I_0 = I \exp \frac{k_0 x}{L} \quad (4-45)$$

Since $N_s = k_0 I/L$ and the dope concentration $N_d = I_d/L$,

$$k_0 N_d = N_s \exp \frac{k_0 x}{L} \quad (4-46)$$

If $k_0 x/L$ is small, N_s will remain nearly constant with distance. Thus, for this system, uniform doping is achieved by having a low segregation-coefficient impurity; in contrast, recall that a high segregation is required for uniformity of concentration in a Teal-Little grown crystal.

The segregation coefficients of most silicon impurity elements used in float zoning are neither very near 1 (except boron), nor very small, so there is difficulty in obtaining a uniform resistivity along the rod. One method of combating these effects of segregation is to saw a series of notches in the rod before zoning and fill each of them with the required amount of dope. It also appears possible to get a flat resistivity profile for k 's less than about 0.5 by doping in both the first and last zones and then making repeated passes in both directions.²⁷ This behavior is illustrated in Fig. 4-33.

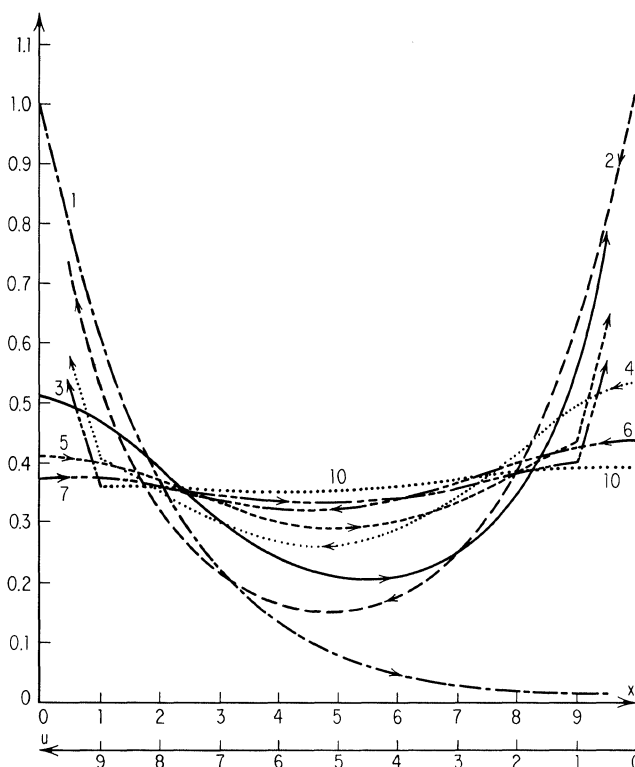


Fig. 4-33. $l = 1$ cm, $k = 0.5$. Graphical representation of the impurity distributions of ten successive passes, which converge slowly to an ultimate impurity distribution. (Braun and Wang.²⁷)

Effective Segregation Coefficient. While the crystal is growing, impurities are constantly being rejected into the melt. If the rejection rate is higher than that which can be transported away by diffusion or stirring, then a concentration gradient will develop at the interface. This is illustrated in Fig. 4-34. If an attempt is made to calculate N_s on the basis of an equilibrium k_0 as previously defined, and the concentration N_l in the main body of the liquid, the increased concentration at the interface can cause serious error. This is normally corrected by considering an “effective” k dependent on growth rate, stirring, geometry, and impurity species, which is defined as the ratio of N_s to N well away from the crystal. k_{eff} is then given by N'_i/N_l (of Fig. 4-34) times the actual k_0 , where N'_i is the concentration in the liquid at the interface.

A simplified analytical expression for k_{eff} can be obtained as follows:²⁸ Consider that despite any stirring that may take place in the melt, there is a small virtually stagnant layer of melt of width $\bar{\delta}$ in which the only flow is that required to replace the crystal being withdrawn from the melt. Outside of this layer the concentration is considered constant (N_l). Inside, the concentration N is described by Fick’s law. If the interface is essentially planar, and if $\bar{\delta}$ is much less than the

lateral dimensions of the crystal, a one-dimension solution is acceptable. Under equilibrium conditions

$$D_l \frac{d^2N}{dx^2} + v \frac{dN}{dx} = 0 \tag{4-47}$$

where D_l = impurity diffusion coefficient in the liquid
 v = crystal growth velocity
 N = concentration at x

The requirements that the sum of the impurity fluxes at the boundary be zero (conservation of the total number of impurities) imposes the boundary condition

$$(N'_l - N_s)v + D_l \frac{dN}{dx} - D_s \frac{dN}{dx} = 0 \tag{4-48}$$

where D_s is the impurity diffusion coefficient in the crystal and N_s is the concentration of impurity in the crystal. Normally $D_s \frac{dN}{dx}$ will be small and can be disregarded. The other boundary condition is that $N'_l = N_l$ at $x = \bar{\delta}$. The solution of Eq. (4-47) then becomes

$$\frac{N - N_s}{N_l - N_s} = \exp \frac{v\bar{\delta} - x}{D_l} \tag{4-49}$$

At the interface

$$\frac{N'_l - N_s}{N_l - N_s} = \exp \frac{v\bar{\delta}}{D} \tag{4-50}$$

Solving for N_s/N_l , which is the effective k , gives

$$k_{\text{eff}} = \frac{k_0}{k_0 + (1 - k_0) \exp(-v\bar{\delta}/D_l)} \tag{4-51}$$

Thus as $v\bar{\delta}/D$ increases from zero, k_{eff} gradually changes from k_0 , and in the limit

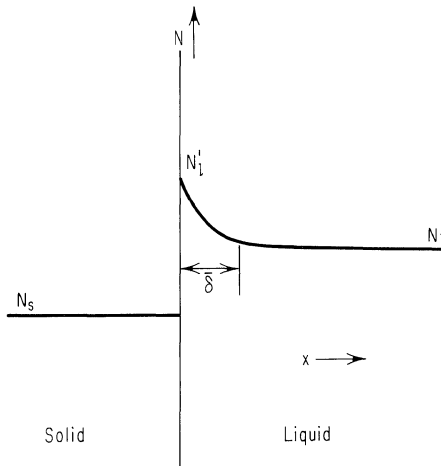


Fig. 4-34. Impurity distribution near crystal-melt interface.

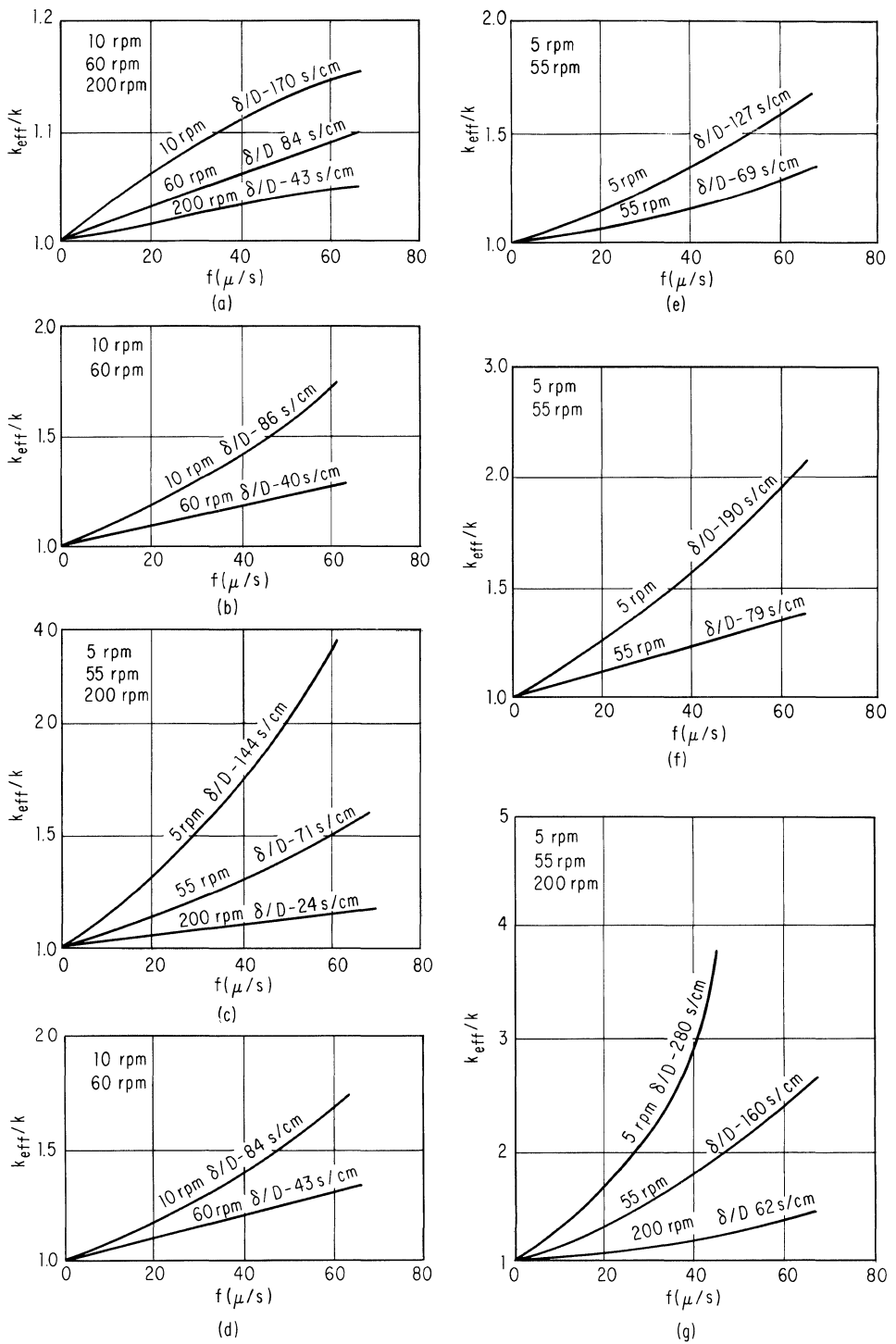


Fig. 4-35. Dependence of effective segregation coefficients of impurities on growth rates and rotation rates: (a) boron, (b) aluminum, (c) gallium, (d) indium, (e) phosphorus, (f) arsenic, (g) antimony. (Kodera.³⁶)

as $v\bar{\delta}/D$ becomes much greater than 1, k_{eff} approaches 1. Figure 4-35 shows some experimental data for the variation of k of silicon with spin and growth rate.²⁹ An alternate approach developed about the same time³⁰ but including the effects of impurity atoms adsorbed on crystal surface as well as solute buildup, predicted an effective segregation coefficient of the form

$$k_{\text{eff}} = k_0 + (k_s - k_0) \exp \frac{-v_i}{v} \quad (4-52)$$

where k_s and v_i are constants. Equation (4-51) is most widely accepted and Table 4-1 gives values of $\bar{\delta}/D$ and D calculated in this manner from the data of Fig. 4-35.²⁹

Faceting. When crystals are grown in or near the [111] direction, there is often a well-defined (111) face formed on the bottom of the crystal. That is, rather than a curved melt-liquid interface determined solely by thermal gradients, a large portion of the interface may be bounded by a (111) plane. It has been experimentally observed that for indium antimonide,³¹ germanium,³² and silicon,³³ the impurity concentration is higher in the faceted region than in the rest of the crystal. Though not reported in silicon, k_{eff} in the faceted portion of some semiconductors is often much greater than 1.

It can be assumed that nucleation is more difficult on (111) planes than on the rest of the solid-liquid interface, and that considerable supercooling of the melt adjacent to the facet is required before a layer does nucleate. Once a layer begins,

Table 4-1. Values of $\bar{\delta}/D$ for Silicon*

Impurity element	Rotation rate, rpm	$\bar{\delta}/D\ell$, s/cm	Diffusion coefficient $D\ell$, cm ² /s
B	10	170 ± 19	$(2.4 \pm 0.7) \times 10^{-4}$
	60	84 ± 37	$(2.4 \pm 0.7) \times 10^{-4}$
	200	43 ± 18	$(2.4 \pm 0.7) \times 10^{-4}$
Al	10	86 ± 34	$(7.0 \pm 3.1) \times 10^{-4}$
	60	40 ± 17	$(7.0 \pm 3.1) \times 10^{-4}$
Ga	5	144 ± 54	$(4.8 \pm 1.5) \times 10^{-4}$
	55	71 ± 26	$(4.8 \pm 1.5) \times 10^{-4}$
	200	24 ± 8	$(4.8 \pm 1.5) \times 10^{-4}$
In	10	84 ± 15	$(6.9 \pm 1.2) \times 10^{-4}$
	60	43 ± 5	$(6.9 \pm 1.2) \times 10^{-4}$
P	5	127 ± 36	$(5.1 \pm 1.7) \times 10^{-4}$
	55	60 ± 19	$(5.1 \pm 1.7) \times 10^{-4}$
As	5	190 ± 53	$(3.3 \pm 0.9) \times 10^{-4}$
	55	79 ± 16	$(3.3 \pm 0.9) \times 10^{-4}$
Sb	5	283 ± 55	$(1.5 \pm 0.5) \times 10^{-4}$
	55	157 ± 57	$(1.5 \pm 0.5) \times 10^{-4}$
	200	62 ± 37	$(1.5 \pm 0.5) \times 10^{-4}$

* From Hiroshi Kodera, Diffusion Coefficients of Impurities in Silicon Melt, *J. Appl. Phys. (Japan)*, vol. 2, pp. 212-219, April, 1963.

it can release its latent heat very quickly to the supercooled liquid and thus grow laterally with a very high velocity determined not by Eq. (4-2), but rather by the ability of atoms to move to an allowable lattice site.³⁴ A derivation of an effective k based on this concept gives

$$k_{\text{eff}} = \frac{k_0}{1 - Av(1 - k_0\tau_s/\tau_i)} \tag{4-53}$$

where A is a function of the system and includes such items as the impurity diffusion coefficient and concentration. τ_s/τ_i is the ratio of dwell times of the solvent and impurity atoms. For small $k_0\tau_s/\tau_i$

$$k_{\text{eff}} \simeq \tau_i/\tau_s \tag{4-54}$$

Constitutional Supercooling. As was discussed in the section on effective segregation coefficients, while a crystal grows there is a solute “pile-up” at the interface (see Fig. 4-34) if any impurities are being rejected. These added impurities reduce the freezing point of the mixture so that for crystal growth, the temperature at the melt-crystal interface must be reduced below that required for growth from a pure melt.³⁵ For dilute solutions the temperature depression will be approximately proportional to the concentration increase. Thus the temperature required for freezing, as a function of distance from the interface, is the inverse of the concentration curve of Fig. 4-34 and is shown as the solid curve of Fig. 4-36. The temperature gradient in the melt is probably quite linear over the same region, with the magnitude depending on such previously discussed parameters as the amount of heat being radiated by the crystal and crucible designs. Several possible values are shown by the dotted lines of Fig. 4-36. If the actual temperature is as shown by line 1, the melt is always above the freezing point except at the solid-liquid interface; but if it is as line 3, then that portion of the melt shown shaded is below the melting point and is “constitutionally supercooled.”

No constitutional supercooling can occur if

$$\frac{dT_{\text{actual}}}{dx} > \frac{dT_e}{dx} \quad \text{at } x = 0 \tag{4-55}$$

where T_e is the equilibrium liquidus temperature. The equilibrium temperature can be written as

$$T_e(x) = T_0 + mN(x) \tag{4-56}$$

where T_0 = melting point of the pure solvent

$N(x)$ = impurity concentration at distance x from the interface

$$m = dT_e/dN$$

The latter will be considered constant for very dilute solutions.

$$\frac{dT_e}{dx} = m \frac{dN}{dx} \tag{4-57}$$

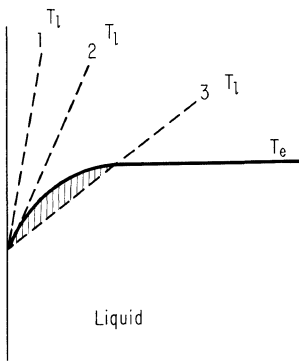


Fig. 4-36. Temperature distribution in the melt and equilibrium liquidus temperature. The depression of T_e is caused by solute “pile-up” at the interface.

Substituting in the value of dN/dx from Eq. (4-48) and the value of N_s/N_l from Eq. (4-51) gives

$$\frac{dT_e}{dx} = \frac{mvN_l(1 - k_0)}{D_l[k_0 + (1 - k_0)e^{-v\delta/D}]} \quad (4-58)$$

The actual temperature gradient (the dotted lines of Fig. 4-36) is given by Eq. (4-4) as

$$\frac{dT_l}{dx} = \frac{k_s(dT_s/dx) - Lv\bar{\delta}}{k_1} \quad (4-59)$$

Combining Eqs. (4-55), (4-58), and (4-59) gives the criteria for no constitutional supercooling as

$$\frac{k_s(dT_s/dx) - Lv\bar{\delta}}{k_1} \geq \frac{mvN_l(1 - k_0)}{D_l[k_0 + (1 - k_0)e^{-v\delta/D}]} \quad (4-60)$$

From this equation it follows that high growth rates, small k_0 's, and small temperature gradients in the crystal all enhance the possibility of the occurrence of supercooling.

Small amounts of supercooling can be tolerated, but if it is as much as 2° for silicon, polygrowth is usually initiated.³⁶ Figure 4-37 shows a crystal which began polygrowth because of this effect. At values less than that required to cause polycrystal growth, cellular structure is observed in many metals³⁷ and occasionally in silicon. As a result of this phenomenon, the maximum doping as calculated from normal solid solubility limits is seldom observed in single crystals. Table 4-2 gives some experimentally observed concentrations and compares them with solid solubility.³⁶

Impurity Concentration Striations. It is often observed that there are cyclic impurity

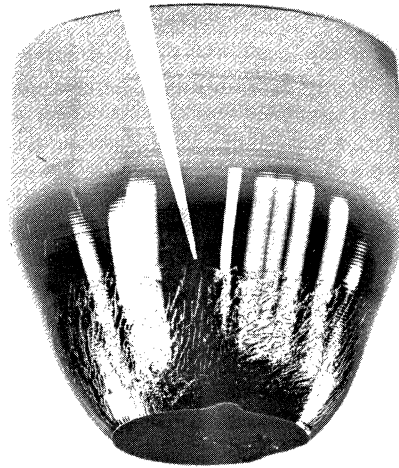


Fig. 4-37. Effect of heavy doping on crystal growth. The marker points to the beginning of polycrystalline growth.

Table 4-2*

Impurity element	C_{S1}, cm^{-3}	$C_{S,max}, \text{cm}^{-3}$
B	3×10^{20}	6×10^{20}
P	8×10^{19}	1.4×10^{20}
Sb	2.9×10^{19}	6.7×10^{19}

* From Hiroshi Kodera, Constitutional Supercooling during the Crystal Growth of Germanium and Silicon, *J. Appl. Phys. (Japan)*, vol. 2, pp. 527-534, 1963.



Fig. 4-38. An electrochemically etched slice exhibiting severe impurity concentration striations. These are usually more pronounced as the doping level approaches the solid solubility limit.

gradients in crystals grown by the Teal-Little process.³⁸ These are caused by variations in growth rate that occur when the center of rotation of the crystal is not coaxial with the thermal gradients. Figure 4-26*b* is a photograph of the external shape of such a crystal, while Fig. 4-38 shows impurity variation as revealed by selective etching. Even though the crystal does not grow in such a severe environment as the one which produced the crystal of Fig. 4-26*b*, these striations still occur.

4-7. MISCELLANEOUS TECHNIQUES

While most of the single-crystal silicon is grown with conventional Teal-Little and float-zone equipment, there have been many different techniques tried, some as substitutes for more standard methods, some for special purposes. The following is an attempt to summarize the more interesting of these.

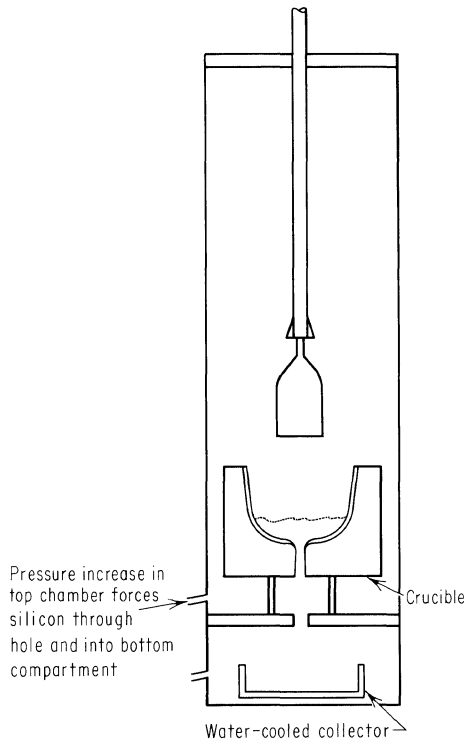
Methods for Saving Fused-silica Liners.

The usual procedure is to allow the silicon remaining in the crucible at the end of the crystal-growing operation to freeze. Since this will cause the fused-silica liner to crack (see Chap. 3), a liner is lost each time a crystal is grown. Since the fused-silica-silicon combination does not break until the temperature has dropped to 700 or 800°C, the silicon remaining in the crucible can be allowed to freeze to the end of the crystal without cracking the liner. Then the crucible temperature is abruptly raised well above the melting point of the silicon so that the frozen button is released from the liner in the manner of an ice cube from a tray.³⁹ Care must be taken to prevent severe slip from being introduced into the crystal during the freezing-melting cycle. One method of doing this is to have only a very small contact area between the crystal and the freezing button and to minimize the temperature of the frozen ingot before it is separated from the liner.

Cracking can also be prevented by emptying the liner before cooling. This may be done by having a small hole in the liner through which the silicon can be forced by differential pressure, but still small enough for surface tension to keep the silicon from leaking out during the growing operation⁴⁰ (Fig. 4-39). This procedure is most applicable to growing crystals for grown-junction transistors because the time of growth after the addition of base and emitter dopes is usually short and quite critical so there is no opportunity to either grow all of the silicon onto the crystal or to use the previous method.

Adding Silicon during Crystal Growing. In order to grow larger crystals than might otherwise be possible or to make the doping more uniform, it is often desirable to add silicon to the melt. The simplest requirement arises if the crucible will

Fig. 4-39. A method of conserving liners.
After the crystal is grown the liner is emptied
by ejecting the silicon into container in bottom.



not hold enough unmelted silicon (because of packing factor) to grow the size crystal desired, but will hold enough molten silicon. It is a straightforward matter to add silicon chunks through a lock of some sort to bring the melt to the desired level. If a crystal is to be grown while the addition occurs, two complications arise: (1) The addition of fresh material to the melt makes temperature control difficult. (2) There is usually a bit of silicon monoxide generated from the SiO_2 . Some of it will often condense on the growing crystal at the melt-solid interface and cause twinning. Both of these difficulties can be eliminated by using a compartmental crucible. Several arrangements have been suggested,⁴¹⁻⁴⁴ but because silicon requires a fused-silica crucible liner, any complicated crucible configuration becomes very expensive. Apparently none of them has been successfully used for silicon.

The top of a vertical silicon rod can be melted and will remain in place because of surface tension. The resulting pool of liquid can be used as the melt for crystal growing.^{45,46} As the liquid is withdrawn from the top, the level is held constant by raising the rod. Figure 4-40 is an illustration of this process. Notice that in the limit as the diameter of the crystal being pulled approaches that of the feedstock, it looks very much like the float-zone process. The length of crystal that can be grown is limited only by the length of the draw mechanism and the supply of rod feed materials so this process is a method of replenishing the supply of melt that is applicable to silicon crystal growing. Rather than depend on surface tension to hold the silicon in place, several variations have been proposed which pro-

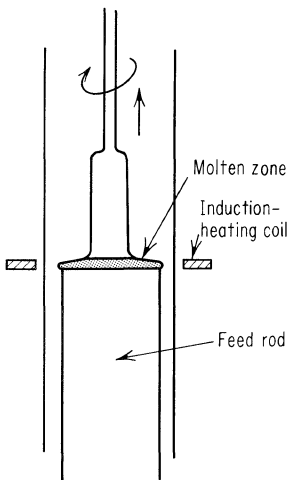


Fig. 4-40. Crystal growing without a crucible.

vide containers for the melt and yet have a means for advancing a feed rod. In one of these the growing is done "upside down" as illustrated in Fig. 4-41.^{47,48,*} In another approach, the silicon is first cast in a fused-silica container, and then without allowing it to cool below a red heat, the top of the ingot is remelted and the crystal grown from the melted section.^{49,50}

Eliminating Crucible Contaminations. Since molten silicon appears to dissolve all known materials the obvious way to eliminate contamination is to remove the crucible altogether, along with the fused-silica liner that normally accompanies it. The process of growing from the top of a rod, as just described, and float zoning both accomplish this goal. Chunks or a single large ingot can be used as its own crucible if heating is done from above.⁵¹ Local heating produces a melt in the middle but the edges never reach the melting point.

Levitation is often used to suspend metals during melting and has been applied to silicon with only limited success.⁵² A modified form of levitation referred to as a "silver cage" has been used for silicon.⁵³ The silicon is contained in a water-cooled silver crucible which acts as part of a transformer to couple from a high-frequency induction heater to the silicon. The water cooling keeps any silicon in contact with the silver well below the Si-Ag eutectic temperature. The induced currents are such that the liquid silicon is slightly raised above the crucible and hence is not contaminated.

Methods of Reducing Concentration Gradients. Since the effective segregation coefficient depends on, and in general increases with, growth, crystals can be grown with variable pull rate in order to reduce the concentration gradient along the crystal length.^{54,55} Figure 4-35 shows some approximate variations of k with growth rate for several impurities. Thus if the initial pull rate were high, more impurities would appear in the crystal than would be predicted by use of the segregation coefficients of Table 6-1. Then, as growth progresses and N_{melt} increases, the growth rate can be progressively slowed down to reduce k_{eff} and keep the $(k_{\text{eff}}N_{\text{melt}})$ product constant. Usually the puller programs are experimentally determined for any given crucible geometry, crystal size, and spin rate.

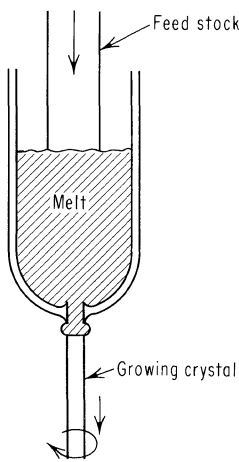


Fig. 4-41. Upside-down crystal growing.

The effective k also depends on the crystal spin rate,⁵⁶ so in principle it too could be varied to minimize resistivity variations along the crystal. In Sec. 4-6 it was shown that a zone moved through a bar would give uniform resistivity along the bar if the segregation coefficient were small. This same process can be applied to vertically grown crystals by growing from a crucible containing two compartments sepa-

* It is also possible to reverse the geometry of the methods of Sterling and of Dash and grow crystals from a hanging drop.

rated by a small orifice.⁵⁷⁻⁶⁰ The growing compartment contains the doped semiconductor, while the supply compartment is filled with high-purity material. If the segregation coefficient is small, the dope concentration will change but little as the crystal is grown, since only a small fraction of the total dope is transferred to the crystal, and the melt volume is held constant by feed from the supply compartment. Because a complicated crucible and fused-silica liner is required for silicon, the process apparently has never been applied to silicon.

When growing from an ingot cast in a fused-silica tube, dope added to the molten zone will result in a constant volume system analogous to those just described.⁴⁹ As in the others, if the doping element has a low segregation coefficient, the concentration in the molten layer will remain substantially constant. However, if k is large, for example, 0.3 for phosphorus and arsenic, the concentration of dope in the molten layer gradually decreases. A continuous reduction of the volume of melt will compensate for this loss. Thus, to produce uniform crystal resistivity,

or
$$\begin{aligned} V(x) &= V_0 - Akx \\ L(x) &= L_0 - kx \end{aligned}$$

- where V = volume of melt
- V_0 = original volume
- L = melt depth
- L_0 = original depth of melt
- A = cross-sectional area (assumed constant)
- x = amount that the liquid level has dropped

Growth of Special Crystal Shapes. Most crystal pullers are designed to produce long round boules, but occasionally other shapes are desired. If disks are required, the puller can be altered as shown in Fig. 4-42 and a wheel-type seed used.^{61,62}

4-8. GROWTH FROM LOW-TEMPERATURE MELTS

Reference to the phase diagrams of Chap. 11 shows that silicon has appreciable solubility in several metals at relatively low temperatures. It is then, in principle, possible to saturate the metal at some temperature and by gradually reducing the temperature, reduce the silicon solubility and grow silicon crystals in the same way that many crystals are grown from aqueous solutions. For example, from the curve of Fig. 4-43, which shows a portion of the gallium-silicon liquidus curve, changing the temperature from 1000 to 900°C reduces the silicon solubility from 20 to 10 atomic per cent. Thus if 70 g of gallium were used (one atomic weight), 6×10^{22} atoms of silicon would be precipitated. This represents 2.8 g of silicon and, if grown on a 1-in.-diameter seed, will produce an additional length of a little less than 1/10 in.

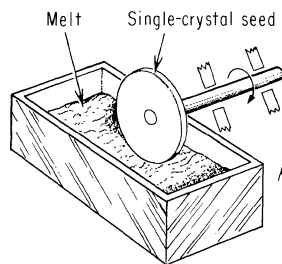


Fig. 4-42. Mechanism for the growth of silicon single-crystal disks directly from the melt.

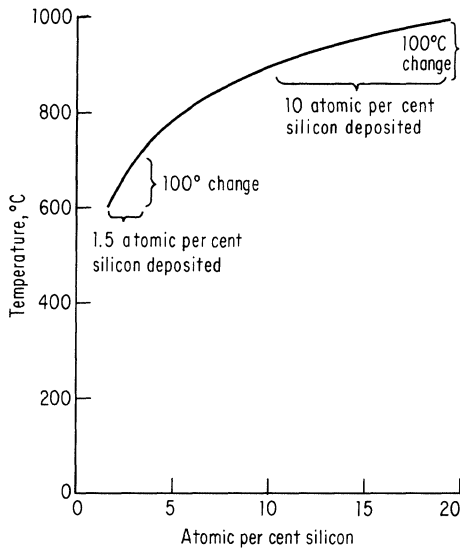


Fig. 4-43. A portion of a gallium-silicon phase diagram and details of silicon growth from a gallium solution.

There are few data available on growth rates required to maintain single-crystal growth in this type of process, but if the criterion of 1 micron/min is chosen (as is common in vapor-phase growth at 1000°C), the 100°C temperature reduction would take over about 40 hr. This represents a dT/dt of 0.04°C/min and requires a rather carefully designed temperature control system to prevent short-term fluctuations from exceeding that value. If instead of operating between 900 and 1000°C, the range of 600 to 700°C were chosen, only one-seventh the amount of silicon would be available for deposition, but the temperature rate of change would be seven times as great for the same growth rate.

The mechanical arrangement for this type of growth may be that of a metal zone moving through a bar of silicon as the heater moves (similar to zone refining),⁶³ the zone progressing by a fixed externally maintained thermal gradient (zone gradient melting, or traveling solvent),⁹ or by the direct reduction of the whole melt temperature (as was assumed in the example).⁶⁴

Although silicon can be grown by any of these methods, to produce high-quality single-crystal growth poses additional problems which have not yet been satisfactorily solved. Some of them are:

1. Initiation of growth is severely hampered by the residual oxide film on the silicon seed.
2. Most applications require a thin layer grown on a relatively thin slice.* If the concentration of silicon in the melt is not carefully controlled before the seed slice is inserted the whole slice may dissolve.
3. The grown layer is saturated with the metal. In applications requiring heavy doping, this is desirable (if the metal used is a proper doping agent). If less dope is required, there is some hope of growing from an electrically inactive metal such as tin.

* This process is sometimes referred to as "solution epitaxy."

4-9. VAPOR-LIQUID-SOLID (VLS) METHOD OF CRYSTAL GROWTH^{65,66}

Instead of growing from a low-temperature melt fed by solid feedstock or dissolved nutrient or by a direct vapor deposition, it is possible to grow from a liquid drop alloy being constantly replenished by a vapor-phase reaction at the liquid surface. The liquid acts as a preferred sink or as a catalyst for silicon deposited at low temperatures from a silicon halide, for example, 950°C, where normal vapor-phase deposition is quite slow. Silicon then freezes at the liquid-solid interface. As silicon continues to freeze, the drop is gradually raised and can give rise to needlelike structures. Au, Pt, Ag, Pd, Cu, and Ni have all been used as the alloying agent.

4-10. GROWTH FROM THE VAPOR

Float-zoned or pulled crystals are very satisfactory for most purposes, but because of the inability to remove doping impurities from the melt once they are added, the impurity level in the growing crystal continually increases. It is true that the resistivity can be increased as the crystal grows, e.g., the grown-junction crystal, but always by compensation, so the limit of usefulness of such a process is rapidly reached. In the case of germanium it is possible to have a series of melt reservoirs, each doped differently, and to transfer the crystal from one to the other. Because of the difficulty of initiating good single-crystal growth on large cross-section seeds, and because of the curved melt-solid interface that normally occurs, such a process is not practical for silicon. If growth is from the vapor, however, the simultaneous deposition of silicon and the appropriate impurity allows doping, and yet the relative deposition rates can be rapidly changed. Thus alternate low- and high-resistivity layers can be grown without the large-scale compensation which would be required for growth from a melt.

The ability to grow silicon from the vapor phase has been recognized for many years, but only when devices became sophisticated enough to require doping profiles unattainable by standard growing and diffusion processes was its potential usefulness recognized.^{17,19,67}

Silicon can be deposited by any of the processes discussed in Chap. 2, so each of them is a potential epitaxial* method. Likewise, direct evaporation and the decomposition of organosilicon compounds are possibilities. The process requirements do differ somewhat from those of bulk silicon manufacturing in that the primary requirement of the latter is for a high-efficiency process, whereas epitaxial deposition requires good control of deposition rate and resistivity and high crystal perfection in the deposited layer.

Deposition from Silicon Tetrachloride.⁶⁸⁻⁷⁷ Experimental curves of deposition rate versus temperature for the hydrogen reduction of silicon tetrachloride follow curves as shown in Fig. 4-44. At the lower temperatures the deposition rate is given by $v = A \exp(-\Delta E/RT)$, where ΔE is the activation energy, A and R are constants, and T is the temperature. At higher temperatures, diffusion processes appear to be the limiting factor. Various reactor designs and flow rates change

* For the origin of the term "epitaxy," see Chap. 1.

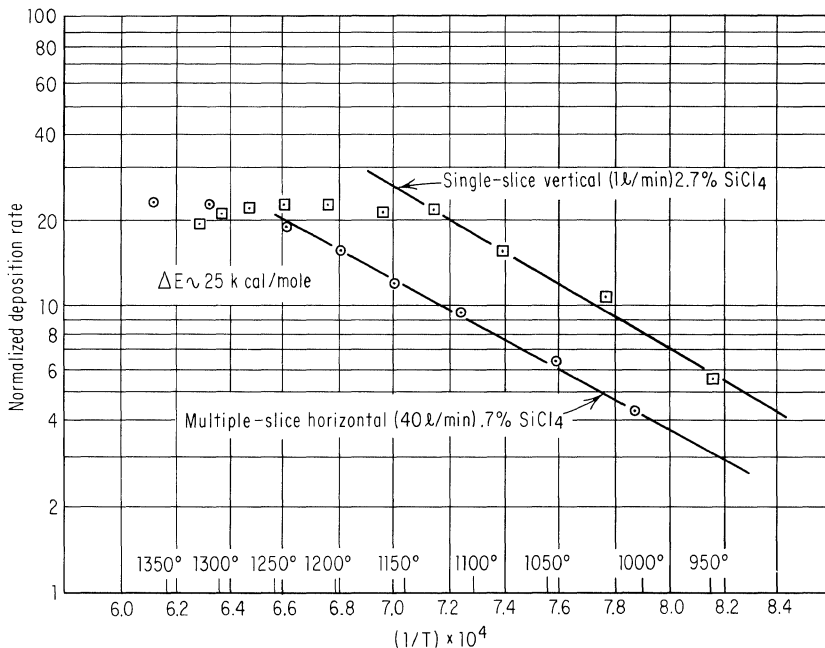


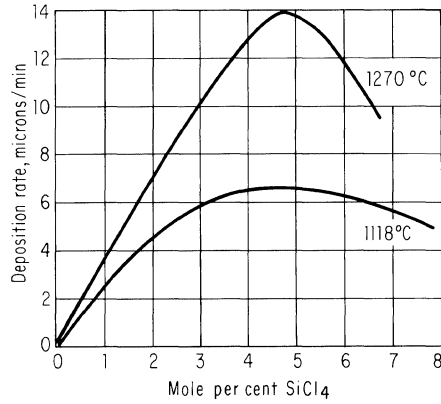
Fig. 4-44. Deposition rate versus $1/T$ for deposition by the hydrogen reduction of SiCl_4 .

the temperature at which diffusion becomes predominant. The more turbulent, or the higher the velocity of, the flow, the higher the temperature required before the reaction becomes diffusion-controlled. In Fig. 4-44 are representative curves for two reactors, one vertical and one horizontal. The ΔE measured from these curves is approximately 25 kcal/mole. Activation energies from 25 to 40 kcal/mole have been reported, but it seems that the apparently higher values were caused by improperly cleaned surfaces. For example, if only a short hydrogen fire is used before deposition, 36 to 40 kcal/mole is obtained, and if thickness versus deposition time is plotted, an induction time of several seconds is often observed and becomes more pronounced at the lower temperatures. If vapor etching (to be described later) is used to clean the surface prior to deposition, the induction period is no longer observed and 25 kcal/mole is obtained for the activation energy. It might be noted that the reported value for the reduction of trichlorosilane is 22 kcal/mole and confirms observations that there is little difference in the deposition behavior of silicon tetrachloride and trichlorosilane.

For an otherwise fixed set of reactor conditions, increasing the concentration of silicon tetrachloride will produce a maximum in the deposition rate and, finally, etching. The maximum depends on the temperature, and some typical curves are shown in Fig. 4-45. Working near this point will reduce the deposition time but may have deleterious side effects, such as more surface defects and lower deposition efficiency.

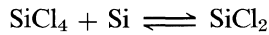
With a fixed concentration, the deposition-rate dependence on flow rate and

Fig. 4-45. Deposition rate versus per cent silicon tetrachloride.

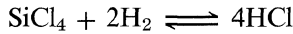


temperature is shown in Fig. 4-46. When the reactor is operating in the temperature-dependent region, the growth rate increases as the degree of misorientation from the (111) plane increases.⁷⁵

By considering the transport reaction

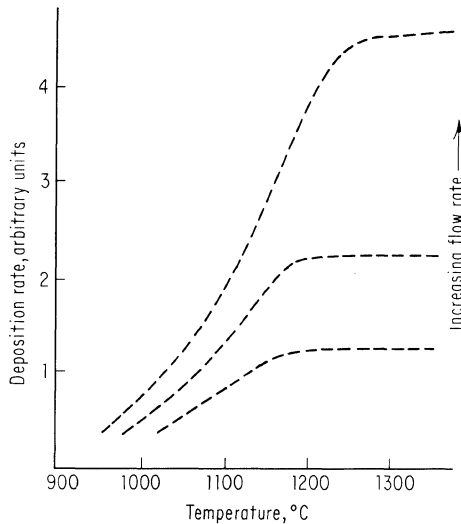


along with the reduction reaction



the silicon yield has been calculated for various deposition conditions and gives reasonable qualitative agreement with experiment. It also predicts the transport within the reactor of silicon in the direction of lower temperatures. For example, if a silicon or a silicon-coated heater is used, silicon can be transferred from the heater to the underside of the slice by this process. More often, however, silicon

Fig. 4-46. The effect of increasing flow rate through the reactor on deposition rate.



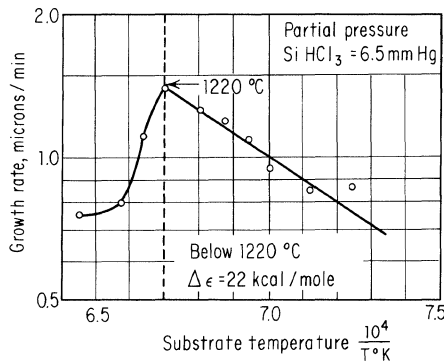


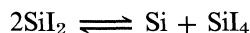
Fig. 4-47. Deposition rate versus temperature for a trichlorosilane deposition. (Charig and Joyce.⁷⁸)

deposition on the underside of the slice occurs because of poor contact with the heater surface which in turn allows feedstock from the gas stream to flow beneath the slice. There are also some reactor conditions, not fully understood, which allow etching to proceed on the underside of the slice and sometimes to produce severe pitting.

Growth from Trichlorosilane (SiHCl₃). Trichlorosilane can be used for epitaxial deposition and in performance appears quite comparable to silicon tetrachloride. Its activation energy is ~22 kcal/mole (as compared to approximately 25 kcal/mole for SiCl₄). At high temperatures there is a reduction in deposition rate similar to that observed under some conditions for SiCl₄. Figure 4-47 shows a typical deposition rate versus temperature curve for SiHCl₃.⁷⁸ It is also interesting to note that whether silicon tetrachloride or trichlorosilane is used in the deposition process, the exit gases show both SiHCl₃ and SiCl₄, as well as HCl and various long-chain silicon polymers.

Growth from Silicon Tetrabromide. Depositions have been made using the hydrogen reduction of silicon tetrabromide, and an activation energy of 15 kcal/mole has been determined. Its general behavior is similar to that of the other halides, but if a bromide is used as a dopant, for example, BBr₃, there are no side reactions generating BCl₃.^{19,79}

Growth by SiI₂ Disproportionation.⁸⁰ Silicon can be deposited by the thermal decomposition of SiI₄ but the process requires low pressures and has a very low deposition rate. An alternate reaction involving the partial reduction of the tetraiodide may be used at higher pressures and faster deposition rates. This reaction may be written as follows:



The di-iodide is unstable and exists only in equilibrium with SiI₄ and iodine but it can be produced *in situ* by the reaction



This process must be carried out in a closed tube with the temperature adjusted to favor the formation of SiI₂ from a silicon source placed at one end and the reduction of the di-iodide at the other end. Such systems are usually static with the

transfer of reactants occurring by diffusion and convection. Some typical operating conditions are:

- Source zone, 1100°C
- Deposition zone, 950°C
- Iodine concentration, ~ 1 mg/cm³ of reactor volume
- Carrier gas, hydrogen at about 300 mm pressure
- Deposition rate, ~ 10 to 15 microns/hr

Single-crystal deposits can be made at temperatures of 800°C or less (which are considerably lower than with the other processes described). Most of the doping elements can be transported by similar reactions, so if the source of silicon is doped, the growing layer will usually have a comparable impurity level.

Variations of growth rate with substrate orientation have been observed, with deposition on a (211) plane being most rapid, followed in order by (110), (111), and (100) planes.

Deposition from Silane.⁸¹⁻⁸³ The reaction kinetics of pyrolytic silane depositions have been studied over a temperature range from 900 to 1300°C for various silane pressures. Figure 4-48 shows the growth rate versus temperature from which an activation energy of approximately 37 kcal/mole is calculated. Between 1100 and 1225°C the rate becomes essentially independent of temperature and thus displays the same characteristics as those shown by silicon tetrachloride and trichlorosilane depositions. Above 1225°C there is a marked decrease in the deposition rate, again similar to the behavior of SiCl₄ and SiHCl₃.

Autodoping. Impurities originally in the substrate often are transferred to the growing layer and may severely limit the resistivity range obtainable in the layer. In less adverse conditions, only the region near the substrate layer interface is affected, where an impurity gradient past the diffusion front is observed.⁸⁴ These impurities can come either from the front of a slice (from experiments performed in a single-slice reactor with regions of high-impurity concentration patterns diffused into the front) or from the back (deduced from the improvement noted when masking is used). That they sometimes get into the gas stream can be seen

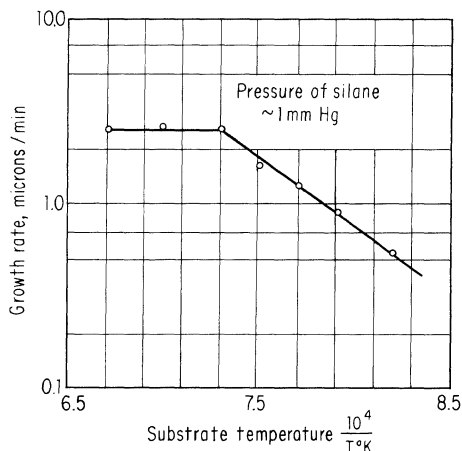


Fig. 4-48. Epitaxial layer growth rate versus temperature for deposition from a silane source. (Joyce and Bradley.⁸¹)

from observing the effects on downstream slices in a multiple-slice reactor, and yet autodoping is observed,⁸³ although to a lesser degree, in silane deposition systems where there can be no etching reaction.

In order to explain the first two observations, the following model has been proposed:⁸⁴

1. A continual etch-deposit mechanism is involved.
2. Silicon and dopant are removed in the ratio in which they are found at the surface of the solid.
3. The incoming gas composition is modified by mixing with it the products of step 2.
4. Silicon and dopant are deposited in the ratio in which they are now present in the gas stream (corrected as necessary for differences in deposition efficiency).

This model predicts the general shape of the observed gradient and also implies that, if the substrate impurity had a lower deposition efficiency than that being used to intentionally dope the layer, the effect would be smaller. The measured deposition rates from PCl_3 , BBr_3 , and SbCl_3 are in the ratio of 1:0.2:0.03⁸⁵ and is in keeping with the observation that autodoping is less pronounced when using antimony-doped substrates.

A combination of out diffusion, surface diffusion, and evaporation from the substrate has been suggested as a possible reason for the effect existing in layers deposited from silane. A long "bake out" period in hydrogen sometimes reduces the dope transport and suggests that the outer few atomic layers may become depleted of impurity by out diffusion.

Methods of Minimizing Diffusion.⁷⁴ During the growing of epitaxial layers it often develops that appreciable diffusion from one layer to the next occurs during deposition. There is a variety of ways these effects manifest themselves, e.g., reduction in amplitude of infrared reflection from a high-low concentration boundary, reduction in the effective layer width of high-resistivity layers, and the movement of p-n junctions. The concentration profile is determined by the diffusion constant-time product and the boundary conditions, each of which will now be examined. The Dt product can be reduced by using a lower deposition temperature, choosing a doping impurity with a much lower D value, or by increasing the deposition rate in order to make the diffusion time t as small as possible. It should be remembered that if high-temperature operations subsequent to the epitaxial deposition are carried out, the diffusion occurring during them may completely overshadow diffusion during deposition.

Since diffusion can occur during the addition of an epitaxial layer, the determination of the amount of diffusion taking place during deposition requires a solution to Fick's equation which involves a moving boundary (see Chap. 7). Calculations show that for

$$\frac{V^2t}{D} \equiv \Gamma > 100$$

and

$$\frac{KVt}{D} < 10$$

(4-61)

where V = growth velocity
 t = deposition time
 D = diffusion constant
 K = out-diffusion rate constant

there is only a small error in using the standard solution for diffusion from a concentration step. A substitution of values appropriate for silicon indicates little likelihood of exceeding these numbers during most deposition cycles. Thus, the calculation of the diffusion occurring near the substrate-epitaxial interface reduces to the geometry of Fig. 4-49, which has Eq. (4-62) as a solution.

$$N(x,t) = \frac{N_1^0}{2} \left(1 - \operatorname{erf} \frac{x}{2\sqrt{D_1 t}} \right) + \frac{N_2^0}{2} \left(1 + \operatorname{erf} \frac{x}{2\sqrt{D_2 t}} \right) \quad (4-62)$$

where $N(x,t)$ is the final distribution of impurities, N_1 is the initial (assumed uniform) concentration in the layer and N_2 that of the substrate. If the impurities are different, and if $D_1 \ll D_2$, a resistivity doubling can occur at the interface.* If Γ of Eq. (4-61) is larger than postulated, slightly more dope is transported than would be expected by Eq. (4-62).

One aid in minimizing diffusion is to always choose the impurity with the lowest diffusion coefficient. In practice, this alone may not provide adequate reduction of diffusion and in addition other reasons may govern the choice of dope. For example, of the n-type dopes, antimony has one of the lowest diffusion coefficients, and is often used both as a substrate and an epitaxial layer dopant. However, the combination of a low segregation coefficient and the inability to easily grow single crystals from melts containing more than about 2 per cent impurity prevents antimony doping of substrates to impurity levels greater than about 10^{19} atoms/cm³. If a very low resistivity epitaxial layer is desired, as for example in low voltage diodes, the limits of solubility will not allow the use of elements like indium and bismuth, even though they do have low diffusion coefficients. There are also prob-

* Another effect which causes increased resistivity, or even type change near the interface, occurs if a heavily n-doped substrate has a small amount of p-dope in it. In this case, the p-dope may diffuse faster than the substrate n-dope and thus produce compensation in the epitaxial layer.

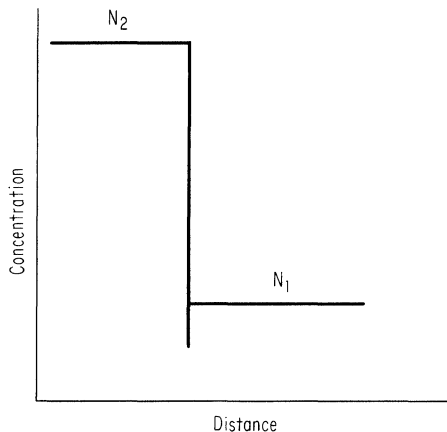


Fig. 4-49. Idealized impurity concentration profile for an epitaxial layer and its substrate.

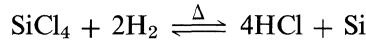
lems in introducing some of the dopes into an epitaxial reactor in a controlled fashion. For example, bismuth bromide and chloride both have melting points above 200°C, so a system using them requires that the complete system be kept at elevated temperatures.

In order to minimize the effects of diffusion, reactor flows and concentration are chosen to give the highest deposition rate, and the reactor is operated at as low a temperature as possible for the surface quality desired. If this temperature is in the region where deposition rate is orientation-dependent, choose the orientation for fastest deposition. (Diffusion in silicon is isotropic so orientation will not affect it).

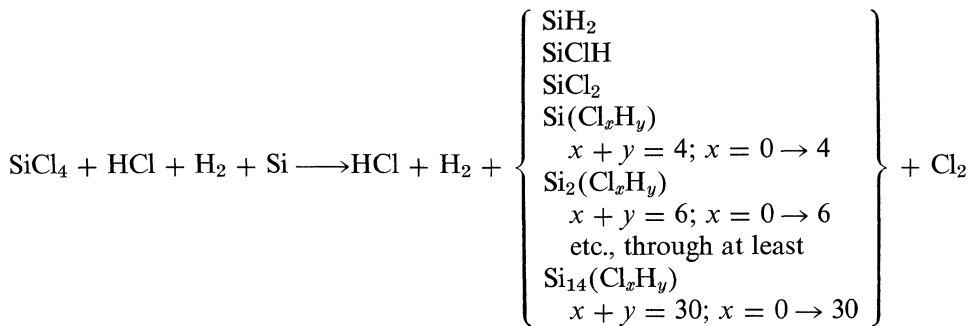
Vapor Etching prior to Epitaxial Deposition. Vapor etching *in situ* immediately prior to epitaxial deposition of silicon has been found to be very desirable, both on chemically and mechanically polished substrates. Epitaxial layers having dislocation densities no greater than that of the substrate and stacking fault densities less than 200/cm² can be grown if the proper vapor etching procedure is carried out. Mechanically polished slices usually have some mechanical damage remaining and even though there is no surface damage detectable on chemically polished surfaces, it is difficult to obtain a perfectly clean residue and oxide-free surface.

There are several potential vapor etches that might be used for silicon removal. Among these are chlorine, bromine, HCl, and SiCl₄ in high concentrations. Of these only HCl has been studied extensively.

The reaction



can be forced to the left by the addition of an excess of HCl. Using this mechanism it is possible to maintain the same flow of SiCl₄ that would be used during deposition. Then to change from etching to deposition merely calls for a termination of the HCl flow. This in turn brings about a gradual change from an etching condition to one of deposition. The skeleton reaction for etching might be written as follows:



For systems involving only HCl plus a carrier gas the reactions might be written as follows:

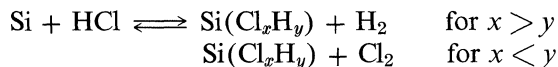


Figure 4-50 shows the etch rate versus HCl concentration at a fixed temperature,

while Fig. 4-51 shows the effect of temperature on a fixed HCl concentration.⁸⁶ All the vapor etches have regions in which they are more selective than polishing. Figure 4-52 delineates the useful area for HCl.⁸⁷ It should be remembered that all these processes are geometry-dependent so that these are only to be considered as “typical.”

Fig. 4-50. Etch rate versus HCl concentration for vapor etching in a horizontal reactor. (Bean and Gleim.⁸⁶)

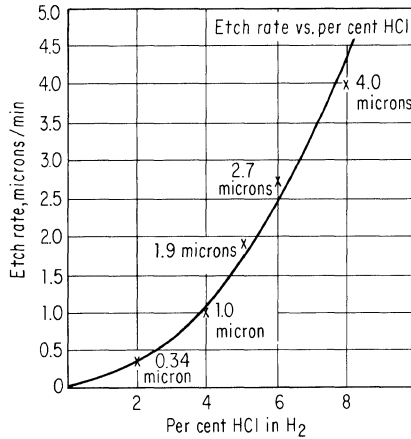


Fig. 4-51. Effect of temperature on vapor-phase etch rate of Silicon (Bean and Gleim.⁸⁶)

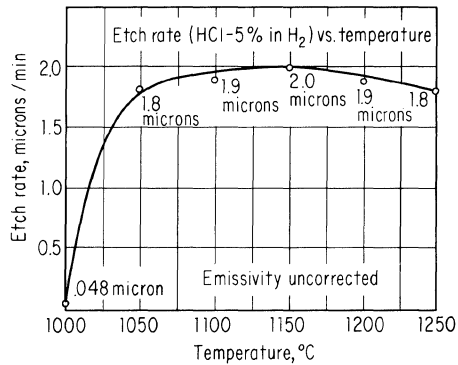
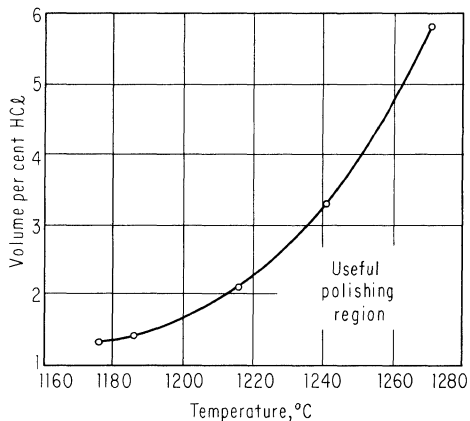


Fig. 4-52. Maximum allowable per cent (by volume) of hydrogen chloride in the etching gas as a function of temperature. (Lang and Stavish.⁸⁷)



Methods of Adding Dope. Doping of the growing layer can be accomplished by two processes. One involves injection of a suitable doping compound into the gas stream externally to the reactor; the second depends on transport of substrate dope into the growing layer. The first method is preferable from a control standpoint and is normally used though the second often occurs simultaneously and must be considered.

If the intent is to set a particular resistivity level and not vary it, a suitable doping compound such as boron tribromide or phosphorus pentachloride can be dissolved in the liquid silicon tetrachloride or trichlorosilane source. Then as the silicon halide is vaporized, some of the dopant will be included. If the liquid mixture is metered as a liquid and flash evaporated, the doping concentration will remain constant as the silicon halide is depleted. If the concentration of halide in the hydrogen stream is determined by vapor pressure, i.e., by the bubbler arrangement, relative amounts of silicon halide and doping halide will change as more and more of the supply is used.

To change the resistivity of the epitaxial layers it is necessary to either add more dope to the feed, dilute the bottle with more silicon halide, or use multiple feed bottles and switch from one to the other. While these direct doping systems have been widely used, systems with a vapor-phase dope addition are easier to change, and where a range of resistivities are to be supplied from a single reactor, they are essential. The more common of these use commercially available doping gases such as diborane, phosphine, and arsine diluted with hydrogen. The concentration of these gases in hydrogen is usually in the parts-per-million range. They may be

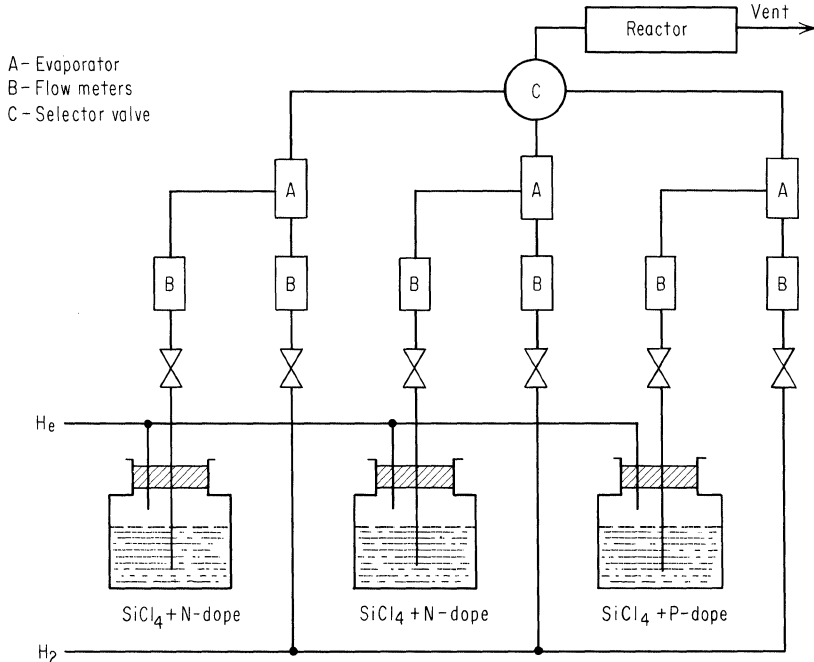


Fig. 4-53. Piping arrangement for liquid doping.

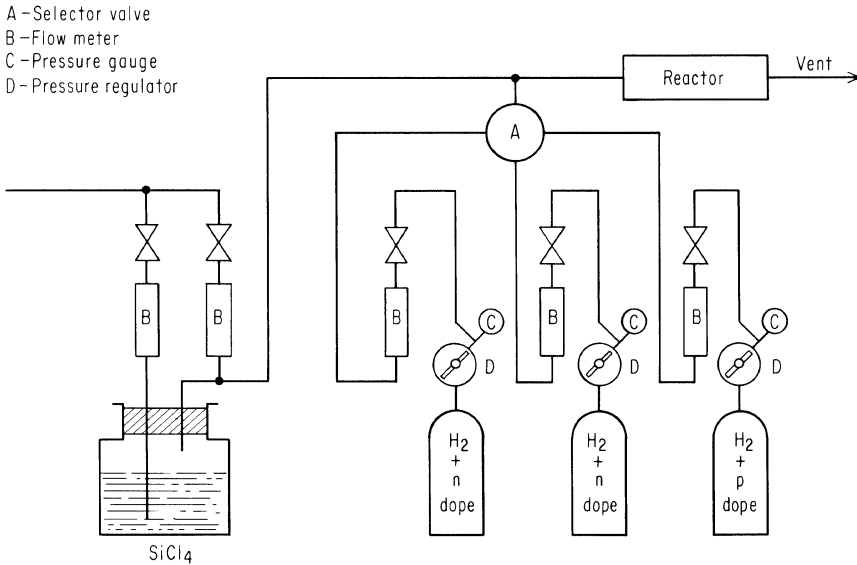


Fig. 4-54. Piping arrangement for gas-phase doping.

fed directly to the reactor or diluted first, depending on the type of flowmeters used and the impurity range desired. Figures 4-53 and 4-54 show plumbing diagrams for these two systems.

Layer Defects. The most common defects appearing in epitaxial layers are dislocations and stacking faults.⁸⁸⁻⁹⁴ For systems that do not use vapor etching, stacking faults and dislocation densities both decrease with increasing deposition temperature and in general follow a curve such as shown in Fig. 4-55. “Tetrahedrons”, such as shown in Fig. 4-56, are a common occurrence if the system is not kept very clean. Their origin has been ascribed to oxide layers and to silicon carbide. If particles from various parts of the reactor settle on the surface during deposition, fast-growing polycrystalline areas usually form. Small quantities of hydrocarbon in the feed stream cause little round silicon carbide balls to form in the layer. Low deposition temperatures usually produce a distinctive surface pattern such as is shown in Fig. 4-57.

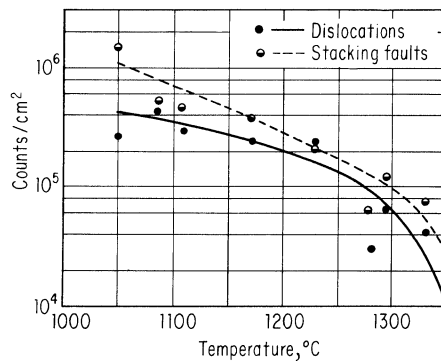


Fig. 4-55. The effect of increased deposition temperature on stacking fault and dislocation density for a non-vapor-etched surface.

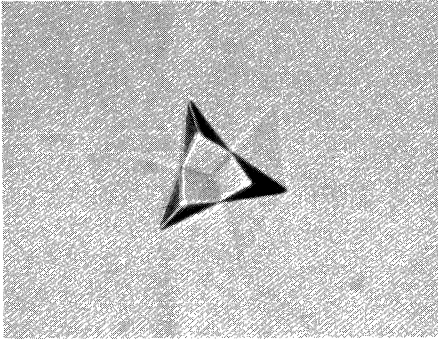


Fig. 4-56. Defect observed in silicon epitaxial layers (magnification approximately $700\times$).

Masking. In order to provide localized epitaxial growth, it is often desired to mask the deposition at some areas on a slice. This may be done either by covering the specified areas of the slice with a material on which silicon will not nucleate, or by covering it with a material that can later be removed, along with any silicon which deposited on it.

Silicon dioxide is very convenient to use as a mask since it can be easily delineated by standard photomask techniques. If the oxide is clean and free from pin holes, silicon nucleation is quite difficult. For example, during a normal cycle little silicon will be deposited on an oxide which is added to the slice *after* insertion into the reactor. Conversely, if the oxide is dirty, or has had a nucleation agent deliberately added, there is usually a uniformly thick layer of silicon grown. In addition, the choice of low flow rates⁹⁵ and reduction of the width of the oxide strips⁹⁶ both reduce the likelihood of nucleation. Figure 4-58 illustrates the difference in the amount of spurious growth which occurs between narrow and wide expanses of oxide. Silicon slices with holes in them, metal masks laying on the surface, and lampblack have also been used to approximately limit deposition, but lack of definition restricts their use.

Silicon Evaporation. It is possible to evaporate silicon in a high vacuum, but if it is deposited on a cold substrate, the layer will be of very high resistivity and apparently amorphous. As the substrate temperature is increased, diffraction

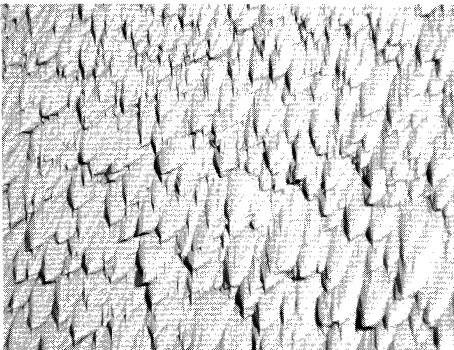
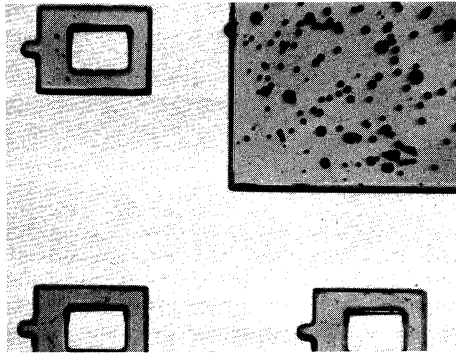


Fig. 4-57. The effect of low deposition temperature on silicon epitaxial surface (magnification approximately $50\times$).

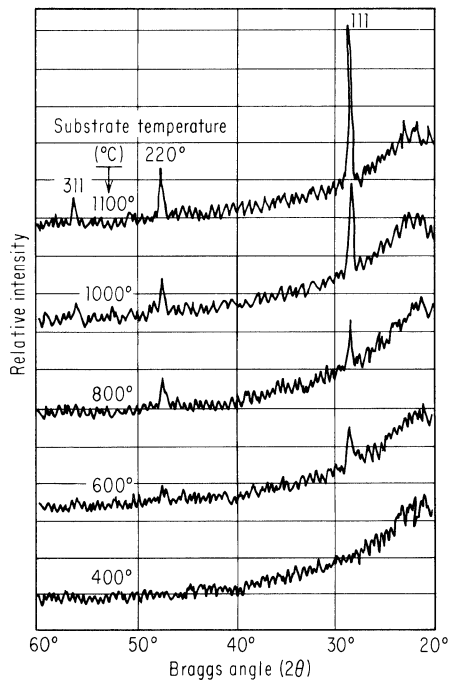
Fig. 4-58. The effect of narrow oxide stripes on spurious nucleation. The smallest rectangles are approximately 5×7 mils.



peaks gradually appear, as shown in Fig. 4-59.⁹⁷ The resistivity of the layer decreases as the temperature of the substrate it is deposited on is raised, and then sometimes goes through another maximum in the temperature range of 800 to 1000°C. The character of this peak seems to be quite dependent on the particular heat treatment given and to the impurity content of the silicon.^{97,98} If the deposition temperature is above about 1100°C and a single crystal silicon substrate is used, the layer appears to be single crystal and can be used for device construction.^{13,99}

Electron beam,^{13,14,100} r-f levitation,⁵² direct ohmic heating,¹⁰¹ and resistance-heated crucibles such as boron nitride⁹⁷ and Al_2O_3 have all been used to vaporize silicon. Most of the systems have been conventional in layout, i.e., the silicon

Fig. 4-59. X-ray diffraction pattern of silicon films vacuum-deposited at the indicated substrate temperatures. (Collins.⁹⁷)



source is separated from the substrate by several inches and has a separate substrate heater. One variation that has been reported is to have the silicon source in the form of a slice separated from the substrate by only a few mils. The complete assembly, silicon source slice, spacer, and silicon substrate is then induction-heated.¹⁰² The quality of film perfection seems to be directly related to the vacuum; 10^{-6} torr is marginal. 10^{-7} and above is to be preferred.

Though film perfection has not yet reached the levels attained by the various vapor reduction processes, there are some advantages to be seen in vacuum depositions. It should, for example, be easier to grow in localized areas by a vacuum deposition. It has been proposed to build microcircuits by the direct deposition of metals by ion beam.¹⁰³ The use of silicon in a programmed beam would even eliminate the need for masks. A vacuum system should have little "dope holdover" and thus can afford rapid change of doping levels or type. Since there is no chemical reaction at the surface, mass transport effects are also eliminated. Major disadvantages at present include complicated equipment, the requirement of very high vacuum, and poor film perfection.

True Epitaxy. Oriented overgrowth of silicon on sapphire, quartz, and germanium substrates has been obtained.¹⁰⁴⁻¹⁰⁶ It is not yet clear whether the crystal perfection and electrical properties will be comparable to more conventionally grown silicon, or if they will be severely degraded because of excessive dislocations and lattice strain.

Polycrystalline Deposits. Polycrystalline silicon deposits have been intentionally made both by vacuum deposition and by vapor decomposition. Some of the films were prepared for use as resistors,^{97,107} but most have been used for device study.¹⁰⁸⁻¹¹⁰ In some instances, such films have been used to make devices similar to those normally constructed of single-crystal material, e.g., solar cells; in others, devices depending on majority carriers were examined; and finally, there have been miniature devices constructed in individual crystallites.

Rheotaxial Growth.^{111,112} In an effort to minimize the effect of a foreign substrate and to enhance the silicon surface mobility so that it may more readily grow as a single-crystal layer, depositions have been made on fluid substrates. The requirements for such a fluid is that it be nonreactive with silicon and with the support material; that its melting point be well above the operating range of any devices to be made; that it be nonconducting when solid; and that its expansion coefficient closely match that of silicon. Various mixtures of Na_2O , MgO , and SiO_2 meet these requirements and have been used on aluminum oxide supports. Silicon has been deposited over the range from 900 to 1200°C, but the most successful temperatures were from 1120 to 1170°C. The film perfection of silicon deposited in this manner is not presently comparable to that deposited on silicon, but it is considerably better than that obtained by direct deposition on the aluminum oxide support.

REFERENCES

1. Saratovkin, D. D.: "Dendritic Crystallization," Consultants Bureau, Inc., New York, 1959.
2. Eagle-Picher Company: "Second Technical Summary Report: Investigation of Inte-

- grally Composed Variable Energy Gap Photovoltaic Solar Energy Converter," Contract DA36-039-SC-85246, 1960.
3. Bolling, G. F., and W. A. Tiller: The Fundamentals of Dendritic Growth, "Metallurgy of Elemental and Compound Semiconductors," vol. 12, Interscience Publishers, Inc., 1961.
 4. Wagner, R. S., and R. G. Treuting: Morphology and Growth Mechanism of Silicon Ribbons, *J. Appl. Phys.*, vol. 32, pp. 2490-2491, 1961.
 5. Buckley, H. E.: "Crystal Growth," John Wiley & Sons, Inc., New York, 1951.
 6. Zerfoss, S. L., R. Johnson, and P. H. Egli: Crystal Growth at High Temperatures, *Trans. Faraday Soc.*, 1949.
 7. Teal, G. K., and J. B. Little: Growth of Germanium Single Crystals, *Phys. Rev.*, vol. 78, p. 647 (A), 1950.
 8. Keck, Levin, Broder, and Lieberman: Crystal Growth by the Tip Fusion Method, *Rev. Sci. Instr.*, vol. 25, p. 298, 1954.
 9. Pfann, W. G.: "Zone Melting," John Wiley & Sons, Inc., New York, 1958.
 10. Petritz, R. L.: Contributions of Materials Technology to Semiconductor Devices, *Proc. IRE*, vol. 50, pp. 1025-1038, 1962.
 11. Medcalf, W. E., and R. H. Fahrig: High-pressure, High Temperature Growth of Cadmium Sulfide Crystals, *J. Electrochem. Soc.*, vol. 105, pp. 719-723, 1958.
 12. Parker, Robert L., and Lawrence M. Kushner: Growth Rates of Zinc Crystals from the Vapor Phase, *J. Chem. Phys.*, vol. 35, pp. 1345-1348, 1961.
 13. Unvala, B. A.: Epitaxial Growth of Silicon by Vacuum Evaporation, *Nature*, vol. 194, pp. 966-967, 1962.
 14. Via, G. G., and R. E. Thur: "Combined Evaporator & Electron Diffraction Apparatus for the Study of Epitaxial Growth," paper presented at the Second International Congress on Vacuum Technology, Washington, D.C., October, 1961.
 15. Van Arkel, Anton Eduard: Manufacture of Bodies from Metals Having a High Melting Point, U.S. Patent 1,601,931, Oct. 5, 1926.
 16. Storks, Keith H., and Gordon Teal: Electrical Translating Materials and Method of Making Them, U.S. Patent 2,441,603, May 18, 1948.
 17. Christensen, H., and G. K. Teal: Method of Fabricating Germanium Bodies, U.S. Patent 2,692,839, Oct. 26, 1954.
 18. Wajda, E. S., and R. Glang: Epitaxial Growth of Silicon p-n Layers from the Vapor Phase, "Metallurgy of Elemental and Compound Semiconductors," vol. 12, Interscience Publishers, Inc., New York, 1961.
 19. Sangster, R. C., E. F. Maverick, and M. L. Croutch: Growth of Silicon Crystals by a Vapor Phase Pyrolytic Deposition Method, *J. Electrochem. Soc.*, vol. 104, pp. 317-319, 1957.
 20. Billig, E.: Growth of Monocrystals of Germanium from an Undercooled Melt, *Proc. Roy. (London) Soc.*, vol. 229, pp. 346-363, 1955.
 21. Shanks, H. R., P. D. Maycock, P. H. Sidles, and G. C. Danielson: Thermal Conductivity of Silicon from 300 to 1300°K, *Phys. Rev.*, vol. 130, pp. 1743-1748, 1963.
 22. Runyan, W. R.: Growth of Large Diameter Silicon and Germanium Crystals by the Teal-Little Method, *Rev. Sci. Instr.*, vol. 30, pp. 535-540, 1959.
 23. Mil'vidskii, M. G., and B. I. Golovin: The Form of the Crystallization Front in Semiconducting Single Crystals Grown from the Melt by the Czochralski Method, *Soviet Phys.-Solid State*, vol. 3, pp. 737-739, 1961.
 24. Gaulé, G. K., and J. R. Pastore: The Role of Surface Tension in Pulling Single Crystals of Controlled Dimensions, "Metallurgy of Elemental and Compound Semiconductors," vol. 12, pp. 201-226, 1961.
 25. Shockley, W.: Crystal Growing Apparatus, U.S. Patent 2,927,008, Mar. 1, 1960.

26. Pfann, W. G.: *Trans. AIME*, vol. 194, p. 747, 1952.
27. Braun, I., and E. Y. Wang: A New Method of Zone Leveling for Materials Having Distribution Coefficients in the Range 0–0.6, *Solid-State Electron.*, vol. 3, pp. 79–90, 1961.
28. Burton, J. A., R. C. Prim, and W. P. Slichter: The Distribution of Solute in Crystals Grown from the Melt. Part I, Theoretical, *J. Chem. Phys.*, vol. 21, pp. 1987–1991, 1953.
29. Kodera, Hiroshi: Diffusion Coefficients of Impurities in Silicon Melt, *J. Appl. Phys. (Japan)*, vol. 2, pp. 212–219, 1963.
30. Hall, R. N.: Segregation of Impurities during the Growth of Germanium and Silicon Crystals, *J. Phys. Chem.*, vol. 57, pp. 836–839, 1953.
31. Hulme, K. F., and J. B. Mullin: Facets and Anomalous Solute Distributions in Indium-antimonide Crystals, *Phil. Mag.*, vol. 4, no. 47, pp. 1286–1288, 1959.
32. Dikhoff, J. A. M.: Cross-sectional Resistivity Variations in Germanium Single Crystals, *Solid-State Electron.*, vol. 1, pp. 202–210, 1960.
33. Mil'vidskii, M. G., and A. V. Berkova: The Development of a Faceting Effect in Silicon Single Crystals during Growth by the Czochralski Method, *Soviet Phys.–Solid State*, vol. 5, pp. 374–377, 1963.
34. Trainor, A., and B. E. Bartlett: A Possible Mechanism of Crystal Growth from the Melt and Its Application to the Problem of Anomalous Segregation at Crystal Facets, *Solid-State Electron.*, vol. 2, pp. 106–114, 1961.
35. Hurle, D. T. J.: Constitutional Supercooling during Crystal Growth from Stirred Melts. I., *Solid-State Electron.*, vol. 3, pp. 37–44, 1961.
36. Kodera, Hiroshi: Constitutional Supercooling during the Crystal Growth of Germanium and Silicon, *J. Appl. Phys., (Japan)*, vol. 2, pp. 527–534, 1963.
37. Tiller, W. A., K. A. Jackson, J. W. Rutter, and B. Chalmers: *Acta Met.*, vol. 1, pp. 428, 1953.
38. Dikhoff, J. A. M.: Inhomogenetics in Doped Germanium and Silicon Crystals, *Philips Tech. Rev.*, vol. 25, pp. 195–206, 1964.
39. Cate, Glen: Personal communication.
40. Runyan, W. R., John W. Ross, and James L. Fischer: Method for Recovery and Reuse of Quartz Containers, U.S. Patent 3,093,456, June 11, 1963.
41. Rusler, G. W.: Crystal Growing Procedure, U.S. Patent 2,892,739, June 30, 1959.
42. Mortimer, G. D.: "Apparatus and Method of Preparing Crystals of the Silicon Germanium Group," U.S. Patent 2,809,136, Oct. 8, 1957.
43. Sparks, M.: Method of Producing Semiconductive Bodies, U.S. Patent 2,727,839, Dec. 20, 1955.
44. Tanenbaum, M.: Semiconductor Crystal Growing, in N. B. Hannay (ed.), "Semiconductors," Reinhold Publishing Corporation, New York, 1959.
45. Sterling, H. F.: Personal communication.
46. Dash, W. C.: Silicon Crystals Free of Dislocations, *J. Appl. Phys.*, vol. 29, p. 736, 1958.
47. Schweickert, H.: Method of Preparing Rod-shaped Crystalline Semiconductor Bodies, U.S. Patent 2,783,168, Feb. 26, 1957.
48. Schweickert, H., and Joachim Haus: Apparatus for Preparing Rod-shaped Crystalline Bodies, Particularly Semiconductor Bodies, U.S. Patent 2,893,847, July 7, 1959.
49. Horn, F. H.: paper presented at Electrochemical Society, 1956.
50. Horn, F. H.: Growth of Uniform Composition Semiconductor Crystals, U.S. Patent 2,904,512, Sept. 15, 1959.
51. Shockley, W., and Richard V. Jones: Crystal Growing Apparatus, U.S. Patent 2,979,386, Apr. 11, 1961.
52. Roth, E. A., E. A. Margerum, and J. A. Amick: Evaporation of Silicon and Germanium by rf Levitation, *Rev. Sci. Instr.*, vol. 33, pp. 686–687, 1962.

53. Sterling, H. F., and R. W. Warren: A Cold Crucible for High-temperature Melting Processes, *Nature*, vol. 192, p. 745, Nov. 25, 1961.
54. Buehler, E., and G. K. Teal: Process for Producing Semiconductive Crystals of Uniform Resistivity, U.S. Patent 2,768,914, Oct. 30, 1956.
55. Hall, R. N.: Semiconductor p-n Junction Units and Method of Making Same, U.S. Patent 2,822,308, Feb. 4, 1958.
56. Hannay, N. B.: Method of Forming Junctions in Silicon, U.S. Patent 2,743,200, Apr. 24, 1956.
57. Leverton, W. F.: Crystal Growing Apparatus and Methods, U.S. Patent 3,025,191, Mar. 13, 1962.
58. Leverton, W. F.: Floating Crucible Technique for Growing Uniformly Doped Crystals, *J. Appl. Phys.*, vol. 29, pp. 1241-1244, 1958.
59. Blackwell, G. R.: A Revised Theory of the Floating Crucible Technique of Crystal Growing, *J. Electron. Control*, vol. 10, pp. 459-463, 1961.
60. Matore, H. F.: General Considerations concerning the Double Crucible Method to Grow Uniformly Doped Germanium Crystals of High Perfection, *Solid-State Electron.*, vol. 6, pp. 163-167, 1963.
61. Teal, G. K.: Method of Producing a Semiconductor, U.S. Patent 2,703,296, Mar. 1, 1955.
62. O'Connor, J. R., and W. A. McLaughlin: Growth of Silicon and Germanium Discs, *J. Appl. Phys.*, vol. 29, p. 222 (L), 1958.
63. Carman, J. N., P. E. Stello, and C. A. Bittmann: Regrowth of Silicon through a Low Melting Zone of Silicon-Gold Eutectic, *J. Appl. Phys.*, vol. 25, p. 543 (L), 1954.
64. Nelson, H.: Epitaxial Growth from the Liquid State and Its Application to the Fabrication of Tunnel and Laser Diodes, *RCA Rev.*, vol. 24, pp. 603-615, 1963.
65. Wagner, R. S., and W. C. Ellis: Vapor-Liquid-Solid Mechanism of Single Crystal Growth, *Appl. Phys. Letters*, vol. 4, pp. 89-90, 1964.
66. New Mechanism Used to Grow Crystals, *Chem. Eng. News*, pp. 48-49, vol. 42, Mar. 16, 1964.
67. Theuerer, H. C., J. J. Kleimack, H. H. Loar, and H. Christensen: Epitaxial Diffused Transistors, *Proc. IRE*, vol. 48, pp. 1642-1643, 1960.
68. Theuerer, H. C.: Epitaxial Silicon Films by Hydrogen Reduction of SiCl_4 , *J. Electrochem. Soc.*, vol. 108, pp. 649-653, 1961.
69. Mark, Albert: Single Crystal Silicon Overgrowths, *J. Electrochem. Soc.*, vol. 108, pp. 880-885, 1961.
70. Tung, S. K.: The Influence of Process Parameters on the Growth of Epitaxial Silicon, in John B. Schroeder (ed.), "Metallurgy of Semiconductor Materials," pp. 87-107, Interscience Publishers, Inc., 1962.
71. Li, C. H.: Epitaxial Growth of Silicon, *J. Electrochem. Soc.*, vol. 109, pp. 952-957, 1962.
72. Bylander, E. G.: Kinetics of Silicon Crystal Growth from SiCl_4 Decomposition, *J. Electrochem. Soc.*, vol. 109, pp. 1171-1175, 1962.
73. Deal, Bruce E.: Epitaxial Deposition of Silicon in a Hot-tube Furnace, *J. Electrochem. Soc.*, vol. 109, pp. 514-517, 1962.
74. Runyan, W. R.: "Methods of Minimizing the Effects of Diffusion during Silicon Epitaxial Deposition," paper presented at the Fall Meeting of the Electrochemical Society, 1963.
75. Tung, S. K.: "The Effects of Substrate Orientation on Epitaxial Silicon Growth," paper presented at the Fall Meeting of the Electrochemical Society, 1963.
76. Steinmaier, W.: Thermodynamical Approach to the Growth Rate of Epitaxial Silicon from SiCl_4 , *Philips Res. Rept.*, vol. 18, pp. 75-81, 1963.
77. Monchamp, R. R., W. J. McAleer, and P. I. Pollak: A Kinetic Study of the System Si-SiCl_4 , *J. Electrochem. Soc.*, vol. 111, pp. 879-881, 1964.

78. Charig, J. M., and B. A. Joyce: Epitaxial Growth of Silicon by Hydrogen Reduction of SiHCl_3 onto Silicon Substrates, *J. Electrochem. Soc.*, vol. 109, pp. 957-962, 1962.
79. Miller, K. J., and M. J. Grieco: Epitaxial P-Type Germanium and Silicon Films by the Hydrogen Reduction of GeBr_4 , SiBr_4 , and BBr_3 , *J. Electrochem. Soc.*, vol. 110, pp. 1-5, 1963.
80. Glang, R., and E. S. Wajda: Status of Vapor Growth in Semiconductor Technology, in John B. Schroeder (ed.), "Metallurgy of Semiconductor Materials," pp. 27-47, Interscience Publishers, Inc., New York, 1962.
81. Joyce, B. A., and R. R. Bradley: Epitaxial Growth of Silicon from the Pyrolysis of Monosilane on Silicon Substrates, *J. Electrochem. Soc.*, vol. 110, pp. 1235-1240, 1963.
82. Bhola, S. R., and A. Mayer: Epitaxial Deposition of Silicon by Thermal Decomposition of Silane, *RCA Rev.*, vol. 24, pp. 511-522, 1963.
83. Mayer, S. E., and D. E. Shea: Epitaxial Deposition of Silicon Layers by Pyrolysis of Silane, *J. Electrochem. Soc.*, vol. 111, pp. 550-556, 1964.
84. Thomas, C. O., D. Kahng, and R. C. Manz: Impurity Distribution in Epitaxial Silicon Films, *J. Electrochem. Soc.*, vol. 109, pp. 1055-1060, 1962.
85. Nuttall, R.: The Dependence on Deposition Conditions of the Dopant Concentration of Epitaxial Silicon Layers, *J. Electrochem. Soc.*, vol. 111, pp. 317-323, 1964.
86. Bean, Kenneth E., and Paul S. Gleim: "Vapor Etching prior to Epitaxial Deposition of Silicon," paper presented at the Fall Meeting of the Electrochemical Society, 1963.
87. Lang, G. A., and T. Stavish: Chemical Polishing of Silicon with Anhydrous Hydrogen Chloride, *RCA Rev.*, vol. 24, pp. 488-498, 1963.
88. Miller, D. P., S. B. Watelski, and C. R. Moore: Structure Defects in Pyrolytic Silicon Epitaxial Films, *J. Appl. Phys.*, vol. 34, pp. 2813-2821, 1963.
89. Chu, T. L., and J. R. Gavaler: A Structural Imperfection in Vapor-grown Silicon, *Phil. Mag.*, ser. 8, vol. 9, pp. 993-1002, 1964.
90. Mendelson, S.: Stacking Fault Nucleation in Epitaxial Silicon on Various Oriented Silicon Substrates, *J. Appl. Phys.*, vol. 35, pp. 1570-1581, 1964.
91. Batsford, K. O., and D. J. D. Thomas: Defects in Vapour-grown Silicon Layers, *Elec. Commun.*, vol. 38, pp. 354-362, 1963.
92. Schwuttke, G. H., and V. Sils: X-ray Analysis of Stacking Fault Structures in Epitaxially Grown Silicon, *J. Appl. Phys.*, vol. 34, pp. 3127-3134, 1963.
93. Batsford, K. O., and D. J. D. Thomas: "Solid-state Electronics," vol. 5, pp. 353-360, Pergamon Press, New York, 1962.
94. Charig, J. M., B. A. Joyce, D. J. Stirland, and R. W. Bicknell: Growth Mechanism and Defect Structures in Epitaxial Silicon, *Phil. Mag.*, vol. 7, pp. 1847-1860, 1962.
95. Joyce, B. D., and J. A. Baldrey: Selective Epitaxial Deposition of Silicon, *Nature*, vol. 195, pp. 485-486, 1962.
96. Schnable, G. L., W. J. Hillegas, Jr., and C. G. Thornton: "Preferential Silicon Epitaxy with Oxide Masking," paper presented at the Fall Meeting of the Electrochemical Society, 1963.
97. Collins, F. M.: Vacuum Evaporated Silicon Films, "Transactions of the Eighth Vacuum Symposium," pp. 899-904, Pergamon Press, New York, 1962.
98. Kataoka, Yukua: Some Properties of Evaporated Silicon Films, *J. Phys. Soc. Japan*, vol. 17, pp. 967-969, 1962.
99. Hale, A. P.: Preparation and Evaluation of Epitaxial Films Prepared by Vacuum Evaporation, *Vacuum*, vol. 13, pp. 93-100, 1963.
100. Richard, M.: Silicon Evaporation in Vacuo, *Le Vide*, vol. 18, no. 104, pp. 100-102, 1963.

101. Kilgore, Ben F., and Richard W. Roberts: Preparation of Evaporated Silicon Films, *Rev. Sci. Instr.*, vol. 34, pp. 11–12, 1963.
102. Handelman, E. T., and E. I. Povilonis: Epitaxial Growth of Silicon by Vacuum Sublimation, *J. Electrochem. Soc.*, vol. 111, pp. 201–206, 1964.
103. Flynt, W. E.: Research on an Ion Beam Deposition System for Microcircuit Fabrication, "Proceedings, Third Symposium on Electron Beam Technology, Boston, March 1961," Alloyd Electronics Corp., Cambridge, Mass., 1961.
104. Mamasevity, H. M., and W. I. Simpson: Single Crystal Silicon on a Sapphire Substrate, *J. Appl. Phys.*, vol. 35, pp. 1349–1351, 1964.
105. Bicknell, R. W., J. M. Charig, B. A. Joyce, and D. J. Stirland: The Epitaxial Deposition of Silicon on Quartz, *Phil. Mag.*, vol. 9, pp. 965–978, 1964.
106. Newman, R. C., and J. Wakefield: Vapor Growth of Germanium-Silicon Alloy Films on Germanium Substrates, *J. Electrochem. Soc.*, vol. 110, pp. 1068–1071, 1963.
107. "Semiconductor Resistive Element," Texas Instruments Incorporated, Final Report, NObsr-854406, 1962.
108. Heaps, J. D., O. N. Tuttle, and A. Nussbaum: Vapor-deposited Polycrystalline Silicon Solar Cells, *IRE Trans. Electron Devices*, vol. ED-8, p. 560, 1961.
109. Bylander, E. G., and M. M. Mitchell: Progress on the Vapor Growth of Silicon p-n Junctions on Insulating Substrates, paper presented at the AIME Conference, Pittsburgh, Pa., Aug. 28, 1962.
110. Bylander, E. G., and R. J. Murphy: Formation of Tunnel Diodes in Vapor-deposited Silicon Microcrystals, *Proc. IEEE*, vol. 51, p. 228 (L), 1963.
111. Rasmanis, E.: Thin Film p-n Junction Silicon Devices, *Semiconductor Products*, June, 1963.
112. Rasmanis, E.: Deposition of Device-quality Silicon Films on a Fluid Surface, paper presented at the Spring Meeting of the Electrochemical Society, 1963.

5

Crystal Habit and Orientation

5-1. CRYSTAL SYSTEMS^{1,*}

Crystals are characterized by an orderly array of their atoms; that is, an arrangement which recurs regularly throughout the crystal. This can be visualized by considering that the whole crystal is composed of a series of little parallelepipeds stacked so that there is no space between them. Each of these boxes may contain many atoms in some peculiar configuration; but for a particular crystal, all boxes and their contents are identical. The corners of the boxes are defined as space-lattice points and each have identical surroundings. In other words, an observer has no way to distinguish one point from another. It can be shown that there are only 14 ways to place the points and construct the parallelepipeds so that they are stacked face-to-face with no gaps.

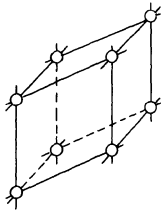
These 14 constructions are usually grouped into seven crystal systems according to the relative length of the three axes and the angles between these axes. These systems are described as follows:

1. *Cubic*. Three equal lengths, mutually perpendicular axes.
2. *Tetragonal*. Three mutually perpendicular axes with two of the axes of equal length.
3. *Orthorhombic*. Three mutually perpendicular, unequal length axes.
4. *Hexagonal*. Three coplanar axes of equal length making a 120° angle with each other and a fourth axis of different length perpendicular to the others; or, two equal length axes making a 120° angle with each other and perpendicular to a third of different length.
5. *Monoclinic*. Three unequal length axes, two of which are perpendicular.
6. *Rhombohedral*. Three equal length axes, having equal, but not 90° , angles.
7. *Triclinic*. Three unequal length axes not at right angles to each other.

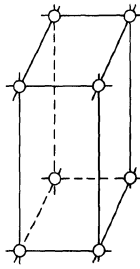
Each of these classes is shown in Fig. 5-1.

The various planes that pass through the crystal are described in terms of Miller indices. These are defined as the reciprocals of the intercepts of the plane in question with the three crystallographic axes. These reciprocals are usually

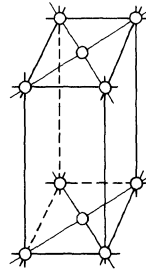
* Superscript numbers indicate items listed in References at the end of the chapter.



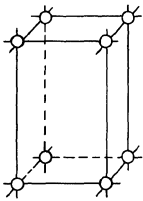
Triclinic



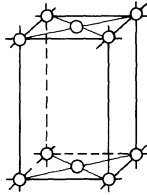
Simple monoclinic



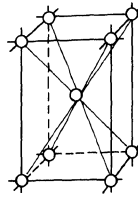
Base-centered monoclinic



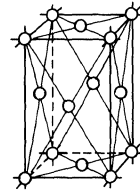
Simple orthorhombic



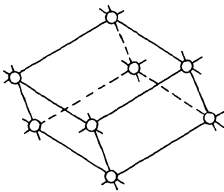
Base-centered orthorhombic



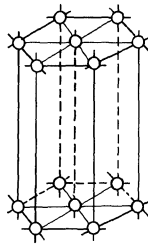
Body-centered orthorhombic



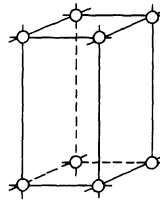
Face-centered orthorhombic



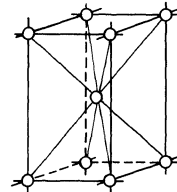
Rhombohedral



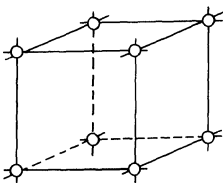
Hexagonal



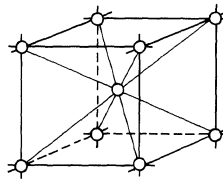
Simple tetragonal



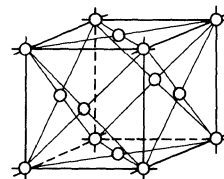
Body-centered tetragonal



Simple cubic



Body-centered cubic



Face-centered cubic

Fig. 5-1. Crystal systems. (From "Mineralogy," 5th ed., by Kraus, Hunt, and Ramsdell. Copyright, 1959. McGraw-Hill Book Company. Used by permission.)

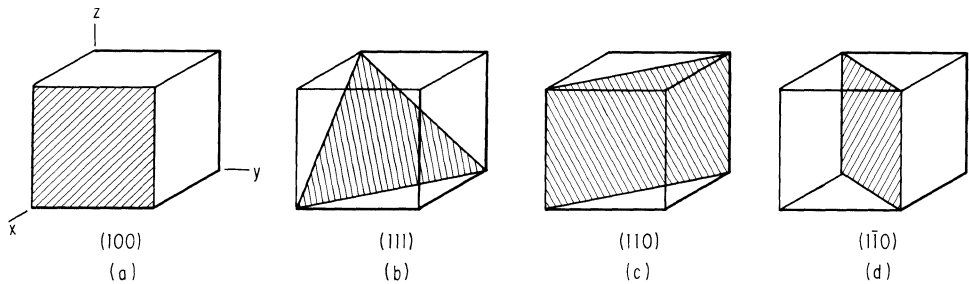


Fig. 5-2. Low indices planes.

expressed as the smallest possible integers having the same ratio and are written as (hkl) . This is illustrated in Fig. 5-2 for the three more common planes.

EXAMPLE 5-1. What are the Miller indices of a plane which cuts the x axis at $\frac{1}{2}$, the y axis at 2, and is parallel with the z axis? The intercepts are $\frac{1}{2}$, 2, ∞ ; the reciprocals are 2, $\frac{1}{2}$, 0; cleared of fractions, the reciprocal ratios become 4, 1, 0, so the Miller indices are (410) .

From the definition of Miller indices just given, a (200) plane, for example, would not be allowed since it could be reduced and expressed as (100) . However, present usage sometimes permits higher-order indices. The lowest-order indices are used to designate the planes forming the boundaries of the unit cell. Thus, in Fig. 5-3,² atoms 1, 2, 4, 5, and 6 would be included in a (100) plane. However, the plane parallel to it and passing through atoms 7, 8, 9, and 10 is a (200) plane. On a gross scale no difference between the two can be detected, so that from a crystallographer's point of view, the original definition is quite adequate. It is only when atomic examinations are made that such distinctions are required.

For cubic crystals of single elements, e.g., silicon, the (100) , the (010) , and the (001) planes are indistinguishable, as are the (110) , the (101) , and the (011) planes.

In the event that a plane crosses an axis on the minus side of the origin, that intercept is written with a bar over it. Figure 5-2*d* illustrates a $(1\bar{1}0)$ plane. If it had crossed both the a and the b axes on the minus side, then it would have been parallel to a (110) plane and may be written as such. In order to indicate a full family of equivalent faces, for example, the group (100) , (010) , (001) , $(\bar{1}00)$, $(0\bar{1}0)$, $(00\bar{1})$; the notation $\{100\}$ is used.

Since the crystal is made up of a large number of atoms arranged repetitively, there will be a multitude of parallel and equally spaced (hkl) planes throughout the crystal. If a is the separation of the "corner" atoms, the spacing of any set of planes in the cubic lattice is given by:³

$$d_{hkl} = \frac{a}{(h^2 + k^2 + l^2)^{1/2}} \quad (5-1)$$

$$a_{\text{silicon}} = 5.42 \text{ \AA} = 5.42 \times 10^{-8} \text{ cm}$$

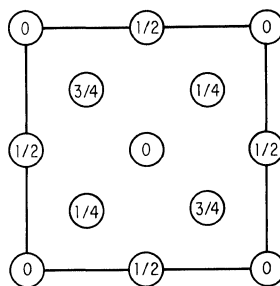
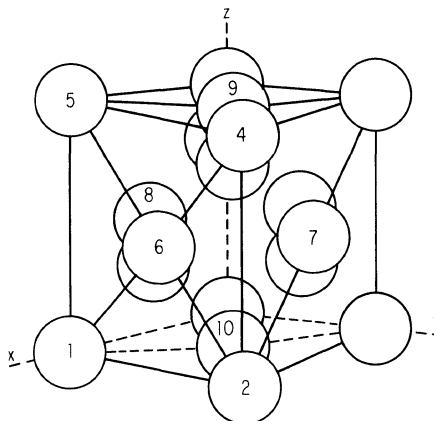


Fig. 5-3. Diamond lattice. (Wyckoff:²)



Spacing of some of the low-indices silicon planes is given in Table 5-1.

The equation for a plane is

$$\frac{h}{a}x + \frac{k}{b}y + \frac{l}{c}z = \text{const}$$

Since silicon is cubic, $a = b = c$, and the equation reduces to

$$hx + ky + lz = \text{const}$$

Two planes hkl and $h'k'l'$ intersect in a line $[uvw]$, and it can be shown that

$$u = \begin{vmatrix} kl \\ k'l' \end{vmatrix} \quad v = \begin{vmatrix} lh \\ l'h' \end{vmatrix} \quad w = \begin{vmatrix} hk \\ h'k' \end{vmatrix}$$

A zone axis is a line (plane edge) parallel to all planes within that particular zone. Thus a $[100]$ zone includes all planes passing through a $[100]$ line and would be the family $(0kl)$.

Table 5-1

d_{100}	5.42 Å
d_{110}	3.83 Å
d_{111}	3.13 Å
d_{123}	1.56 Å

The angle α between any two planes (hkl) and $h'k'l'$ is given by:³

$$\cos \alpha = \frac{hh' + kk' + ll'}{\sqrt{(h^2 + k^2 + l^2)(h'^2 + k'^2 + l'^2)}} \quad (5-2)$$

EXAMPLE 5-2. The angle between a (110) and a (111) plane is given by:

$$\begin{aligned} \cos \alpha &= \frac{1 + 1 + 0}{\sqrt{(1 + 1 + 1)(1 + 1)}} = \frac{2}{\sqrt{6}} \\ \alpha &= 35.26^\circ \end{aligned}$$

A tabulation of angles between some common planes is given in Table 5-2.*

The indices of a direction through the crystal are determined by:

1. Considering that travel starts at the origin and is to go through some point p in the lattice.
2. Reaching that point by going a distance u along the x axis, a distance v parallel to the y axis, and a distance w parallel to the z axis.
3. Expressing ratio of $u:v:w$ as the smallest possible set of integers $h:k:l$. These are the direction indices and are written as $[hkl]$. A complete set of equivalent directions is written as $\langle hkl \rangle$.

For a cubic system, a direction will always be perpendicular to a plane with the same indices, but in other systems this is not generally true.

5-2. SILICON STRUCTURE

Silicon belongs to the cubic crystal system and has a diamond structure.² This is characterized by having each atom symmetrically surrounded by four equally spaced neighbors. Figure 5-3 shows an isometric and a planar view of the position of the atoms with respect to the crystal axes x , y , and z . The number in each circle is the distance that particular atom lies below the plane of the paper. Another way of visualizing the atom's position is to consider the lattice as two interwoven face-centered cubes with the origin of one displaced $\frac{1}{4}$, $\frac{1}{4}$, $\frac{1}{4}$ from the other. This is shown in Fig. 5-4. We can extend Fig. 5-3 as shown in Fig. 5-5. Neither Fig. 5-3 nor 5-4 shows the location of the bonds between atoms that hold the crystal together. Figure 5-6a shows the complete bonding for one atom, while Fig. 5-6b shows the same atoms as in Fig. 5-3, but with bonds drawn in.⁴

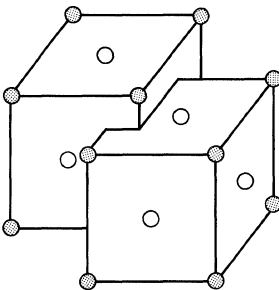


Fig. 5-4. Diamond lattice shown as two interwoven face-centered cubes.

Examination of Figs. 5-3 to 5-6 shows that the atoms combine to form well-defined sheets with spacing between the sheets varying according to their orientation. For example, looking down upon a (001) face (Fig. 5-3), there are three sheets of atoms equally spaced between consecutive (100) planes. Figure 5-7 shows these spacings and some of the others to be observed while looking in the [001] direction.

* A more complete listing may be found in Peavler and Lenusky, "Angles between Planes in Cubic Crystals," IMD Special Report, no. 8, American Institute of Mining, Metallurgical and Petroleum Engineers.

Table 5-2. Angles between Crystallographic Planes (and between Crystallographic Directions) in Crystals of the Cubic System

{HKL}	{hkl}	Values of angles between HKL and hkl planes (or directions)					
100	100	0.00	90.00				
	110	45.00	90.00				
	111	54.74					
	210	26.56	63.43	90.00			
	211	35.26	65.90				
	221	48.19	70.53				
	310	18.43	71.56	90.00			
110	311	25.24	72.45				
	110	0.00	60.00	90.00			
	111	35.26	90.00				
	210	18.43	50.77	71.56			
	211	30.00	54.74	73.22	90.00		
	221	19.47	45.00	76.37	90.00		
	310	26.56	47.87	63.43	77.08		
111	311	31.48	64.76	90.00			
	111	0.00	70.53				
	210	39.23	75.04				
	211	19.47	61.87	90.00			
	221	15.79	54.74	78.90			
	310	43.09	68.58				
	311	29.50	58.52	79.98			
210	210	0.00	36.87	53.13	66.42	78.46	90.00
	211	24.09	43.09	56.79	79.48	90.00	
	221	26.56	41.81	53.40	63.43	72.65	90.00
	310	8.13	31.95	45.00	64.90	73.57	81.87
	311	19.29	47.61	66.14	82.25		
211	211	0.00	33.56	48.19	60.00	70.53	80.40
	221	17.72	35.26	47.12	65.90	74.21	82.18
	310	25.35	40.21	58.91	75.04	82.58	
	311	10.02	42.39	60.50	75.75	90.00	
221	221	0.00	27.27	38.94	63.61	83.62	90.00
	310	32.51	42.45	58.19	65.06	83.95	
	311	25.24	45.29	59.83	72.45	84.23	
310	310	0.00	25.84	36.87	53.13	72.54	84.26
	311	17.55	40.29	55.10	67.58	79.01	90.00
311	311	0.00	35.10	50.48	62.96	84.78	

5-3. CRYSTAL HABIT

Silicon belongs to the hexoctahedral class, and the preferred growth habit is octahedral (Fig. 5-8), i.e., bounded by the family of {111} planes. Usually, however, externally imposed constraints prevent well-defined faces from forming. Crystals grown from the vapor usually have the fewest of these constraints and often develop rather large facets. Small octahedrons sometimes are to be observed from nucleation on oxide during selective epitaxial depositions. In the manufac-

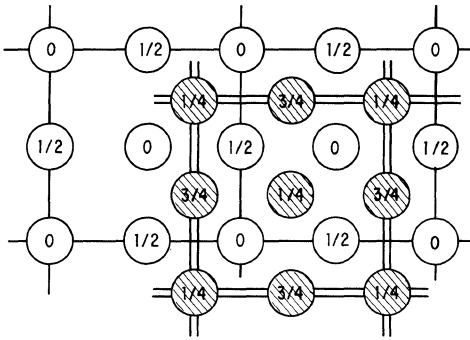


Fig. 5-5. Two face-centered cubes combined to form a diamond lattice.

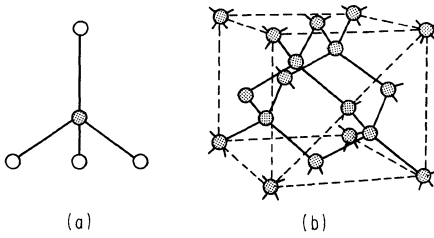


Fig. 5-6. Location of silicon bonds. (Shockley.⁴)

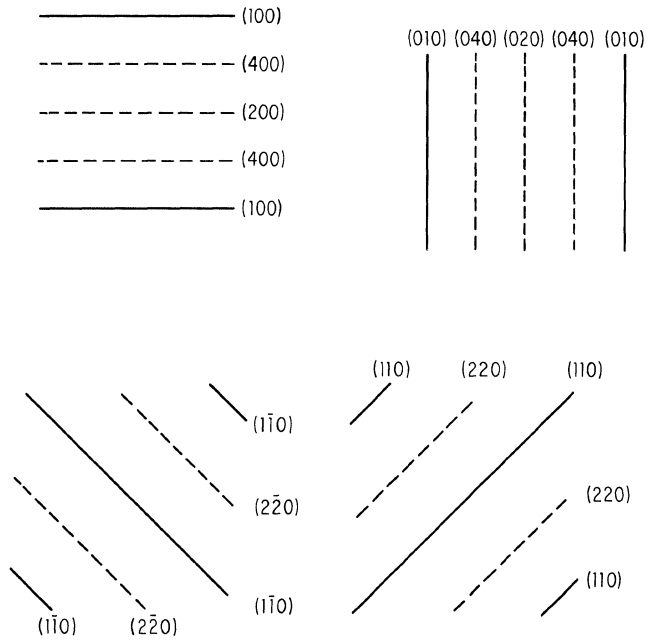


Fig. 5-7. Intercepts of atomic sheets with (001) plane.

ture of bulk silicon, large, beautiful single crystals sometimes grow out from the furnace walls (see Fig. 5-9). In this case, the constraint appears to be one of a silicon-halide concentration gradient in the feed stream which promotes a length increase. Crystals grown in this fashion invariably have the long axis in the $[111]$ direction.

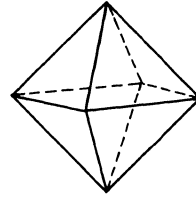


Fig. 5-8. Octahedron.

Occasionally, single crystals will form on the surface of a pool of molten silicon. These are almost always flat, regular six-sided platelets bounded by $\{111\}$ planes. If a small amount of molten silicon is extruded from a crack in an otherwise frozen ingot, single crystals sometimes form and are usually octahedral.

Though thermal gradients in the melt allow little face development in crystals grown from the melt, there are vestiges which always occur and give characteristic markings to crystals grown in different crystallographic directions. In general, the smaller the thermal gradient, the better developed the faces will be. Figure 5-10 shows the effect of radial thermal gradients on the top of crystals grown in the $[100]$ direction. The crystal on the left was grown in a melt with a very small radial gradient so that its shape was determined primarily by the slow growing (111) faces. The middle crystal is intermediate, and the one on the right was grown in such a manner that the thermal gradients completely determined its shape.

If the crystal is grown in the $[111]$ direction, and if the top is quite flat, the (111) plane perpendicular to the growth direction will be exposed and there will be large "flats" visible, such as the flat which corresponds to face 1 of the octahedron of Fig. 5-11a. If the crystal is growing out at an angle near 70° to the melt surface, (111) planes corresponding to faces 2, 3, and 4 will each be tangent to the growing conical crystal at one place, and about each of these points, portions of the planes will grow and produce small flats. If the crystal is then tapered in at the bottom with the same angle, three more faces of the octahedron will be tangent and will produce flats. In the octahedron of Fig. 5-11b, one of these faces is labeled "5." The other two are not visible. Note that the flats produced on the bottom are rotated 60° from those appearing on the top. It is also possible to grow the crystal top nearly flat and have all six of the (111) planes just discussed form ridges or flats on the crystal top. The ridges apparently form when planes

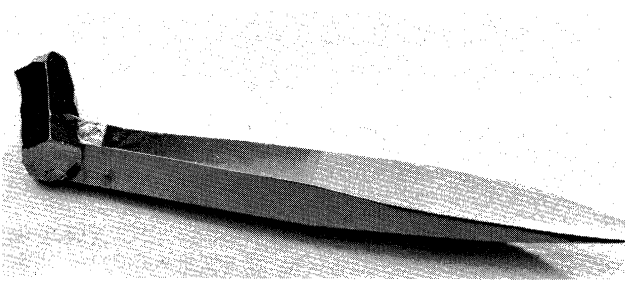


Fig. 5-9. Single silicon crystal grown from vapor phase (length, approximately 3.5 in.).

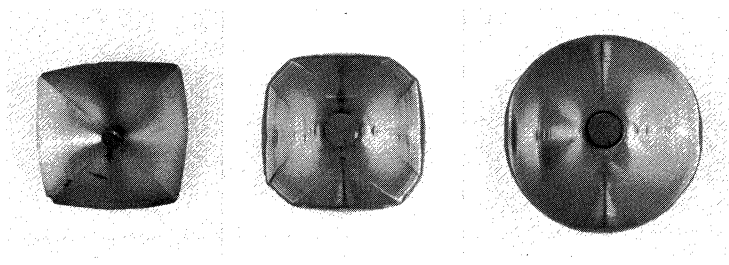


Fig. 5-10. The effect of thermal gradients in the melt on crystal shape.

2, 3, 4, 5, 6, and 7 are trying to grow and intersect planes 1 or 8 (the horizontal ones) which are also growing out into the melt.

When the crystal is grown as a right circular cylinder, there are three equally spaced flats extending down the side. Each of these is a succession of small {111} growth planes intersecting the surface of the crystal and presenting a shingled appearance as they progress down the crystal. The gross effect is that of a somewhat rough (110) plane extending down the crystal. Planes cutting the crystal parallel with the direction of growth and along the ribs are {110}. Planes cutting the crystal parallel with the direction of growth and midway between the ribs are {211}. These various configurations are shown in Fig. 5-12.

If a crystal is grown from the melt in a [100] direction, the top will be squarish and normally have four equally spaced ribs extending radially out from the seed. These will extend down the sides of the crystal as flats. However, where the transition is made from top to side growth, there will be flats developing instead of normal ribs. In the event that the crystal is grown cone-shaped, and if the angle the cone makes with the plane of growth is approximately 54° [coinciding with the angle a (111) plane makes with a (100) plane], flats will extend the full length of the cone. Since {110} planes are perpendicular to some (111) and (100) planes, it follows that a plane cutting the crystal along the ribs and perpendicular to the plane of growth is a (110) plane. It further follows that other (100) planes cut the crystal along the diagonals of the square top. These details are shown in Fig. 5-13.

EXAMPLE 5-3. Find the position of marking (either flats or ridges) down the sides of a crystal grown in the [112] direction.

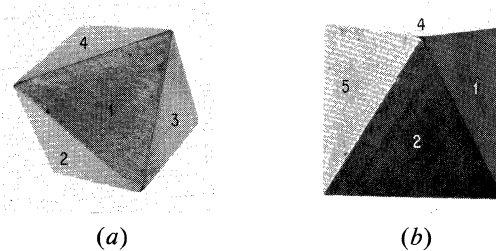


Fig. 5-11. Views of octahedrons.

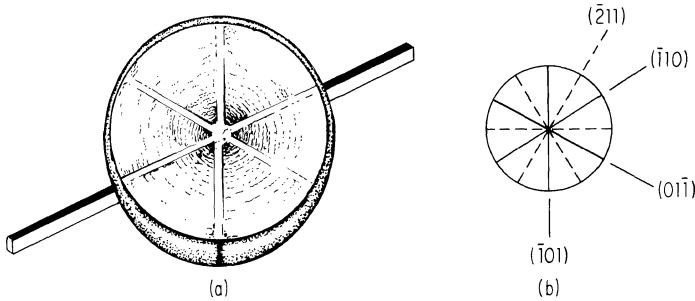


Fig. 5-12. Views of various planes cutting a crystal grown in $[111]$ direction.

SOLUTION. In general, it can be concluded that markings will occur on the growing crystal only where (111) planes are tangent to the periphery of the melt-crystal interface. Thus, find the trace of (111) planes on the (112) growth plane. Then, where these lines are tangent to a circle representing the crystal cross section, marks will appear.

5-4. ROUGH ORIENTATION

If a crystal of some orientation has been grown, how does one choose the proper cutting direction in order to expose a particular plane?

One method is to grow the crystal in the $[100]$ direction, then cut it into a cube with the (100) faces exposed as illustrated in Fig. 5-13. Next, mark the desired intercepts on the three edges and cut accordingly.

EXAMPLE 5-4. To expose a (123) face: Since the Miller indices are the reciprocals of the intercepts, the plane must cut the x axis at unit distance, the y axis at $\frac{1}{2}$ unit, and the z axis at $\frac{1}{3}$ unit. The unit length is quite arbitrary since any length chosen will give a plane parallel to that described by any other unit length. This process is shown in Fig. 5-14.

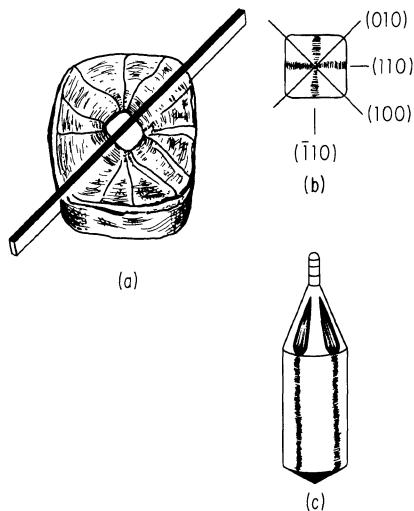


Fig. 5-13. Views of various planes cutting a crystal grown in $[100]$ direction.

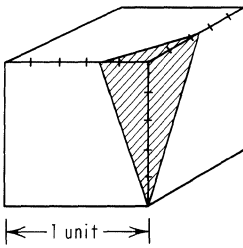


Fig. 5-14. A (123) plane exposed by cutting off a corner of a cube bounded by {100} planes.

Another useful method is to calculate the angle the required plane makes with two planes already known in the crystal. Then, if the desired plane should make an angle of 90° with one of these two reference planes, orienting and sawing are quite simple.

EXAMPLE 5-5. To expose a (311) plane: A check of Table 5-2 shows that this plane is perpendicular to one of the {110} family. Since it is easy to locate (110) faces in a crystal grown in the [111] direction (see Fig. 5-12), use such a crystal as starting material. Table 5-2 also lists a series of values for the angle between (311) and (111) planes. These numbers cover the whole family of planes {111} so that care must be taken to choose the correct one. The application of Eq. (5-2) shows that the (311) plane is perpendicular to the (01 $\bar{1}$) plane, and that the (01 $\bar{1}$) plane is perpendicular to a (111) plane. Accordingly, the required angle is that between the (311) plane and the (111) plane (29.5°). The crystal is mounted on a horizontal sawing block with one set of ribs vertical. A cross cut making an angle of 29.5° with the vertical will expose the desired (311) plane. This is shown in Fig. 5-15.

The crystal is mounted on a horizontal sawing block with one set of ribs vertical. A cross cut making an angle of 29.5° with the vertical will expose the desired (311) plane. This is shown in Fig. 5-15.

5-5. X-RAY ORIENTATION

The methods described in the previous section make it possible to estimate to within a few degrees the orientation of a cut. However, it is often necessary to cut slices or expose faces that are accurately oriented to within a few minutes and to check with similar accuracy the orientation of already cut slices.

There are two methods normally used. One is by measuring the Bragg angle from the desired plane and comparing it to the cut face; another is an optical method dependent on light reflections from etch figures in the silicon surface.

If an X-ray beam impinges on a crystal, it will be scattered by the various atoms it strikes in the crystal. Normally, the scattering will be random, but if a proper relation is established between the geometry of the incoming beam and the atomic arrangement, then in-phase or coherent scattering will occur. In particular it can be shown that if a parallel, monochromatic X-ray beam of wavelength λ strikes a crystal in such a manner that the grazing angle of incidence θ and the spacing d between the planes of atoms follow the relation $n\lambda = 2d \sin \theta$, where n is an integer, the beam will appear to be reflected at the same angle. This angle is called the Bragg angle. The derivation of this expression may be found in any standard text on X-rays, such as "X-rays in Practice" by Wayne T. Sproul. However, the qualitative explanation is as follows: If the length of the path of the portion of the beam reflected from two adjacent planes differs by an integral number of wave-

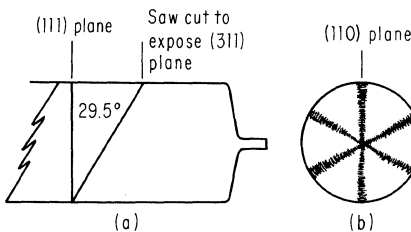
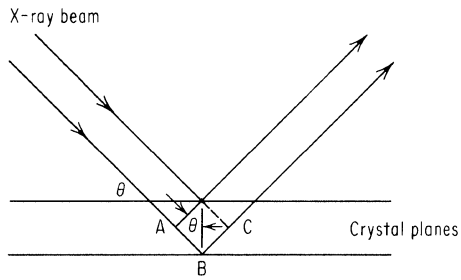


Fig. 5-15. Method of cutting a (311) plane from a crystal grown in the <111> direction.

Fig. 5-16. Geometry for X-ray diffraction.



lengths, then the two portions will be in phase and will add. If any other path length occurs, then partial or complete cancellation will occur. The condition for the path lengths to differ by a full wavelength is seen from Fig. 5-16 to be that which makes the distance ABC equal to the wavelength. Thus

$$\lambda = 2d \sin \theta \tag{5-3}$$

or

$$\theta = \frac{\lambda}{2d}$$

If the wavelength of the X rays used and the spacing of the desired plane are known, the angle at which coherent scattering or “reflection” is expected can be calculated. Then, if an arrangement such as is shown in Fig. 5-17 is used, the source and detector may be set at the proper angles and the surface of the crystal rocked until a maximum occurs. It follows that the desired crystallographic plane makes an angle θ with the beam and thus lies along the reference plane A . If the surface of the crystal does not also lie in this plane, then it is misoriented by the difference between itself and the reference plane.

Various manufacturers, such as G.E. and Philips, make X-ray equipment expressly designed for orientation work. In these, the detector may be set at twice the Bragg angle, and the crystal holder slowly rotated (usually by hand) about one axis only. If the crystal is badly misoriented, it is conceivable that the X-ray maximum cannot be found since no amount of adjustment about one axis can bring a randomly oriented plane into position to reflect into the detector. Some latitude is built into the machines, however, in that the detector usually has a slit or line aperture so that if the beam is deflected slightly to the side, it may still be found. The observed angle will not, however, be the correct one.

Normally, an auxiliary holder is added which allows the crystal to be rotated about two axes so that a true maximum can be found and the alignment more

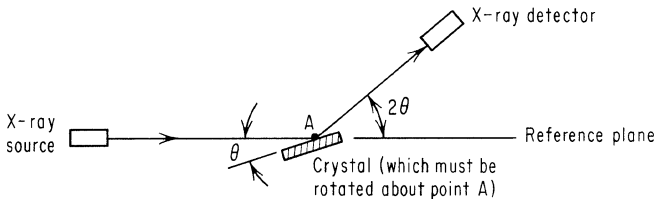


Fig. 5-17. X-ray crystal orientation.

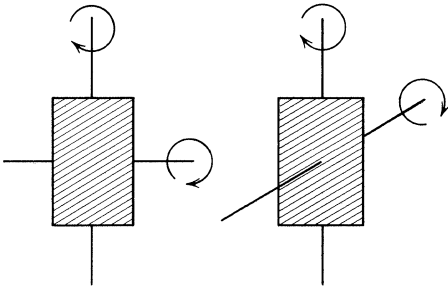


Fig. 5-18. Methods of rotating crystal holder.

accurately performed. Two ways of effecting the added degree of freedom of the holder are shown in Fig. 5-18. They are equivalent so a choice can be made on the basis of ease of mechanical construction.

Orientation for sawing can be done either by building a combination crystal jig which can be used in both the X-ray machine and the saw, or by having a sawing jig only. The latter is simpler to construct, but requires the cutting of a test slice, checking the slice orientation, and then making the required corrections.

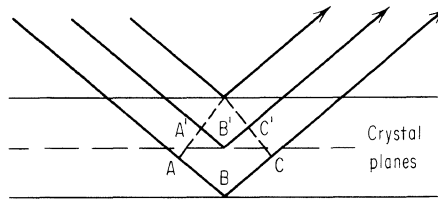
Some types of crystals, such as silicon, have atoms interspersed between the major crystallographic planes. For example, reference to Fig. 5-3 shows that (100) planes do not include the atoms inside the box. These extra atoms sometimes scatter X rays in such a manner as to prevent a maximum from occurring at the expected Bragg angle. This can be visualized by imagining a sheet of atoms spaced halfway between the normal reflecting plane (see Fig. 5-19). If the angle is adjusted so that the distance ABC is a whole wavelength in order to give constructive interference with the ray from plane 1, then $A'B'C'$ is one-half a wavelength and so will cancel out the ray from plane 1. However, if the angle is changed to be appropriate for a spacing of $d/2$, then reflection will be observed.

The planes that will give reflections may be calculated from the position of the atoms in the unit cell. For the diamond lattice, which silicon has, these calcula-

Table 5-3. Planes from Which X-ray Reflections Are to Be Expected, Their Spacing, and the Bragg Angle When Using the Copper $K\alpha_1$ Line

Allowable planes	$h^2 + k^2 + l^2$	d_{hkl}	$\text{Sin } \theta$	θ_{hkl}°	$2\theta_{hkl}^\circ$
111	3	3.1354	0.24566	14.21	28.42
220	8	1.9200	0.40117	23.65	47.30
311	11	1.6374	0.47041	28.06	56.12
400	16	1.3576	0.56736	34.56	69.12
331	19	1.2459	0.61822	38.18	76.36
422	24	1.1085	0.69485	44.00	88.00
511, 333	27	1.0452	0.73694	47.46	94.92
440	32	0.9599	0.80242	53.36	106.72
531	35	0.9179	0.83914	56.05	114.10
620	40	0.8586	0.89709	63.78	127.56
533	43	0.8281	0.93014	68.45	136.90
444	48	0.7838	0.98271	79.33	158.66

Fig. 5-19. Reflections from an intermediate plane.



tions show that if the sum of the square of the Miller indices equals one of the series 3, 8, 11, 16, 19, etc., then reflections will occur.

$$\begin{aligned} h^2 + k^2 + l^2 &= (4n - 1) && \text{for } n = \text{any odd integer} \\ h^2 + k^2 + l^2 &= 4n && \text{for } n = \text{any even integer} \end{aligned} \quad (5-4)$$

These results are summarized in Table 5-3.

EXAMPLE 5-6. Will the (100) plane yield a reflection? If not, what is the lowest indices plane parallel to it that will?

$$h^2 + k^2 + l^2 = 1^2 + 0 + 0$$

Since 1 is not included in the allowable numbers determined by Eq. (5-4) or listed in Table 5-3, no reflections will occur. Similarly none will be observed for the (200) or the (300) plane. The (400) plane does, however, reflect.

If it is desirable to X-ray orient parallel to the (100) plane, it is necessary to look for the (400) plane. The spacing is 1/4 that of the (100) planes.

EXAMPLE 5-7. What angle must one use for orienting (110) planes? The $K\alpha_1$ line of a copper target tube will be used. Reference to Eq. (5-4) shows that the lowest-order reflecting planes parallel to a (110) plane is the (220). d_{110} is found from Table 5-1 to be 3.84 Å. Thus, the d_{220} spacing is 1.92 Å. The X-ray emission spectrum from a copper target includes α_1 , α_2 , and β components in the K series. A nickel filter removes the β peak, and since the $K\alpha$ doublet is easily resolved on sensitive equipment, the $K\alpha_1$ peak ($\lambda_{\alpha_1} = 1.54050 \text{ Å}$)* alone is used. Thus, from Eq. (5-3),

$$\begin{aligned} \sin \theta &= \frac{1.54}{2 \times 1.92} = 0.40 \\ \theta &= 23.6^\circ \end{aligned}$$

5-6. OPTICAL ORIENTATION⁵⁻⁹

When the proper chemicals are used, silicon can be preferentially etched so that (111) planes are exposed. That is, the etch rate in the [111] direction is slower than in other directions. Such selectivity creates well-defined patterns on the surface and can be used to determine the surface orientation. Thus, if the surface were originally near a (111) plane, there would be little three-sided inverted pyramids (tetrahedrons) etched in the surface. If a (100) plane is etched, then four-sided pyramids will result. Originally, the etch figures were individually examined microscopically, but more recent equipment depends on large-scale reflections.

* M. E. Straumanis, P. Borgeaud, and W. J. James, Perfection of the Lattice of Dislocation-free Silicon, Studied by the Lattice Constant and Density Method, *J. Appl. Phys.*, vol. 32, pp. 1382-1384, 1961.

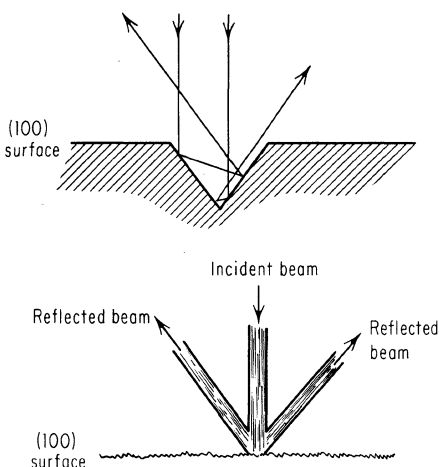


Fig. 5-20. Reflections from etch pits.

If a parallel beam of light shines on the surface, the exposed (111) faces will reflect the light back in the manner shown in Fig. 5-20. In the case of a four-sided pyramidal hole, light will be reflected back as four symmetric rays plus the one reflected back from the unetched surface. Further, if the original light is normal to the (100) plane (not necessarily to the exposed face), then the reflecting planes, and consequently the rays, will be symmetrically spaced. When an arrangement such as shown in Fig. 5-21 is used, the reflected rays will appear as spots on the screen. Usually the etch used exposes not only (111) faces, but others of the same zone, for example, 110, 113. These also reflect and cause what would normally be well-defined spots to become long ovals. Figure 5-22 shows patterns typical of the more common planes and the relation between these spots and other crystallographic directions. If the crystal is mounted so that it can be tilted, adjustments can be made until the spots are symmetrically arranged about the center. The amount of misorientation can then be determined by the amount of tilting required.

The accuracy of the optical system depends both on the care with which the optical system is built and on the ability of the etch to leave flat surfaces. If, for example, the etching procedures leave steps or slightly curved surfaces, then the accuracy will be impaired. The best results have been reported using either molten salts or metals and are of the order of 3 min. However, boiling for five minutes in a 5 per cent solution of NaOH will give an etch surface good enough for 15 min accuracy.

5-7. TWINNING^{10,11}

Occasionally, two or more crystals of the same material will grow in such a manner that at the intersection they share a common plane and sheet of atoms, but

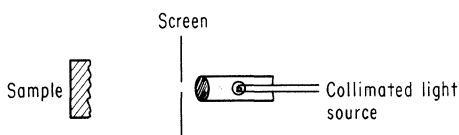


Fig. 5-21. Optical orienting arrangement.

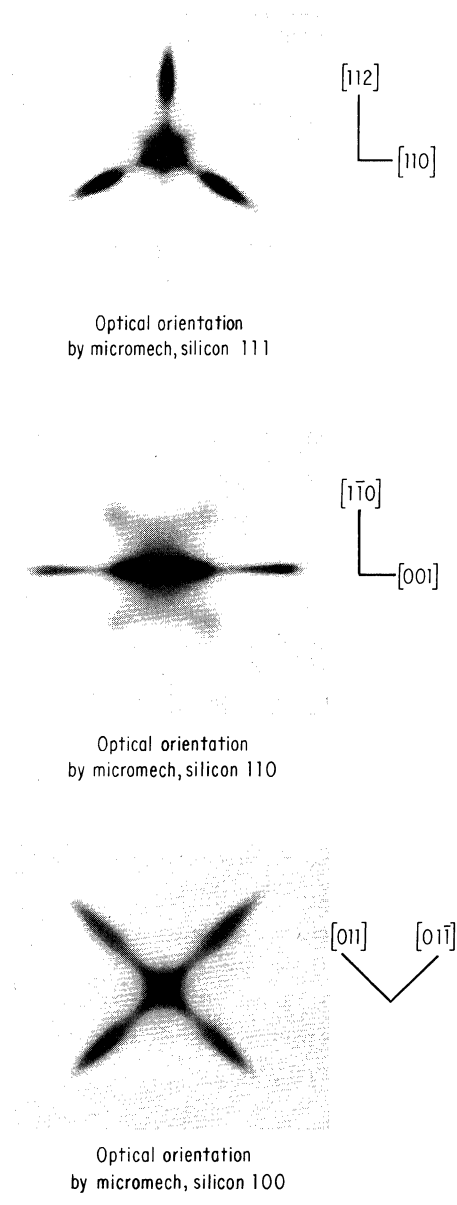


Fig. 5-22. Optical orientation patterns.
(Courtesy Micromech Manufacturing Co.)

otherwise their orientation is different. This is referred to as twinning, and for a given material the orientation between the two crystals is fixed. A discussion of the crystal symmetry properties which determine the orientation will not be given; instead the reader is referred to crystallography texts for details.

Based on geometric laws, crystals with the diamond lattice may twin with either a (111) or a (112) common plane, and for these crystals the twinned portion appears as a reflection of the original crystal in the twin plane.¹² This is illustrated by Fig. 5-23. If actual atomic structure and low-energy requirements are consid-

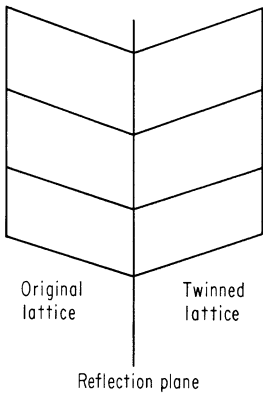


Fig. 5-23. Reflection twin.

ered, only (111) twinning would be expected and has been experimentally confirmed for diamond,^{12,13} silicon,¹⁴ and germanium.¹⁵⁻¹⁷

In order to visualize the relative orientation of such crystals, consider the two cubes in Fig. 5-24a. First cut off a corner of one of the cubes along a (111) plane as shown. Then remove a corner of the second cube, again along a (111) plane, and join them together as shown in Fig. 5-24b. Thus, while the two cubes have a common (111) plane, their relative orientation is different. Figure 5-24c shows twinned octahedrons as they would look under ideal growth conditions.

If twinning occurs while a crystal is being grown from the melt, the new growth plane can be predicted since it must make the same angle with the (111) twin plane as the original plane. This is illustrated in Fig. 5-25. One method of determining the new growth-plane indices is to refer to a tabulation of angles and find one that fits, however, the indices of the new plane with respect to the axis of the old one may also be calculated directly from the following three simultaneous equations.¹²

$$\begin{aligned} ht + ku + lv &= -hp - kq - lr \\ kt - hu &= kp - hq \\ lt - hv &= lp - hr \end{aligned}$$

where (hkl) = indices of the twin plane
 (pqr) = indices of the original plane
 (tuv) = indices of the new plane

If the twinning occurs while a crystal is being grown in the [100] direction, the twin plane will make an angle of 54.7° with the plane of growth so that if the crystal length is increased enough, a segment with no twinned material will result. However, the new orientation will be of the {221} family. In the case of an original [111] growth direction, the twin boundary will usually make an angle of 70.53° with the growing plane so that the next segment of the crystal will be grown in the [511] direction. Almost invariably, however, it will immediately twin again and proceed as a $(\bar{1}\bar{1}\bar{1})$. In rare occasions the growing (111) plane may be the twin plane. In this case further growth is in the $[\bar{1}\bar{1}\bar{1}]$ direction. If the crystal is

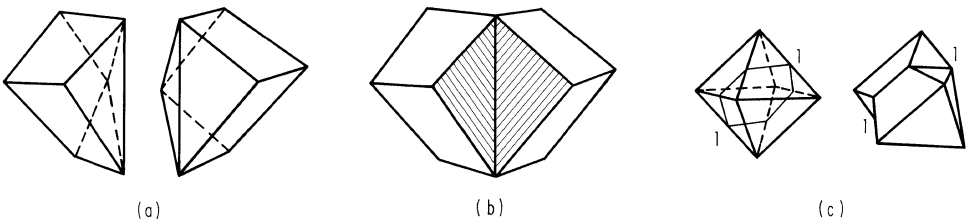


Fig. 5-24. Octahedral twin geometry.

growing in a plane such as the (211), then the twin plane may be the one perpendicular to the growth plane, so that any twins formed continue to propagate themselves as long as the crystal is grown. Some of the twin possibilities for silicon are summarized in Table 5-4.

5-8. DETECTION OF TWINNING

In the case of silicon grown from the melt, the gross shape of the crystal or boule is determined more by the thermal conditions of the melt than by its natural tendency to expose certain faces. Consequently, detection of twins is usually accomplished by observing the boundary between the differently oriented regions. Normally, a line is visible where the common plane intersects the boule surface. Sometimes, however, it will be hidden by surface blemishes such as an oxide film. Twin boundaries that intersect the bottom of the crystal usually are more discernible than those that do not. While careful search by a trained observer will usually yield all twins, a better procedure is to lightly sandblast the crystal and then give it a short etch. This surface treatment sharply delineates all boundaries and makes them clearly visible to even untrained observers.

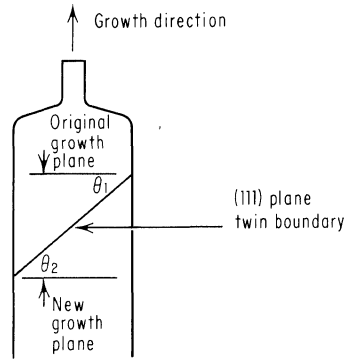


Fig. 5-25. Twinning geometry in crystal growing from melt. Since the same growth direction is maintained throughout the crystal, θ_1 must equal θ_2 .

5-9. GRAIN BOUNDARIES

If different portions of an ingot nucleate randomly and then grow together, the contact surface is a grain boundary. In this case there is no fixed relationship

Table 5-4

Original plane	Twinning plane	New plane
100	111	$\bar{1}\bar{2}\bar{2}$
	$\bar{1}\bar{1}\bar{1}$	122
	$\bar{1}\bar{1}\bar{1}$	122
	$\bar{1}\bar{1}\bar{1}$	122
110	111	$\bar{1}\bar{1}\bar{4}$
	$\bar{1}\bar{1}\bar{1}$	110
	$\bar{1}\bar{1}\bar{1}$	110
	$\bar{1}\bar{1}\bar{1}$	$\bar{1}\bar{1}\bar{4}$
111	111	$\bar{1}\bar{1}\bar{1}$
	$\bar{1}\bar{1}\bar{1}$	511
	$\bar{1}\bar{1}\bar{1}$	151
	$\bar{1}\bar{1}\bar{1}$	115

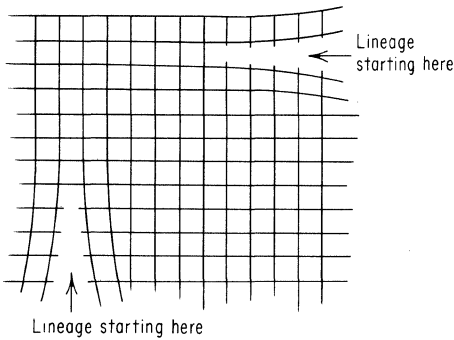


Fig. 5-26. Lineage structure.

between the two orientations in contact so that there will, in general, be a mismatch of atoms and planes. The same techniques used in detecting twin boundaries are applicable for grain boundaries.

5-10. LINEAGE

In the event that a crystal starts to grow in an orderly fashion and gradually develops misalignment, the misaligned portion is called a lineage structure. This is illustrated by Fig. 5-26. If the misalignment is very severe, the joints become grain boundaries and may be observed with standard etching techniques. If there are only small deviations, detection is usually by X-ray techniques.

REFERENCES

1. Kraus, E. H., W. F. Hunt, and L. S. Ramsdell: "Mineralogy," McGraw-Hill Book Company, New York, 1959.
2. Wyckoff, R. W. G.: "Crystal Structures," Interscience Publishers, Inc., New York, 1960.
3. Wood, Elizabeth A.: "Crystal Orientation," Columbia University Press, New York, 1963.
4. Shockley, William, "Electrons and Holes in Semiconductors," D. Van Nostrand Company, Princeton, N.J., 1950.
5. Wolff, G. A., J. M. Wilbur, Jr., and J. C. Clark: Etching and Orientation Measurements of Diamond Type Crystals by Means of Light Figures, *Z. Elektrochem.*, vol. 61, pp. 101-106, 1957.
6. Schwuttke, G. H.: Determination of Crystal Orientation by High Intensity Reflectograms, *J. Electrochem. Soc.*, vol. 106, pp. 315-317, 1959.
7. Wynne, R. H., and Colman Goldberg: Preferential Etch for Use in Optical Determination of Germanium Crystal Orientations, *J. Metals*, vol. 5, p. 436, 1953.
8. Faust, J. W., Jr.: "Etches for Imperfections in Silicon and Germanium," paper presented at the Electrochemical Society Meeting, May, 1955.
9. Honess, Arthur P.: "The Nature, Origin and Interpretation of the Etch Figures on Crystals," John Wiley & Sons, Inc., New York, 1927.
10. Cahn, R. W.: Twinned Crystals, *Advan. Phys.*, vol. 3, pp. 363-446, 1954.
11. Buerger, M. J.: The Genesis of Twin Crystals, *American Mineralogist*, vol. 30, pp. 469-482, 1945.
12. Slawson, Chester B.: Twinning in the Diamond, *American Mineralogist*, vol. 35, pp. 193-206, 1950.

13. Sutton, J. R.: "Diamond: A Descriptive Treatise," Thomas Murby & Co., London, 1928.
14. Salkowitz, E. I., and F. W. Von Batchelder: Twinning in Silicon, *J. Metals*, vol. 4, p. 165, 1952.
15. Ellis, W. C.: Twin Relationships in Ingots of Germanium, *J. Metals*, vol. 2, p. 886, 1950.
16. Ellis, W. C., and R. G. Treuting: Atomic Relationships in the Cubic Twinned State, *J. Metals*, vol. 3, pp. 53-55, 1951.
17. Ellis, W. C., and Jacqueline Fageant: Orientation Relationships in Cast Germanium, *J. Metals*, vol. 6, pp. 291-294, 1954.

6

Doping Procedures

6-1. EFFECTS OF IMPURITIES ON RESISTIVITY

The conductivity σ due to impurities in a semiconductor is given by:

$$\sigma = eN\mu \quad (6-1)$$

where e = electronic charge

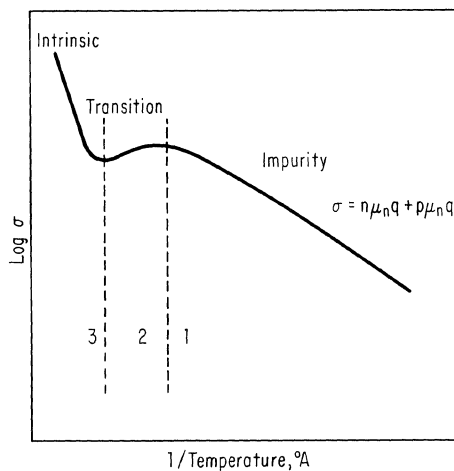
N = number of ionized impurities per unit volume

μ = drift mobility of the current carrier

For the more commonly used silicon doping elements (B, Ga, Al, In, As, P, and Sb) at room temperatures and for concentrations less than perhaps $5 \times 10^{19}/\text{cm}^3$, each impurity atom occupies a substitutional site. The majority is ionized and contributes to the conductivity. Thus, the N of Eq. (6-1) becomes the number of impurities in the silicon. If, however, the temperature is reduced sufficiently, the conductivity drops accordingly.

The general character of the conductivity variation with temperature is shown in the graph below.

The high resistivity in region 1 is due to the temperature being too low for the impurities to be ionized. Region 2 has normal "extrinsic" conductivity in



which transistors are normally operated. The increase in resistivity with temperature is caused by the mobility decrease with increasing temperature. Region 3 has intrinsic conduction, i.e., the temperature is high enough for valence to conduction band transitions so that the conduction is primarily due to thermally generated carriers rather than to impurities. In this region the conductivity varies exponentially with temperature.

Some impurities enter into the lattice interstitially rather than substitutionally and may not be ionized at room temperature. That is, they will not contribute to conductivity until the temperature is raised appreciably. They may, however, act as traps for carriers already present and so raise the resistivity. This can be visualized as follows.

Consider an n-type impurity with an ionization energy too high to be activated at room temperature. Its extra electron will then remain bound to the atom. On the other hand, any mobile hole which drifts into the vicinity will be "trapped" by the extra electron and will then be prevented from participating in the conductivity. Gold is one such element that behaves in this manner and is also amphoteric, i.e., can act either as a donor or an acceptor. Thus, as gold is added to either n- or p-type material, it will immobilize the free carriers (either holes or electrons) and increase the resistivity. After an excess of gold has been added, however, it does dope p-type (approximately 10^5 ohm-cm). The quantitative effect of gold and silver on silicon of various resistivities is given in Chap. 8.

In addition, it is possible to have impurities dispersed in the bulk material so that they can contribute to conductivity and then, by various heating and cooling cycles, cause the impurities to precipitate along dislocations where they behave as an inert aggregate in a silicon matrix.

For the present these effects will all be neglected so that Eq. (6-1) is adequate. In the event that there are both p- and n-type impurities in the material, then it is only the excess of one over the other that contributes to the conductivity.

Equation (6-1) has been plotted for a wide range of impurity levels and is shown in Figs. 6-1 to 6-4.^{1,*} The impurity levels are shown as N_d (number of donor atoms/cm³) or N_a (number of acceptor atoms/cm³) versus resistivity, but if the total impurity content is low enough for the mobility to be independent of the total number of carriers (both n- and p-type), then it is acceptable to use these curves for $N_d - N_a$ versus resistivity.

EXAMPLE 6-1. How many atoms/cm³ of phosphorus will be required to dope silicon to 0.75 ohm-cm? From Fig. 6-2 it is found that the required concentration is 7.5×10^{15} atoms/cm³.

While Figs. 6-1 to 6-4 are plotted in terms of impurities/cm³, it is often desirable to express the impurity content in ppb, which really means atoms of impurity/billion silicon atoms and not parts by weight or parts by volume. Since by definition 1 g atomic weight of any element contains 6×10^{23} atoms

$$\frac{28 \text{ (atomic weight of silicon)}}{2.3 \text{ (density of silicon)}} = 12.1 \text{ cm}^3$$

* Superscript numbers indicate items listed in References at the end of the chapter.

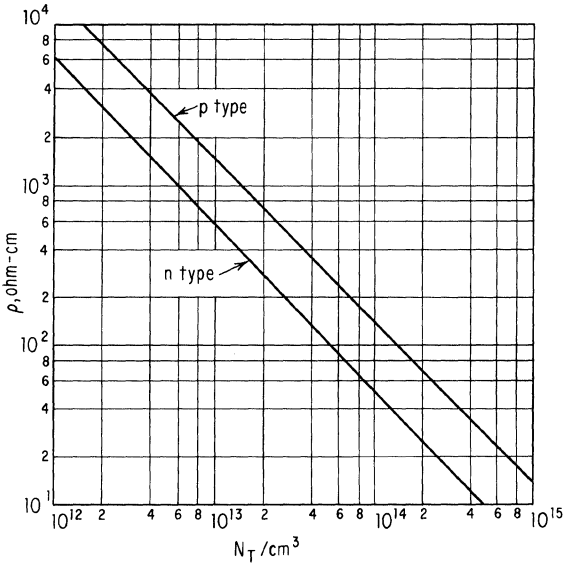


Fig. 6-1. Resistivity versus impurity density for $|N_a - N_d|$ between 10^{12} and 10^{15} impurities/cm³. (Extrapolated from Irvin.¹)

from which 1 cm³ contains $6 \times 10^{23}/12.1 = 5 \times 10^{22}$ atoms. Thus, 1 ppb = 5×10^{13} atoms/cm³.

EXAMPLE 6-2. A sample of silicon has 2 ppb of phosphorus and 1 ppb of boron. What is its resistivity?

The net impurity content is 1 ppb n-type. This corresponds to 5×10^{13} atoms/cm³, which gives, from Fig. 6-1, a resistivity of 100 ohm-cm.

EXAMPLE 6-3. How many milligrams of arsenic per gram of silicon must be incorporated into the lattice to give a resistivity of 0.1 ohm-cm if there is already 6 ppb of boron in the silicon? From Fig. 6-3 it is found that 0.1 ohm-cm requires 9×10^{16} n-type impurities/cm³. Thus 9×10^{16} atoms/cm³ plus enough to compensate for the 6 ppb boron already there, or 9×10^{16} plus 3×10^{14} arsenic atoms/cm³ will be required. Since the density of silicon is

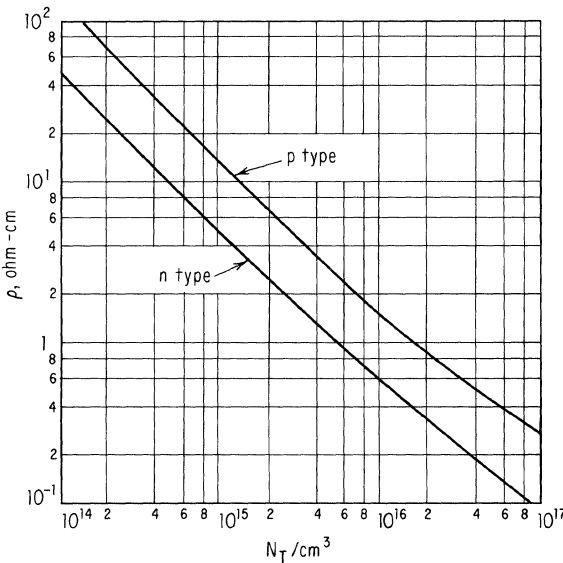
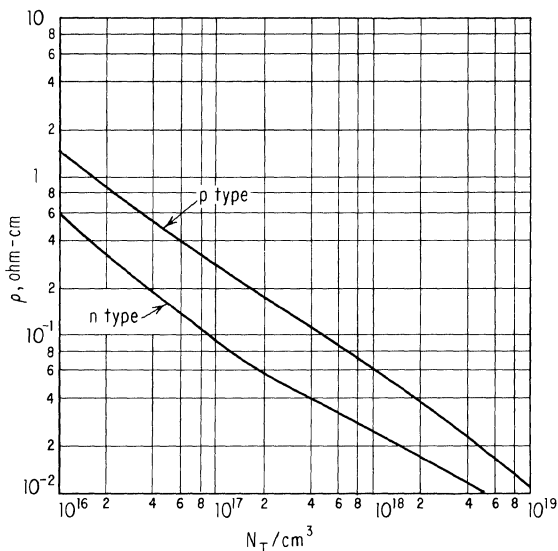


Fig. 6-2. Resistivity versus impurity density for $|N_a - N_d|$ between 10^{14} and 10^{17} impurities/cm³. (Irvin.¹)

Fig. 6-3. Resistivity versus impurity density for $|N_a - N_d|$ between 10^{16} and 10^{19} impurities/cm³. (Irvin.¹)



2.32 g/cm³, $9.03 \times 10^{16}/2.32$ or 3.87×10^{16} atoms of arsenic per gram of silicon will be required. The 3.87×10^{16} atoms of arsenic weighs $(3.87 \times 10^{16}) / (6 \times 10^{23}) \times 75$ g (75 is the atomic weight of arsenic*), or finally 4.8 μ g of arsenic per gram of silicon must be introduced into the silicon lattice to reduce the resistivity to 0.1 ohm-cm.

6-2. EFFECT OF SEGREGATION COEFFICIENT ON RESISTIVITY

The previous section was devoted to calculations involved in determining the amount of impurity required in the silicon crystal to give the desired resistivity.

* For convenience, the atomic weight and density of several of the more common doping elements are tabulated and included as Table 6-1.

Fig. 6-4. Resistivity versus impurity density for $|N_a - N_d|$ between 10^{18} and 10^{20} impurities/cm³. (Irvin.¹)

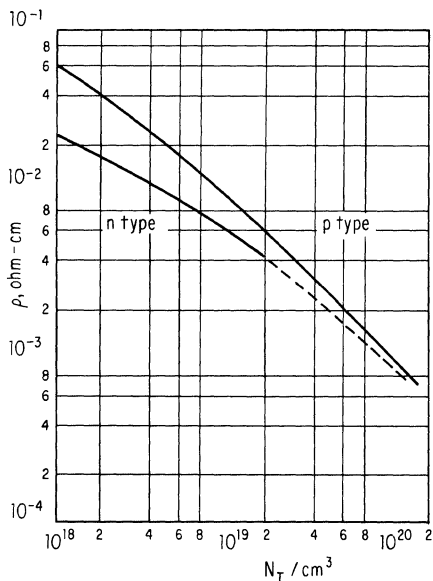


Table 6-1. Miscellaneous Doping Information

Element	Atomic weight	Segregation coefficient ²	Atoms/mg	Melting point, °C	Boiling point, °C
B	10.82	0.80	5.55×10^{19}	2300	>2550
Al	26.97	0.0020	2.23×10^{19}	660	1800
Ga	69.22	0.0080	8.69×10^{18}	29.8	1600
In	114.76	4×10^{-4}	5.25×10^{18}	155	1450
Tl	204.39	2.68×10^{18}	304	1650
P	30.98	0.35	1.94×10^{19}	44	280
As	74.91	0.3	8.03×10^{18}	Sublimes	
Sb	121.76	0.023	4.94×10^{18}	630	1380
Bi	209.00	7×10^{-4}	2.88×10^{18}	271	1450
Zn	65.38	$\sim 1 \times 10^{-5}$	9.22×10^{18}	420	907
Cu	63.57	4×10^{-4}	9.47×10^{18}	1083	2300
Au	197.2	2.5×10^{-5}	3.05×10^{18}	1063	2600
Pt	195.23	3.08×10^{18}	1773	4300
Fe	55.84	8×10^{-6}	1.08×10^{19}	1535	3000
Ni	58.69	1.02×10^{19}	1455	2900
Co	58.94	8×10^{-6}	1.02×10^{19}	1495	3000
Li	6.94	0.01	8.69×10^{19}	186	>1220

These calculations will now be extended so that the amount of dope that must be added to the charge can also be determined. These procedures are applicable to crystals grown from the melt but not to those grown from the vapor. For the latter the amount of impurities incorporated into the silicon depends on the relative reaction rates of various compounds and will be discussed in conjunction with vapor-phase crystal growth.

As materials freeze, they usually reject impurities into the remaining melt so that purification occurs. In some instances (none reported in silicon) the reverse occurs so that the freezing portion has a higher concentration of impurity than the adjacent liquid. In either case, a segregation, or distribution, coefficient k is defined as the ratio of the concentration of impurity being incorporated into the solid to the impurity concentration in the melt at the liquid-solid interface. That is

$$N_{\text{solid}} = kN_{\text{liquid}} \quad (6-2)$$

Thus, the more impurity that is rejected, the smaller k is. If no segregation occurs, i.e., the same concentration of impurity is in the melt as is in the frozen portion, then $k = 1$.

Since k for silicon is less than 1, as the crystal is grown, the impurity concentration in the melt steadily increases and this in turn causes a similar increase in the concentration level of the growing crystal. For the present, k will be assumed to be independent of crystal-growth parameters such as pull rate, speed of rotation, and growth direction. In actual practice this is not so, and these variations can, in fact, be used for a variety of useful purposes.

The expression for the concentration level in the solid as a function of the amount in the original melt and the fraction solidified is given by³

$$N_s = kN_{m,0}(1 - X)^{k-1} \quad (6-3)$$

where X is the fraction of the melt solidified and $N_{m,0}$ is the melt concentration at the start of freezing.

Figure 6-5 shows the behavior of Eq. (6-3) for a number of k values corresponding to the more common dopes. The initially frozen portion has its impurity level reduced by a factor of $1/k$ over that originally in the charge, but as the last portion of the melt freezes, its concentration will be higher than was originally in the melt. For low values of k this will occur very close to the final freezing end and so is not shown in the figure. The lower the segregation coefficient, the higher the final concentration must be since ultimately one must account for all the dope. However, for k 's near 1 it will occur much sooner, i.e., from Fig. 6-5, for $k = 0.9$, the concentration in the solid is greater than that in the original melt (though not by much) for the last 50 per cent of the silicon frozen.

It is experimentally observed that if there is about 2 per cent by weight or more of impurity in the melt, it is impossible to grow single crystals of silicon. It can be expected then that as a crystal is grown from a melt heavily doped with a low-segregation-coefficient element, some point will be reached beyond which twinning or polycrystalline growth occurs.* In many cases it will be this effect that will limit the impurity concentration that can be obtained in a single crystal rather than the limit of solubility of the dopant in silicon at its melting point.

EXAMPLE 6-4. What is the lowest resistivity that can be obtained in an antimony-doped single crystal?

Using the criterion of 2 per cent maximum impurity† in the melt for single-crystal growth, the maximum amount of antimony allowed will be 0.046 g/cm³. From Table 6-1, 46 mg of Sb contains $46 \times 4.94 \times 10^{18}$ or 2.3×10^{20} atoms. There is, therefore, approximately 2×10^{20} atoms/cm³ of Sb in the melt. Since antimony has a segregation coefficient of 0.023, the amount introduced into the crystal is 4×10^{18} atoms/cm³. From Fig. 6-3 this corresponds to a resistivity of approximately 0.01 ohm-cm, which is in close agreement with the experimentally observed value.

In the event that there is more than one impurity present, it is assumed that they

* This is due to constitutional supercooling and is considered in greater detail in Chap. 4.
 † See Chap. 4 for more precise numbers.

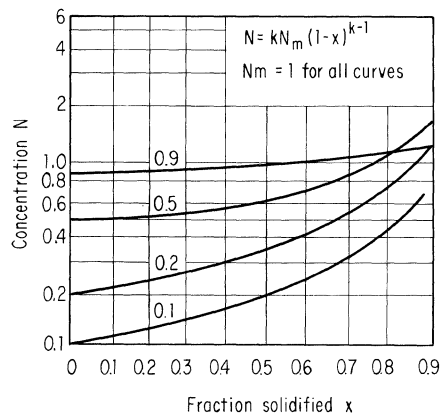


Fig. 6-5. Impurity concentration versus fraction solidified for normal freezing. (Pfann.³)

behave independently of each other so that the total impurity concentration along a crystal can be obtained by adding the concentration of each impurity calculated from Eq. (6-3). The resistivity along the crystal can then be determined from the resistivity-impurity concentration curves.

EXAMPLE 6-5. The initial concentration of antimony in the melt is 10^{16} atoms/cm³. What will be the resistivity of the crystal when $\frac{1}{2}$ of the melt has been grown if there is no other impurity present and if the original silicon had 4 ppb boron in it?

Reference to Table 6-1 gives the segregation coefficient of Sb as 0.023. From a direct substitution into Eq. (6-1) or by reading from Fig. 6-4, the resistivity is found to be 1.3 ohm-cm. Four parts per billion equals 2×10^{14} atoms/cm³. Table 6-1 gives the segregation coefficient of boron as 0.8. Substitution into Eq. (6-3) gives a concentration at the halfway point of almost exactly equal to the initial concentration in the melt, or 2×10^{14} . The excess n-type impurity is then $8 \times 10^{14} - 2 \times 10^{14}$ so that the resistivity is now 1.6 ohm-cm, or an increase of about 20 per cent because of the residual boron.

Since boron is a common residual impurity in silicon, curves showing the behavior of resistivity versus crystal length with varying amounts of n-type dope and boron are shown in Figs. 6-6 to 6-11.

6-3. METHODS OF DOPING

Having determined the amount of dope required, there still remains the problem of introducing it into the melt in a safe and reproducible fashion.

Indium. Available in purities of 99.999 per cent. It boils above 1450°C and will alloy with silicon at any temperature above 300°C. It can be added directly to a charge before or after melt-in without fear of losses due to excessive evaporation. Since it has such a low segregation coefficient (4×10^{-4}), large quantities are required for normal doping. Because of this, the amounts required per charge are normally large enough to be directly weighed and handled without difficulty.

Gallium. Available in purities of 99.999 per cent. It boils above 1600°C so it may be added to the charge before or after melt-in without loss due to evaporation.

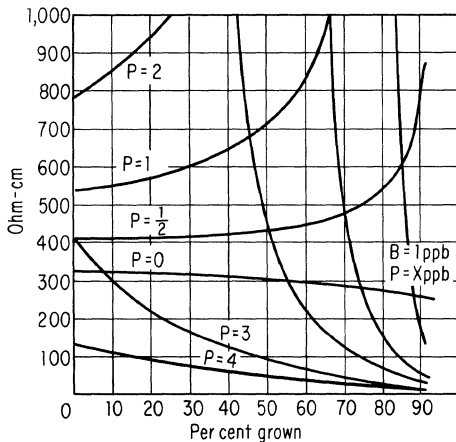


Fig. 6-6. Calculated effect of 1 ppb boron on the resistivity of phosphorus-doped crystals.

Fig. 6-7. Calculated effect of 1 ppb boron on the resistivity of phosphorus-doped crystals.

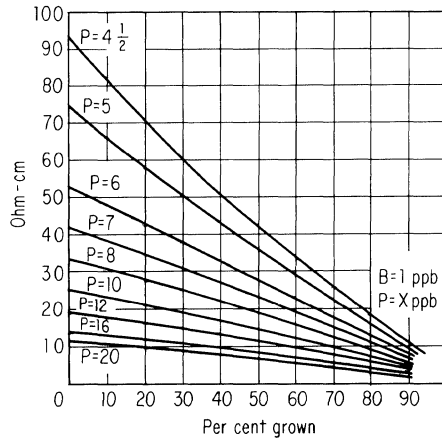


Fig. 6-8. Calculated effect of 4 ppb boron on the resistivity of phosphorus-doped crystals.

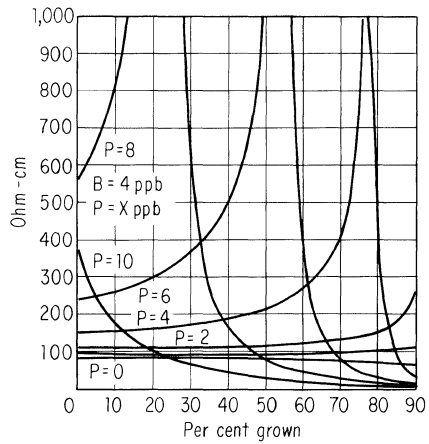
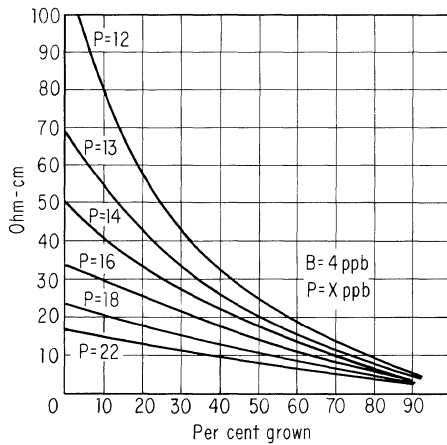


Fig. 6-9. Calculated effect of 4 ppb boron on the resistivity of phosphorus-doped crystals.



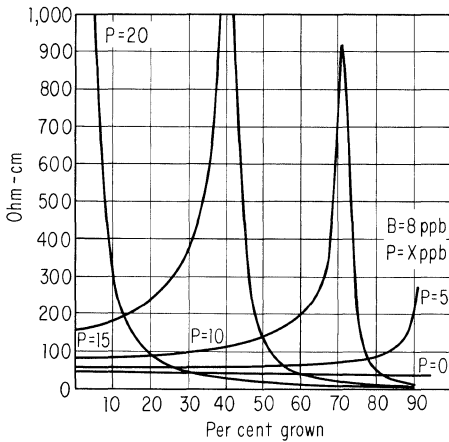


Fig. 6-10. Calculated effect of 8 ppb boron on the resistivity of phosphorus-doped crystals.

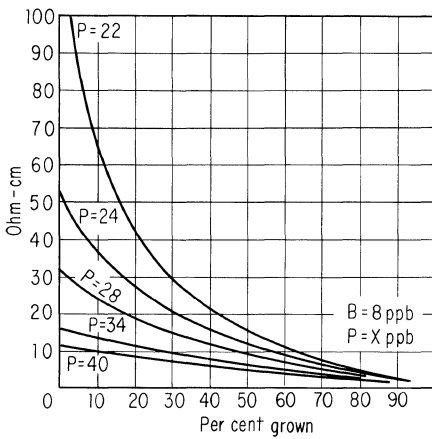


Fig. 6-11. Calculated effect of 8 ppb boron on the resistivity of phosphorus-doped crystals.

It melts at 29.7°C, however, so that there is a problem in transporting it to a melt. Presumably, the desire to add it after the silicon has been melted would only occur in the growing of grown-junction crystals and represents a relatively small usage. Gallium cannot be dropped down a dope tube, for example, without a probable partial or complete loss due to wetting and sticking to the silica. Even with the wetting problem, however, small fused-silica buckets suspended above the melt have been used to directly add molten gallium to the melt. While still frozen, small pieces of gallium may be wrapped in indium foil, and then the combination can be added to the melt. Since the segregation coefficient of gallium is a factor of 20 greater than that of indium, most of the doping will be due to the gallium (unless a ridiculously large indium wrapper is used). If gallium were to be used in grown-diffused crystals, it could be added as a compound such as gallium arsenide. The arsenic would not bother since some sort of heavy n-type dope is usually added at the same time.

Aluminum. High-purity aluminum is available and since it alloys with silicon at temperatures below 600°C and does not boil until 1000°C, it can be used with no difficulty.

Boron. High-purity boron is difficult to obtain. It reacts with molten silicon quite slowly and has such a high segregation coefficient that it must almost always be diluted before using in order to obtain anything approaching precision doping. It then becomes appropriate to make boron-silicon alloys of various boron concentrations. Otherwise, weighing would be difficult and there would be a large risk of inadvertently losing the dope charge after it is weighed but before melt-in. The percentage of boron to be used will, of course, depend on the final crystal resistivity desired, but 0.01 to 1 per cent by weight is a useful range. Since elemental boron reacts slowly, it is necessary when making the alloy to allow from 30 min to 2 hr for complete solution in the molten silicon. The process is speeded up by using a fused-silica paddle to stir the mixture and by keeping the molten silicon as hot as possible without the fused-silica container softening and collapsing. After complete solution, there are several paths to pursue in order to prepare the alloy for use. The charge may be cooled, cracked, mixed, and used. This has the advantage of simplicity but affords no purification. A boule (not necessarily a single crystal) can be grown from the melt, sliced, powdered, and used. This gives a one-stage purification and leaves the alloy in a form that can be easily handled. As a further refinement, the original charge can either be cast or grown as a long, thin rod and then zone-refined for additional purity. In any of these procedures care must be taken in the reduction-to-powder process in order to prevent contamination. If the alloy is sawed into thin slices, they can be carefully cleaned and then broken quite easily as contrasted to the difficulty of reducing large chunks to powder. If such contrivances as ball mills or normal mortar and pestles are used, unwanted contamination will almost certainly occur. A mortar and pestle made of high-purity silicon will work nicely with thin slices and will only dilute the alloy a small amount, but will not add unwanted impurities.

Bismuth. Apparently this is little used, but it can be added directly since it alloys with silicon at relatively low temperatures and does not boil until above 1450°C.

Antimony. Antimony is available in purities of 99.999 per cent. Because of its low segregation coefficient, large amounts may be needed to dope so that the amount of impurities in it is much more important than in boron, for example, where much smaller amounts are required. It may be used as an alloy or added directly to the charge or melt. If an alloy is to be made, then there are some precautions that must be taken. Since it does have a low segregation coefficient, uncontrolled freezing may very well precipitate pure antimony along grain boundaries during the final stages of freezing. This makes good mixing imperative if reproducibility is to be expected. A better procedure is to grow a boule and use only a portion of it so that the concentration variation from one end to the other is restricted to perhaps 2:1. Another method which will yield a more uniform doping rod is to cast the alloy in a separate mold. If the mold is tubular and properly cooled, the silicon will freeze fast enough to prevent much segregation along the rod. It may then be cut up, powdered, and mixed. This approach has the disadvantage of not including a purification stage. The cast rod might be zone-refined, but because of the low segregation of antimony, the variation along the rod would be increased. It has also been suggested that the dope be made

directly in pellet form by using a shot tower process. Such a method has been used for germanium but apparently not for silicon.

Arsenic. Arsenic sublimates at 615°C at atmospheric pressure and does not react with silicon below that temperature. Because of the high (0.3) segregation coefficient, an alloy is usually required in order to simplify doping. If undiluted arsenic is used, it must be added after the silicon is melted, otherwise it will all sublime and not dissolve. When arsenic is added to the melt, there is, of course, still a great deal lost by sublimation so that if an alloy is to be made, there is little likelihood of accurately predicting the composition. It is available in purities of 99.999 per cent.

Phosphorus. Since phosphorus is quite reactive, its introduction into molten silicon is somewhat of a problem. In addition it has a segregation coefficient of 0.35 so that normal usage requires a dilution before use. It can be added to the silicon as a compound rather easily (usually as a phosphate), and then if the other elements of the compound have been chosen to have low segregation coefficients, either a float-zoned cast rod, or a normal crystal-pulling operation will produce a good quality dope. It can also be introduced into the melt from a gaseous compound, such as phosphorus trichloride, or may be codeposited with silicon during manufacture.

6-4. DISCUSSION OF CRYSTAL YIELDS

Occasionally, the actual resistivity, or the amount of crystal in the desired resistivity range, is different from that calculated according to the preceding directions. This section will consider some of the reasons for such occurrences and, in addition, will suggest methods of improving yields over that predicted by simple theory.

Material Variability. The unknown variation of residual Groups IIIA and VA elements in the raw silicon can cause considerable variation in yield when the desired doping level is less than ten times the average initial impurity level.

Despite these variations, if one assumes that the variability within a lot is small, although the variation from lot to lot may be much larger, then a small series of crystals can be grown and the doping for maximum yield can be determined from these.

Doping Variability.

1. In order to prevent contamination of the melt from the machine itself, a strict cleaning schedule must be maintained.
2. There are occasional errors which arise from improper weighing, loss of dope during transfer to the charge, and accidental choice of incorrect dope.
3. If a volatile dope such as pure arsenic is used, then varying quantities may be lost as it is added to the melt. If any precision doping is to be done, an alloy or compound should be used.

Even if no losses occur in transferring to the melt, some of the dope is continuously evaporating during the growing process. In general this is helpful since it reduces the increased concentration of dope normally occurring during growth and thus gives more uniform resistivity profiles.

However, if difficulty in growing causes the cycle to be much longer than normal, enough dope may evaporate to adversely affect yields.

4. The dope itself may be nonuniform, particularly in alloys. If an attempt is made to make a dope with a higher concentration than the solid solubility of the dopant in the silicon, then the excess will segregate out along grain boundaries and cause tremendous variations in concentration through the ingot.
5. After the dope is made, it must be broken into small pieces and reduced to a powder and thoroughly mixed before good uniformity can be expected. Care must be taken that the act of grinding does not add contaminants. If grinding is done in an aluminum-oxide-bearing container, for example, enough particles of aluminum oxide may be added to the dope to change a low-concentration n dope to p-type. In order to prevent possible contamination of the lot during use, it should be divided into smaller quantities and stored in sealed glass ampoules until needed.

Resistivity Variation along Crystal. Because of the tendency for the impurity to remain in the melt as the crystal is grown, the concentration of impurity in the melt is continually increased, so that the quantity of dope in the crystal also increases. If a ± 25 per cent resistivity spread of n-type material is required, yields of less than 50 per cent will result. Typically, the best 5 to 9 ohm-cm n-type yield is 50 per cent. There are, however, some things that can be done to increase this yield.

1. The segregation coefficient generally varies with growth rate; i.e., the faster the growth, the higher the segregation coefficient. Accordingly, a programmed pull rate can be used so that the initial pull is high and, as the concentration builds up, the pull is reduced.⁴
2. A compensating dope can be added part of the way through the growing. In general, compensation is not desirable and should be considered only as a last resort.
3. Some method of removing the excess dope from the melt as it accumulates can be used. If growth is carried out under reduced pressure, then the rate of evaporation can be adjusted to at least partially compensate for the dope being rejected by the growing crystal. It has been reported that phosphorous dope works well in this application.⁵ It does have the disadvantage of requiring a vacuum puller with its added complexity.

Another approach is to use a cold-walled chamber, a large area melt surface, and a normal atmosphere. Then useful evaporation may still occur.

4. Crystals can be grown from constant volume melts maintained either by continuously introducing feed material or by the periodic addition of new melt. Several continuous feed systems have been devised, but they are complicated and growing yields would probably be low. However, if some fixed fraction of the melt is grown, the crystal removed, and an equal amount of new material and appropriate dope added, then the process can be repeated. Thus, for example, if the expected yield of 5 to 9 ohm-cm material is 50 per cent, then 50 per cent of the melt would be withdrawn so that the whole crystal would be usable.

Then, in principle, the process could be continued many times until the unusable $\frac{1}{2}$ charge that remained in the machine at the end of the cycle would be insignificant when compared to the quantity of good material already produced.

Such a machine has the capability of yielding 99+ per cent usable material, but there is a series of limiting factors which would preclude reaching that yield.

- a. Although it has been assumed that only one type of dope is present in the beginning silicon, this is, unfortunately, not true. A calculation based on 3 ppb boron impurity (and no other p-type), and a desired 5 to 9 ohm-cm n-type crystal indicates about an 80 to 85 per cent maximum yield if an n-type dope with a k of 0.3 is used.
- b. The material variability will prevent starting the crystal at exactly the right resistivity every time.
- c. The gradual solution of the liner will limit the growing time and, hence, maximum yield. However, calculations show that a above will actually be the limiting factor.

Lack of Radial Resistivity Uniformity. If the liquid beneath the growing crystal-melt interface is not stirred, the impurities being rejected by the crystal will cause a concentration increase in the liquid adjacent to the crystal. This changes the effective impurity concentration in the melt and is reflected in the resistivity of the growing crystal. If the crystal is rotating and no convection currents are assumed, the relative velocity of the crystal and melt varies from zero at the middle to a maximum at the edge. If there are convection currents, they will generally oppose the stirring currents and could conceivably yield little stirring anywhere across the melt-solid boundary. It is this variable and unpredictable stirring that is primarily responsible for radial resistivity gradients. The effect of convection currents can be minimized by simultaneously rotating the crucible and crystal, but this still does not give stirring at the center of the crystal. It can be shown, however, if both crystal and crucible are rotated with the same angular velocity and if the centers are displaced by the radius of the crystal, then the liquid is swept over the whole crystal-growing surface at near uniform velocity.

REFERENCES

1. Irvin, J. C.: Resistivity of Bulk Silicon and of Diffused Layers in Silicon, *Bell System Tech. J.*, vol. 41, pp. 387-410, 1962.
2. Trumbore, F. A.: Solid Solubilities of Impurity Elements in Germanium and Silicon, *Bell System Tech. J.*, vol. 39, pp. 205-233, 1960.
3. Pfann, W. G.: Principles of Zone Melting, *Trans. AIME*, vol. 194, p. 747, 1952.
4. Buehler, E., and G. K. Teal: Process for Producing Semiconductive Crystals of Uniform Resistivity, U.S. Patent 2,768,914, Oct. 30, 1956.
5. Ziegler, G.: Quantitative Consideration of Evaporation During Crucible-free Zone Melting, *Z. Metallk.*, vol. 49, pp. 491-494, 1958.

7

Diffusion

7-1. ELEMENTARY THEORY

The simple theory of diffusion assumes that one species of impurity will diffuse independently of any other, and that the diffusion rate is independent of the concentration. Neither of these assumptions is rigorously true, but they are accurate enough for many calculations.*

The amount of material diffusing per unit time is proportional to the concentration gradient and is transported in the direction of lower concentration. For the one-dimensional case, Fick's first law of diffusion states that^{1-4,†,‡}

$$J = -D \frac{\partial N}{\partial x} \quad (7-1)$$

where J = diffusion current

D = diffusion constant[§]

N = concentration of the diffusing substance

x = distance coordinate

From this it can be shown that if D is independent of concentration, the concentration change with time may be expressed as

$$\frac{\partial N}{\partial t} = D \frac{\partial^2 N}{\partial x^2} \quad (7-2)$$

or, in general coordinates,

$$\frac{\partial N}{\partial t} = D \nabla^2 N \quad (7-3)$$

In case D is not a constant, Eq. (7-3) becomes

$$\frac{\partial N}{\partial t} = \vec{\nabla} \cdot (D \vec{\nabla} N) \quad (7-4)$$

*See the section on diffusion constants for an elaboration of these assumptions and a discussion of diffusion mechanisms.

† These are general references to diffusion and heat-flow processes.

‡ Superscript numbers indicate items listed in References at the end of the chapter.

§ See the section on diffusion constants for numbers appropriate for silicon.

There are two general categories of solutions that might be considered. One is the steady-state condition in which the concentration at any point is invariant with time. Such a set of circumstances could, for example, eventually arise from a source on one side of a plate diffusing through the plate and evaporating from the other side, or from diffusion into a surface which is slowly evaporating. This is discussed in Case 7. The other solutions are transient and are applicable over the time range before the concentration becomes time-independent.

Most diffusions are made normal to a large surface area and do not extend very far into the parent material so that a one-dimensional solution to Fick's equation is usually adequate. Several different boundary conditions falling into this category are of use and will be discussed.

Case 1. Diffusion from an Infinite Source. If the initial concentration in the bulk of the solid is negligible, and the surface concentration is N_0 impurity atoms/cm³ and remains constant, then³

$$N(x,t) = N_0 \left(1 - \operatorname{erf} \frac{x}{2\sqrt{Dt}} \right)^* \quad (7-5)$$

This equation is plotted in Fig. 7-1a using semilogarithmic coordinates and in Fig. 7-1b with linear coordinates.

In the event that the concentration N_1 in the bulk is uniform, but not negligible, and is the same element as N_0 ,⁵

$$N(x,t) = N_1 + (N_0 - N_1) \left(1 - \operatorname{erf} \frac{x}{2\sqrt{Dt}} \right) \quad (7-6)$$

This is the case often encountered in making one-step transistor emitter and base diffusions. Such diffusions are usually made from a "glassy source" on the surface of the silicon. This glassy layer maintains the surface concentration fixed at some surface concentration N_0 , independent of the length of the diffusion.

If an n-type diffusion is being made into p-type material of concentration N' , or

* See the following section for a brief discussion of error functions.

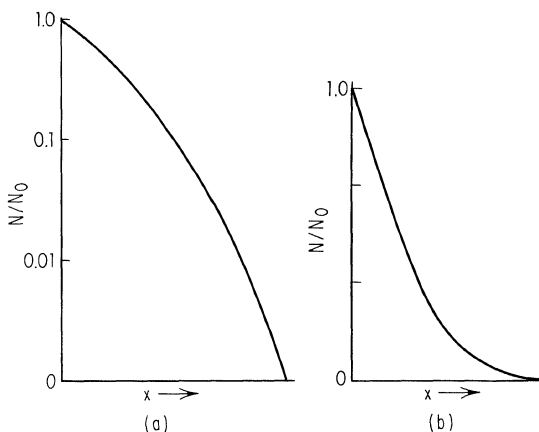


Fig. 7-1. Impurity concentration versus depth for diffusion from an infinite source.

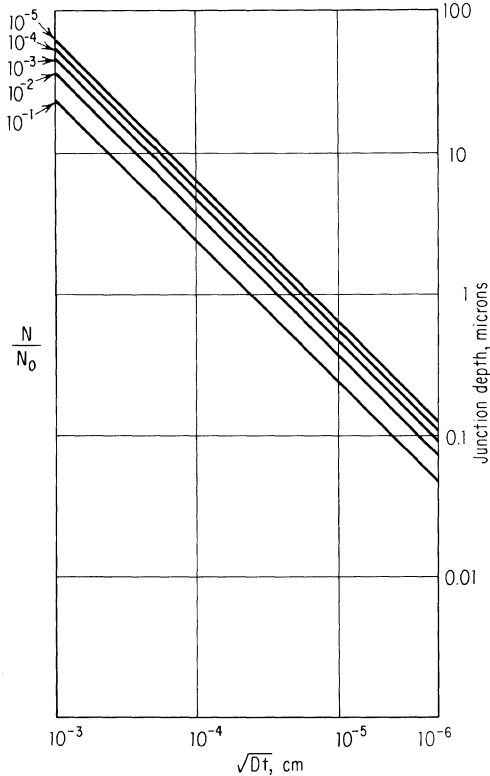


Fig. 7-2. Junction depth versus \sqrt{Dt} for various ratios of N_1/N_0 .

vice versa, then a junction will occur where $N(x,t) = N'$, or when

$$N_0 \left(1 - \operatorname{erf} \frac{x_j}{2\sqrt{Dt}} \right) = N' \tag{7-7}$$

The value of x_j for which this occurs can be calculated or an approximate value obtained from Fig. 7-2. If a second diffusion, with impurity type opposite to that of the first, is now made, a second junction will occur when

$$N_0 \left(1 - \operatorname{erf} \frac{x}{2\sqrt{D't'}} \right) + N' = N_0 \left(1 - \operatorname{erf} \frac{x}{2\sqrt{Dt}} \right) \tag{7-8}$$

where N'_0 is surface concentration of the second diffusant, and $D't'$ is its diffusion-time product.

Sometimes the two diffusions are done simultaneously, but more often they will be done in sequence, and quite likely at different temperatures. The Dt product required in the equation for each diffusion is then the sum of the Dt 's for that step and all following ones. This is discussed in the next section.

Figure 7-3 shows the individual impurity distributions and the net impurity distribution ($N_A - N_D$) as described by Eq. (7-8). Equation (7-8) assumes that the second diffusant N'_0 is a different species than the original N' slab doping (collector doping). In the event N' and N'_0 are the same element, then Eq. (7-6) must be used rather than Eq. (7-5) for the distribution, so that Eq. (7-8) now becomes

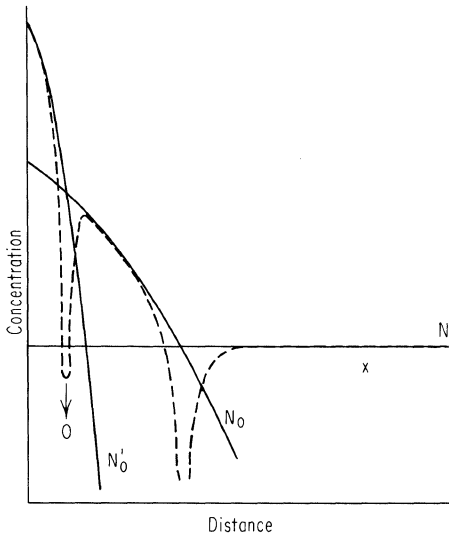


Fig. 7-3. Impurity distribution described by Eq. (7-8).

$$(N'_0 - N'_1) \left(1 - \operatorname{erf} \frac{x}{2\sqrt{D't'}} \right) + N'_1 = N_0 \left(1 - \operatorname{erf} \frac{x}{2\sqrt{Dt}} \right) \quad (7-9)$$

While tedious calculations are required to get precise junction locations and profiles for the various distributions considered, it is often quite satisfactory to use a simple graphical analysis. This will be described in the following section on numerical calculations.

During the design of transistors it is also of interest to know the maximum base doping and its location. The location $x_{b,\max}$ is found by setting $\partial N/\partial x = 0$ and solving for x . After a double diffusion corresponding to Eq. (7-8)

$$N(x,t) = N' + N'_0 \left(1 - \operatorname{erf} \frac{x}{2\sqrt{D't'}} \right) - N_0 \left(1 - \operatorname{erf} \frac{x}{2\sqrt{Dt}} \right) \quad (7-10)$$

and

$$\frac{\partial N}{\partial x} = -N'_0 \frac{1}{\sqrt{\pi D't'}} e^{-x^2/4D't'} + N_0 \frac{1}{\sqrt{\pi Dt}} e^{-x^2/4Dt} \quad (7-11)$$

By setting Eq. (7-11) equal to zero, $x_{b,\max}$ can be solved directly and N_{\max} can then be found by substituting $x_{b,\max}$ into Eq. (7-10).⁶ For the specific case of simultaneous diffusion, so that $t = t'$,

$$x_{b,\max} = \left(\frac{4t}{1/D - 1/D'} \log \frac{N_0}{N'_0} \sqrt{D'/D} \right)^{1/2} \quad (7-12)$$

From this equation it can be seen that $x_{b,\max}/\sqrt{Dt}$ is time-independent so that when it is substituted into Eq. (7-10) to calculate N_{\max} , N_{\max} is also time-independent. Thus, while the position of maximum base concentration may change with time, the maximum concentration itself remains constant.

High-frequency transistor performance depends among other things on the base

resistance. As can be seen from Fig. 7-3 a number proportional to base conductance would be

$$\frac{\int (\text{Base concentration as a function of } x) dx}{\text{Base width}} \tag{7-13}$$

The integral is sometimes referred to as the ‘‘Gummel number’’⁷ and can either be solved analytically or by approximation, depending on the distribution involved.

Case 2. Bilateral Diffusion. If simultaneous diffusions from an infinite source are made from each side of a slab of finite thickness a , the distribution is given by³

$$N(x,t) = N_0 \left[1 - \frac{4}{\pi} \left(\epsilon^{-y} \sin \frac{\pi x}{a} + \frac{1}{3} \epsilon^{-9y} \sin \frac{3\pi x}{a} + \frac{1}{5} \epsilon^{-25y} \sin \frac{5\pi x}{a} + \dots \right) \right] \tag{7-14}$$

where $y = \pi^2 Dt/a^2$.

It should be observed that as y becomes smaller, progressively more terms are required, and that for very small y , corresponding to a semi-infinite medium, the Case 1 solution is easier to use. The behavior of Eq. (7-14) for two values of y is shown in Fig. 7-4.

In the event that diffusion is only from one side of the thin slice of thickness a , as for example if an oxide mask were used on one side, then the solution would be the same as the bilateral case for a thickness of $2a$. That is,

$$N(x,t) = N_0 \left[1 - \frac{4}{\pi} \left(\epsilon^{-y'} \sin \frac{\pi x}{2a} + \frac{1}{3} \epsilon^{-9y'} \sin \frac{3\pi x}{2a} + \dots \right) \right] \tag{7-15}$$

where $y' = \pi^2 Dt/4a^2$. This is illustrated in Fig. 7-5 and arises because the solution of the bilateral case is symmetrical about $x = a/2$. Diffusion for periods of time long enough for the bilateral set of solutions to prevail is not very common, but occasionally is used to obtain a reasonably uniform distribution of some fast diffuser like gold or copper.

If the back side is not bounded by an impermeable face, but by one in which J across it is given by* $J = -K[N_e - N(a)]$

* For a definition of symbols see Case 4.

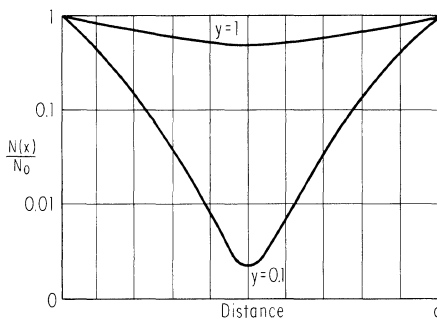


Fig. 7-4. Impurity distribution for bilateral diffusion.

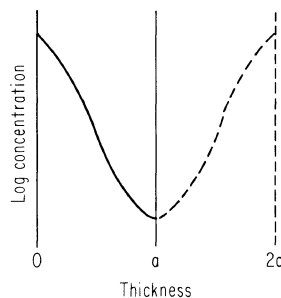


Fig. 7-5. Diffusion into one side of a slice of width a .

then⁸
$$\frac{N(x,t)}{N_0} = A_0 - 2 \sum_1^{\infty} A_n \sin \left(\alpha_n \frac{x}{a} \right) \exp \left(\frac{-\alpha_n^2 D t}{a^2} \right) \quad (7-16)$$

where
$$A_0 = \frac{K[a - (1 - N_e/N_0)x] + D}{D + Ka}$$

$$A_n = \frac{K^2 a^2 + \alpha_n^2 D^2}{\alpha_n(K^2 a^2 + KaD + \alpha_n^2 D^2)}$$

and α_n are the positive roots of the equation

$$\tan \alpha_n = \frac{-\alpha_n D}{aK}$$

Case 3. Diffusion from a Limited Source. If instead of having an infinite source of concentration N_1 at the surface, only a limited supply of S impurities per unit area is available, the solution is³

$$N(x,t) = \frac{S}{\sqrt{\pi D t}} \epsilon^{-x^2/4Dt} \quad (7-17)$$

In this case, since the total amount of impurity is fixed, continued diffusion reduces the surface concentration. Figure 7-6 illustrates this behavior.

Often, in order to get controlled low-surface concentration, a two-step diffusion is used. In this process, a very short normal diffusion of the type described by Eq. (7-5) is first made. For this first diffusion N_0 will be high and determined probably by either the solid solubility limit of the impurity or by the concentration in a glassy layer that sometimes forms on the surface of the silicon. After the initial short diffusion is made, the slices are removed from the furnace, any glassy layer source removed, and the slices put into a clean furnace for further diffusion. For this second step, the thin layer from the first diffusion will act as a limited source for the second step. In the event the Dt product of the second diffusion is long compared to the first one, the thin layer will appear as a surface source so that Eq. (7-17) is applicable. The value for S is the total number of impurities per cm^2 which entered the surface during the first diffusion and is given by

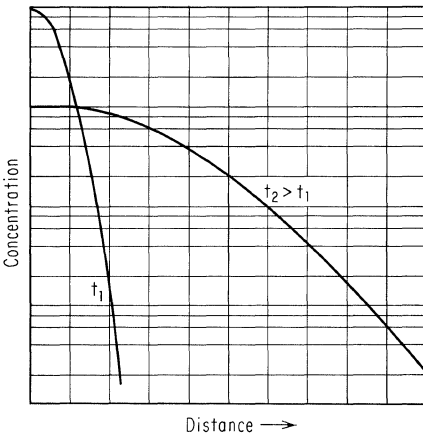


Fig. 7-6. Behavior of diffusion from a limited source for two different times.

$$S = \int_0^\infty N(x) dx = \int_0^\infty N_0 \left(1 - \operatorname{erf} \frac{x}{2\sqrt{Dt}}\right) dx = \frac{2N_0}{\sqrt{\pi}} \sqrt{Dt} \quad (7-18)$$

If this value for S is substituted into Eq. (7-17),

$$N(x,t) = \frac{2N_0}{\pi} \sqrt{\frac{Dt}{D't'}} \epsilon^{-x^2/4D't'} \quad (7-19)$$

The primes indicate the second diffusion. The possibility of D' being different from D arises because the two steps of the diffusion may be made at different temperatures. Sometimes the second diffusion will not be long compared to the first one, so the assumption that the first diffusion will behave as a thin source is not valid. The solution under this condition is⁹

$$N(x,t,t') = N_0 \frac{2}{\sqrt{\pi}} \int_{\sqrt{\beta}}^\infty \epsilon^{-m^2} \operatorname{erf}(\alpha m) dm \quad (7-20)$$

where

$$\alpha = \sqrt{\frac{Dt}{D't'}}$$

$$\beta = \frac{x^2}{4(Dt + D't')}$$

The integral has been evaluated by Smith for various α 's and β 's and is tabulated in the next section.¹⁰

The surface concentration after the second diffusion is given by

$$N_{\text{sur}} = N_0 \frac{2}{\pi} \tan^{-1} \sqrt{\frac{Dt}{D't'}} \quad (7-21)$$

Case 4. In and Out Diffusion with a Rate Limitation at the Surface. In Case 1, the surface concentration was determined directly and immediately by some external phase. In some circumstances, however, there is a rate-limiting process involved in the transfer of impurities from the source phase to the surface. For example, if a gas were used as the source, the amount of impurities actually penetrating the surface might depend not only on the concentration in the gas phase, but also on a sticking probability. In out diffusion, there is usually an energy barrier to the direct transfer of atoms from the solid to the gas, so there is a probability of escape involved.

If it is assumed that the transport of material across the surface is proportional to the difference between the actual surface concentration $N(0)$ and the equilibrium concentration N_e , the flux J across the surface is given by

$$J = K[N_e - N(0)]$$

where K is the rate constant.

The solution equivalent to Case 1, but with this as an added boundary condition, is given by¹¹

$$N(x,t) = N_1 + (N_e - N_1) \epsilon^{-y^2} \{ \epsilon^{y^2} (1 - \operatorname{erf} y) - \epsilon^{(y+Z)^2} [1 - \operatorname{erf}(y+Z)] \} \quad (7-22)$$

where

$$y = \frac{x}{2\sqrt{Dt}}$$

$$Z = \frac{K}{D}\sqrt{Dt}$$

For $Z \rightarrow \infty$, that is, K is so much larger than D that there is no rate limiting, then N_e becomes N_0 and Eq. (7-22) reduces to Eq. (7-6). If $N_e = 0$ and $Z \rightarrow \infty$, then Eq. (7-22) becomes

$$N(x,t) = N_1 \operatorname{erf} \frac{x}{2\sqrt{Dt}} \tag{7-23}$$

and represents out diffusion with no rate limitation.

Equation (7-22) has little application to silicon since apparently K is always small, though no numbers appear to have been published. Figure 7-7 is a graphical solution to Eq. (7-22) for $N_e = 0$, i.e., out diffusion, for various values of K .*

Case 5. Diffusion from a Concentration Step. If at $t = 0$, $N(-x)$ equals a constant N_1 and $N(+x)$ equals a constant N_2 ,³

$$N(x,t) = \frac{N_1}{2} \left(1 - \operatorname{erf} \frac{x}{2\sqrt{Dt}} \right) + \frac{N_2}{2} \left(1 + \operatorname{erf} \frac{x}{2\sqrt{Dt}} \right) \tag{7-24}$$

so that the diffusion from each side can be considered independent of the other,

* For graphical solutions to the in-diffusion case, the reader is referred to Smits and Miller, *Bell Telephone System, Tech. Publ., Monographs*, no. 3119.

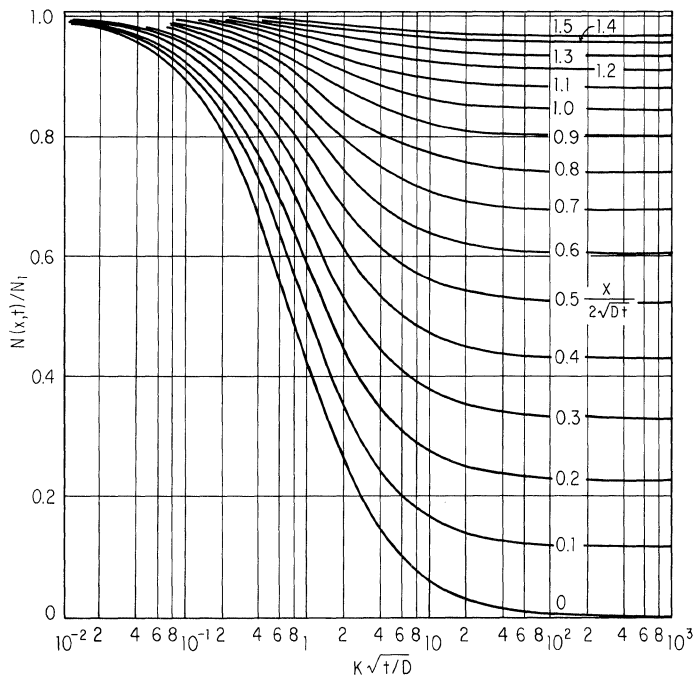


Fig. 7-7. Graphical solution to Eq. (7-22). (Miller and Smits.⁸⁰)

and the actual distribution is given by the sum of the individual solutions regardless of whether N_1 and N_2 are the same impurity. The initial distribution and one at some later time are shown in Fig. 7-8. In the event the step is not at $x = 0$, but rather at $x = a$, it then becomes necessary to substitute $(x - a)$ for x in Eq. (7-24). Before proceeding further with this case it is to be observed that in actual practice one does not suddenly obtain an initial distribution as shown in Fig. 7-8, but that the crystal had to be grown in a finite time at elevated temperatures, so that by the time some reasonable thickness layer was added, either from a melt or from vapor, some diffusion has already occurred; and that there is the possibility that the moving boundary close to the initial concentration step will require a different solution from that given by Eq. (7-24). It will be shown in the next case that under most circumstances, this effect is trivial and can be neglected. The diffusion during crystal growth is not trivial however, and in fact it is quite often that distribution which is desired.¹² Since it is legitimate to neglect effects of the moving boundary, one can assume the initial concentration as shown in Fig. 7-8 and calculate the concentration at the end of the process by means of Eq. (7-24) and the time and temperature of growth. Likewise, if there is further processing involved, the total diffusion can be calculated by using the effective Dt product as described earlier and discussed in the next section.

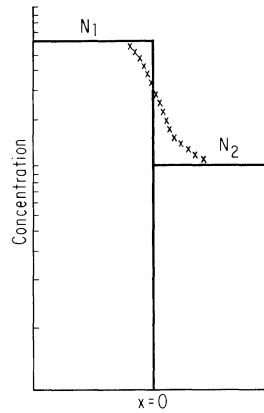


Fig. 7-8. Impurity distribution for diffusion from a concentration step.

This case describes the distribution that occurs during grown-junction crystal growing and during epitaxial deposition and is quite an important one. In particular, the ability to epitaxially grow alternate layers of different doping levels and impurities opens up a vast array of doping distributions not realizable with simple multiple diffusions from one or two surfaces and, simultaneously, makes the determination of the profile much more involved.

Single Step.

1. If the impurities on each side are different but of the same type, and if the one with the highest concentration has a much lower diffusion coefficient than the other, then the profile will be as shown in Fig. 7-9, and the resistivity will increase. The limit of this occurs when $D_1 = 0$, at which time, $N_2(0+,t) = N_2^0/2$, so that the resistivity very close to the original step can rise to twice the original value. Continued diffusion for reasonable values of D and $N_1^0 \gg N_2^0$ will however soon eliminate this resistivity maximum.
2. If $N_1^0 = N_2^0$ but is of opposite type, for example, $N_n^0 = N_p^0$, then the position of junction will remain fixed, independent of the D 's and t 's. Likewise, if $N_n^0 > N_p^0$, the junction will move into the p side as time increases, regardless of the relative values of D_n and D_p . The amount of movement however does depend on D_n , D_p , and t , as well as on N_p^0 and N_n^0 , and can be found by approximation from the equation

$$\frac{N_n^0}{N_p^0} = \frac{1 + \operatorname{erf} x_j/2\sqrt{D_p t}}{1 - \operatorname{erf} x_j/2\sqrt{D_n t}} \tag{7-25}$$

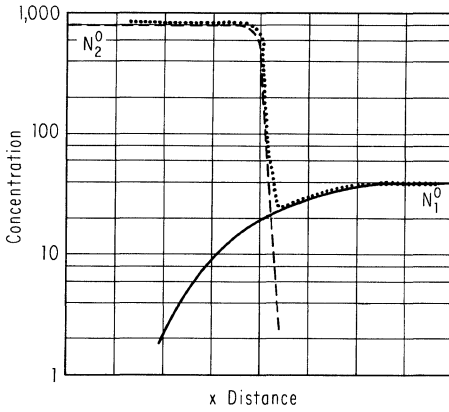


Fig. 7-9. Diffusion from a concentration step when the impurities on each side are different.

Multiple Steps. In the event multiple layers are grown and all doped with different impurities, the diffusions can be considered to proceed independently. The final distribution is the sum of the distributions arising from the various steps and is most easily determined graphically. Similarly, if each concentration step is far

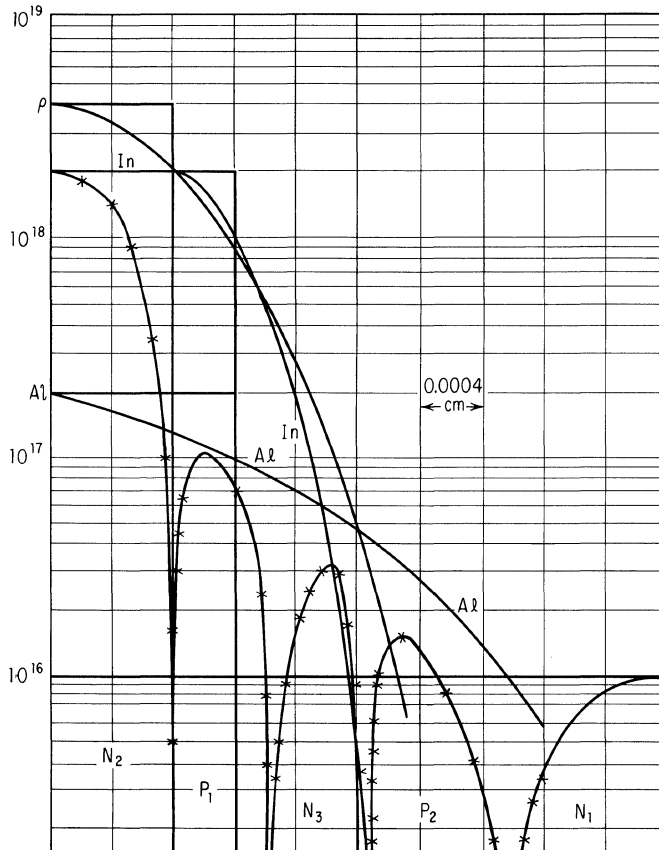


Fig. 7-10. n-p-n-p-n structure derived from diffusion of a three-layer structure.

enough removed from its neighbors to behave independently, then again, the sum of the individual solutions is adequate. If neither simplification occurs, each case must be solved according to its individual boundary conditions. The number of possibilities are endless and, for example, Fig. 7-10 illustrates a configuration that can occur after an initial rather simple distribution which can be generated either by growing from the melt or by vapor-phase deposition.¹³

Case 6. Diffusion from a Concentration Step in Which the Material Thickness on One Side of the Step Is Initially Zero and Increases Linearly with Time.¹⁴ This is illustrated in Fig. 7-11. The diffusion equation to be solved now becomes

$$D \frac{\partial^2 N}{\partial x^2} = \frac{\partial N}{\partial t} + v \frac{\partial N}{\partial x} \tag{7-26}$$

instead of Eq. (7-2). The origin is held fixed at the surface and v is the velocity at which the material thickness increases. Three sets of boundary conditions may be considered.

- (1) Boundary conditions: $N(0,t) = N_1$
 $N(\infty,t) = 0$
 $N(x,0) = 0$

This corresponds to the original semi-infinite slab having zero concentration and the layer being added having N_1 impurities/cm³ in it at the time of addition. This is shown in Fig. 7-12. Equation (7-26) with these boundary conditions has a solution

$$N(x,t) = \frac{N_1}{2} \left[\operatorname{erfc} \left(\frac{x - vt}{2\sqrt{D_1 t}} \right) + e^{vx/D_1} \operatorname{erfc} \frac{x + vt}{2\sqrt{D_1 t}} \right] \tag{7-27}$$

- (2) Boundary conditions: $N(x,0) = N_2$
 $N(\infty,t) = N_2$
 $J = (K + v)N(0,t)$

This assumes the added layer has no impurities in it ($N = 0$), that the rate of loss at the surface is determined by a rate constant K , and that $N_e = 0$. For this set of conditions

$$N(x,t) = N_2 - \frac{N_2}{2} \left[\operatorname{erfc} \left(\frac{x - vt}{2\sqrt{D_2 t}} \right) + \frac{K + v}{K} e^{vx/D_2} \operatorname{erfc} \frac{x + vt}{2\sqrt{D_2 t}} \right] + N_2 \left(\frac{2K + v}{2K} \right) e^{[(K+v)/D_2](x+Kt)} \times \operatorname{erfc} \frac{x + (2K + v)t}{2\sqrt{D_2 t}} \tag{7-28}$$

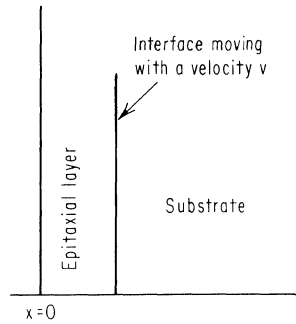


Fig. 7-11. Moving boundary geometry.

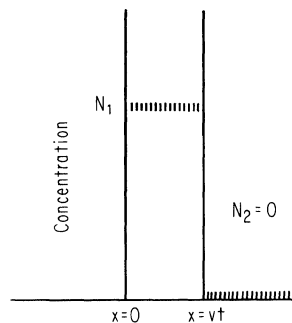


Fig. 7-12. Imaginary concentration profile before diffusion has occurred.

Usually K will be very small for silicon so that Eq. (7-28) reduces to

$$N(x,t) = \frac{N_2}{2} \left[1 + \operatorname{erf} \frac{x - vt}{2\sqrt{D_2t}} \right] \quad (7-29)$$

(3) The original material has an impurity concentration of N_2 impurities/cm³, and the layer has a concentration of N_1 impurities/cm³ as it is being added. If the impurities are different on each side of the step, e.g., in an epitaxial deposition where one side might be an arsenic-doped substrate, and the growing layer is doped with phosphorus on the other side, the solution is the sum of the solutions to boundary conditions (1) and (2). For K equal to zero, the solution is the sum of Eqs. (7-27) and (7-29) or

$$N(x,t) = \frac{N_1}{2} \left[\operatorname{erfc} \left(\frac{x - vt}{2\sqrt{D_1t}} \right) + e^{vx/D_1} \operatorname{erfc} \frac{x + vt}{2\sqrt{D_1t}} \right] + \frac{N_2}{2} \left(1 + \operatorname{erf} \frac{x - vt}{2\sqrt{D_2t}} \right) \quad (7-30)$$

In order to compare deviations of the solutions of Eq. (7-26) from the simpler version of Case 5, it is convenient to consider Eqs. (7-27) and (7-28) for various values of v^2t/D and Kvt/D .

Direct numerical calculations show that $N(x,t)$ of Eq. (7-27) (plotted in Fig. 7-13) differs only a few per cent from that of Eq. (7-24) for $v^2t/D = 100$, and that agreement is better for larger v^2t/D . For $v^2t/D > 100$ and $Kvt = 0$, Eqs. (7-24) and (7-28) are in agreement to within a fraction of a per cent, and again the agreement becomes better as v^2t/D becomes larger. For $Kvt/D = 10$ and $v^2t/D > 100$, agreement is to within a few per cent. Using values of diffusion

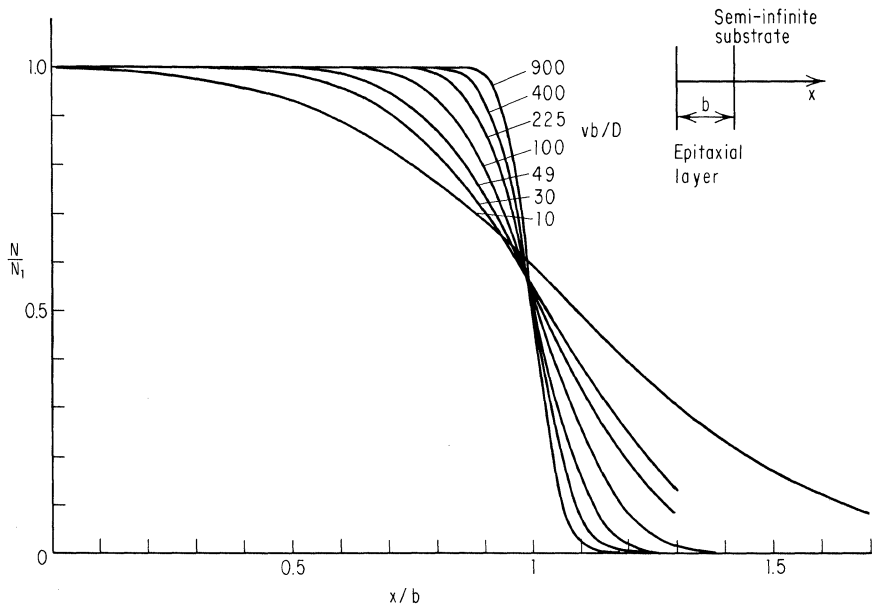


Fig. 7-13. Distribution of impurity added with growing layer. (Rice.¹⁴)

coefficients appropriate for silicon and growth velocities and times normal for epitaxial deposition, it is virtually impossible to realize a $v^2t/D < 100$. No good values of K are available, but apparently K is low enough to consider negligible.

Case 7. Diffusion into a Medium with the Boundary Moving in the Direction of Diffusion. The boundary is considered moving in the $+x$ direction with uniform velocity v . The boundary conditions then become

$$\begin{aligned} N(x,0) &= 0 && \text{for } t = 0, x > 0 \\ N(vt,t) &= N_0 && \text{for all } t\text{'s} \end{aligned}$$

Again the equation to be solved is

$$D \frac{\partial^2 N}{\partial x^2} = \frac{\partial N}{\partial t} \quad (7-31)$$

With the change of variable $x' = x - vt$, Eq. (7-31) becomes

$$D \frac{\partial^2 N}{\partial x'^2} + v \frac{\partial N}{\partial x'} = \frac{\partial N}{\partial t} \quad (7-32)$$

This equation has a solution¹⁵

$$N(x - vt, t) \equiv N(x', t) = \frac{N_0}{2} \left[\left(\operatorname{erfc} \frac{x' + vt}{2\sqrt{Dt}} \right) + \epsilon^{-vx'/D} \operatorname{erfc} \frac{x' - vt}{2\sqrt{Dt}} \right] \quad (7-33)$$

where x' is the distance measured from the actual boundary at any given time. Comparison of this solution with that of Eq. (7-27) of Case 6, which was the addition of material rather than its removal, shows, as expected, that the two solutions are identical except for the reversal of the sign of v .

Equation (7-33) applies where simultaneous diffusion and evaporation are occurring or where some vapor etching process can proceed coincidentally with the diffusion.

Since the diffusion front moves more slowly at larger x , it is possible to reach a condition where the amount of material removed per unit time just matches the forward motion of the front, so that with respect to the actual (moving) boundary, the front is stationary. The requirements for this condition may be found by setting $\partial N/\partial t$ of Eq. (7-32) equal to zero.¹⁶ This gives

$$N(x) = N_0 \epsilon^{-vx'/D} \quad (7-34)$$

Now, if the original material has an initial doping concentration of N' impurities of the opposite type, a junction will occur where $N = N'$, and the depth x' would be independent of time and given by

$$x' = \frac{D}{v} \log \frac{N_0}{N'} \quad (7-35)$$

if enough time had elapsed for the steady-state condition to prevail. An estimate of this time can be obtained by assuming it to be comparable to the time required to evaporate a layer of thickness x' . Thus

$$t_{\text{equil}} \approx \frac{D}{v^2} \log \frac{N_0}{N'} \quad (7-36)$$

Case 8. Diffusion through a Layer of Medium 1 into a Semi-infinite Block of Medium 2. If the diffusion coefficient in medium 1 is D_1 and in medium 2 is D_2 , then

$$D_1 \frac{\partial^2 N_1}{\partial x^2} = \frac{\partial N_1}{\partial t} \quad \text{for } -a < x < 0$$

$$D_2 \frac{\partial^2 N_2}{\partial x^2} = \frac{\partial N_2}{\partial t} \quad \text{for } x > 0$$
(7-37)

If there is no discontinuity in concentration at the interface between mediums 1 and 2, then the boundary conditions are as follows (see Fig. 7-14):

(1) The current J_1 in medium 1 at $x = 0$ equals the current J_2 in medium 2 at $x = 0$, i.e.,

$$J_1 = J_2 = D_1 \frac{\partial N_1}{\partial x} = D_2 \frac{\partial N_2}{\partial x}$$
(7-38)

(2) $N_1(0,t) = N_2(0,t)$

(3) $N_1(-a,t) = N_0$

(4) $N_2(x,t) \rightarrow 0$ as $x \rightarrow \infty$

These boundary conditions, combined with the Eq. (7-37), give¹⁷

$$N_1(x,t) = N_0 \sum_{j=0}^{\infty} \left(\frac{1-\mu}{1+\mu} \right)^j \left(\operatorname{erfc} \frac{a(2j+1)+x}{L_1} - \frac{1-\mu}{1+\mu} \operatorname{erfc} \frac{a(2j+1)-x}{L_1} \right)$$
(7-39)

$$N_2(x,t) = \frac{2\mu N_0}{1+\mu} \sum_{j=0}^{\infty} \left(\frac{1-\mu}{1+\mu} \right)^j \operatorname{erfc} \left[\frac{a(2j+1)}{L_1} + \frac{x}{L_2} \right]$$
(7-40)

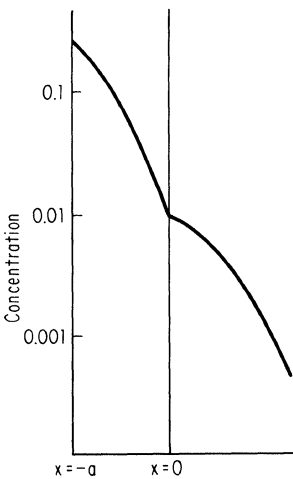


Fig. 7-14. Diffusion through a thin layer into a semi-infinite medium.

where $\mu = \frac{D_1}{D_2}$

$$L_1 = 2 \sqrt{D_1 t}$$

$$L_2 = 2 \sqrt{D_2 t}$$

If a/L_1 is greater than or equal to 1, then one term in the summation will be a good approximation, so that

$$N_1(x,t) \approx N_0 \left(\operatorname{erfc} \frac{a+x}{L_1} - \frac{1-\mu}{1+\mu} \operatorname{erfc} \frac{a-x}{L_1} \right)$$
(7-41)

$$N_2(x,t) \approx \frac{2\mu N_0}{1+\mu} \operatorname{erfc} \left(\frac{a}{L_1} + \frac{x}{L_2} \right)$$
(7-42)

In the event that $N_2(0,t) < N_1(0,t)$ and is given by $N_2(0,t) = kN_1(0,t)$, i.e., if there is a segregation coefficient less than 1 for an impurity moving from medium 1 to medium 2, then another solution is in order. For the case of $a/L > 1$ and $N_2(0,t)$ not limited by the diffusant's maximum solubility in medium 2¹⁸

$$N_1(x,t) \approx N_0 \left(\operatorname{erfc} \frac{a+x}{L_1} - \frac{k-\mu}{k+\mu} \operatorname{erfc} \frac{a-x}{L_1} \right) \quad (7-43)$$

$$N_2(x,t) \approx \frac{2k\mu}{k+\mu} N_0 \operatorname{erfc} \left(\frac{a}{L_1} + \frac{x}{L_2} \right) \quad (7-44)$$

This is illustrated in Fig. 7-15.

Case 9. Diffusion through an Oxide Growing on the Silicon Surface.¹⁹ As the oxide grows it devours silicon, so the silicon-silicon oxide boundary moves in the direction of diffusion. Since the density of the grown oxide is comparable to that of silicon, the silicon oxide–ambient interface moves in the opposite direction. These conditions are illustrated in Fig. 7-16. $Z = 0$ in Fig. 7-16 merely represents a stationary reference plane. The x coordinates are associated with the oxide, the y 's with the silicon. Consider that the thickness a of the oxide is given by

$$a = (a_0^2 + \sigma^2 t)^{1/2} \quad (7-45)$$

- where a_0 = initial thickness
- σ = oxidation rate constant
- t = diffusion (growing) time

The boundary conditions are

$$\begin{aligned} N_1(x=0,t) &= N \\ N_2(y=\infty,t) &= 0 \\ kN_1(x=a,t) &= N_2(y=0,t) \end{aligned}$$

For region 1, which is the oxide layer,

$$D_1 \frac{\partial^2 N_1}{\partial x^2} = \frac{\partial N_1}{\partial t} \quad (7-46)$$

For region 2, the silicon layer,

$$D_2 \frac{\partial^2 N_2}{\partial y^2} + \frac{\sigma^2}{2r(a_0^2 + \sigma^2 t)^{1/2}} \frac{\partial N_2}{\partial y} = \frac{\partial N_2}{\partial t} \quad (7-47)$$

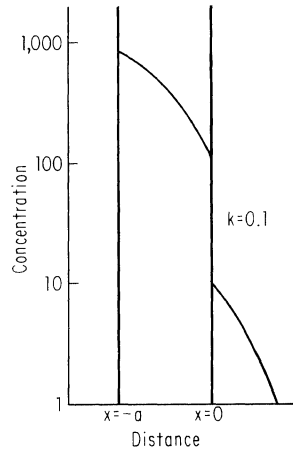


Fig. 7-15. Diffusion through a thin layer into a semi-infinite medium when k is less than 1.

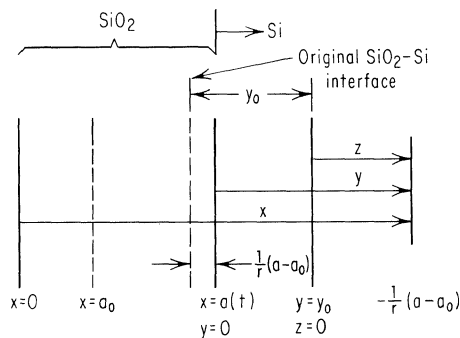


Fig. 7-16. Coordinates for the moving boundary problem. (Tsai.¹⁹)

where r is the volume ratio of silicon dioxide to silicon, k a segregation coefficient,* and the multiplier of $\partial N_2/\partial y$ is the velocity with which the silicon-silicon oxide surface moves. The solutions to these equations are

$$N_1(x,t) = N_0 \left[1 - \frac{DF \operatorname{erf} x/2\sqrt{D_1t}}{(DF + (1/k) \operatorname{erfc} \sigma/2r\sqrt{D_2}) \operatorname{erf} a/2\sqrt{D_1t}} \right] \quad (7-48)$$

$$N_2(y,t) = N_0 \frac{\operatorname{erfc} \{(\sigma/2\sqrt{D_2}) [(1/r) + (y/a)]\}}{DF + (1/k) \operatorname{erfc} (\sigma/2r\sqrt{D_2})} \quad (7-49)$$

where
$$D = \sqrt{\frac{D_2}{D_1}} \epsilon^{-\sigma^2/4r^2D_2} - \frac{\sigma\sqrt{\pi}}{2r\sqrt{D_1}} \operatorname{erfc} \frac{\sigma}{2r\sqrt{D_2}} \quad (7-50)$$

and
$$F = \frac{\sigma\sqrt{t}}{a} \epsilon^{a^2/4D_1t} \operatorname{erf} \frac{a}{2\sqrt{D_1t}} \quad (7-51)$$

Using numbers appropriate for silicon, it can be shown that for k of the order of 1, the terms containing k can be neglected. Rather sketchy data indicate that k for phosphorus¹⁸ is probably less than 0.1 and for boron²⁰ about 0.016.

This case is particularly applicable to the planar method of making devices, where it is usual to simultaneously diffuse and grow the oxide for the next step. It may become more complicated however because some diffusions are two-step processes in which one step may involve oxide growth and diffusion from a source already in the silicon.

If the diffusing impurity forms a glassy layer with the silicon oxide, the diffusant concentration will generally be much higher in that region than in the bulk of the oxide. If enough impurity is present, i.e., a very high surface concentration, the glassy layer may grow at the expense of the oxide layer, so that the oxide-layer thickness decreases rather than increases. When the whole layer becomes converted to glass, the concentration at the silicon surface will abruptly increase. Data indicate that this occurs for concentration of boron above 10^{19} atoms/cm³ and probably for phosphorus as well.²⁰ Thus, if it is desired to calculate the impurity concentration on the silicon surface, it is necessary to know which condition prevails and to have the appropriate diffusion constants. Unfortunately, there are only scattered values available and it is difficult to tell whether they are representative of the impurity diffusing through the oxide or of the movement of the glass-oxide interface.

* The k defined above is the reciprocal of the one used in Ref. 19. This change was made in the interest of uniformity of presentation.

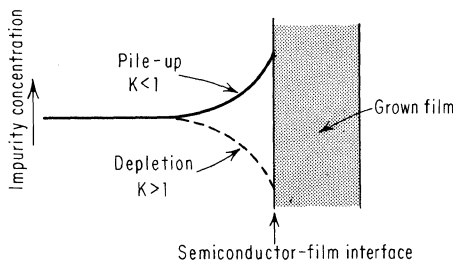
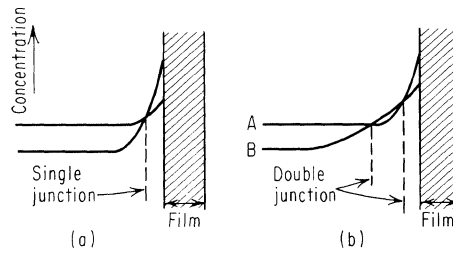


Fig. 7-17. Change of impurity distribution during silicon oxidation. (Atalla and Tannenbaum,²¹)

Fig. 7-18. Formation of junction by impurity redistribution during oxidation. (Atalla and Tannenbaum.²¹)



It is often desirable to determine the effectiveness of a thin layer (oxide or otherwise) as a mask. This can be done by examining the amount of impurity that can diffuse through the mask layer during a diffusion run or by examining the concentration at the silicon surface. The latter can be found by setting $x = 0$ in Eq. (7-40) or (7-42) and solving for N_2 , or by setting $y = 0$ in Eq. (7-49) and solving for N_2 . Similarly, if the allowable level of N_2 is known, then the maximum diffusion time (mask failure condition) can be found from these same equations.

Apparently the segregation coefficients of most impurities in the silicon-silicon oxide system favor the impurities remaining in the silicon,* so an oxidation step without any external diffusion source can still increase the concentration of impurities near the boundary.²¹ Conversely, for the cases where k is less than 1, the growing oxide can act as a sink and deplete the silicon near the surface. These possibilities are indicated schematically in Fig. 7-17. In principle it is possible to have both p- and n-type impurities in the original slice and, by this stacking-up effect, introduce either one or two junctions, depending on the relative concentration and diffusion rates. This is shown in Fig. 7-18.

7-2. DIFFUSION ALONG A GRAIN BOUNDARY

An appropriate model is shown in Fig. 7-19 and consists of a thin lamella ($2a$ wide) of material in which the diffusivity is very high, sandwiched between two thick regions in which diffusion proceeds at a normal rate.^{22,23} N is the concentration outside the lamella, and D is the diffusion coefficient. Inside the layer, N' is the concentration and D' the diffusion coefficient. Thus

$$\begin{aligned}
 D \nabla^2 N &= \frac{\partial N}{\partial t} && \text{outside the layer} \\
 D' \nabla^2 N' &= \frac{\partial N'}{\partial t} && \text{inside the layer}
 \end{aligned}
 \tag{7-52}$$

At the boundary between the two media ($x = \pm a$), $N' = N$ and $D' \partial N' / \partial x = D \partial N / \partial x$, i.e., it will be

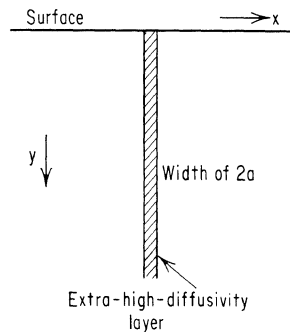


Fig. 7-19. Geometry for diffusion along grain boundaries.

* This effect is difficult to understand considering that results of studies performed on diffusions through an already present oxide indicate just the opposite for phosphorus. One explanation is that there is a significant rate limiting process involved in the transfer of impurities across the interface, and it has really been the effects of this process that have been reported in both cases.

assumed that the segregation coefficient between the layer and the main body of the medium is 1, and that the limits of solubility are the same in both the layer and the bulk. If y is much greater than a , the concentration in the layer can be expressed as a power series.

$$N'(x,y,t) = N'_0(y,t) + N'_1(y,t)x + \frac{N'_2(y,t)x^2}{2} + \dots \quad (7-53)$$

But since N' is symmetrical with respect to x , only even powers of x remain. To a first approximation

$$N'(x,y,t) = N'_0(y,t) + \frac{N'_2(y,t)x^2}{2} \quad (7-54)$$

Substituting in the boundary conditions and eliminating N'_0 and N'_2 give

$$D' \frac{\partial^2 N}{\partial y^2} + \frac{D}{a} \frac{\partial N}{\partial x} = \frac{\partial N}{\partial t} \quad (7-55)$$

for the concentration outside the layer. Fisher²² considered an asymptotic solution and Whipple²³ developed a complete solution of Eq. (7-55) for the case of an infinite source at the surface.

$$N = \operatorname{erfc} \left(\frac{y}{\sqrt{Dt}} + \frac{y}{2\sqrt{\pi Dt}} \right) \int_1^\Delta \epsilon^{-y^2/4Dt\sigma} \times \left\{ \operatorname{erfc} \frac{1}{2} \left[\sqrt{\frac{\Delta-1}{\Delta-\sigma}} \left(\frac{\sigma-1}{\beta} + \frac{x-a}{\sqrt{Dt}} \right) \right] \right\} \frac{d\sigma}{\sigma^{3/2}} \quad (7-56)$$

where
$$\Delta = \frac{D'}{D} \quad \beta = \frac{D'}{D-1} \frac{a}{\sqrt{Dt}}$$

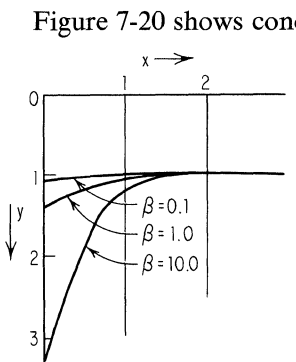


Fig. 7-20. Isoconcentration profile for different values of β . (From "Diffusion in Solids" by Paul G. Shewmon. Copyright © 1963. McGraw-Hill Book Company. Used by permission.)

Figure 7-20 shows concentration curves for various values of β .¹ If time is held constant, these show the effect of different ratios of D'/D . It can be seen that there is little difference until β becomes about 1. If it is assumed that the width of the fast diffusing region ($2a$) is 4 Å (about one atomic plane spacing), $D = 10^{-11}$ cm²/sec (boron at 1250°C), and $t = 10^5$ sec (approximately 28 hr), then D'/D must be greater than 5×10^4 before there is an appreciable effect. This is to be expected since the grain boundary region is so thin that a high diffusivity is required in order to transport much impurity along it.

The same sort of data plotted in Fig. 7-20 can be rearranged as shown in Fig. 7-21. In this case consider that β does not vary because of changes in D'/D , but rather because of an increase in time. It then becomes possible to observe changes in the shape of the diffusion front as it progresses. The spike angle broadens and the per cent increase in penetration depth at the

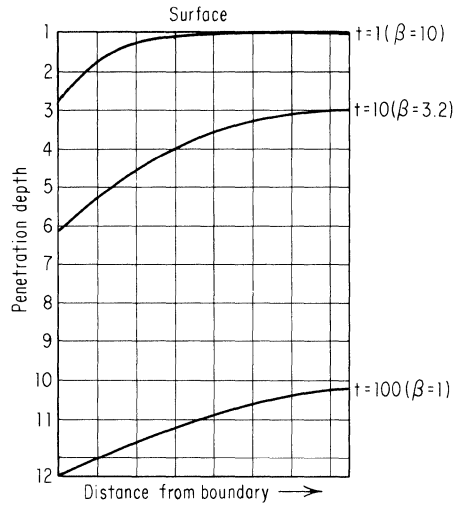


Fig. 7-21. Sketch showing penetration near a grain boundary for various values of time. (Adapted from Whipple.²³)

spike tip decreases. Figure 7-22 shows actual data from a phosphorus diffusion.²⁴ Wood, Austin, and Milford²⁵ have used a computer to obtain various numerical solutions to Whipple's equation and have published some of these.

In order to make experimental data a little more amenable to interpretation, Queisser, Hubner, and Shockley²⁴ have developed a "spike-velocity" method of analysis which uses the same boundary conditions as Whipple's, but derives the solution in terms of different parameters. Their solution is

$$v(\tan \theta)^{-1} = \frac{W_d \sin^2 \theta - W_0}{2D} \quad (7-57)$$

where v = velocity with which the spike tip advances

θ = angle between a concentration curve and a surface normal, measured at $x = a$

$W_d = 2[(D'/D) - 1]a \equiv$ effective width for flux enhancement

$W_0 = (D'/D)W_d \equiv$ effective width for concentration enhancement

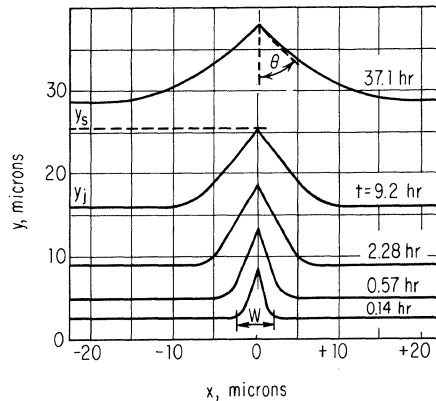


Fig. 7-22. p-n junction profiles or isoconcentration lines for phosphorus diffusion at 1200°C from measurements on photomicrographs of stained, beveled junctions. (Queisser, Hubner, and Shockley.²⁴)

In principle, it is possible to get values of both D' and a , but recall that previous calculations indicated that D'/D had to be in the order of 10^4 before any noticeable deviation from a normal profile occurred. Thus W_0 is so small and the inaccuracies of measuring v , D , and θ so large that in practice only W_d and, accordingly, aD'/D can be determined. Limited data on this ratio are available and are tabulated in the section of diffusion constants.²⁶

Apparently there is little or no increase in diffusion along silicon twin boundaries as in the incoherent grain boundaries just discussed. First-order twins (111), second-order twins (221),²⁷ and stacking faults²⁸ have been examined and showed no anomalous behavior.

7-3. FIELD-AIDED DIFFUSION

If there is an electric field applied during diffusion, if the diffusion impurity is ionized, and if the field is in the proper direction to enhance the diffusion current,

$$D \frac{\partial^2 N}{\partial x^2} - v \frac{\partial N}{\partial x} = \frac{\partial N}{\partial t} \quad (7-58)$$

where v is the velocity imparted to the diffusing ion by the field.³ This equation as written is the same as that used for the moving boundary cases, e.g., Eq. (7-26) or (7-32), so that the solutions derived for them can be used if the boundary conditions are appropriate. Under the influence of the field, $v = \mu E$, where μ is the mobility and E the field,

$$\frac{D}{\mu} = \frac{kT}{qz}$$

where k is Boltzmann's constant, q the electronic charge, and qz the ionic charge, so that v in Eq. (7-26) or (7-32) can be replaced by $EzDq/kT$.

A rough idea of the effect of such a field can be obtained by comparing the value of $EDzqt/kT$ with the values of x of interest. E will be restricted to a few volts/cm by the I^2R heating of the sample and the desired diffusion temperature. Choosing a D of 10^{-12} cm²/sec, a temperature of 1200°C, an E of 2 volts/cm, and a time of 1 hr gives a vt product of approximately 5.6×10^{-8} cm. Thus, for the Groups VA and IIIA elements, the effect is small. However, some of the elements, such as copper, lithium, and zinc are very fast diffusers,²⁹⁻³¹ so that the application of a field can rather quickly redistribute them. Other equally fast diffusers such as iron apparently are un-ionized and so have shown no measurable field enhancement.²⁹

It is also possible to have built-in fields due to the impurity distribution itself, and these fields sometimes can produce a twofold increase in the effective diffusion coefficient. Such circumstances occur when the doping level is high enough that extrinsic conduction still occurs at diffusion temperatures (a curve showing n_i versus temperature may be found in Chap. 8). The holes (or electrons) associated with the impurity have a much higher diffusion coefficient and thus tend to outrun the atom. However, this would cause a space charge to build up, so the net result is that charge carriers drag the atoms along faster than normally.^{32,33}

7-4. NUMERICAL CALCULATIONS

The more simple solutions can be calculated quite easily and many are amenable to very rapid graphic analysis. Examples of these will be given, but for the more complex cases, or where many variations are to be considered, computer solutions are very helpful, but will not be discussed.

Simple error function algebra and error function, coerror function, and Smith's function tables are included at the end of this section (see Tables 7-1 to 7-3). The error and exponential function tables are extensive enough to allow computation of N/N_0 ratios from 1 to about 10^{-6} , e.g., from 10^{20} atoms/cm³ down to 10^{14} atoms/cm³; however, the Smith functions are considerably more restricted.

EXAMPLE 7-1. If gallium is diffused into a thick slice of silicon with no previous gallium in it, at a temperature of 1100°C for 3 hr, what is the final distribution of gallium if the surface concentration is held fixed at 10^{18} atoms/cm³?

1. The boundary conditions fit Case 1, Eq. (7-5), i.e.,

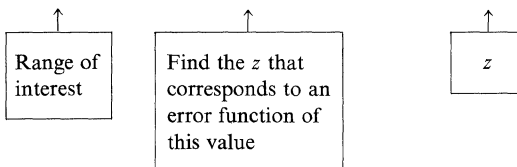
$$\frac{N(x,t)}{N_0} = \operatorname{erfc} \frac{x}{2\sqrt{Dt}}$$

2. Reference to Fig. 7-28 gives D for gallium at 1100°C as 7×10^{-13} cm²/sec.
3. Three hours is 10.8×10^3 sec.
4. A combination of 2 and 3 gives a Dt product of 75.6×10^{-10} cm², or

$$2\sqrt{Dt} = 17.2 \times 10^{-5} \text{ cm}$$

5. Suppose that concentrations in the range of from 10^{18} to 10^{14} are of interest; then the following table can be filled out and the results conveniently plotted on semi-log paper.

$N(x)$	$\frac{N(x)}{N_0}$	$\operatorname{erfc}^{-1} \frac{x}{2\sqrt{Dt}}$	x
10^{18}	1	0.0	0
10^{17}	0.1	1.17	2.0×10^{-4} cm
10^{16}	0.01	1.82	3.1×10^{-4} cm
10^{15}	10^{-3}	2.33	4.0×10^{-4} cm
10^{14}	10^{-4}	2.76	4.7×10^{-4} cm



Graphical Analysis. Since the solutions to many of the diffusion problems of interest involve only the sum of coerror functions, $\operatorname{erfc} (x/2\sqrt{Dt})$ may be plotted for various values of \sqrt{Dt} . Then, for a single element diffusion, concentration profiles can be read directly from the curves. This is also applicable to some of

the more complex solutions (see, for example, Fig. 7-10). For diffusions from steps and/or several diffusions from an exterior boundary, individual profiles can be traced from these curves onto an overlying piece of graph paper with the same coordinates. From these, the summation giving the overall net impurity distribution with distance can be quickly drawn.

The y coordinates of the master curve (Fig. 7-23) are in terms of N/\bar{N} and are plotted on a logarithmic scale, so that N_0 (or $N_0/2$ in the case of diffusion from a step) on the overlay can be matched against $N/\bar{N} = 1$ on the master curve (MC). Mirror image curves are provided to cover diffusion in both the $+$ and $-x$ directions.

EXAMPLE 7-2. Suppose that an epitaxial substrate is doped with 10^{18} atoms/cm³ of arsenic and 5×10^{17} atoms/cm³ of boron. To this is added an epitaxial layer doped with 5×10^{15} atoms/cm³ of antimony and the whole thing held at 1250°C for 100 min. Determine the final net impurity concentration.

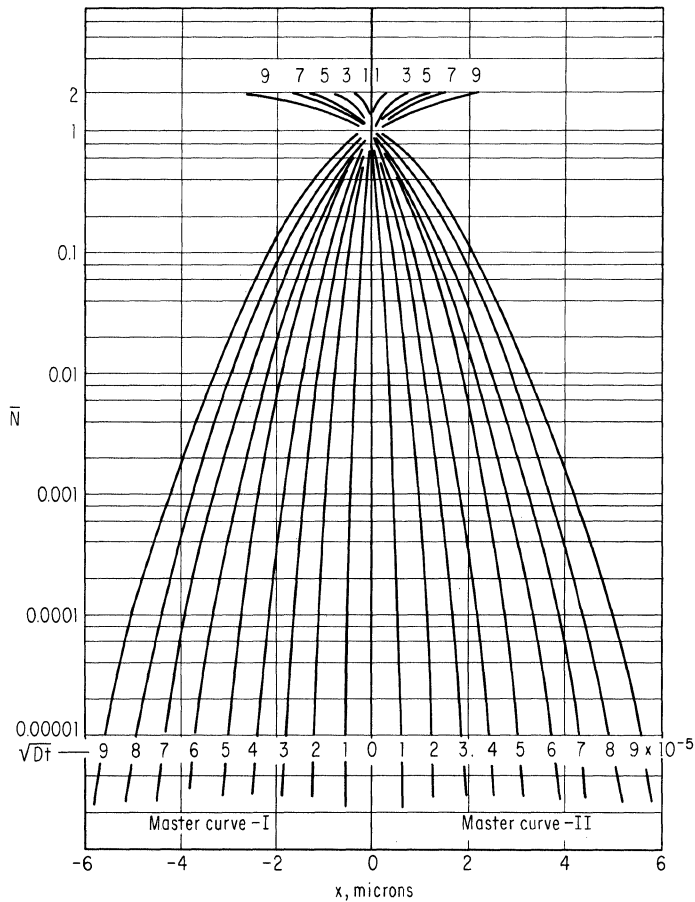
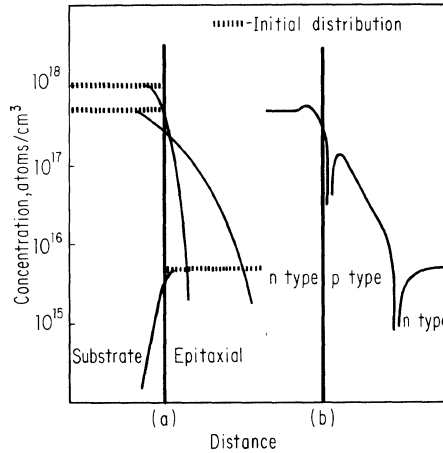


Fig. 7-23. Master curve.

Fig. 7-24. Diffusion from epitaxial substrate which has both n- and p-type dope in it. Notice that for this particular choice, a p layer is formed in the epitaxial layer.



1. The respective \sqrt{Dt} 's are: arsenic, 1.9×10^{-5} ; antimony, 1.9×10^{-5} ; boron, 6.9×10^{-5} .
2. Using master curve I as a guide, sketch in the profiles for arsenic and boron. Be sure to match $N/\bar{N} = 2$ on the master curve with 10^{18} and 5×10^{17} respectively on the overlay.
3. Using master curve II, sketch in the antimony profile, again being sure to match $N/\bar{N} = 2$ with the initial concentration. These three distributions are shown in Fig. 7-24a.
4. Add together the arsenic and antimony concentrations and subtract from them the boron concentration. Note that for this particular case the antimony concentration is very small compared to the amount of arsenic present, so its contribution in the $-x$ direction can be neglected. The final distribution is shown in Fig. 7-24b.

Because it is impractical to hope for graph paper to match the scale of Fig. 7-23, the reader can easily reproduce master curves I and II to his chosen scale. The range of values in Fig. 7-23 covers \sqrt{Dt} 's from 10^{-5} to 9×10^{-5} cm and x 's from 0 to 6 microns. However, since the argument of the erfc function is the ratio of x to $2\sqrt{Dt}$, a scale change can be effected merely by multiplying both values by the same constant, e.g., the curves can also be \sqrt{Dt} 's from 10^{-4} to 9×10^{-4} and x 's from 0 to 60 microns.

Effect of Time Varying Temperature. Often it is desirable to calculate the total amount of diffusion that occurs during a series of temperature cycles. For example, in order to know the final impurity profile in the vicinity of an epitaxial layer-substrate interface after a device has been constructed, it is necessary to consider the diffusion that occurred not only during the deposition cycle, but also during subsequent diffusion, oxide growth, and contact addition steps. Similarly, if a slow cool after diffusion is used, it is necessary to consider the amount of diffusion which took place during the cool-down cycle. In order to compute the total diffusion, an effective Dt product must be found. If a series of discrete times at fixed temperatures is used, then the solution is³⁴

$$Dt_{\text{eff}} = \sum D_1 t_1 + D_2 t_2 + D_3 t_3 + \dots$$

EXAMPLE 7-3. Suppose that a thick silicon epitaxial layer doped with arsenic to a resistivity of 1 ohm-cm were deposited on a 0.001 ohm-cm arsenic-doped substrate. The deposition was at 1250°C for 15 min. Afterward the slice was subjected to an oxidation step of 1 hr at 1150°C and a 2-hr diffusion at 1000°C. Determine the profile in the vicinity of the epitaxial layer-substrate interface after these operations.

1. Reference to Fig. 7-26 gives

$$\begin{aligned} D_{1250} &= 6 \times 10^{-13} \text{ cm}^2/\text{sec} \\ D_{1150} &= 1 \times 10^{-13} \text{ cm}^2/\text{sec} \\ D_{1000} &= 8 \times 10^{-15} \text{ cm}^2/\text{sec} \end{aligned}$$

2. $\Sigma Dt = 900 \times 6 \times 10^{-13} + 3,600 \times 10^{-13} + 7,200 \times 8 \times 10^{-15} = 9.6 \times 10^{-10} \text{ cm}^2$
3. Equation (7-24) is the appropriate one for these boundary conditions, and for the specific case of $D_1 = D_2$, it reduces to

$$N(x,t) = N_1 + \frac{N_2 - N_1}{2} \left(1 - \operatorname{erf} \frac{x}{2\sqrt{Dt}} \right)$$

4. After converting 1 ohm-cm and 0.001 ohm-cm to equivalent impurity concentrations

$$N(x) = 5.2 \times 10^{15} + 5 \times 10^{19} \left(1 - \operatorname{erf} \frac{x}{6.3 \times 10^{-5} \text{ cm}} \right)$$

If the temperature varies continuously with time, then $\int_0^t D(T) dt$ is required. Since $D = D_0 \exp(-A/T)$, and T is now a function of time,

$$Dt_{\text{eff}} = D_0 \int \exp\left(\frac{-A}{T}\right) dt$$

This equation has been explicitly solved for the special case of a linear decrease of temperature with time and is given by³⁵

$$Dt_{\text{eff}} = \frac{D(T_0)T_0^2}{AR} \left[1 - \frac{2T_0}{A} + \left(\frac{6T_0}{A}\right)^2 + \dots \right]$$

where $T = T_0 - Rt$ defines both T_0 and R . In general, however, it appears more appropriate to plot $D(t)$ versus t and use numerical integration to obtain an approximate Dt_{eff} .

Multiple Diffusions.³⁴ After a single diffusion of the type described in Case 1, $N(x,t)$ is given by

$$N(x,t_1) = N_0 \operatorname{erfc} \frac{x}{2\sqrt{D_1 t_1}}$$

If the surface concentration is now increased to a new value N'_0 and diffusion continued for an additional time t_2 ,

$$N(x,t_1 t_2) = N_0 \operatorname{erfc} \frac{x}{2\sqrt{D_1 t_1 + D_2 t_2}} + (N'_0 - N_0) \operatorname{erfc} \frac{x}{2\sqrt{D_2 t_2}}$$

Similarly for three diffusions

$$N(x, t_1, t_2, t_3) = N_0 \operatorname{erfc} \frac{x}{2\sqrt{D_1 t_1 + D_2 t_2 + D_3 t_3}} + (N'_0 - N_0) \operatorname{erfc} \frac{x}{2\sqrt{D_2 t_2 + D_3 t_3}} + (N''_0 - N'_0) \operatorname{erfc} \frac{x}{2\sqrt{D_3 t_3}}$$

or, for the general case

$$N(x) = \sum (N_j - N_{j-1}) \operatorname{erfc} \frac{x}{2 \left(\sum_{k=1}^{n-1} D_K t_K - \sum_{k=0}^{j-1} D_K t_K + D_n t_n \right)^{1/2}}$$

Error Function Algebra.³

$$\operatorname{erf} z = \frac{2}{\sqrt{\pi}} \int_0^z \epsilon^{-\alpha^2} d\alpha = \frac{2}{\sqrt{\pi}} \left[z - \frac{z^3}{3 \cdot 1!} + \frac{z^5}{5 \cdot 2!} + \dots \right]$$

$$\operatorname{erfc} z = (1 - \operatorname{erf} z) = \frac{2}{\sqrt{\pi}} \int_z^\infty \epsilon^{-\alpha^2} d\alpha$$

$$\operatorname{erf}(0) = 0$$

$$\operatorname{erf}(\infty) = 1$$

$$\operatorname{erf}(-z) = -\operatorname{erf} z$$

$$\frac{d}{dz} (\operatorname{erf} z) = \frac{2}{\sqrt{\pi}} \epsilon^{-z^2}$$

$$\frac{d^2}{dz^2} (\operatorname{erf} z) = \frac{-4}{\sqrt{\pi}} z \epsilon^{-z^2}$$

7-5. DIFFUSION PROCESSES

Two requirements for a diffusion process are a means of heating the slices and a source of impurity. The temperature range for silicon is approximately from 900 to 1300°C. The temperature profile required of the furnace depends somewhat on circumstances, but in general, for good control, the portion where slices are placed should be uniform to within a few degrees and controlled as a function of time to the same tolerance. These are all straightforward matters of furnace design and are apparently easily met.

The diffusant source requirements are not so straightforward, and in general compromises must be made. Some desirable features are:

1. The surface concentration should be reproducible from run to run.
2. The surface concentration should be continuously variable over a concentration range of several orders of magnitude with the upper limit being the solid solubility of the impurity in silicon.
3. No compounds difficult or impossible to remove should be formed on the surface.
4. No cracking of the slice should occur because of surface films added before or formed during the diffusion (alloying or thermal mismatch).

Table 7-1. Error Function, erf(z) *

z	erf(z)	z	erf(z)	z	erf(z)	z	erf(z)
0.00	0.000 000	0.50	0.520 500	1.00	0.842 701	1.50	0.966 105
0.01	0.011 283	0.51	0.529 244	1.01	0.846 810	1.51	0.967 277
0.02	0.022 565	0.52	0.537 899	1.02	0.850 838	1.52	0.968 413
0.03	0.033 841	0.53	0.546 464	1.03	0.854 784	1.53	0.969 516
0.04	0.045 111	0.54	0.554 939	1.04	0.858 650	1.54	0.970 586
0.05	0.056 372	0.55	0.563 323	1.05	0.862 436	1.55	0.971 623
0.06	0.067 622	0.56	0.571 616	1.06	0.866 144	1.56	0.972 628
0.07	0.078 858	0.57	0.579 816	1.07	0.869 773	1.57	0.973 603
0.08	0.090 078	0.58	0.587 923	1.08	0.873 326	1.58	0.974 547
0.09	0.101 281	0.59	0.595 936	1.09	0.876 803	1.59	0.975 462
0.10	0.112 463	0.60	0.603 856	1.10	0.880 205	1.60	0.976 348
0.11	0.123 623	0.61	0.611 681	1.11	0.883 533	1.61	0.977 207
0.12	0.134 758	0.62	0.619 411	1.12	0.886 788	1.62	0.978 038
0.13	0.145 867	0.63	0.627 046	1.13	0.889 971	1.63	0.978 843
0.14	0.156 947	0.64	0.634 586	1.14	0.893 082	1.64	0.979 622
0.15	0.167 996	0.65	0.642 029	1.15	0.896 124	1.65	0.980 376
0.16	0.179 012	0.66	0.649 377	1.16	0.899 096	1.66	0.981 105
0.17	0.189 992	0.67	0.656 628	1.17	0.902 000	1.67	0.981 810
0.18	0.200 936	0.68	0.663 782	1.18	0.904 837	1.68	0.982 493
0.19	0.211 840	0.69	0.670 840	1.19	0.907 608	1.69	0.983 153
0.20	0.222 703	0.70	0.677 801	1.20	0.910 314	1.70	0.983 790
0.21	0.233 522	0.71	0.684 666	1.21	0.912 956	1.71	0.984 407
0.22	0.244 296	0.72	0.691 433	1.22	0.915 534	1.72	0.985 003
0.23	0.255 023	0.73	0.698 104	1.23	0.918 050	1.73	0.985 578
0.24	0.265 700	0.74	0.704 678	1.24	0.920 505	1.74	0.986 135
0.25	0.276 326	0.75	0.711 156	1.25	0.922 900	1.75	0.986 672
0.26	0.286 900	0.76	0.717 537	1.26	0.925 236	1.76	0.987 190
0.27	0.297 418	0.77	0.723 822	1.27	0.927 514	1.77	0.987 691
0.28	0.307 880	0.78	0.730 010	1.28	0.929 734	1.78	0.988 174
0.29	0.318 283	0.79	0.736 103	1.29	0.931 899	1.79	0.988 641
0.30	0.328 627	0.80	0.742 101	1.30	0.934 008	1.80	0.989 091
0.31	0.338 908	0.81	0.748 003	1.31	0.936 063	1.81	0.989 525
0.32	0.349 126	0.82	0.753 811	1.32	0.938 065	1.82	0.989 943
0.33	0.359 279	0.83	0.759 524	1.33	0.940 015	1.83	0.990 347
0.34	0.369 365	0.84	0.765 143	1.34	0.941 914	1.84	0.990 736
0.35	0.379 382	0.85	0.770 668	1.35	0.943 762	1.85	0.991 111
0.36	0.389 330	0.86	0.776 100	1.36	0.945 561	1.86	0.991 472
0.37	0.399 206	0.87	0.781 440	1.37	0.947 312	1.87	0.991 821
0.38	0.409 009	0.88	0.786 687	1.38	0.949 016	1.88	0.992 156
0.39	0.418 739	0.89	0.791 843	1.39	0.950 673	1.89	0.992 479
0.40	0.428 392	0.90	0.796 908	1.40	0.952 285	1.90	0.992 790
0.41	0.437 969	0.91	0.801 883	1.41	0.953 852	1.91	0.993 090
0.42	0.447 468	0.92	0.806 768	1.42	0.955 376	1.92	0.993 378
0.43	0.456 887	0.93	0.811 564	1.43	0.956 857	1.93	0.993 656
0.44	0.466 225	0.94	0.816 271	1.44	0.958 297	1.94	0.993 923
0.45	0.475 482	0.95	0.820 891	1.45	0.959 695	1.95	0.994 179
0.46	0.484 655	0.96	0.825 424	1.46	0.961 054	1.96	0.994 426
0.47	0.493 745	0.97	0.829 870	1.47	0.962 373	1.97	0.994 664
0.48	0.502 750	0.98	0.834 232	1.48	0.963 654	1.98	0.994 892
0.49	0.511 668	0.99	0.838 508	1.49	0.964 898	1.99	0.995 111

* For a more complete table, see L. J. Comrie, "Chambers Six Figure Mathematical Tables," vol. 2, W. & R. Chambers, Ltd., Edinburgh, 1949, or "Tables of the Error Function and Its Derivative," National Bureau of Standards Applied Mathematics Series, no. 41, Oct. 22, 1954.

Table 7-1. Error Function, erf(z)* (continued)

<i>z</i>	erf(<i>z</i>)						
2.00	0.995 322	2.50	0.999 593	3.00	0.999 977 91	3.50	0.999 999 257
2.01	0.995 525	2.51	0.999 614	3.01	0.999 979 26	3.51	0.999 999 309
2.02	0.995 719	2.52	0.999 634	3.02	0.999 980 53	3.52	0.999 999 358
2.03	0.995 906	2.53	0.999 654	3.03	0.999 981 73	3.53	0.999 999 403
2.04	0.996 086	2.54	0.999 672	3.04	0.999 982 86	3.54	0.999 999 445
2.05	0.996 258	2.55	0.999 689	3.05	0.999 983 92	3.55	0.999 999 485
2.06	0.996 423	2.56	0.999 706	3.06	0.999 984 92	3.56	0.999 999 521
2.07	0.996 582	2.57	0.999 722	3.07	0.999 985 86	3.57	0.999 999 555
2.08	0.996 734	2.58	0.999 736	3.08	0.999 986 74	3.58	0.999 999 587
2.09	0.996 880	2.59	0.999 751	3.09	0.999 987 57	3.59	0.999 999 617
2.10	0.997 021	2.60	0.999 764	3.10	0.999 988 35	3.60	0.999 999 644
2.11	0.997 155	2.61	0.999 777	3.11	0.999 989 08	3.61	0.999 999 670
2.12	0.997 284	2.62	0.999 789	3.12	0.999 989 77	3.62	0.999 999 694
2.13	0.997 407	2.63	0.999 800	3.13	0.999 990 42	3.63	0.999 999 716
2.14	0.997 525	2.64	0.999 811	3.14	0.999 991 03	3.64	0.999 999 736
2.15	0.997 639	2.65	0.999 822	3.15	0.999 991 60	3.65	0.999 999 756
2.16	0.997 747	2.66	0.999 831	3.16	0.999 992 14	3.66	0.999 999 773
2.17	0.997 851	2.67	0.999 841	3.17	0.999 992 64	3.67	0.999 999 790
2.18	0.997 951	2.68	0.999 849	3.18	0.999 993 11	3.68	0.999 999 805
2.19	0.998 046	2.69	0.999 858	3.19	0.999 993 56	3.69	0.999 999 820
2.20	0.998 137	2.70	0.999 866	3.20	0.999 993 97	3.70	0.999 999 833
2.21	0.998 224	2.71	0.999 873	3.21	0.999 994 36	3.71	0.999 999 845
2.22	0.998 308	2.72	0.999 880	3.22	0.999 994 73	3.72	0.999 999 857
2.23	0.998 388	2.73	0.999 887	3.23	0.999 995 07	3.73	0.999 999 867
2.24	0.998 464	2.74	0.999 893	3.24	0.999 995 40	3.74	0.999 999 877
2.25	0.998 537	2.75	0.999 899	3.25	0.999 995 70	3.75	0.999 999 886
2.26	0.998 607	2.76	0.999 905	3.26	0.999 995 98	3.76	0.999 999 895
2.27	0.998 674	2.77	0.999 910	3.27	0.999 996 24	3.77	0.999 999 903
2.28	0.998 738	2.78	0.999 916	3.28	0.999 996 49	3.78	0.999 999 910
2.29	0.998 799	2.79	0.999 920	3.29	0.999 996 72	3.79	0.999 999 917
2.30	0.998 857	2.80	0.999 925	3.30	0.999 996 94	3.80	0.999 999 923
2.31	0.998 912	2.81	0.999 929	3.31	0.999 997 15	3.81	0.999 999 929
2.32	0.998 966	2.82	0.999 933	3.32	0.999 997 34	3.82	0.999 999 934
2.33	0.999 016	2.83	0.999 937	3.33	0.999 997 51	3.83	0.999 999 939
2.34	0.999 065	2.84	0.999 941	3.34	0.999 997 68	3.84	0.999 999 944
2.35	0.999 111	2.85	0.999 944	3.35	0.999 997 838	3.85	0.999 999 948
2.36	0.999 155	2.86	0.999 948	3.36	0.999 997 983	3.86	0.999 999 952
2.37	0.999 197	2.87	0.999 951	3.37	0.999 998 120	3.87	0.999 999 956
2.38	0.999 237	2.88	0.999 954	3.38	0.999 998 247	3.88	0.999 999 959
2.39	0.999 275	2.89	0.999 956	3.39	0.999 998 367	3.89	0.999 999 962
2.40	0.999 311	2.90	0.999 959	3.40	0.999 998 478	3.90	0.999 999 965
2.41	0.999 346	2.91	0.999 961	3.41	0.999 998 582	3.91	0.999 999 968
2.42	0.999 379	2.92	0.999 964	3.42	0.999 998 679	3.92	0.999 999 970
2.43	0.999 411	2.93	0.999 966	3.43	0.999 998 770	3.93	0.999 999 973
2.44	0.999 441	2.94	0.999 968	3.44	0.999 998 855	3.94	0.999 999 975
2.45	0.999 469	2.95	0.999 970	3.45	0.999 998 934	3.95	0.999 999 977
2.46	0.999 497	2.96	0.999 972	3.46	0.999 999 008	3.96	0.999 999 979
2.47	0.999 523	2.97	0.999 973	3.47	0.999 999 077	3.97	0.999 999 980
2.48	0.999 547	2.98	0.999 975	3.48	0.999 999 141	3.98	0.999 999 982
2.49	0.999 571	2.99	0.999 976	3.49	0.999 999 201	3.99	0.999 999 983

* For a more complete table, see L. J. Comrie, "Chambers Six Figure Mathematical Tables," vol. 2, W. & R. Chambers, Ltd., Edinburgh, 1949, or "Tables of the Error Function and Its Derivative," National Bureau of Standards Applied Mathematics Series, no. 41, Oct. 22, 1954.

Table 7-2. $\operatorname{erfc}(z)$

z	$\operatorname{erfc}(z)$	z	$\operatorname{erfc}(z)$
0	1.000 00	2.00	0.004 68
0.10	0.887 54	2.10	0.002 98
0.20	0.777 30	2.20	0.001 86
0.30	0.671 37	2.30	0.001 14
0.40	0.571 61	2.40	0.000 689
0.50	0.479 50	2.50	0.000 407
0.60	0.396 14	2.60	0.000 236
0.70	0.322 20	2.70	0.000 134
0.80	0.257 90	2.80	0.000 075
0.90	0.203 09	2.90	0.000 041
1.00	0.157 30	3.00	0.000 022 09
1.10	0.119 80	3.10	0.000 011 65
1.20	0.089 69	3.20	0.000 006 03
1.30	0.065 99	3.30	0.000 003 06
1.40	0.047 72	3.40	0.000 001 52
1.50	0.033 90	3.50	0.000 000 743
1.60	0.023 65	3.60	0.000 000 356
1.70	0.016 21	3.70	0.000 000 167
1.80	0.010 91	3.80	0.000 000 77
1.90	0.007 21	3.90	0.000 000 35

Table 7-3. Smith Function* (continued across on facing page)

$\beta \backslash \alpha$	0.1	0.2	0.3	0.4	0.5	0.6	0.7	0.8	0.9	1.0	1.1	1.2
0.1	0.09015	0.08155	0.07376	0.06672	0.06035	0.05459	0.04938	0.04467	0.04040	0.03655	0.03306	0.02990
0.2	0.17838	0.16119	0.14566	0.13162	0.11894	0.10748	0.09713	0.08777	0.07931	0.07167	0.06477	0.05853
0.3	0.26295	0.23723	0.21403	0.19310	0.17422	0.15719	0.14182	0.12795	0.11545	0.10416	0.09398	0.08479
0.4	0.34254	0.30837	0.27761	0.24993	0.22501	0.20259	0.18240	0.16422	0.14786	0.13314	0.11988	0.10794
0.5	0.41626	0.37374	0.33557	0.30132	0.27058	0.24299	0.21822	0.19599	0.17603	0.15812	0.14203	0.12759
0.6	0.48366	0.43290	0.38751	0.34692	0.31062	0.27814	0.24908	0.22308	0.19982	0.17900	0.16036	0.14368
0.7	0.54464	0.48580	0.43340	0.38673	0.34515	0.30809	0.27505	0.24562	0.21937	0.19596	0.17508	0.15645
0.8	0.59940	0.53264	0.47347	0.42100	0.37447	0.33317	0.29652	0.26398	0.23508	0.20940	0.18657	0.16628
0.9	0.64829	0.57380	0.50812	0.45017	0.39903	0.35385	0.31393	0.27864	0.24742	0.21979	0.19532	0.17365
1.0	0.69176	0.60975	0.53784	0.47475	0.41935	0.37066	0.32783	0.29013	0.25693	0.22765	0.20183	0.17903
1.1	0.73033	0.64100	0.56318	0.49529	0.43600	0.38415	0.33877	0.29900	0.26411	0.23348	0.20655	0.18286
1.2	0.76448	0.66808	0.58465	0.51232	0.44950	0.39486	0.34726	0.30574	0.26946	0.23772	0.20991	0.18553
1.3	0.79470	0.69148	0.60276	0.52634	0.46035	0.40327	0.35377	0.31078	0.27336	0.24074	0.21225	0.18734
1.4	0.82144	0.71164	0.61797	0.53781	0.46901	0.40979	0.35870	0.31449	0.27616	0.24286	0.21385	0.18855
1.5	0.84509	0.72899	0.63069	0.54714	0.47586	0.41482	0.36238	0.31720	0.27815	0.24431	0.21492	0.18933
1.6	0.86601	0.74388	0.64130	0.55469	0.48123	0.41865	0.36511	0.31914	0.27953	0.24530	0.21562	0.18983
1.7	0.88454	0.75666	0.65010	0.56076	0.48542	0.42153	0.36710	0.32051	0.28048	0.24595	0.21607	0.19014
1.8	0.90095	0.76759	0.65739	0.56562	0.48865	0.42369	0.36854	0.32147	0.28112	0.24638	0.21636	0.19033
1.9	0.91549	0.77693	0.66340	0.56948	0.49114	0.42529	0.36956	0.32213	0.28154	0.24665	0.21653	0.19045
2.0	0.92838	0.78491	0.66833	0.57254	0.49303	0.42646	0.37029	0.32258	0.28182	0.24682	0.21664	0.19051
2.5	0.97404	0.81009	0.68228	0.58029	0.49735	0.42887	0.37165	0.32335	0.28225	0.24707	0.21678	0.19059
3.0	0.99920	0.82094	0.68698	0.58234	0.49825	0.42928	0.37183	0.32343	0.28229	0.24708	0.21679	0.19059
∞	1.02843	0.82795	0.68892	0.58291	0.49843	0.42933	0.37184	0.32343	0.28229	0.24709	0.21679	0.19059

* From R.C.T. Smith, Conduction of Heat in the Semi-infinite Solid with a Short Table of an Important Integral, *Australian J. Phys.*, vol 6, pp. 127-130, 1953.

5. Purity of source must be high enough that spurious doping does not occur. Similarly if a compound is used, either the other component(s) must be electrically inactive or have very low solubilities and diffusion rates.
6. The source must have a long enough life that a reasonable length run can be made without additional material being required and preferably so that many such runs can be made.
7. For a commercially feasible system, it should be possible to meet the above requirements simultaneously over an area of many slices.

Diffusion processes can be broken into two broad categories: closed tube and open tube. In the first, the semiconductor is placed in a tube, along with some suitable dopant.³⁶ The tube is then evacuated, sealed, and put in a furnace for the required time. The impurity is normally contained in a bulb connected with a small tube to the main chamber in order to prevent surface attack or alloying of the silicon by the dopant. Pure elements may be used as a source.

In the open-tube system, a continuous flow of gas is maintained across the slices during diffusion. The source is usually deposited on the surface of the slice in a previous step or carried in by the gas stream. An example of the first is a "paint-on" source, in which some evaporable liquid containing the desired diffusing element is used to coat the slice by dipping or spraying.³⁷ The addition of a compound such as boron trichloride to the gas flow through the furnace is representative of one class of gas-stream-carried dopants.³⁸ Similarly, the impurity source may be a solid kept at a high enough temperature by an auxiliary furnace to

1.3	1.4	1.5	1.6	1.7	1.8	1.9	2.0	2.5	3.0	4.0	5.0	β α
0.02705	0.02446	0.02213	0.02002	0.01811	0.01638	0.01481	0.01340	0.00811	0.00491	0.00180	0.00066	0.1
0.05289	0.04779	0.04319	0.03903	0.03527	0.03187	0.02880	0.02603	0.01568	0.00945	0.00343	0.00125	0.2
0.07651	0.06903	0.06228	0.05620	0.05071	0.04575	0.04128	0.03725	0.02228	0.01333	0.00477	0.00171	0.3
0.09720	0.08752	0.07881	0.07097	0.06391	0.05756	0.05183	0.04668	0.02766	0.01640	0.00577	0.00204	0.4
0.11462	0.10297	0.09251	0.08312	0.07468	0.06711	0.06030	0.05419	0.03178	0.01866	0.00645	0.00224	0.5
0.12875	0.11538	0.10340	0.09268	0.08308	0.07448	0.06678	0.05988	0.03475	0.02021	0.00688	0.00236	0.6
0.13982	0.12499	0.11174	0.09992	0.08936	0.07993	0.07150	0.06398	0.03677	0.02120	0.00712	0.00242	0.7
0.14824	0.13219	0.11790	0.10519	0.09387	0.08379	0.07481	0.06680	0.03806	0.02180	0.00724	0.00244	0.8
0.15444	0.13741	0.12230	0.10889	0.09699	0.08642	0.07702	0.06867	0.03885	0.02213	0.00730	0.00245	0.9
0.15889	0.14109	0.12535	0.11141	0.09907	0.08814	0.07844	0.06985	0.03931	0.02231	0.00733	0.00246	1.0
0.16200	0.14361	0.12739	0.11307	0.10041	0.08923	0.07933	0.07056	0.03956	0.02240	0.00734	0.00246	1.1
0.16411	0.14529	0.12872	0.11412	0.10125	0.08989	0.07985	0.07098	0.03969	0.02244	0.00735	0.00246	1.2
0.16552	0.14638	0.12956	0.11478	0.10176	0.09028	0.08016	0.07122	0.03976	0.02246	0.00735	0.00246	1.3
0.16643	0.14706	0.13008	0.11517	0.10205	0.09051	0.08033	0.07134	0.03979	0.02247	0.00735	0.00246	1.4
0.16700	0.14749	0.13039	0.11540	0.10222	0.09063	0.08042	0.07141	0.03980	0.02247	0.00735	0.00246	1.5
0.16736	0.14774	0.13057	0.11552	0.10231	0.09070	0.08046	0.07144	0.03981	0.02247	0.00735	0.00246	1.6
0.16757	0.14789	0.13067	0.11559	0.10236	0.09073	0.08049	0.07146	0.03981	0.02247	0.00735	0.00246	1.7
0.16770	0.14797	0.13073	0.11563	0.10239	0.09075	0.08050	0.07147	0.03982	0.02247	0.00735	0.00246	1.8
0.16777	0.14802	0.13076	0.11565	0.10240	0.09075	0.08050	0.07147	0.03982	0.02247	0.00735	0.00246	1.9
0.16781	0.14804	0.13078	0.11566	0.10240	0.09076	0.08051	0.07147	0.03982	0.02247	0.00735	0.00246	2.0
0.16786	0.14807	0.13079	0.11567	0.10241	0.09076	0.08051	0.07147	2.5
0.16786	0.14807	0.13079	0.11567	0.10241	0.09076	0.08051	0.07147	3.0
0.16786	0.14807	0.13079	0.11567	0.10241	0.09076	0.08051	0.07147	0.03982	0.02247	0.00735	0.00246	∞

Table 7-4. Summary of Diffusion Processes

1. Closed-tube System:
Semiconductor plus doping element, alloy, or compound
2. Open-tube System:
 - a. Paint-on or evaporated source
 - b. Direct gas source
 - c. Vaporization of liquid sources
 - d. Vaporization of solid sources
 - e. Box source

have appreciable vapor pressure. An inert gas is then used to sweep the vapor into the main diffusion furnace. One example of this is a phosphorus diffusion using a P_2O_5 source kept at a few hundred degrees.³⁹

Another variation of the open-tube system is the "box technique," in which the source and slices are held at the same temperature in a box with a tight-fitting lid.⁴⁰

These processes are summarized in Table 7-4, and some are illustrated schematically in Fig. 7-25.

Procedures for Various Elements.

Aluminum. Fuller and Ditzenberger³⁶ used metallic aluminum in a closed tube. Miller and Savage⁴¹ used metallic aluminum, but contained it and the slices in a silicon container placed in an open-ended tantalum tube.

Antimony. Antimony trioxide (Sb_2O_3) can be used directly as a source in a closed tube³⁶ or in a box¹⁹. In the box system it is possible to use some other ingredient such as silica powder as a diluent to reduce the vapor pressure and thus give some measure of control to surface concentration. In an open tube, antimony tetraoxide (Sb_2O_4) has been used with either a wet* nitrogen or wet hydrogen carrier, and a source temperature of 900°C.³⁹ Antimony pentachloride (Sb_3Cl_5) is a liquid at room temperature, and it can be used in a bubbler arrangement as a source.

Arsenic. Fuller and Ditzenberger used arsenic trioxide (As_2O_3) in a closed tube, Frosch and Derick³⁹ used an open tube with the arsenic trioxide held at 235°C and with a carrier of nitrogen saturated with water vapor at 30°C, water-saturated hydrogen (30°C), or dry oxygen. Armstrong⁴² used arsenic trioxide and a carrier gas composed of 99.4 per cent nitrogen, 0.6 per cent oxygen, water less than 1.5 ppm. He gives the following relation between surface concentration and source temperature:

N_0	Source temperature, °C
8×10^{18} atoms/cm ³	210
2×10^{18} atoms/cm ³	183
8×10^{17} atoms/cm ³	163
10^{17} atoms/cm ³	150

* If silicon is held at high temperatures in a nonoxidizing atmosphere selective etching sometimes occurs. Also, some of the reaction products of the doping agent-silicon reaction may be volatile and thus cause undesired erosion. The addition of water vapor³⁹ prevents these reactions.

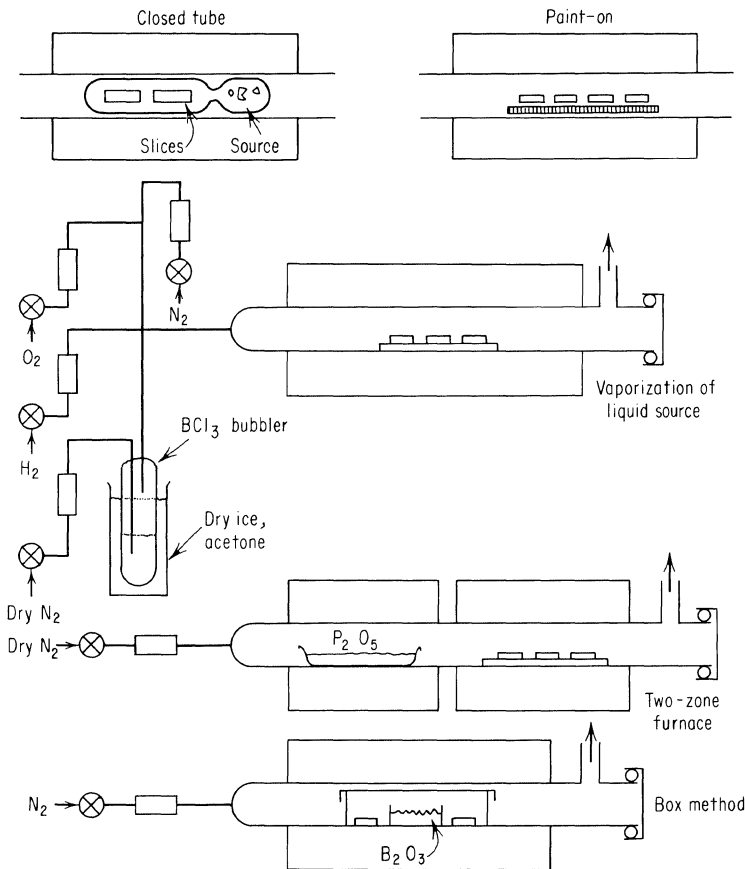


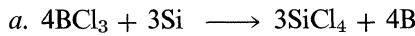
Fig. 7-25. Diffusion methods.

Bismuth. Fuller and Ditzenberger used bismuth oxide in a closed tube.

Boron. Since boron is one of the more important diffusants in silicon technology it has been studied extensively. Fuller and Ditzenberger originally used B_2O_3 in a closed tube, and since then all the other methods listed in Table 7-5 have been tried by various people.

1. Elemental boron has been evaporated onto the silicon surface and diffused in a closed tube.
2. B_2O_3 has been evaporated onto slices and then the diffusion made in a closed tube.
3. Boron powder appears to be useful as a source in a closed-tube system, but it is presumably some suboxide present in small quantities that actually contributes the boron.
4. Williams⁴³ used a thin layer of B_2O_3 deposited on the slices by evaporating a few drops of methyl alcohol saturated with B_2O_3 . The diffusion was then carried out in an open tube.

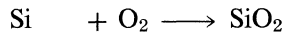
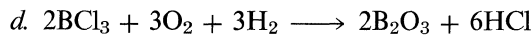
5. A trimethyl borate-saturated nitrogen carrier can be used in an open tube.⁴⁴ This process has the disadvantage of producing carbon or carbonaceous material as the trimethyl borate decomposes. The end product appears to be a layer of B_2O_3 on the slice surface.
6. Cline and Seed³⁷ used glassy layers of potassium silicates and borates in an attempt to obtain a uniform and reproducible surface concentration. In one case, potassium silicate was used on the slice in conjunction with a B_2O_3 source located upstream from the slices. In other cases the boron was available from the paint-on, which consisted of varying amounts of potassium tetraborate, potassium hydroxide, and potassium silicate.
7. The box system has been used with pure B_2O_3 and with various amounts of SiO_2 as a means of reducing surface concentration.^{40,45} Yatsko and Kesperis prepared their sources by mixing boric and silicic acid powders together, hydrolyzing with high-purity water, drying, and sintering. By varying the composition from 0.2 per cent boron to 80 per cent B_2O_3 , surface concentrations of from 4×10^{18} to 4×10^{20} were obtained at a temperature of $1129^\circ C$. Surface pitting occurred if pure B_2O_3 was used at temperatures above $1025^\circ C$.
8. Boron trichloride³⁸ or boron tribromide can be fed into the gas stream and used for doping. Again, in order to prevent pitting, an oxidizing atmosphere is required. In order to examine more closely the behavior of halide doping, consider the following possible reactions.



In either of these cases, silicon removal occurs because silicon tetrachloride is volatile at these temperatures. If water vapor is introduced simultaneously,



or if O_2 and H_2O are added



For these two cases, the silicon is covered with a protective oxide stable at diffusion temperatures and simultaneously coated with boric oxide. The boric oxide and silicon oxide will then form a glassy layer and the source is quite similar to that which occurs in the other process.

Since all but the first process ends with B_2O_3 deposited on the slice, it is also of interest to consider the B_2O_3 + slice reactions. Experimentally it is observed that if only a small amount of B_2O_3 is present or if there is a thick initial oxide, the film remaining after diffusion can be removed in HF and the silicon, after diffusion, presents a clean surface. If the amount of B_2O_3 is further increased, a brown film forms between the HF soluble glass

and the silicon surface. This film is apparently boron and can be dissolved by refluxing in a solution designed to dissolve boron.*

If the amount of B_2O_3 is further increased an additional film with a low electrical conductivity forms between the boron and the silicon. Attempts to analyze this layer have been inconclusive, but it is presumably a boron-silicon compound, possibly SiB_6 , whose existence has been confirmed.⁴⁷ This latter film appears insoluble in any solvent that will not dissolve silicon, so its removal is difficult, and its occurrence is to be avoided if possible. Several boron sources appropriate for open-tube diffusion are summarized in Table 7-5.

Carbon. Carbon has been diffused by Newman and Wakefield into silicon in a closed-tube system using three sources: barium carbonate, carbon dioxide, and acetylene. In each case β -silicon carbide formed on the surface.⁴⁸

Copper. Copper diffusions have been made by evaporating thin layers of copper onto the silicon surface or more commonly^{49,50} by plating from a copper nitrate solution.

Gallium. Fuller and Ditzenberger used gallium oxide in an evacuated closed tube. Kurtz and Gravel⁵¹ used the two-zone system with high-purity gallium as the source and 400 ml/min of dry argon as the carrier gas. No pitting was observed. Goetzberger and Queisser used Ga_2O_3 in an open tube, but had to use a wet nitrogen flow in order to obtain appreciable doping.²⁶

Gold. Gold has been diffused both from evaporated and electroplated sources.⁵⁰ It can be done either in a closed tube or in an open tube with an inert atmosphere.

Indium. Fuller and Ditzenberger used indium oxide in a closed tube as a source. Evaporated indium was also used but usually led to surface pitting.

Iron. Anhydrous $FeCl_3$ or pure iron in a quartz tube has been used for iron diffusions.⁵²

Lithium. Kessler, Tompkins, and Blanc have summarized and suggested various sources for diffusion into germanium which should also be applicable to silicon. These include an oil suspension source, tin-lead alloy, evaporated metallic lithium, $LiOH$, and $LiOH-LiCl$ mixtures.⁵³

Manganese. Carlson put a $MnCl_2$ solution on the silicon slice and subsequently heated it in an evacuated quartz tube for diffusion and solubility studies.⁵⁴

Phosphorus. Fuller and Ditzenberger used P_2O_5 in a closed tube. Since then, a great variety of combinations have been tried with about the same results as for boron, i.e., the most reproducible diffusion occurs when phosphorus can combine with the silicon oxide to form a glassy layer on the surface. P_2O_5 has most commonly been used in a two-zone furnace³⁹ with a very dry gas as a carrier. P_2O_5 is hygroscopic so it in general is very difficult to maintain the whole system moisture-free. If this is not done, excessive pitting of the silicon surface usually occurs. However, Lothrop reports that a usable source is the azeotrope of phosphorus pentoxide and water.⁵⁵ This has a composition of 92.4 per cent P_2O_5 and 7.6 per cent H_2O and is prepared by heating metaphosphoric acid in a platinum boat for

* For example,⁴⁶ 50 cm³ H_2O , 10 cm³ HNO_3 , 5 cm³ HCl , and 2 cm³ H_2SO_4 .

Table 7-5. Impurity Sources for Open-tube Diffusion of Boron*.⁶²

Original impurity source	Room temperature state	Temperature range of source during diffusion, °C	Impurity concentration range	Advantages	Disadvantages
Boric acid	Solid	600–1200	High and low	Readily available Proven source	Source contaminates tube Control is difficult
Boron tribromide	Liquid	10–30	High and low	Clean system Good control over wide range of impurity concentration Can use in non-oxidizing diffusion	Geometry of system is important
Methyl borate	Liquid	10–30	High	Simple to prepare and operate	Restricted to high surface concentration
Boron trichloride	Gas	Room temperature	High and low	Same as boron tribromide Accurate control by gas metering equipment Easy installation and operation	
Diborane	Gas	Room temperature	High and low	Same as boron trichloride	Highly toxic

* From A. M. Smith and R. P. Donovan, "Impurity Diffusion in Silicon," paper presented at the Third Annual Microelectronics Symposium, St. Louis, April, 1964 (Ref. 62).

several hours at 800°C. In addition he has examined PCl_3 , PF_5 , POCl_3 , and PH_3 . Mackintosh⁵⁶ has used a box with phosphorus glass as a source. The glass was a mixture of P_2O_5 and CaO . Weight ratios of from 6:1 to 50:1 of P_2O_5 - CaO were used with no noticeable difference in performance or surface concentration. The diffusion was done in an atmosphere of dry oxygen with a flow of 1 liter/min. Schmidt and Owen⁵⁷ doped anodic grown oxide with phosphorus and used it as a source. The phosphorus was incorporated from an acidic solution. Shortes and Wurst⁵⁸ have used sputtered silicon oxide films doped with appropriate elements for gallium-arsenide diffusion sources. This same process should be directly applicable to silicon diffusions. Maekawa used a two-zone furnace with $\text{H}_4\text{P}_2\text{O}_7$ as a source. 600 cm³/min of nitrogen was used as a carrier. Surface concentrations ranged from 2×10^{18} atom/cm³ to 1.5×10^{21} as the source temperature was varied from 300 to 600°C.⁵⁹ Table 7-6 summarizes some sources suitable for open-tube diffusions.

Silver. Evaporated films and plating from AgNO_3 solutions have been used as sources.⁶⁰

Thallium. Fuller and Ditzenberger used thallium oxide in a closed tube.

Zinc. Carlson⁶¹ used zinc alloyed to the silicon surface and also zinc plated from zinc chloride as sources for diffusion.

7-6. DIFFUSION COEFFICIENTS

There are several possible ways in which the atoms can physically make their way through the lattice. For example, it can be by:

1. Direct interchange.
2. Ring interchange in which several cooperative moves occur simultaneously.
3. Occupation of interstitial positions and movement between atoms.
4. Movement into an adjacent vacant site.

It is by the last two mechanisms that diffusion in silicon occurs.

Since the diamond lattice is very open, atomic movement is considerably easier than in a close-packed structure and a somewhat different diffusion model is required. For diffusion from substitutional sites (Fig. 7-26*d*) a model which con-

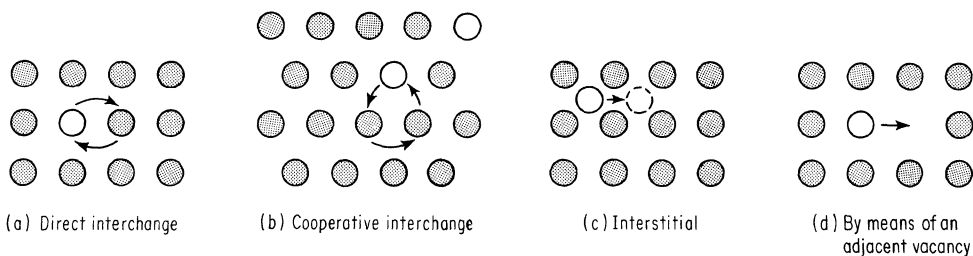


Fig. 7-26. Various mechanisms for the movement of atoms through a lattice: (a) direct interchange; (b) cooperative interchange; (c) interstitial; (d) by means of an adjacent vacancy. The last two processes occur in silicon.

Table 7-6. Impurity Sources for Open-tube Diffusion of Phosphorus*

Original impurity source	Room temperature state	Temperature range of source during diffusion, °C	Impurity concentration range	Advantages	Disadvantages
Red phosphorus	Solid	200–300	Low ($<10^{20}$ cm ⁻³)	Low surface concentration	Variable composition and vapor pressure
Phosphorus pentoxide	Solid	200–300	High ($>10^{20}$ cm ⁻³)	Proven source for high surface concentration	Sensitive to water vapor Requires frequent tube cleaning
Ammonium phosphate	Solid	450–1200	High and low	Avoids water vapor dependence	Purification is marginal
Phosphorus oxychloride	Liquid	2–40	High and low	Clean system Good control over wide range of impurity concentrations	Geometry of system is important
Phosphorus trichloride	Liquid	170	High and low	Same as phosphorus oxychloride Can be used in non-oxidizing diffusion	
Phosphine	Gas	Room temperature	High and low	Same as phosphorus trichloride Accurate control by gas metering Easy installation and operation	Highly toxic

* From A. M. Smith and R. P. Donovan, "Impurity Diffusion in Silicon," paper presented at the Third Annual Microelectronics Symposium, St. Louis, April, 1964.

siders the size of the impurity ion and the coulomb interaction between the impurity and charged vacancies predicts the faster diffusion of p-type than n-type impurities in silicon (and the opposite in germanium) and, in both cases, is in agreement with experiment.⁶³ In the case of interstitial diffusion, the older theory had to be revised to account for the small fraction of activation energy arising from lattice distortion and the much larger fraction due to electrostatic interactions. An interesting observation based on this revision is that there is an optimum ion size for rapid diffusion, which thus qualitatively explains why copper, with its larger diameter, diffused more rapidly than lithium.⁶⁴ Unfortunately, however, these theories are not refined enough to give usable absolute values of diffusion coefficients.

If there is a distribution of a particular impurity between the interstitial and substitutional sites, the effective diffusion coefficient is given by a weighted combination of the two individual coefficients, D_i and D_s . Thus $D_{\text{eff}} = D_i f + D_s(1 - f)$ where f is the fraction in interstitial sites.¹ If f is a function of concentration, D_{eff} will also vary with concentration, and deviations from the diffusion front predicted by the simple solutions to Fick's equation may be quite severe. Gold and copper apparently both behave in this manner.^{65,66}

Effect of Dislocations on Diffusion Coefficient. Because of the rapid diffusion along dislocations, it would appear that there should be marked differences in effective diffusion rates depending on the dislocation density in the material. The effective D will be given by

$$D_{\text{eff}} = D_i(1 - f) + D_p f$$

or

$$D_{\text{eff}} = D_l + fD_p \quad \text{when } f \text{ is small}$$

where D_l = normal diffusion coefficient

D_p = diffusion coefficient along a dislocation pipe

There have been conflicting data presented concerning observation of the effect in germanium,^{67,68} but apparently nothing has been published relating to silicon. The reasons for the discrepancies are probably the large errors inherent in determining the diffusion coefficient* and the smaller than anticipated magnitude of enhancement. For example, if the separation between dislocations is much greater than a diffusion length $2\sqrt{Dt}$, the pipes become clogged, and D_{eff} is less than predicted.⁶⁹ If the pipes themselves move, as during plastic deformation or annealing, D_{eff} may again become equal to (but never greater than) that predicted by the above equation.

Effect of Vacancies on Diffusion Coefficient. For the substitutional diffusion process which depends on vacancies, the diffusion coefficients should be enhanced if the number of vacancies were increased over the equilibrium number. By generating a continuous supply of vacancies through ion bombardment the coefficient

* In an effort to obtain greater sensitivity, silicon epitaxial layers with dislocation densities ranging from 1,000/cm² to 10⁶/cm² have been grown on substrates of similar resistivities and then diffused from the edge. By this procedure, the penetration depths in high- and low-dislocation density material could be measured on the same slice. The results for 1200°C boron diffusion were erratic but indicated a D enhancement of about 20 per cent for the highest-dislocation density material.

for both phosphorus and boron has been increased several orders of magnitude.⁷⁰ It has also been suggested that as a result of the lattice damage caused by very high concentration of impurity, an excess of vacancies is available near the diffusion front and causes "emitter push."^{*}

Effect of Crystal Orientation on Diffusion Coefficient. For the general case of diffusion in a crystal, D is given by

$$D = \begin{vmatrix} D_{11} & D_{12} & D_{13} \\ D_{21} & D_{22} & D_{23} \\ D_{31} & D_{32} & D_{33} \end{vmatrix} \quad (7-59)$$

When the x , y , and z axes coincide with the crystallographic axes the three-dimensional Fick's second law becomes

$$\frac{\partial N}{\partial t} = D_{xx} \frac{\partial^2 N}{\partial x^2} + D_{yy} \frac{\partial^2 N}{\partial y^2} + D_{zz} \frac{\partial^2 N}{\partial z^2} \quad (7-60)$$

By making the substitution

$$\alpha = \frac{x\sqrt{D}}{\sqrt{D_{xx}}} \quad \beta = \frac{y\sqrt{D}}{\sqrt{D_{yy}}} \quad \gamma = \frac{z\sqrt{D}}{\sqrt{D_{zz}}}$$

Eq. (7-60) reduces to

$$\frac{\partial N}{\partial t} = D \frac{\partial^2 N}{\partial \alpha^2} + \frac{\partial^2 N}{\partial \beta^2} + \frac{\partial^2 N}{\partial \gamma^2} \quad (7-61)$$

which can be solved in the normal fashion.³ For the special case of a cubic crystal, the off diagonals of Eq. (7-59) become zero and $D_{11} = D_{22} = D_{33}$.¹ Thus the diffusion coefficient for silicon would be expected to be independent of crystallographic orientation.

Experimental Values. In the solution of the various boundary conditions it was assumed that D was concentration-independent, and while this is apparently true for many of the normally used impurities at low concentrations, it certainly is not true for some of them at high concentrations. Because of this effect, coupled with measurement difficulties, many of the literature values are probably somewhat in error. The following values of diffusion constants (Figs. 7-27 to 7-33) are considered to be typical, but not necessarily the most correct, nor has an effort been made to include all published values. It is usual to plot D versus $1/T$, but in the interest of usability the Groups IIIA's and VA's have been plotted in terms of degrees centigrade.

Methods of Measuring Diffusion Coefficients.

1. When the surface concentration is known; D assumed constant; the distribution function known, for example, erfc ; and the diffusant is of opposite type from that originally in the slice, the diffusion constant can be calculated from a measured

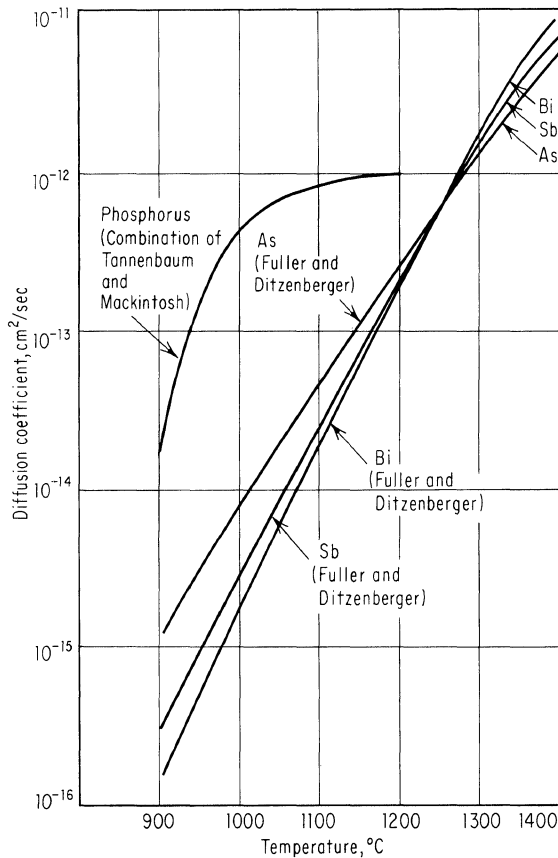
* "Emitter push" is the term applied to the extra penetration of base impurity directly under the emitter window which often occurs during transistor manufacture. See, for example, Baruch et al.⁸¹ and Jaccodine.⁸²

Table of W_D Values*

Bismuth.....	Qualitatively very large grain boundary diffusion
Gallium.....	Diffusion temperature 1150°C, constant source, grain boundary in (100) plane, angle of misfit = 10.5° $W_D = 19$ microns
Boron.....	Diffusion temperature 1000°C, constant source, grain boundary in (100) plane, angle of misfit = 10.5° $W_D = 1.7$ microns
Indium.....	No observed increase in diffusion along boundary
Phosphorus.....	Diffusion temperature 1050°C, constant source, $W_D = 19$ microns
Antimony.....	Diffusion temperature 1300°C, constant source, grain boundary in (100) plane, angle of misfit 10.7° $W_D = 78$ microns

* Data taken from A. Goetzberger and H. Queisser, "Structural Imperfections in Silicon p = n Junctions," Shockley Transistor Corp. Interim Scientific Report, no. 1, Contract AF19(604)-8060, Aug. 31, 1961.

Fig. 7-27. Low concentration-diffusion coefficients for n-type impurities. For most of the impurities, the various literature values are quite close to those shown. In the case of phosphorus, however, a broad spread of D 's appear. The curve shown seems to be the upper limit of values. A lower limit, represented by Howard's data,^{5,83} may be drawn through the points (1000°C, 5.5×10^{-15} cm²/sec), (1100°C, 1.11×10^{-13} cm²/sec), (1300°C, 1.17×10^{-11} cm²/sec).



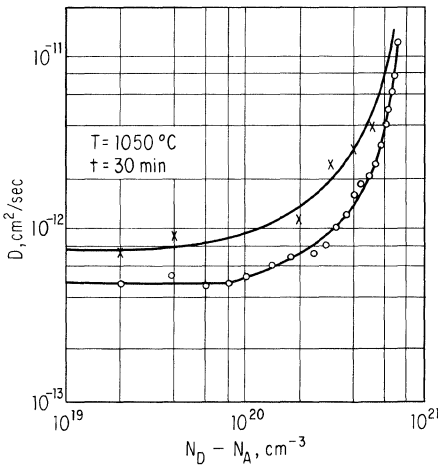


Fig. 7-28. Effect of concentration on the diffusion coefficient of phosphorus in silicon. (Tannenbaum.⁷¹)

value x_j of the junction depth, the initial slice doping level, the diffusion time, and Eq. (7-7).

$$\frac{N'}{N_0} = 1 - \operatorname{erf} \frac{x_j}{2\sqrt{Dt}}$$

2. If the surface concentration is not known, but two slices of different initial

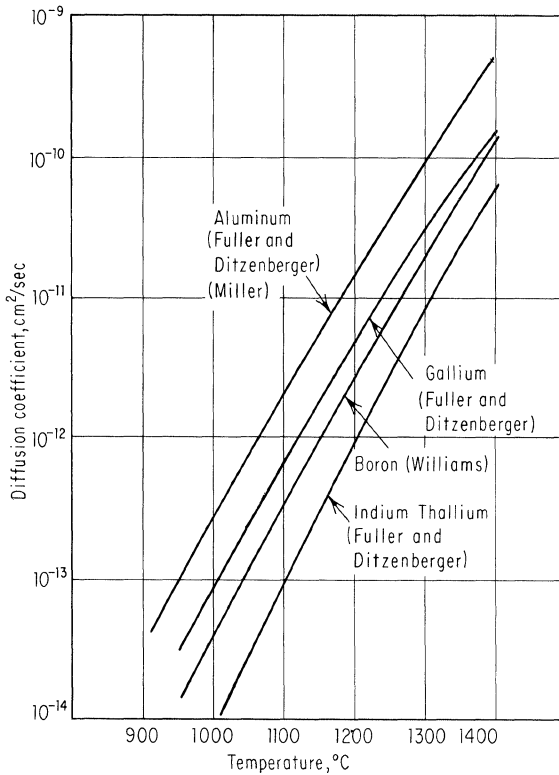
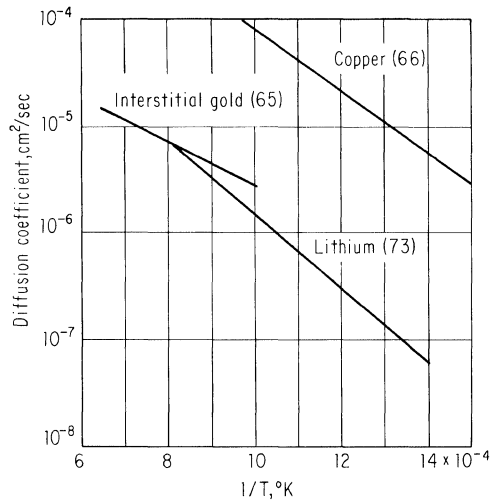


Fig. 7-29. Low concentration-diffusion coefficients for p-type impurities. The variously reported boron D 's can be included in a band with the data shown as an upper limit and those of Kurtz and Yee,⁸⁴ which are about one-fourth the values shown, as the lower limit.

Fig. 7-30. Diffusion coefficients for fast diffusers in silicon.



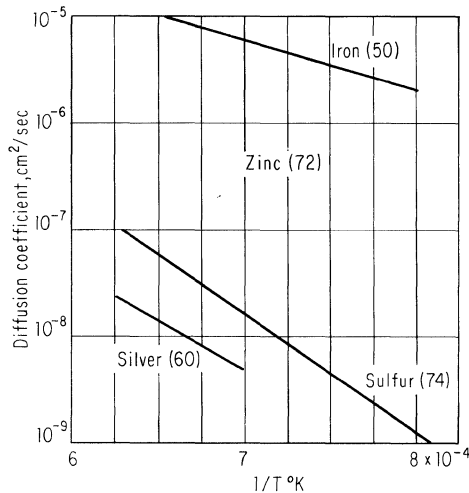
doping can be simultaneously diffused so that both surface concentrations are the same,⁷⁸

$$\frac{N'}{N''} = \frac{1 - \operatorname{erf}(x_j/2\sqrt{Dt})}{1 - \operatorname{erf}(x_j''/2\sqrt{Dt})}$$

where N' and N'' indicate the impurity concentration originally in the two slices. Reference to Fig. 7-2 shows that x_j is not very sensitive to N' , so N' and N'' should be widely separated.

3. If, as in Case 1, a p-n junction is formed during diffusion and the distribution function is known, both the surface concentration and the diffusion coefficient can be found by appropriate measurements. The average conductance $\bar{\sigma}$ of the diffused layer is given by

Fig. 7-31. Diffusion coefficients for fast diffusers in silicon.



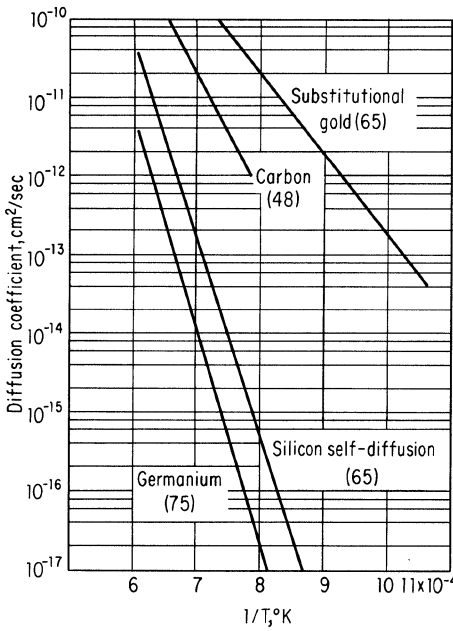


Fig. 7-32. Miscellaneous diffusion coefficients for impurities in silicon.

$$\sigma = \frac{\int_0^{x_j} \sigma(x) dx}{x_j} \tag{7-62}$$

where

$$\sigma(x) = q\mu(N) |N(x) - N'| \tag{7-63}$$

$\mu(N)$ is the carrier mobility and is a function of a totally ionized impurity density of $N(x) + N'$; $M|N(x) - N'|$ is the density of carriers, M being the fraction of uncompensated diffused impurity atoms which are ionized and $N(x)$ the total density of diffused impurity atoms at depth x . When the doping level is very high all the impurities may not be ionized so that $N_{ion}/N(x)$ is much less than 1. These effects can be expressed in terms of an effective mobility $\mu_{eff}(N)$ defined by

$$\mu_{eff} = \frac{\sigma}{N(x)q}$$

This relation has been experimentally determined and is available in the literature.

A knowledge of $\mu(x)$, N' , the determination of $\bar{\sigma}$ from a four-point probe reading, and the functional relation of $N(x)$ versus x , enables $N(0)$, the surface concentration, to be calculated from Eqs. (7-62) and (7-63). For the specific cases of an erfc, a gaussian (limited source), and a linear variation of $N(x)$ with x , surface concentration versus σ has been computed and plotted for a variety of starting resistivities.*

4. Quite often neither the distribution function nor surface concentration is known, so the problem becomes one of first determining the impurity profile and from that, the diffusion constant.

* These curves will not be reproduced here. Instead the reader is referred to Irvin.⁷⁹

- a. A radioactive doping element may be used and the concentration as a function of depth determined by an incremental removal of silicon.⁷⁸
- b. If a diode can be made and reverse-biased so that the space-charge region moves primarily into the layer whose impurity profile is desired, a measurement of diode capacitance versus applied voltage will allow computation of $N(x)$.⁷⁸
- c. If a value of sheet resistance of the diffused layer is measured by a four-point probe, a small amount of the layer removed by lapping, and a new value of sheet resistance read, then the average resistivity of the layer removed is given by

$$R = \frac{R_{1s}R_{2s}}{R_{2s} - R_{1s}} \Delta x \quad (7-64)$$

where Δx = thickness removed

R_{1s} = sheet resistance before layer removal

R_{2s} = sheet resistance after layer removal

A repetition of this process will give a resistivity versus depth profile that can be converted into an $N(x)$ curve.

The problem of determining the diffusion constant from the measured impurity profile still remains. If examination of the data shows that $N(x)$ follows an error or exponential decrease with distance, D can be determined as before. But if because of the boundary conditions or a concentration dependent D some other relation exists, a technique such as that of Boltzmann-Matano must be used to calculate D .¹

5. If a fast diffuser is known to be fully ionized, a small amount can be introduced in a very limited area and its movement observed as a function of time while under the influence of an electric field. From these measurements, the mobility μ can be determined, and by use of the Einstein relation $D/\mu = kT/q$, D can also be calculated.³⁰

6. If a fast diffuser forms ion pairs with a very slow diffuser, the rate of pairing, which is reflected as a change in carrier mobility, can be measured, and from this the diffusion coefficient of the fast diffuser is determined.⁷⁸

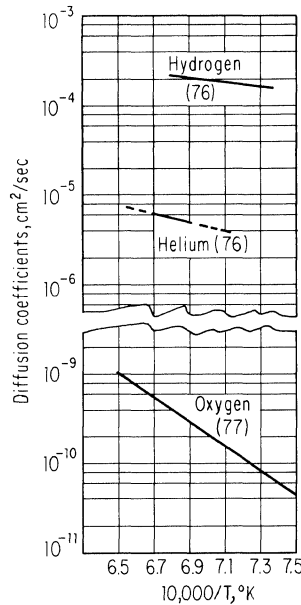


Fig. 7-33. Diffusion coefficients for gases in silicon.

REFERENCES

1. Shewmon, Paul G.: "Diffusion in Solids," McGraw-Hill Book Company, New York, 1963.
2. Barrier, Richard M.: "Diffusion in and through Solids," Cambridge University Press, New York, 1951.
3. Jost, W.: "Diffusion in Solids, Liquids and Gases," Academic Press, Inc., New York, 1962.
4. Carslaw, H. S., and J. C. Jaeger: "Conduction of Heat in Solids," Oxford University Press, Fair Lawn, N.J., 1948.

5. Smits, F. M.: Diffusion in homöopolaren Halbleitern, in "Ergebnisse der exacten Naturwissenschaften," vol. 31, pp. 167-219, Springer-Verlag Ohg, Berlin, 1959.
6. Ratcliff, Gordon (Texas Instruments Incorporated): Private communication.
7. Gummel, H. K.: Measurement of the Number of Impurities in the Base Layer of a Transistor, *Proc. IRE*, vol. 49, p. 834, 1961.
8. Fabricius, E. D.: Diffusion of Impurities in a Thin Semiconductor Slab, *J. Appl. Phys.*, vol. 33, pp. 753-754, 1962.
9. Wackwitz, R. C. (Texas Instruments Incorporated): Unpublished work.
10. Smith, R. C. T.: Conduction of Heat in the Semi-infinite Solid with a Short Table of an Important Integral, *Australian J. Phys.*, vol. 6, pp. 127-130, 1953.
11. Smits, F. M., and R. C. Miller: Rate Limitation at the Surface for Impurity Diffusion in Semiconductors, *Phys. Rev.*, vol. 104, pp. 1242-1245, 1956.
12. Cornelison, B., and W. A. Adcock: Transistors by Grown-diffused Techniques, *IRE WESCON Conv. Record*, pt. 3, pp. 22-27, 1957.
13. Anderson, R. E. (Texas College of Arts and Industries), and W. R. Runyan (Texas Instruments Incorporated): Unpublished work.
14. Rice, Warren R.: Diffusion of Impurities during Epitaxy, *Proc. IEEE*, vol. 52, pp. 284-295, 1964.
15. Kucher, T. I.: The Problem of Diffusion in an Evaporating Solid Medium, *Soviet Phys.-Solid State*, vol. 3, pp. 401-404, 1961.
16. Batdorf, R. L., and F. M. Smits: Diffusion of Impurities into Evaporating Silicon, *J. Appl. Phys.*, vol. 30, pp. 259-264, no. 2, 1959.
17. Allen, R. B., H. Bernstein, and A. D. Kurtz: Effect of Oxide Layers on the Diffusion of Phosphorus into Silicon, *J. Appl. Phys.*, vol. 31, pp. 334-337, 1960.
18. Sah, C. T., H. Sello, and D. A. Tremere: Diffusion of Phosphorus in Silicon Oxide Films, *Phys. Chem. Solids*, vol. 11, pp. 288-298, 1959.
19. Tsai, Joseph C. C., "The Simultaneous Diffusion of Donor and Acceptor Impurities into Silicon," Ph.D. thesis, Ohio State University, Columbus, 1962.
20. Horiuchi, Shiro, and Jiro Yamaguchi: Diffusion of Boron in Silicon through Oxide Layer, *J. Appl. Phys.*, (Japan) vol. 1, pp. 314-323, 1962.
21. Atalla, M. M., and E. Tannenbaum: Impurity Redistribution and Junction Formation in Silicon by Thermal Oxidation, *Bell System Tech. J.*, vol. 39, pp. 933-946, 1960.
22. Fisher, J. C.: Calculation of Diffusion Penetration Curves for Surface and Grain Boundary Diffusion, *J. Appl. Phys.*, vol. 22, pp. 74-77, 1951.
23. Whipple, R. T. P.: Concentration Contours in Grain Boundary Diffusion, *Phil. Mag.*, vol. 45, pp. 1225-1236, 1954.
24. Queisser, H. J., K. Hubner, and W. Shockley: Diffusion along Small-angle Grain Boundaries in Silicon," *Phys. Rev.*, vol. 123, pp. 1245-1254, 1961.
25. Wood, Van E., Alfred E. Austin, and Frederick J. Milford: Theoretical Solutions of Grain-boundary Diffusion Problems, *J. Appl. Phys.*, vol. 33, pp. 3574-3579, 1962.
26. Goetzberger, A., and H. Queisser: "Structural Imperfections in Silicon p-n Junctions," Shockley Transistor Corp. Interim Scientific Report, no. 1, Contract AF19(604)-8060, Aug. 31, 1961.
27. Queisser, H. J.: "Failure Mechanisms in Silicon Semiconductors," Shockley Transistor Corp. Final Report, Contract AF30(602)2556, Jan. 15, 1963.
28. Watelski, Stacy (Texas Instruments Incorporated): Unpublished work.
29. Gallagher, C. J.: Electrolysis of Copper in Solid Solution, *J. Phys. Chem. Solids*, vol. 3, pp. 82-86, 1957.
30. Fuller, C. S., and J. C. Severiens: Mobility of Impurity Ions in Germanium and Silicon, *Phys. Rev.*, vol. 96, pp. 21-24, 1954.

31. Malkovich, R. Sh., and N. A. Alimbarashvili: The Effect of an Electric Field on the Diffusion of Zinc in Silicon, *Soviet Phys.-Solid State*, vol. 4, pp. 1725-1727, March, 1963.
32. Bardeen, Brattain, and Shockley: Investigation of Oxidation of Copper by Use of Radioactive Cu Tracer, *J. Chem. Phys.*, vol. 14, pp. 714-721, 1946.
33. Shockley, W.: Field Enhanced Donor Diffusion in Degenerate Semiconductor Layers, *J. Appl. Phys.*, vol. 32, p. 1402 (L), 1961.
34. Wackwitz, R. C.: Analytic Solution of the Multiple Diffusion Problem, *J. Appl. Phys.*, vol. 33, p. 2909 (L), 1962.
35. Killoran, Daniel Richard: "The Effective Duration of a Linear Slow-Cool," *J. Electrochem. Soc.*, vol. 109, p. 170 (L), 1962.
36. Fuller, C. S., and J. A. Ditzenberger: Diffusion of Donor and Acceptor Elements in Silicon, *J. Appl. Phys.*, vol. 27, pp. 544-554, 1956.
37. Cline, J. E., and R. G. Seed: Diffusion into Silicon from Glassy Layers, *J. Electrochem. Soc.*, vol. 105, pp. 700-701, 1958.
38. Fuller, C. S., and J. A. Ditzenberger: Diffusing of Boron and Phosphorus into Silicon, *J. Appl. Phys.*, vol. 25, p. 1439 (L), 1954.
39. Frosch, D. J., and L. Derick: Surface Protection and Selective Masking during Diffusion in Silicon, *J. Electrochem. Soc.*, vol. 104, pp. 547-552, 1957.
40. D'Asaro, L. A.: Diffusion and Oxide Masking in Silicon by the Box Method, *Solid-State Electron.*, vol. 1, pp. 3-12, 1960.
41. Miller, R. C., and A. Savage: Diffusion of Aluminum in Single Crystal Silicon, *J. Appl. Phys.*, vol. 27, pp. 1430-1432, 1956.
42. Armstrong, W. J.: The Diffusivity of Arsenic in Silicon, *J. Electrochem. Soc.*, vol. 109, pp. 1065-1067, 1962.
43. Williams, E. L.: Boron Diffusion in Silicon, *J. Electrochem. Soc.*, vol. 108, pp. 795-798, 1961.
44. Smythe, R. L., and J. Brixey (Texas Instruments Incorporated): Private communication.
45. Yatsko, R. S., and J. S. Kesperis: A Modified Closed Box System for the Diffusion of Boron into Silicon, *J. Electrochem. Soc.*, vol. 107, pp. 911-915, 1960.
46. Hampel, Clifford (ed.): "Rare Metals Handbook," Reinhold Publishing Corporation, New York, 1954.
47. Cline, Carl F.: An Investigation of the Compound Silicon Boride (SiB_6), *J. Electrochem. Soc.*, vol. 106, pp. 322-325, 1959.
48. Newman, R. C., and J. Wakefield: Diffusion and Precipitation of Carbon in Silicon, "Metallurgy of Semiconductor Materials," Metallurgical Society Conferences, vol. 15, Interscience Publishers, Inc., New York, 1962.
49. Fuller, C. S., J. D. Struthers, J. A. Ditzenberger, and K. B. Wolfstirn: Diffusivity and Solubility of Copper in Germanium, *Phys. Rev.*, vol. 93, pp. 1182-1189, 1954.
50. Struthers, J. D.: Solubility and Diffusivity of Gold, Iron and Copper in Silicon, *J. Appl. Phys.*, vol. 27, p. 1560, 1956; *J. Appl. Phys.*, vol. 28, p. 516, 1957.
51. Kurtz, A. D., and C. L. Gravel: Diffusion of Gallium in Silicon, *J. Appl. Phys.*, vol. 29, pp. 1456-1459, 1958.
52. Collins, C. B., and R. O. Carlson: Properties of Silicon Doped with Iron or Copper, *Phys. Rev.*, vol. 108, pp. 1409-1414, 1957.
53. Kessler, J. O., B. E. Tompkins, and J. Blanc: Variable-characteristic p-n Junction Devices Based on Reversible Ion Drift, *Solid-State Electron.*, vol. 6, pp. 297-307, 1963.
54. Carlson, R. O.: Properties of Silicon Doped with Manganese, *Phys. Rev.*, vol. 104, pp. 937-941, 1956.
55. Lothrop, Robert P.: Diffusion of Phosphorus in Silicon from the Azeotrope of Phosphorus Pentoxide and Water, *J. Appl. Phys.*, vol. 33, p. 2656 (L), 1962.

56. Mackintosh, I. M.: The Diffusion of Phosphorus in Silicon, *J. Electrochem. Soc.*, vol. 109, pp. 392–401, 1962.
57. Schmidt, P. F., and Alan E. Owen: "Use of Doped Anodic Oxide Films on Silicon for Device Fabrication," paper presented at the Spring Meeting of the Electrochemical Society, 1963.
58. Shortes, S. R., and E. C. Wurst: "Diffusion of n and p-type Impurities into GaAs from Doped SiO₂ Films," paper presented at the New York Meeting of the Electrochemical Society, 1963.
59. Maekawa, S.: Diffusion of Phosphorus into Silicon, *J. Phys. Soc. Japan*, vol. 17, pp. 1592–1597, 1962.
60. Boltaks, B. I., and Hsüeh Shih-yin: Diffusion, Solubility, and the Effect of Silver Impurities on Electrical Properties of Silicon, *Soviet Phys.-Solid State*, vol. 2, pp. 2383–2388, 1961.
61. Carlson, R. O.: Double Acceptor Behavior of Zinc in Silicon, *Phys. Rev.*, vol. 108, pp. 1390–1393, 1957.
62. Smith, A. M., and R. P. Donovan: "Impurity Diffusion in Silicon," paper presented at the Third Annual Microelectronics Symposium, St. Louis, April, 1964.
63. Swalin, R. A.: Model for Solute Diffusion in Crystals with the Diamond Structure, *J. Appl. Phys.*, vol. 29, pp. 670–674, 1958.
64. Weiser, K.: Theory of Diffusion and Equilibrium Position of Interstitial Impurities in the Diamond Lattice, *Phys. Rev.*, vol. 126, pp. 1427–1436, 1962.
65. Wilcox, W. R., and T. J. La Chapelle: Mechanism of Gold Diffusion into Silicon, *J. Appl. Phys.*, vol. 35, pp. 240–246, 1964.
66. Hall, R. N., and J. H. Racette: Diffusion and Solubility of Copper in Extrinsic and Intrinsic Germanium, Silicon, and Gallium Arsenide, *J. Appl. Phys.*, vol. 35, pp. 379–397, 1964.
67. Widmer, H.: Effect of Dislocations on Self-diffusion in Germanium, *Phys. Rev.*, vol. 125, pp. 30–32, 1962.
68. Heldt, L. A., and J. N. Hobstetter: The Effect of Dislocations on Diffusion in Germanium, *Acta Met.*, vol. 11, pp. 1165–1168, 1963.
69. Ruoff, A. L., and R. W. Balluffi: Strain-enhanced Diffusion in Metals. II. Dislocation and Grain Boundary Short-circuiting Models, *J. Appl. Phys.*, vol. 34, pp. 1848–1853, 1963.
70. Strack, Hans: Ion Bombardment of Silicon in a Glow Discharge, *J. Appl. Phys.*, vol. 34, pp. 2405–2409, 1963.
71. Tannenbaum, Eileen: Detailed Analysis of Thin Phosphorus-diffused Layers in p-type Silicon, *Solid-State Electron.*, vol. 2, pp. 123–132, 1961.
72. Fuller, C. S., and F. J. Morin: Diffusion and Electrical Behavior of Zinc in Silicon, *Phys. Rev.*, vol. 105, p. 379, 1957.
73. Fuller, C. S., and J. C. Severiens: Mobility of Impurity Ions in Germanium and Silicon, *Phys. Rev.*, vol. 96, pp. 21–24, 1954.
74. Carlson, R. O., R. N. Hall, and E. M. Pell: Sulfur in Silicon, "Advances in Semiconductor Science," Pergamon Press, New York, 1959.
75. Petrow, D. A., J. M. Schaschkow, and A. S. Belanovski: Diffusion of Impurities in Silicon, in M. Schön and H. Welker (eds.), "Semiconductors and Phosphors," pp. 653–655, Interscience Publishers, Inc., New York, 1958.
76. Wieringen, A. V., and N. Warmoltz: On the Permeation of Hydrogen and Helium in Single Crystal Silicon and Germanium at Elevated Temperatures, *Physica*, vol. 22, pp. 849–865, 1956.

77. Haas, C.: The Diffusion of Oxygen in Silicon and Germanium, *J. Phys. Chem. Solids*, vol. 15, pp. 108–111, 1960.
78. Hannay, N. B. (ed.): “Semiconductors,” p. 236, Reinhold Publishing Corporation, New York, 1959.
79. Irvin, J. C.: Resistivity of Bulk Silicon and of Diffused Layers in Silicon, *Bell System Tech. J.*, vol. 41, pp. 387–410, 1962.
80. Miller, R. C., and F. M. Smits: Diffusion of Antimony out of Germanium and Some Properties of the Antimony-Germanium System, *Phys. Rev.*, vol. 107, pp. 65–70, 1957.
81. Baruch, P., C. Constantin, J. C. Pfister, and Mme. R. Saintesprit: Vacancy Enhanced Diffusion in Silicon, discussions of the Faraday Society, no. 31, pp. 76–85, 1961.
82. Jaccodine, R. J.: “Collector DiP in Diffused Devices,” paper presented at the Fall Meeting of the Electrochemical Society, 1964.
83. Howard, B. T.: “Phosphorus Diffusion in Silicon,” paper presented at the Fall Meeting of the Electrochemical Society, 1957.
84. Kurtz, A. D., and R. Yee: Diffusion of Boron into Silicon, *J. Appl. Phys.*, vol. 31, pp. 303–305, 1960.

8

Electrical Properties

8-1. RESISTIVITY

The resistivity of a semiconductor is given by

$$\rho = \frac{1}{q(\mu_n n + \mu_p p)} \quad (8-1)$$

where q = electronic charge

n and μ_n = number and mobility of electrons

p and μ_p = number and mobility of holes*

If there are no impurities in the silicon, equal numbers of electrons and holes are thermally generated, and the product (np) is given by

$$\begin{aligned} np = n_i^2 &= 1.5 \times 10^{33} T^3 \exp\left(\frac{-1.21}{kT}\right) \\ &= 1.9 \times 10^{20} \text{ cm}^{-6} \quad \text{at } 300^\circ \text{K} \end{aligned} \quad (8-2)$$

where k = Boltzmann's constant

T = temperature

This is plotted in Fig. 8-1.1,2,† Since the np product remains constant at a given temperature, the contribution due to the minority carriers becomes relatively unimportant as the doping level is increased over n_i . At room temperature, nearly all impurities are ionized, and

$$\rho \approx \frac{1}{q\mu_{p,n}N_{A,D}} \quad (8-3)$$

so a combination of $N_{A,D}$ and the mobility allows the resistivity to be calculated as a function of doping. Room temperature curves are given in Figs. 6-1 to 6-4.

If the resistivity is desired as a function of temperature, then the variation of mobility with temperature and the fraction ionized must both be considered. This fraction depends on the activation energy of the particular impurity in ques-

* Carrier terminology commonly used in semiconductor physics is summarized in Table 8-1.

† Superscript numbers indicate References listed at the end of the chapter.

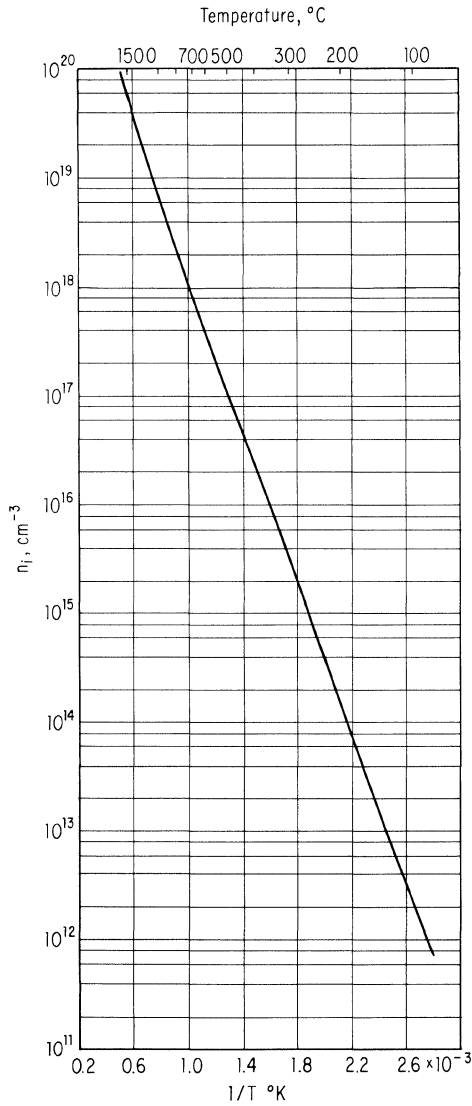


Fig. 8-1. Intrinsic carrier concentration n_i versus reciprocal temperature. (Adapted from Morin and Maita¹ and Hall and Racette.²)

tion and the temperature. Figures 8-2 and 8-3 show such curves for antimony- and boron-doped silicon respectively.* The decrease in activation energy with impurity concentration was taken into account in computing the curves. Reference to Table 8-2 shows that the various n-type dopants have similar activation energies, and a comparison is made in Fig. 8-2 with experimental results on arsenic- and phosphorus-doped silicon. It can also be seen that other p-type dopants have significantly different activation energies. To illustrate the effect of these differ-

* Calculations by Henry Riser and Stacy Watelski are based on Brooks-Herring equation for ionized impurity scattering.

Table 8-1. Carrier Terminology Commonly Used in Semiconductor Physics

n	number of electrons
p	number of holes
p_n	equilibrium hole density in n-type material
n_n	equilibrium electron density in n-type material
n_p	equilibrium electron density in p-type material
p_p	equilibrium hole density in p-type material
n_i	equilibrium electron density in intrinsic material
p_i	equilibrium hole density in intrinsic material
N_D	the number of donor (n-type) impurities per cc
n_d	the number of electrons on donor centers (un-ionized donor impurities)
N_A	the number of acceptor (p-type) impurities per cc
n_a	the number of electrons on the acceptor centers (ionized acceptor impurities)

In general, all the impurities added will be ionized so that

$$\begin{aligned}n_d &= 0 \\n_n &= N_D \\n_a &= N_A\end{aligned}$$

Under equilibrium conditions,

$$\begin{aligned}n - (N_D - n_d) &= p - n_a \\p + (N_D - n_d) &= n + n_a \\pn &= n_i^2\end{aligned}$$

ences, Figs. 8-4 and 8-5 give calculated resistivities of indium- and gallium-doped silicon.

Sometimes impurities which have deep-lying levels, such as gold, are added for lifetime control. Since their activation energies are very large, only a small amount is ionized at room temperature, and so will contribute little to conductivity. The un-ionized atom will, moreover, act as a trap for free carriers available from other types of impurities and will thus generally decrease p or n and give higher resistivities, regardless of whether the silicon is n- or p-type. Figures 8-6 to 8-11 show the calculated resistivity as a function of gold concentration in boron- and antimony-doped silicon.* It should be observed that while extremely high resistivities are obtainable at room temperature, the effect becomes progressively less as the temperature increases. Figure 8-12 shows calculated room temperature resistivity for silver added to silicon.⁵

8-2. MOBILITY

The mobility of Eq. (8-1) may be calculated from equations developed by Brooks,⁶ Herring,⁷ and Conwell and Weisskopf,⁸ and depends both on temperature and impurity concentration.⁷ Figures 8-13 and 8-14 show μ_n and μ_p as a function of impurity concentration at room temperature.† For these curves it was assumed that there was no compensation. In the event that compensation does occur, approximate mobilities can still be obtained by determining the impurity mobility

* Calculations by D. C. Gupta; computer program by Ron Wackwitz.

† Calculations by Henry Riser and Stacy Watelski are based on Brooks-Herring equation for ionized impurity scattering.

μ_I for the desired degree of compensation and then combining it with the lattice mobility to give a total mobility. Figure 8-15 gives μ_I versus impurity concentration.* If compensation is present,⁹

$$\mu_{IC} = \frac{|N_A - N_D|}{N_A + N_D} \mu_{IU} \tag{8-4}$$

where μ_{IC} = compensated impurity mobility
 N_A and N_D = number of acceptors and donors
 μ_{IU} = impurity mobility of uncompensated material with $|N_A - N_D|$ impurities/cm³

* Calculations by Henry Riser and Stacy Watelski are based on Brooks-Herring equation for ionized impurity scattering.

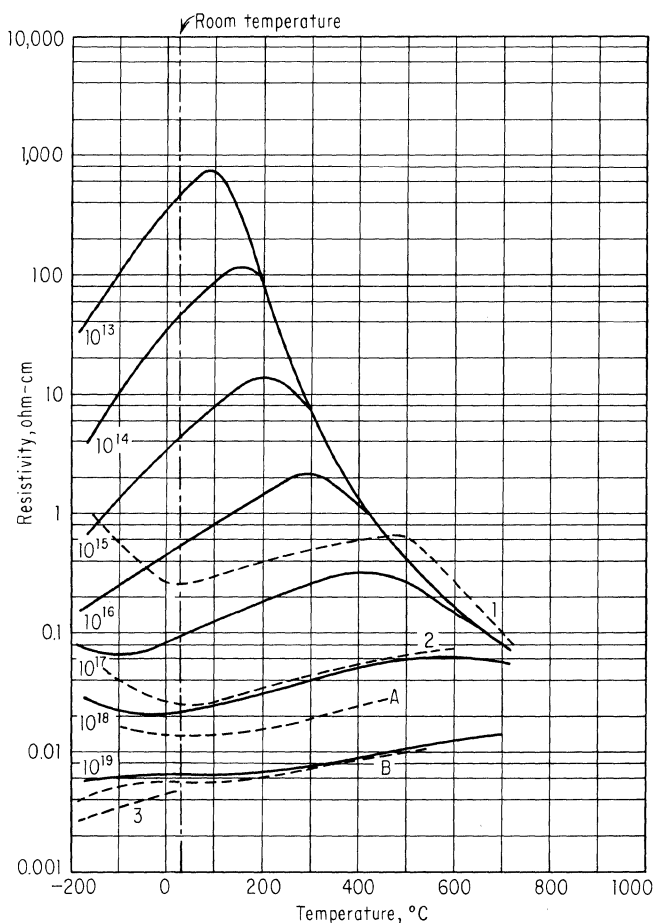


Fig. 8-2. Resistivity versus temperature for n-type silicon. Solid lines are calculated values for Sb-doped silicon. Dashed lines are experimental: (A) 1.7×10^{18} arsenic; (B) 1.1×10^{19} phosphorus (Chapman, Tufte, Zook, and Long³); (1) 1×10^{17} phosphorus; (2) 1.3×10^{18} phosphorus; (3) 1.7×10^{19} phosphorus. (Pearson and Bardeen.⁴)

Thus, by knowing N_A and N_D , a new μ_I can be calculated. Figure 8-16 shows total mobility versus μ_I , so a combination of this curve and the μ_I just determined allows evaluation of the compensated mobility.

8-3. DRIFT MOBILITY

Drift mobility, the mobility of minority carriers, is to a first approximation the same as the majority carrier, or conductivity, mobility just discussed. With this

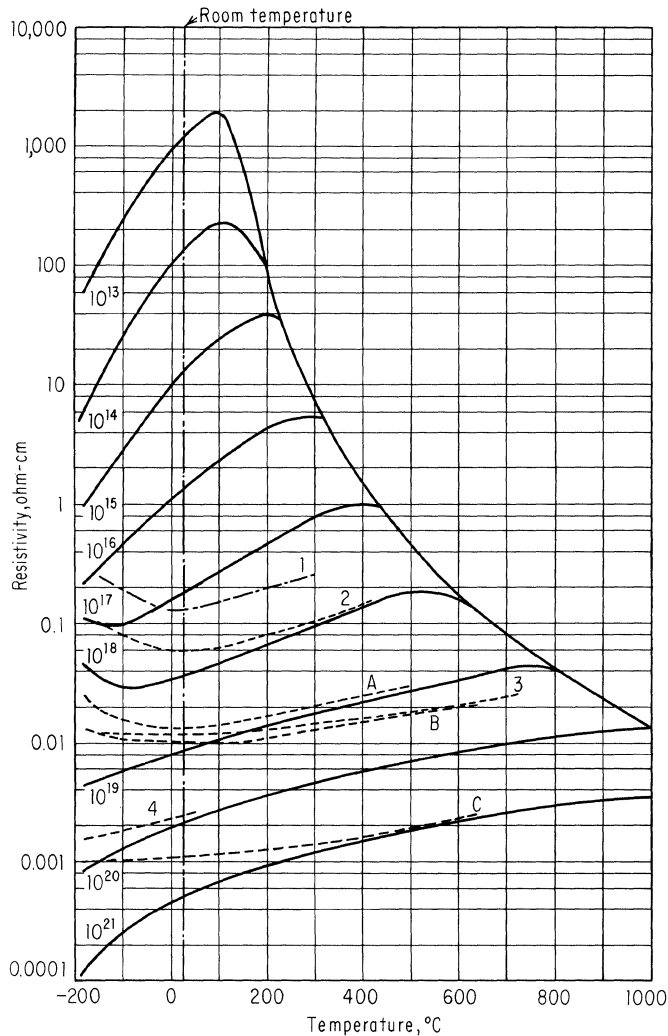


Fig. 8-3. Resistivity versus temperature for boron-doped silicon. Solid lines are calculated for $E_A = 0.045$ ev. Dashed lines are experimental: (A) 6×10^{18} , (B) 1×10^{19} , (C) 1×10^{20} (Chapman, Tufte, Zook, and Long³); (1) 6×10^{17} , (2) 1.3×10^{18} , (3) 1.4×10^{19} , (4) 1.2×10^{20} . (Pearson and Bardeen.⁴)

Table 8-2

Impurity	Donor or acceptor	Below conduction band, ev	Above valence band, ev
Ag*	D	0.31	
	A	0.21
Al†	A	0.057
As†	D	0.049	
Au†	D	0.33
	A	0.54	
B†	A	0.045
Cu†	A	0.49
	D	0.24
Fe†	D	0.55	
	D	0.40
Ga†	A	0.065
In†	A	0.16
Li†	D	0.033	
Mn†	D	0.53	
P†	D	0.044	
Sb†	D	0.039	
	D	0.18	
S‡	D	0.37	
	A	0.55	
Zn†	A	0.30
	A	0.30

* B. I. Boltaks, and Hsüeh Shih-yin, Diffusion, Solubility and the Effect of Silver Impurities on Electrical Properties of Silicon, *Soviet Phys.-Solid State*, vol. 2, pp. 2383-2386, 1961.

† Richard H. Bube, "Photoconductivity of Solids," John Wiley & Sons, Inc., New York, 1960.

‡ R. O. Carlson, R. N. Hall, and E. M. Pell, Sulfur in Silicon, "Advances in Semiconductor Science," pp. 81-83, Pergamon Press, New York, 1959.

assumption the mobility ratio $\mu_p/\mu_n \equiv b$ can be calculated from Fig. 8-15. This is shown in Fig. 8-17.

8-4. HALL COEFFICIENT AND HALL MOBILITY

In extrinsic silicon, the Hall coefficient in the limit of small magnetic field is given by

$$R_n = -\frac{r_n}{en} \quad \text{or} \quad R_p = \frac{r_p}{ep} \quad (8-5)$$

for n- and p-type material respectively. The r_i are constants of proportionality which depend on the details of the scattering process and the detailed electronic structure of silicon.

The Hall coefficient can be measured directly in a long, thin slab.^{10,*} It is given by

$$R = 10^{-8} V_y \frac{t}{I_x B_z} \quad (8-6)$$

* For additional details see O. Lindberg, Hall Effect, *Proc. IRE*, vol. 40, pp. 1414-1419, 1952.

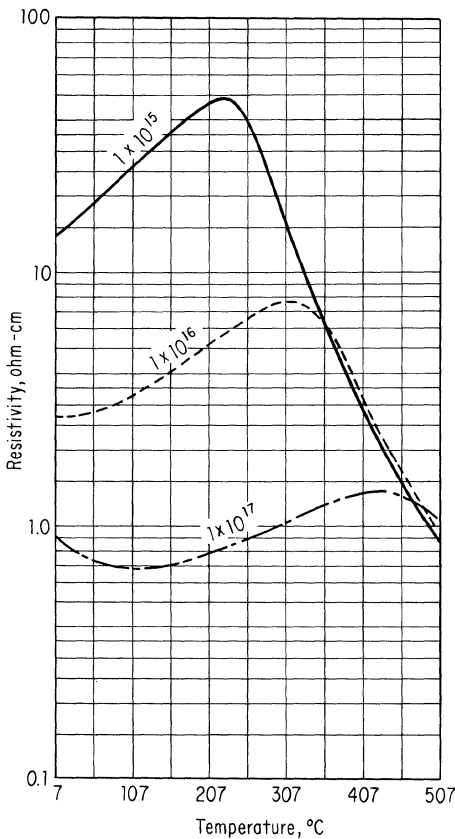


Fig. 8-4. Calculated values of resistivity versus temperature for indium-doped silicon, $E_A = 0.160$ ev.

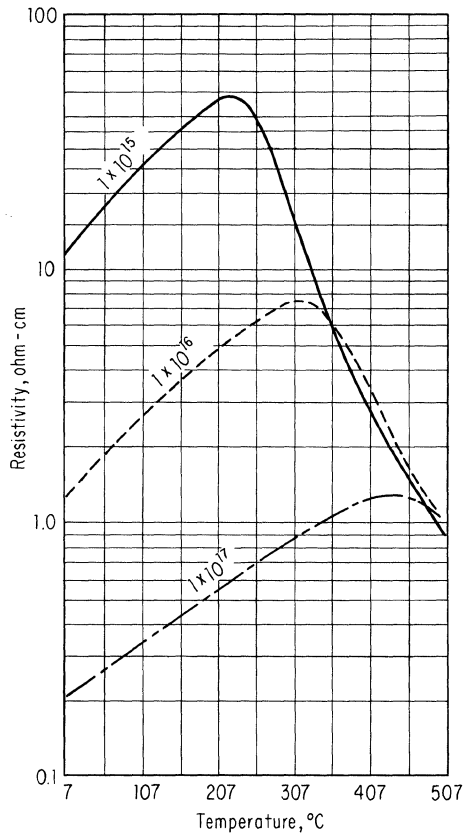


Fig. 8-5. Calculated values of resistivity versus temperature for gallium-doped silicon, $E_A = 0.065$ ev.

where V_y = Hall voltage (volts)
 t = thickness of the sample in the z direction (cm)
 I_x = current (amp)
 B_z = magnetic induction (gauss)

The ratio of the Hall coefficient to the resistivity has the dimensions of mobility and is called the Hall mobility. In n-type material $\mu_{Hn} = r_n \mu_n$ and in p-type material $\mu_{Hp} = r_p \mu_p$. If the r_i are known, it is possible to determine both the concentration and mobility of the majority carrier from electrical measurements.

The Hall mobility as measured by a number of investigators is shown as a function of resistivity in Figs. 8-18 and 8-19 for n- and p-type silicon. Calculated and measured values of conductivity mobility are also shown in these figures.* The

* Data in Figs. 8-18 to 8-20 were collected and analyzed by W. M. Bullis and R. Nasby.

scatter in the experimental data is quite large but approximate values for the ratios r_n and r_p can be computed from the curves. These are shown in Fig. 8-20. At very low resistivities, the assumptions made in the calculations of conductivity mobility are no longer valid, but in this region the value of r_i is 1.

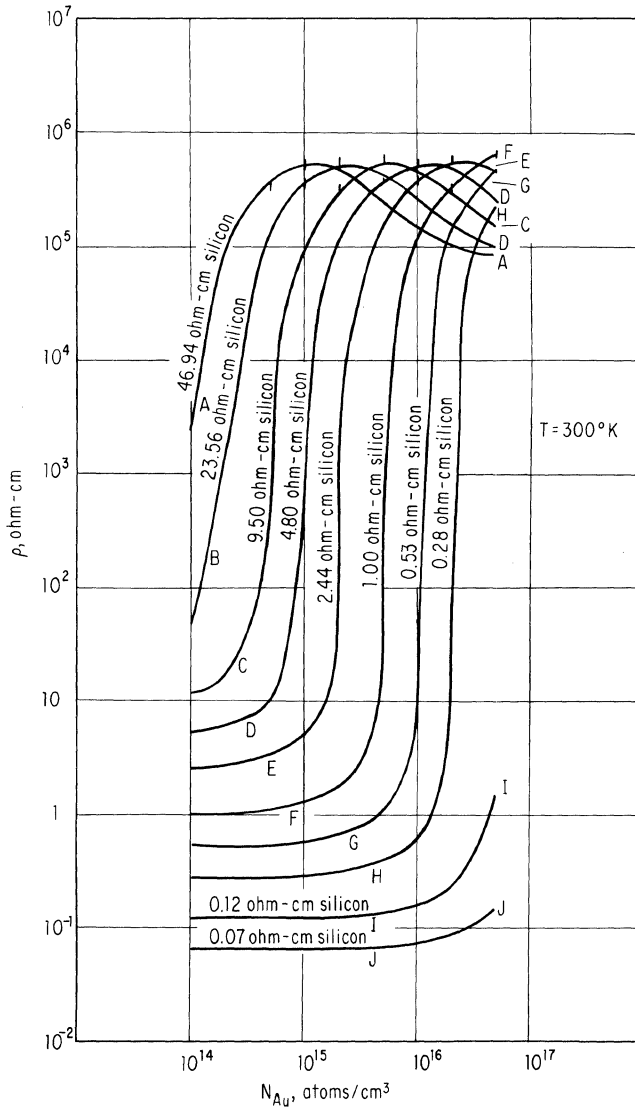


Fig. 8-6. Calculated values of resistivity versus gold concentration in phosphorus-doped silicon at $T = 300^\circ\text{K}$. Gold levels: 0.54 and 0.35 ev. Phosphorus level: 0.044 ev. Because of the difficulties in making precise calculations, these curves, and those of Figs. 8-7 to 8-11 should be considered only as illustrating trends.

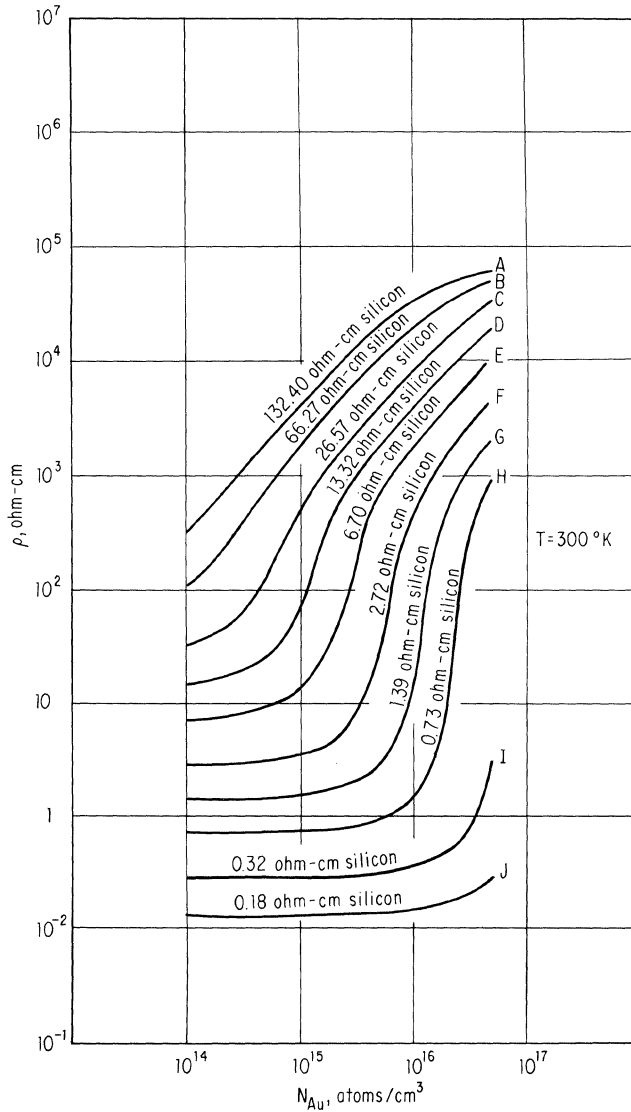


Fig. 8-7. Resistivity versus gold concentration in boron-doped silicon at $T = 300^\circ\text{K}$. Gold levels: 0.54 and 0.35 ev. Boron level: 0.045 ev.

8-5. EFFECTS OF HIGH FIELD ON RESISTIVITY

In Eq. (8-1), the assumption was made that μ (the mobility) and the number of carriers are independent of the applied electric field. For high fields this is not correct. In the range of 10^3 to 10^5 volts/cm, the number of carriers does remain constant, but the mobility decreases appreciably. Figure 8-21 shows the variation of mobility with field strength for high-resistivity n-type silicon.¹⁹ In the range above 10^5 volts/cm, carriers can obtain high enough velocity between collisions to

form new carriers. This is usually observed in the space-charge region of reverse-biased diodes where it is possible to get the high fields quite readily and is called "avalanche." If yet higher fields can be obtained, then zener breakdown, i.e., the field-induced direct transition of carriers from the valence to the conduction band, can be observed.

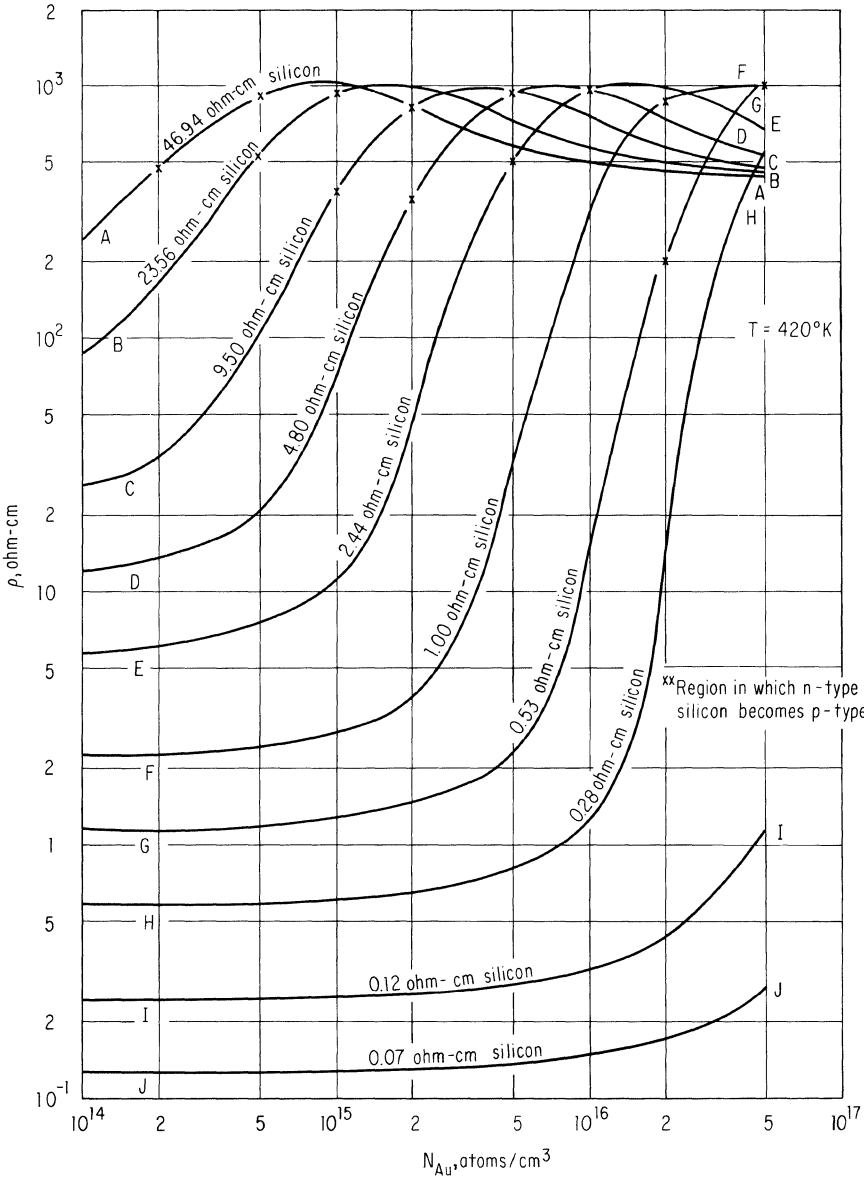


Fig. 8-8. Resistivity versus gold concentration in phosphorus-doped silicon at $T = 420^\circ\text{K}$. Gold levels: 0.54 and 0.35 ev. Phosphorus level: 0.045 ev.

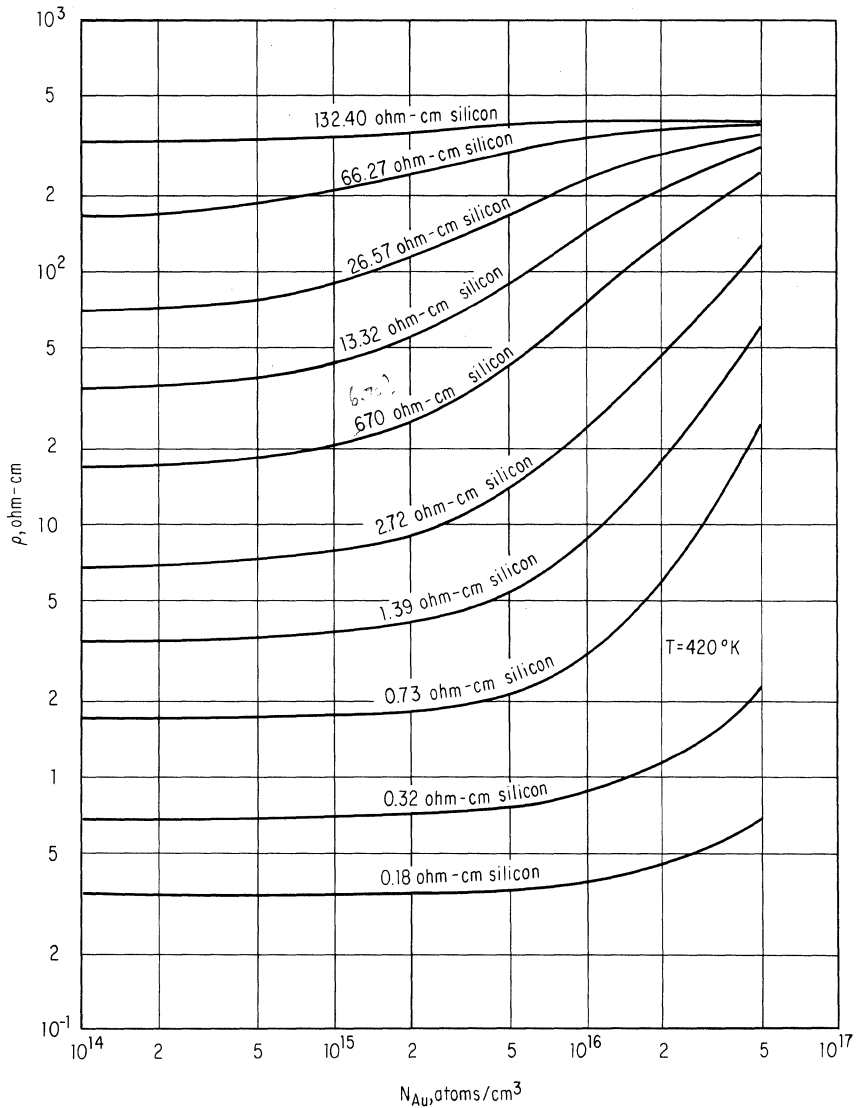


Fig. 8-9. Resistivity versus gold concentration in boron-doped silicon at $T = 420^\circ\text{K}$. Gold levels: 0.54 and 0.35 ev. Boron level: 0.045 ev.

8-6. WIDTH OF SPACE-CHARGE REGION IN p-n JUNCTIONS

The width of the space-charge region at a given applied voltage across the junction, and thus the field, is a function of the impurity atom distribution within the region. If the junction is an "abrupt" one, i.e., a uniform concentration on each side, and one concentration level is many times greater than the other, avalanche breakdown voltage versus the impurity concentration of the low concentration side is as shown in Fig. 8-22.²⁰ This curve and the data from Figs. 6-1 to 6-4 can be

combined into Fig. 8-23 which enables avalanche breakdown or “reach-through” voltage,* the width of the depletion region, resistivity, and impurity concentration to be determined graphically if any one of these values is known.

For example, if the starting material is 4 ohm-cm p-type, moving horizontally from the 4 ohm-cm part to the p-type curve shows that the corresponding impurity concentration is approximately 3×10^{15} atoms/cm³. Following this isoconcentration line until it intersects the breakdown curve gives a space-charge width of 0.3 mil. Moving horizontally to the breakdown voltage scale on the left gives a breakdown of approximately 130 volts.

In the event that the layer available for the space-charge region to expand in was

* Reach-through occurs when the material dimensions rather than the applied voltage limit the movement of the space-charge region. For example, the resistivity of the material might be such that it would have a 100-micron-thick space-charge region at breakdown, but if the thickness of the slice on which the devices were made was only 35 microns, then reach-through would occur when the space-charge boundary reached the contact.

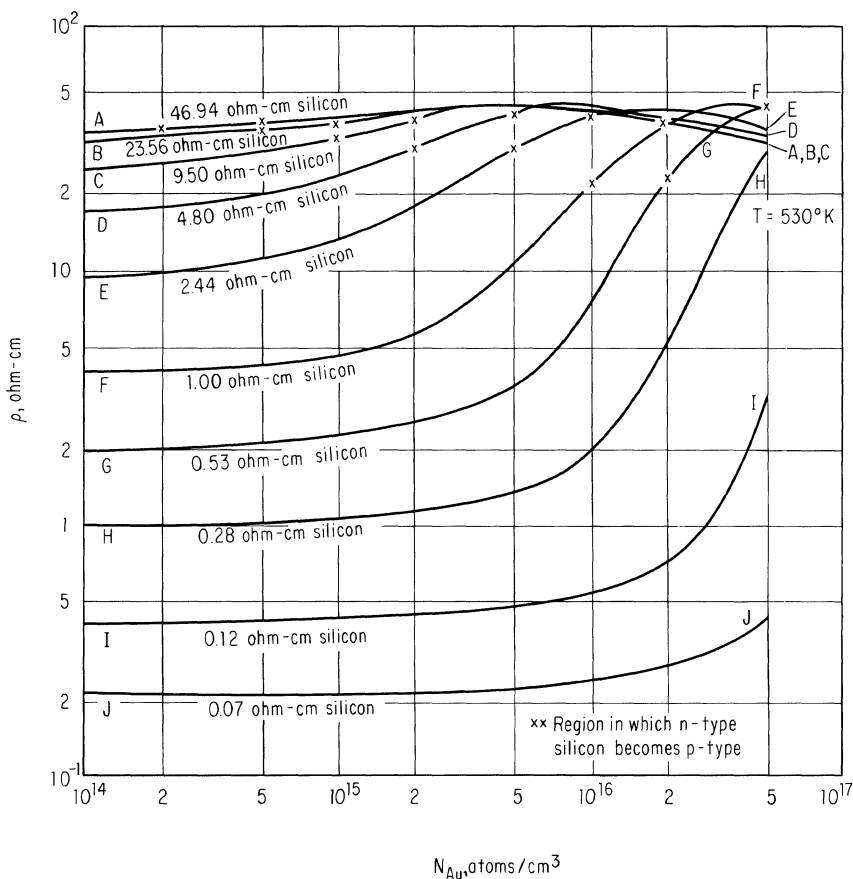


Fig. 8-10. Resistivity versus gold concentration in phosphorus-doped silicon at $T = 530^\circ K$. Gold levels: 0.54 and 0.35 ev. Phosphorus level: 0.044 ev.

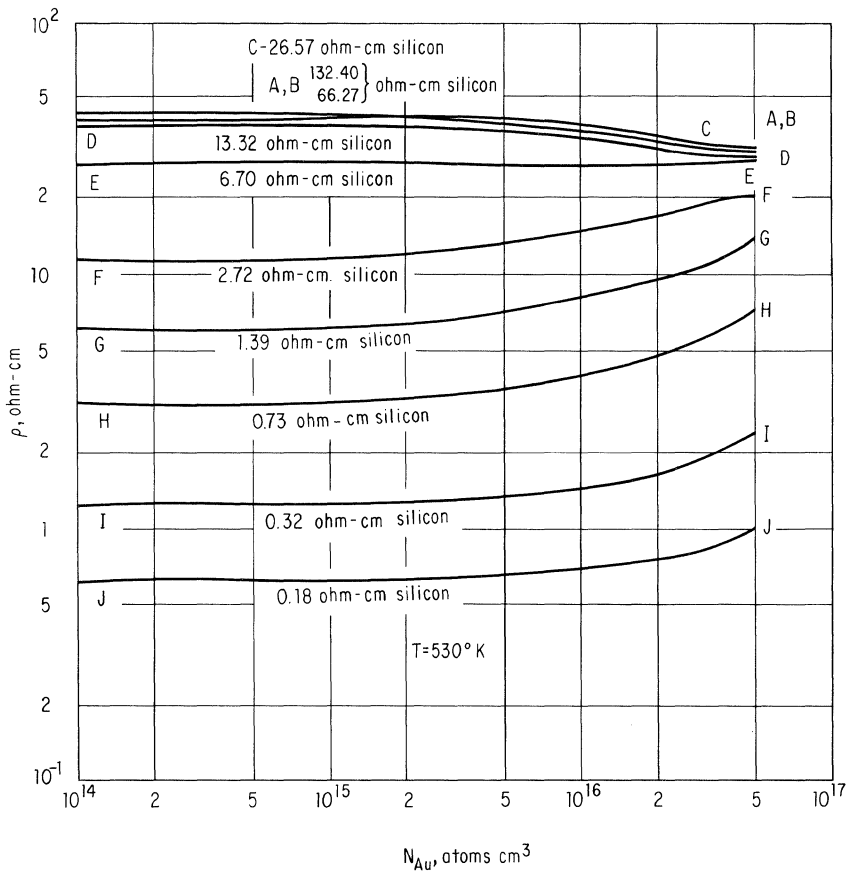


Fig. 8-11. Resistivity versus gold concentration in boron-doped silicon at $T = 530^\circ K$. Gold levels: 0.54 and 0.35 ev. Boron level: 0.045 ev.

limited to some value less than 0.3 mil, for example, 0.1 mil, then breakdown would be determined by that thickness rather than the impurity concentration. Moving to the left from the point of intersection of the 0.1-mil line with the iso-concentration curve gives a reach-through breakdown of approximately 15 volts.

8-7. EFFECTS OF PRESSURE

The pressure dependence of the absorption edge is given by $dE/dP = -1.5 \times 10^{-12} \text{ ev}/(\text{dyne})(\text{cm}^2)$.²¹

The application of very high pressures apparently produces a phase transition and reduces the resistivity several orders of magnitude. Figure 8-24 shows typical behavior.²²

Uniaxial tension, as well as hydrostatic pressure, causes resistivity changes in both p- and n-type silicon. This change can be expressed in terms of a tensor with three independent components π_{11} , π_{12} , and π_{44} . That is, if $\Delta_{ij} = \delta\rho_{ij}/\rho_0$ equals

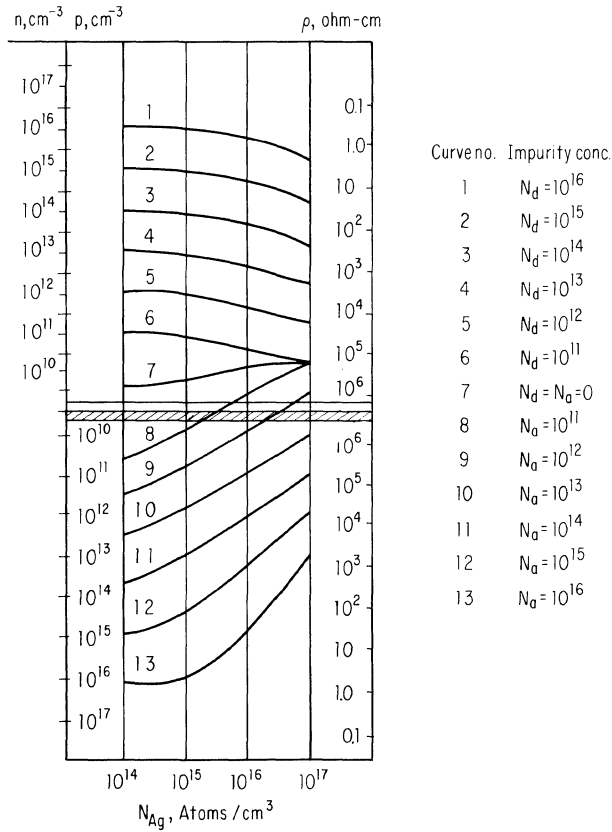


Fig. 8-12. Carrier density and resistivity versus silver concentration in silicon at $T = 18^\circ\text{C}$. (Boltaks and Shih-yin.⁵)

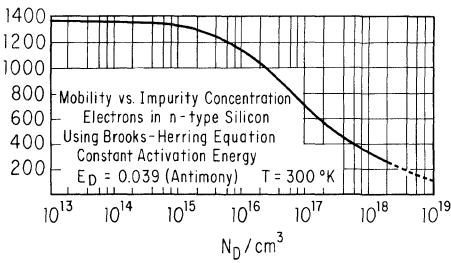


Fig. 8-13. Electron mobility versus impurity concentration in n-type silicon. Calculated using Brooks-Herring equation for ionized impurity scattering, $E_D = 0.039$ eV (antimony), and $T = 300^\circ\text{K}$.

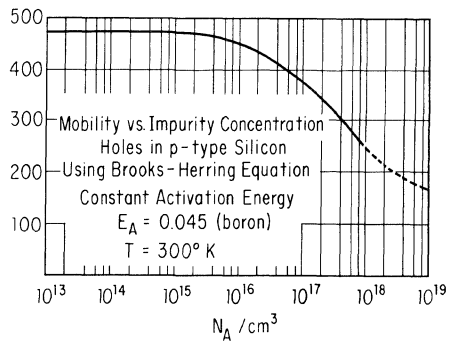


Fig. 8-14. Hole mobility versus impurity concentration in p-type silicon. Calculated using Brooks-Herring equation for ionized impurity scattering, $E_A = 0.045$ eV (boron), and $T = 300^\circ\text{K}$.

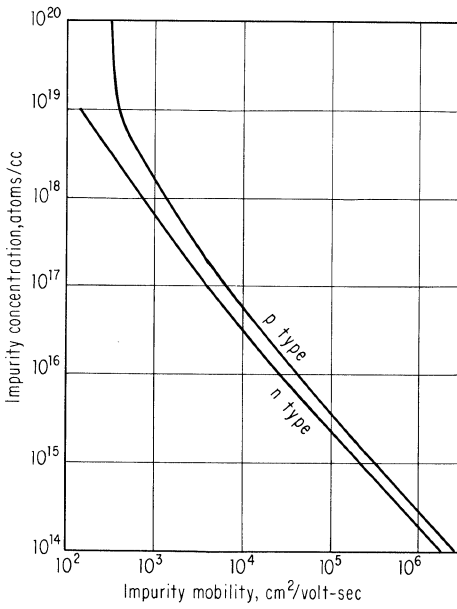


Fig. 8-15. Impurity mobility versus total impurity concentration for n- and p-type silicon. $T = 300^{\circ}\text{K}$.

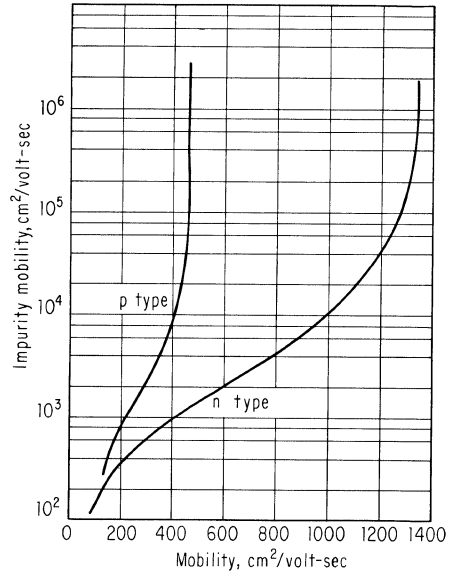


Fig. 8-16. Impurity mobility versus total mobility for n- and p-type silicon. $T = 300^{\circ}\text{K}$.

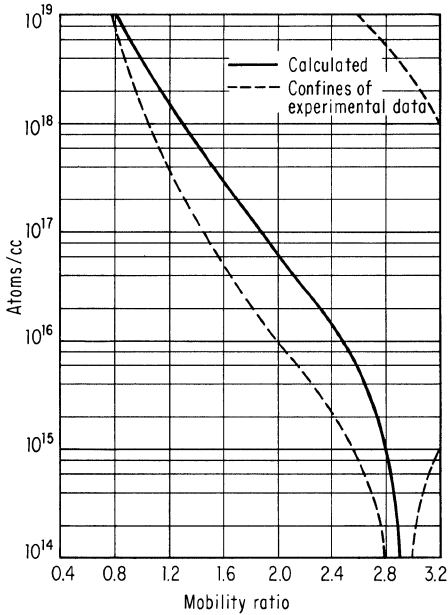


Fig. 8-17. Mobility ratio versus impurity concentration in silicon. $T = 300^{\circ}\text{K}$.

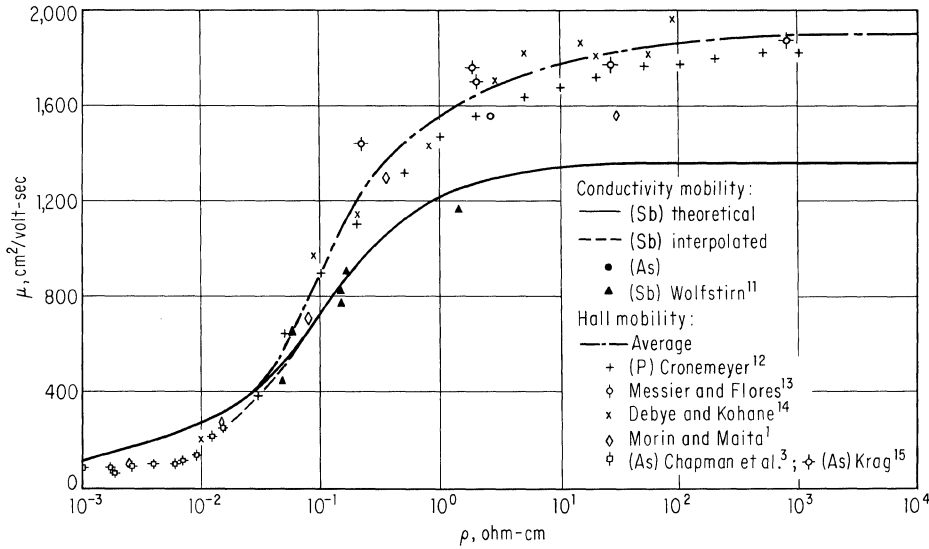


Fig. 8-18. Electron mobility versus resistivity in n-type silicon at 300°K.

the change of resistivity measured in the *j*th direction for a stress applied in the *i*th direction divided by the original resistivity, then

$$[\Delta] = [\pi][T] \tag{8-7}$$

where *T* is the applied stress.²³ For colinear stress, current, and electric field,

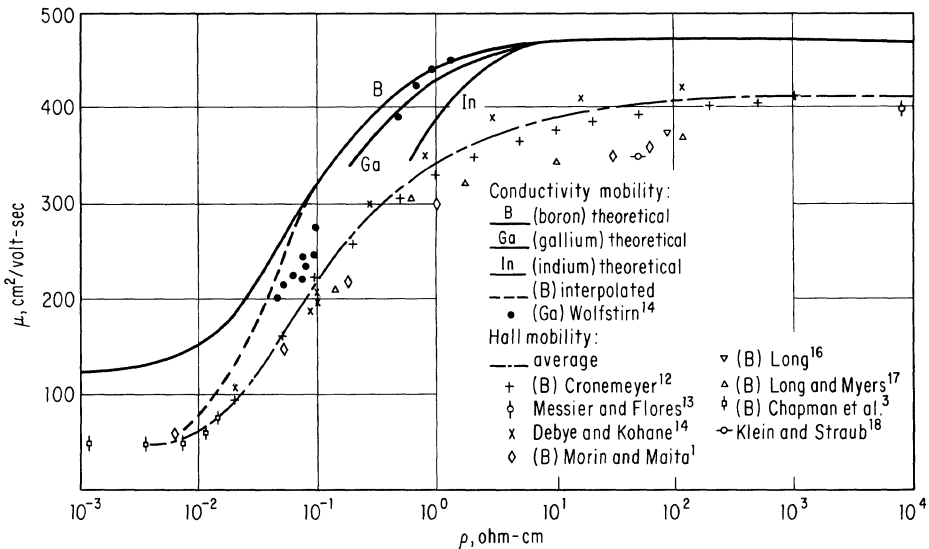


Fig. 8-19. Hole mobility versus resistivity in p-type silicon at 300°K.

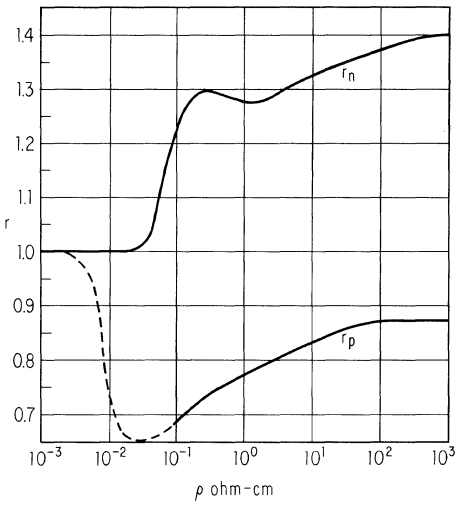


Fig. 8-20. Ratio of Hall mobility to conductivity mobility versus resistivity for uncompensated silicon at 300°K.

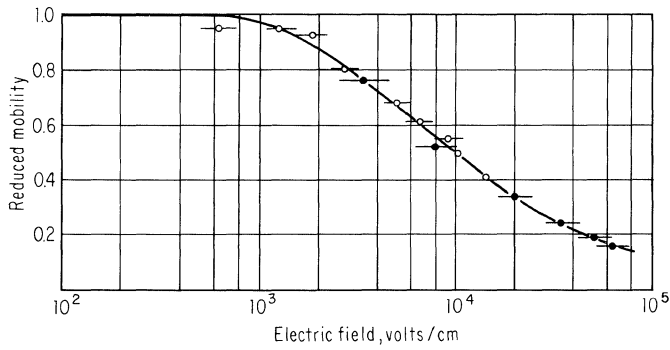


Fig. 8-21. Variation of reduced mobility with electric field applied to 70 ohm-cm silicon along the $\langle 111 \rangle$ direction. Carrier concentration assumed constant. (Davies and Gosling,¹⁹)

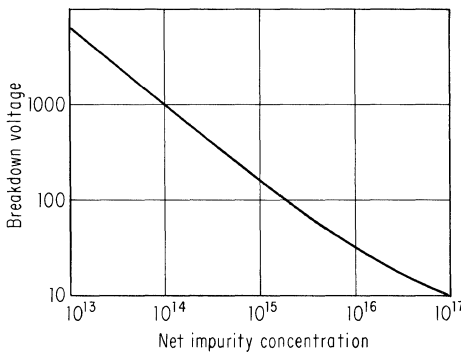


Fig. 8-22. Experimental values of breakdown voltage versus $|N_A - N_D|$ for abrupt silicon p-n junctions. (Shields,²⁰)

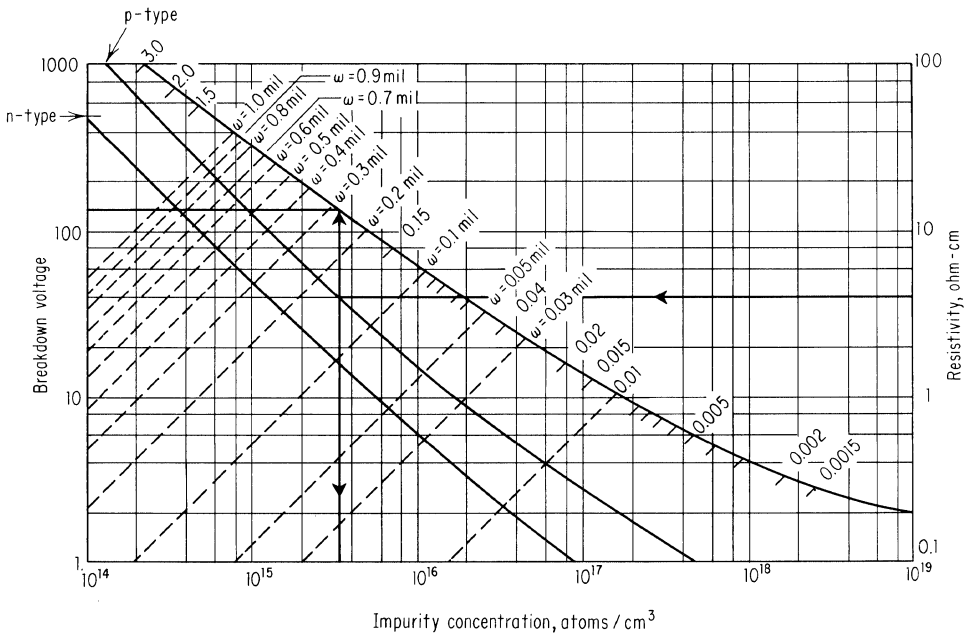


Fig. 8-23. Breakdown voltage versus impurity concentration for an abrupt junction. When starting with either impurity concentration or breakdown voltage, move to top curve for width of space-charge region at breakdown. Then move across or down for breakdown voltage or impurity concentration. n- and p-type curves are used to convert from resistivity to impurity concentration. (Courtesy of Stacy Watelski.)

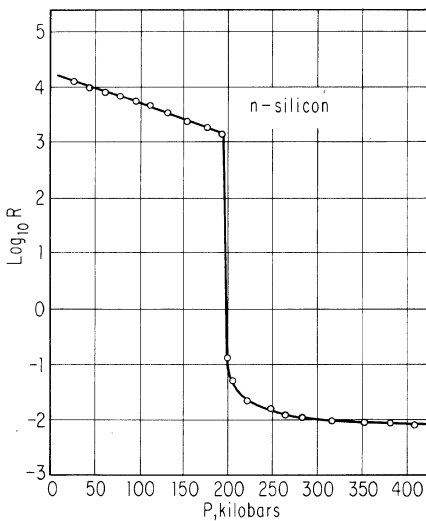


Fig. 8-24. Resistance versus pressure for n-type silicon. (Minomura and Drickamer.²²)

Table 8-3

Crystal direction	π_l , cm ² /dyne	Y_l (silicon), dynes/cm ²
[100]	π_{11}	1.301×10^{12}
[111]	$\frac{1}{3}\pi_{11} + \frac{2}{3}(\pi_{12} + \pi_{44})$	1.878×10^{12}
[110]	$\frac{1}{2}(\pi_{11} + \pi_{12} + \pi_{44})$	1.690×10^{12}

the longitudinal piezoresistance coefficient π_l is given by²⁴

$$\pi_l = \frac{1}{\sigma_l} \frac{\Delta\rho}{\rho_0} = \pi_{11} + 2(\pi_{44} + \pi_{12} - \pi_{11})(m_1^2 m_2^2 + m_1^2 m_3^2 + m_2^2 m_3^2) \quad (8-8)$$

where σ_l = longitudinal stress in the direction l

$\Delta\rho$ = change in resistivity due to stress σ_l

ρ_0 = resistivity in zero stress condition

m_1, m_2, m_3 = direction cosines of direction l with respect to principal crystallographic directions [100], [010], [001]

The principal crystal directions of concern in silicon piezoresistive devices are the [111], [110], and [100] directions. Table 8-3 gives the longitudinal piezoresistance coefficients in terms of the independent π coefficients and Young's modulus for each of these directions. Most of the data taken has been in terms of π_l and is summarized in Fig. 8-25.^{25,30}

8-8. ENERGY BANDS

The energy band spectrum for silicon is shown in Figs. 8-26 and 8-27.^{26,31}

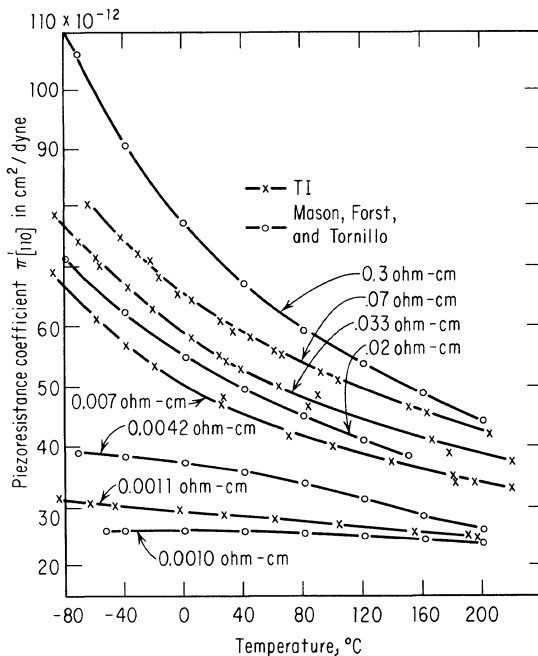


Fig. 8-25. Temperature dependence of piezoresistivity in silicon for various p-type impurity concentrations. (Sobey.²⁵)

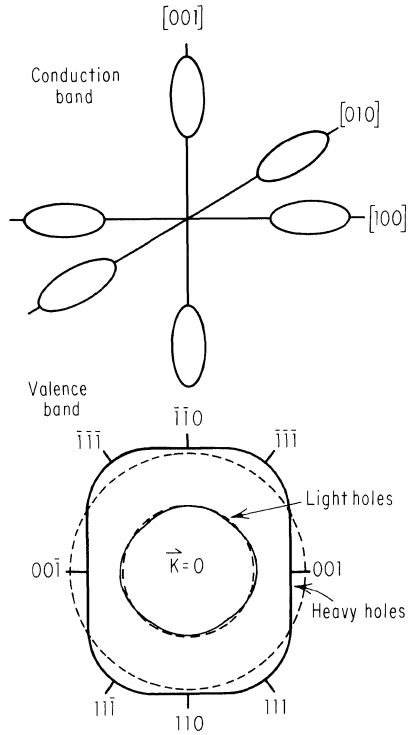


Fig. 8-26. Top: schematic of constant energy contours or valleys around the conduction band edges in silicon. The six ellipsoidal valleys in the $\langle 100 \rangle$ directions are evident. Bottom: cross section of a constant energy contour near the valence band edge in silicon in the (110) plane. (Hannay,²⁶)

8-9. EFFECTIVE MASSES FOR ELECTRONS AND HOLES²⁷

Effective masses are given in the following tabulation:

<i>For Electrons*</i>	<i>For Holes</i>
Longitudinal $\approx 0.98 m$	$m_1 \approx 0.49 m$
Transverse $\approx 0.19 m$	$m_2 \approx 0.16 m$
Conductivity $\approx 0.26 m$	$m_3 \approx 0.24 m$
Density of states $\approx 0.33 m$	Density of states $\approx 0.55 m$

* m is the electron rest mass, 9.1072×10^{-28} g.

Table of Useful Numbers

Avogadro number	6.023×10^{23} /mole
Boltzmann constant	1.38×10^{-16} erg/ $^{\circ}$ K
Stefan-Boltzmann constant	5.67×10^{-5} erg/(cm^2)(sec)($^{\circ}$ K ⁴)
Charge on electron	1.6×10^{-19} coul
Permittivity of free space	8.85×10^{-14} farad/cm
Joule	10^7 ergs
Joule	watt-sec = va-sec
Gram-calorie	4.18 joules
Erg	dyne-cm
Electron volt	1.6×10^{-12} erg
Coulomb	amp-sec
Faraday	9.65×10^4 coul
Ampere	1.036×10^{-5} faraday/sec

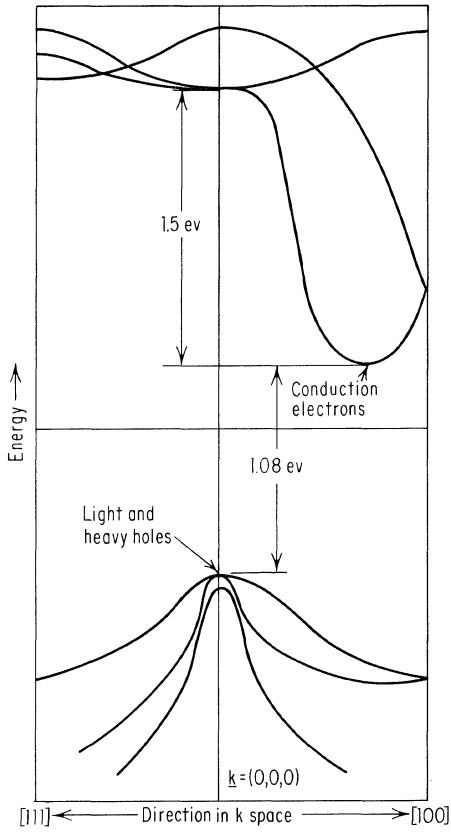


Fig. 8-27. Energy as a function of wave vector k for the [111] and [100] directions in silicon. (Hannay.²⁶)

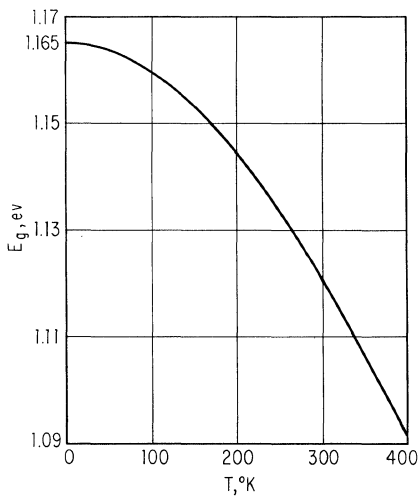
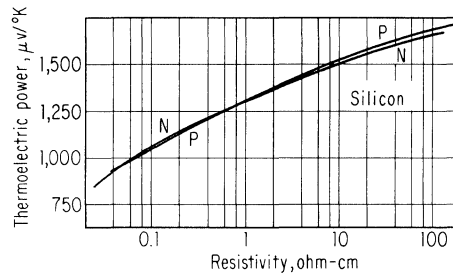


Fig. 8-28. Variation of E_g with temperature. (Smith.²⁷)

Fig. 8-29. Thermoelectric power versus resistivity for silicon at room temperature. (Geballe and Hull.²⁸)



8-10. MISCELLANEOUS EFFECTS

Variation of Energy Gap with Temperature.²⁷ Figure 8-28 shows the variation of energy gap with temperature. The slope in the linear region is given by

$$\frac{dE_g}{dT} = -2.4 \times 10^{-4} \text{ ev}/^\circ\text{C}$$

Thermoelectric Power. Figure 8-29 shows the thermoelectric power versus resistivity for silicon near room temperature.²⁸

Dielectric Constant. The dielectric constant has been measured directly for frequencies of between 500 cps and 30 mcps and found to be 11.7.²¹ The silicon was doped with gold and then cooled to liquid nitrogen temperature so that the resistivity would be high (approximately 10¹⁰ ohm-cm). Other measurements have been made of the complex dielectric constant by microwave techniques at 24 gcps for relatively low-resistivity material. From these data the high-resistivity dielectric constant was calculated to be between 12.6 and 14.6.²⁹

REFERENCES

1. Morin, F. J., and J. P. Maita: Electrical Properties of Silicon Containing Arsenic and Boron, *Phys. Rev.*, vol. 96, pp. 28-35, 1955.
2. Hall, R. N., and J. H. Racette: Diffusion and Solubility of Copper in Extrinsic and Intrinsic Germanium, Silicon, and Gallium Arsenide, *J. Appl. Phys.*, vol. 35, pp. 379-397, 1964.
3. Chapman, P. W., O. N. Tuftte, J. D. Zook, and D. Long: Electrical Properties of Heavily Doped Silicon, *J. Appl. Phys.*, vol. 34, pp. 3291-3295, 1963.
4. Pearson, G. L., and J. Bardeen: Electrical Properties of Pure Silicon Alloys Containing Boron and Phosphorus, *Phys. Rev.*, vol. 75, pp. 865-883, 1949.
5. Boltaks, B. I., and Hsüeh Shih-yin: Diffusion, Solubility and the Effects of Silver Impurities on the Electrical Properties of Silicon, *Soviet Phys.-Solid State*, vol. 2, pp. 2383-2388, 1961.
6. Brooks, H.: Electrical Properties of Germanium and Silicon, in L. Martan (ed.), "Advances in Electronics and Electron Physics," vol. VII, pp. 156-160, Academic Press Inc., New York, 1955.
7. Debye, P. P., and E. M. Conwell: Electrical Properties of n-type Germanium, *Phys. Rev.*, vol. 93, pp. 693-706, 1954.

8. Conwell, E. M., and V. F. Weisskopf: Theory of Impurity Scattering in Semiconductors, *Phys. Rev.*, vol. 77, p. 388, 1950.
9. Smith, R. A.: "Semiconductors," pp. 148–153, Cambridge University Press, London, 1959.
10. Smith, R. A.: "Semiconductors," pp. 100–102, Cambridge University Press, London, 1959.
11. Wolfstirn, K. B.: Hole and Electron Mobilities in Doped Silicon from Radiochemical and Conductivity Measurements, *J. Phys. Chem. Solids*, vol. 16, pp. 279–284, 1960.
12. Cronmeyer, D. C.: Hall and Drift Mobility in High-resistivity Single Crystal Silicon, *Phys. Rev.*, vol. 105, pp. 522–523, 1957.
13. Messier, J., and J. M. Flores: Temperature Dependence of Hall Mobility and μ_H/μ_D for Silicon, *J. Phys. Chem. Solids*, vol. 24, pp. 1539–1542, 1963.
14. Debye, P. P., and T. Kohane: Hall Mobility of Electrons and Holes in Silicon, *Phys. Rev.*, vol. 94, pp. 724–725, 1954.
15. Krag, W. E.: Galvanomagnetic Effects in n-type Silicon, *Phys. Rev.*, vol. 118, pp. 435–450, 1960.
16. Long, D.: Galvanomagnetic Effects in p-type Silicon, *Phys. Rev.*, vol. 107, pp. 672–677, 1960.
17. Long, D., and J. Myers: Weak Field Magnetoresistance in p-type Silicon, *Phys. Rev.*, vol. 109, pp. 1098–1102, 1958.
18. Klein, C. A., and W. D. Straub: Carrier Density, Mobility Ratio and Impurity Concentration of High Resistivity p-type Silicon, *Bull. Am. Phys. Soc.*, ser. 2, vol. 4, p. 28, 1959.
19. Davies, E. A., and D. S. Gosling: Non-ohmic Behavior in Silicon, *J. Phys. Chem. Solids*, vol. 23, pp. 413–416, 1962.
20. Shields, J.: Breakdown in Silicon p-n Junctions, *J. Electron. Control*, vol. 6, pp. 130–148, 1959.
21. Moss, T. S.: "Optical Properties of Semiconductors," Academic Press Inc., New York, 1959.
22. Minomura, S., and H. G. Drickamer: Pressure Induced Phase Transitions in Silicon, Germanium and some III-V Compounds, *J. Phys. Chem. Solids*, vol. 23, pp. 451–456, 1962.
23. Smith, Charles S.: Piezoresistance Effect in Germanium and Silicon, *Phys. Rev.*, vol. 94, pp. 42–49, 1954.
24. Pfann, W. G., and N. Thurston: Semiconducting Stress Transducers Utilizing the Transverse and Shear Piezoresistance Effects, *J. Appl. Phys.*, vol. 32, pp. 2008–2019, 1961.
25. Sobey, Arthur E.: Unpublished work.
26. Hannay, N. B. (ed.): "Semiconductors," Reinhold Publishing Corporation, New York, 1959.
27. Smith, R. A.: "Semiconductors," pp. 347–351, Cambridge University Press, London, 1959.
28. Geballe, T. H., and G. W. Hull: Seebeck Effect in Silicon, *Phys. Rev.*, vol. 98, pp. 940–947, 1959.
29. Anderson, R. E.: Dielectric Properties of Silicon, "Studies on the Thermal and Electrical Properties of Silicon," University of Texas Progress Report, June, 1958.
30. Mason, W. P., J. J. Forst, and L. M. Tornillo: Recent Developments in Semiconductor Strain Transducers, preprint no. 15-NY 60, ISA Fall Instrumentation-Automation Conference, New York, 1960.
31. Brooks, H.: Theory of the Electrical Properties of Germanium and Silicon, in "Advances in Electronics and Electron Physics," vol. VII, Academic Press Inc., New York, 1955.

Optical Properties

9-1. ABSORPTION COEFFICIENTS

The absorption spectrum of silicon can be divided into three areas of interest. The first is wavelengths shorter than those corresponding to the band edge, the second is the transition region near the edge, and the third is longer wavelengths.

Figure 9-1 shows the absorption coefficient in the region from 0.1 to 1.1 microns.^{1,2,*} The absorption is due to carriers being raised from the valence to the conduction band. The increased absorption below about 0.33 micron is presumably due to the beginning of direct transitions. Decreasing temperature shifts the absorption edge to shorter wavelengths. This is shown in Figs. 9-2 and 8-28. Pressure also affects the absorption edge and shifts it to shorter wavelengths.³ This is shown in Fig. 9-3. Details of the absorption near the band edge are shown in Fig. 9-4.⁴

In the long-wavelength region, free carriers, the lattice, impurities, defects, and the carriers associated with the impurities and defects all contribute to the absorption. Figure 9-5⁵ shows typical data from 1.1 to 40 microns for n-type silicon.

* Superscript numbers indicate items listed in References at the end of the chapter.

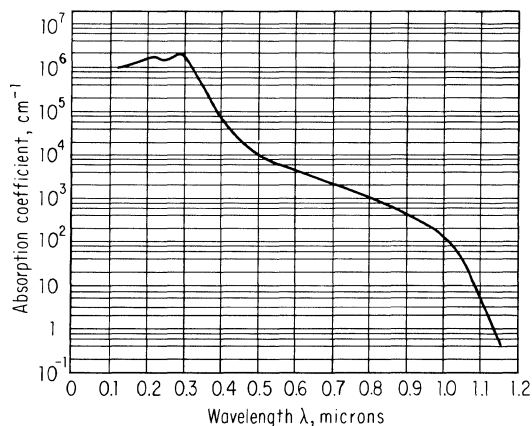


Fig. 9-1. Room temperature absorption coefficient versus wavelength. (Adapted from Dash and Newman¹ and Philipp and Taft.²)

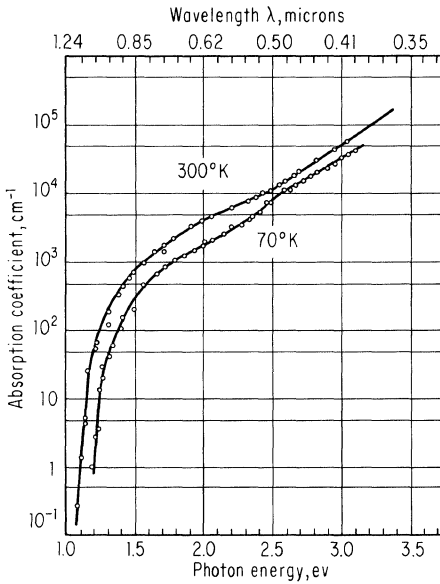


Fig. 9-2. Absorption as a function of wavelength for high-purity, single-crystal silicon. Resistivity >20 ohm-cm. (Dash and Newman.¹)

Figure 9-6⁶ extends the range to beyond 250 microns. There are some absorption bands at 2.3, 9.1, 16, and 19.4 microns, but other than that, α appears to be predominantly due to free carriers and varies as λ^2 . The deviation of the long-wavelength data from the λ^2 dependence is thought to be due to experimental error. Figure 9-7 shows the absorption for p-type silicon.⁷ The characteristics are similar to those of n-type silicon except that the 2.3-micron band is absent.

Since the major part of the absorption coefficient at room temperature and above is due to free carriers, an increase in temperature with a corresponding increase in the number of carriers causes the absorption coefficient to also increase. Figures 9-8 to 9-10 show this effect for high-resistivity n- and p-type material over the wavelength range of from 2.5 to 6 microns (which is the region in which silicon optical elements usually operate).⁸

If the contribution due to the free carriers (as determined by long-wavelength measurements) is subtracted from the measured value a number attributable to the lattice is obtained.⁹ This is shown in Fig. 9-11.

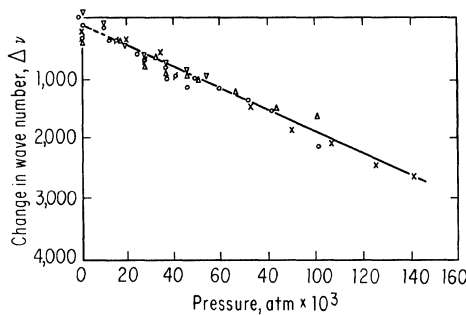


Fig. 9-3. Shift of single-crystal, p-type silicon absorption edge with pressure. ($\alpha = 25 \text{ cm}^{-1}$, $\Delta\nu$ measured from $10,000 \text{ cm}^{-1}$, $\rho = 0.08 \text{ cm}^{-1}$.) (Slykhouse and Dric-kamer.³)

Absorption Bands. The absorption band at 2.3 microns is thought to be caused by excitation of carriers from the conduction band minima to higher bands.⁵ Oxygen in silicon gives rise to the 9.1- and 19.4-micron bands¹⁰⁻¹² which are shown in more detail in Figs. 9-12 and 9-13. The absorption coefficient is proportional to the amount of oxygen present and is often used as a measure of the oxygen content of silicon crystals.¹³ Figure 9-14 shows the 9.1-micron absorption coefficient versus oxygen content.

If silicon which has ionized impurities at room temperature is cooled enough to freeze out the carriers, then transitions may occur between their levels and the valence or conduction bands. Spectra for the Group IIIA and VA elements are shown in Figs. 9-15 and 9-16.¹⁴⁻¹⁷

Radiation-induced Bands. Neutron and electron irradiation of silicon produces a series of absorption bands which depend on the type and amount of initial impurity.¹⁸ One band, which occurs for either neutron or high-energy electron bombardment, appears at 1.8 microns and is observed in high-resistivity n-type and in p-type samples. Apparently the defect responsible for the absorption has an energy level about 0.21 eV below the conduction band and will not absorb if occupied by electrons. Another band is observed at 3.3 microns in low-resistivity n-type material. Presumably in this case a level is introduced at 0.21 eV below the conduction band which will only absorb if it is filled with electrons.

A 3.9-micron band is observed in neutron-irradiated low-resistivity p-type samples which have been annealed. This absorption is probably due to acceptors

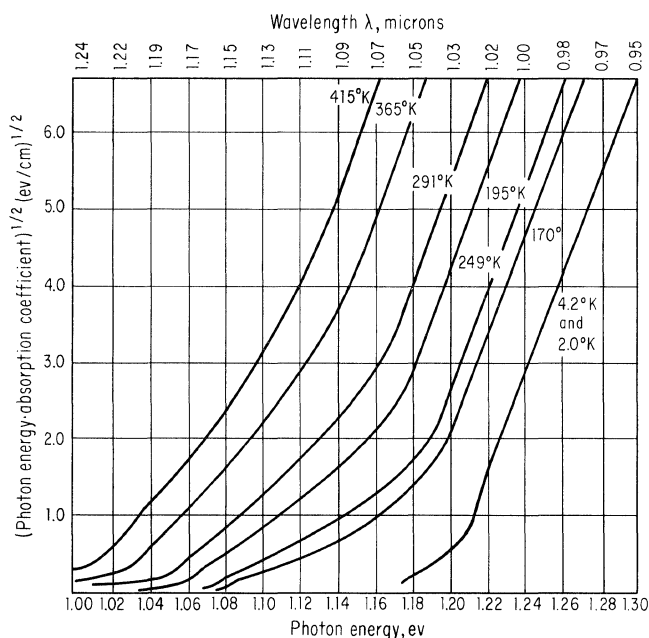


Fig. 9-4. Details of absorption near the band edge. (MacFarlan, McLean, Quarrington, and Roberts.⁴)

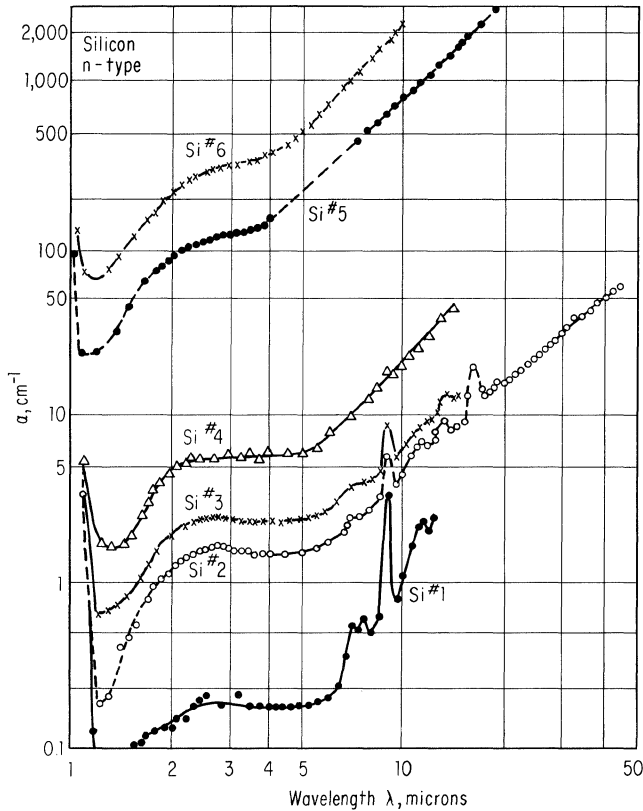


Fig. 9-5. Absorption coefficient of n-type silicon as a function of wavelength. (Spitzer and Fan.⁵)

associated with vacancies. Some low-resistivity n-type samples show a 5.5-micron absorption band which is attributed to a bound electron at about 0.16 eV below the conduction band. Occasionally samples which exhibit the 3.9-micron absorption band after annealing also show a 6-micron band after further annealing. There are also bands (not associated with annealing) that have been observed at 20.5, 27, and 30.1 microns.

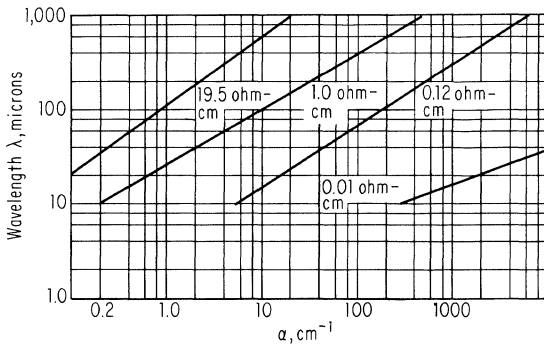
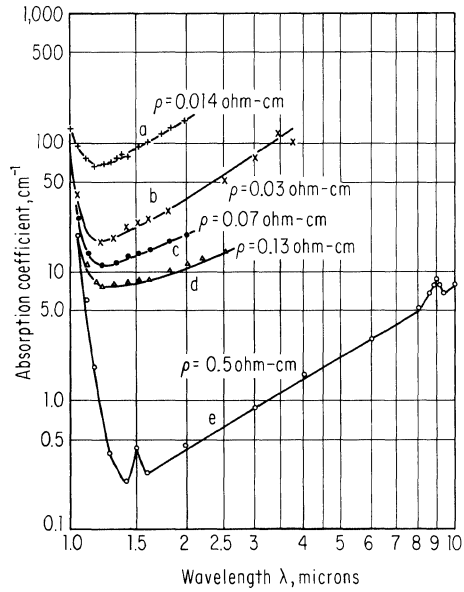


Fig. 9-6. Absorption coefficient of n-type silicon as a function of wavelength at room temperature. (Jones and Hilton.⁶)

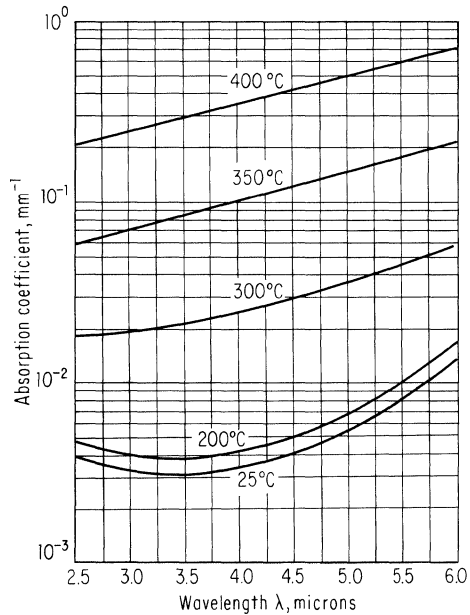
Fig. 9-7. Absorption coefficient of p-type silicon as a function of wavelength (Fan and Becker.⁷)



If oxygen-containing silicon is irradiated with high-energy electrons, defects are introduced which cause an absorption band at 12 microns and which have an associated electrical level 0.17 eV below the conduction band. These defects are apparently due to a vacancy with an oxygen atom bridging two of the dangling bonds.¹⁹

Other than introducing the various absorption bands just discussed, neutron

Fig. 9-8. Absorption coefficient versus wavelength at different temperatures (n-type single-crystal silicon).



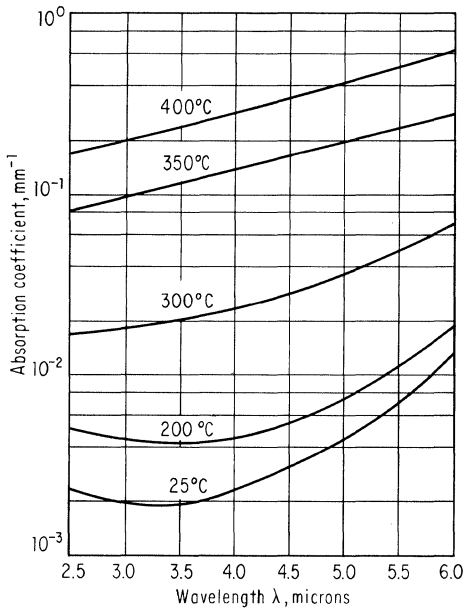


Fig. 9-9. Absorption coefficient versus wavelength at different temperatures (p-type single-crystal silicon).

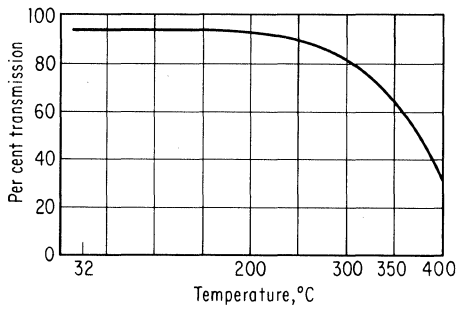


Fig. 9-10. Transmission through coated silicon plate as a function of temperature.

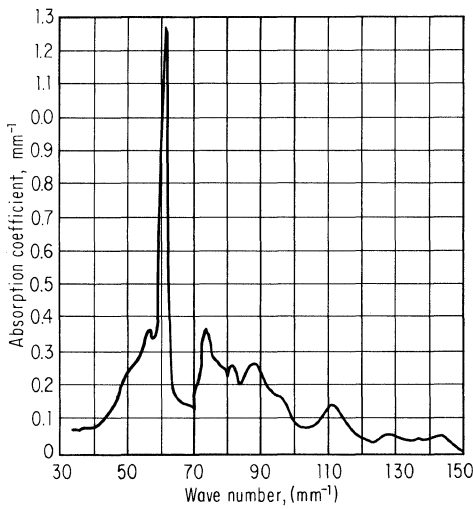


Fig. 9-11. Silicon lattice absorption bands. (Johnson.⁹)

Fig. 9-12. Absorption coefficient of silicon at room temperature: (a) pulled from a quartz crucible, (b) prepared by float-zone technique. (Kaiser, Keck, and Lange.¹⁰)

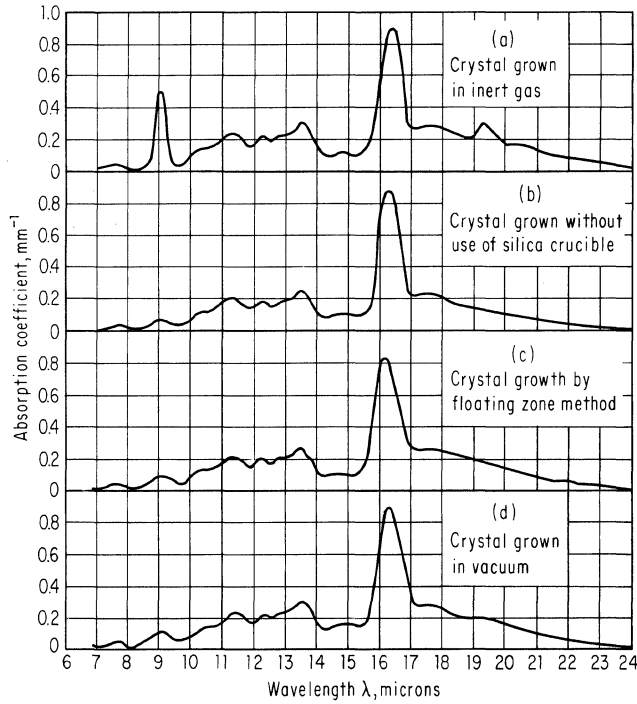
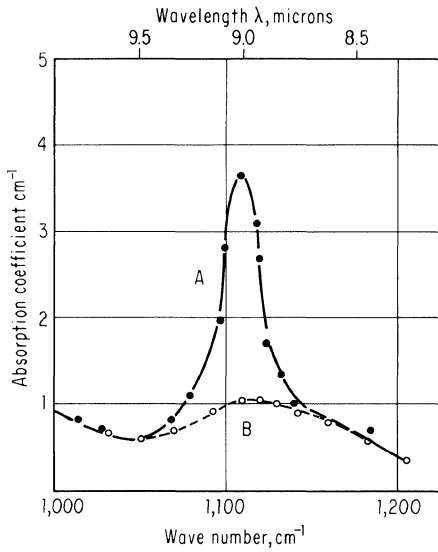


Fig. 9-13. The absorption coefficient as a function of wavelength in the 6- to 24-micron range for specimens of four silicon crystals prepared in different ways. (Green, Hogarth, and Johnson.¹²)

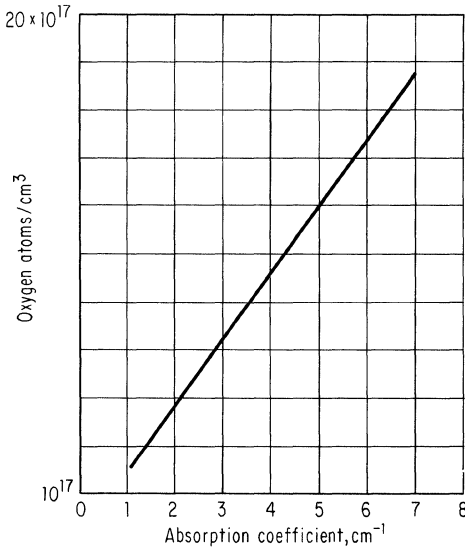


Fig. 9-14. Oxygen content versus absorption coefficient. (Kaiser and Keck.¹³)

irradiation of silicon usually decreases the absorption coefficient. This is attributed to the removal of free carriers during bombardment.⁷ Because of the possibility of increasing the transmission of low-cost, low-purity silicon to a level acceptable for infrared optical components, considerable additional data have been collected in the 2- to 6-micron region.²⁰ Figure 9-17 shows typical changes in the absorption coefficient observed in this range. It was, however, concluded that such a process is presently economically impractical because of the steady decline in the price of high-purity silicon and the expense associated with neutron bombardment.

Effects of Mechanical Damage. Bands have been observed at 2.8, 3.3, and 4.8 microns in crushed silicon and are attributed to defect states produced close to the surface during the crushing.²¹ This spectrum is shown in Fig. 9-18.

Calculation of Transmission from α . The transmission of parallel radiation normal to the surface of a plane parallel plate is given by the relation

$$\frac{I}{I_0} = \frac{e^{-\alpha x}(1 - R)^2}{1 - R^2 e^{-2\alpha x}} \tag{9-1}$$

- where α = absorption coefficient
- x = sample thickness
- I_0 = incident radiation
- I = transmitted radiation
- R = reflection coefficient

The reflection coefficient is given by

$$R = \left(\frac{n_1 - n_2}{n_1 + n_2} \right)^2 \tag{9-2}$$

where n_1 is the index of refraction of air and n_2 that of silicon.

Conversions. To convert from photon energy in electron volts to wavelength

in microns, multiply the reciprocal of electron volts by 1.237, for example, λ (microns) = 1.237/ev.

- 1 angstrom = 10^{-8} cm
- 1 micron = 10^{-6} meters
- 1 wave number = 1/wavelength

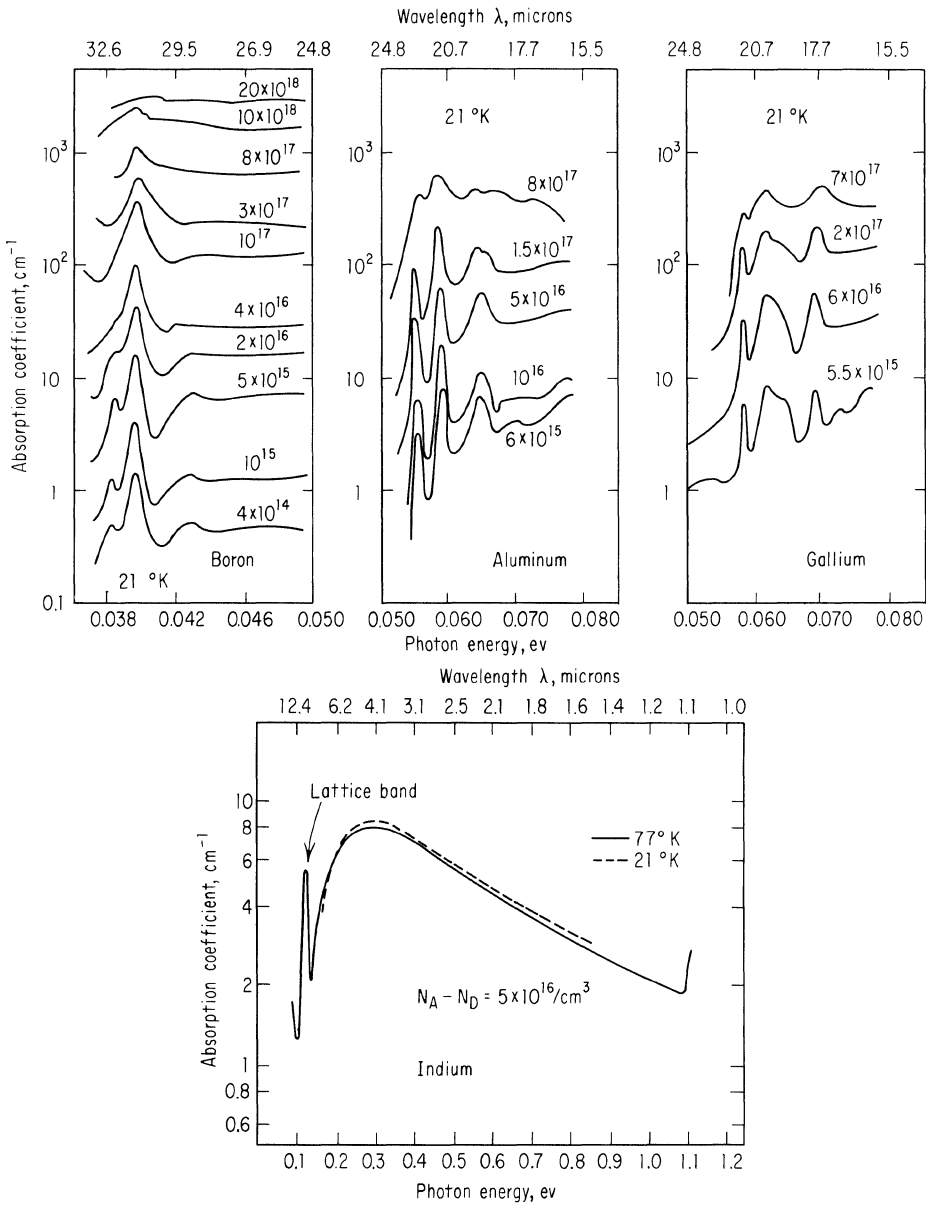


Fig. 9-15. Absorption spectra of p-type impurities in silicon. (Newman.^{14,15})

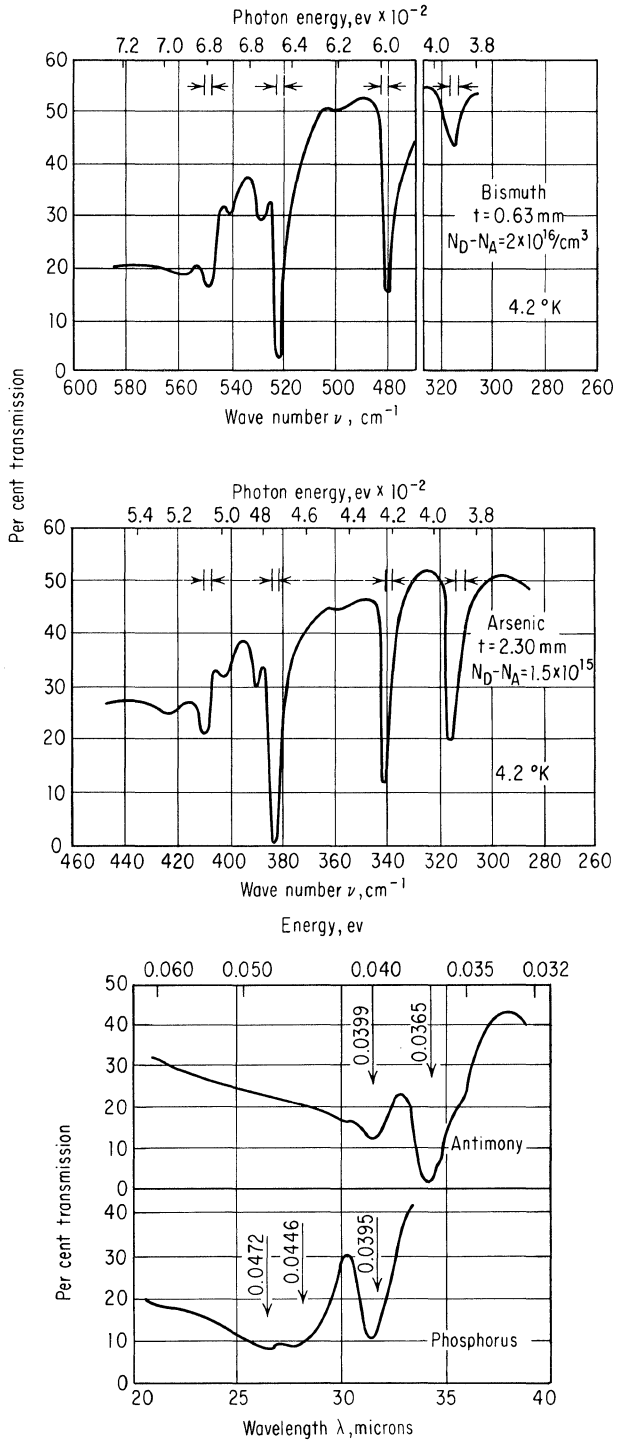


Fig. 9-16. Absorption spectra of n-type impurities in silicon. (Hrostowski and Kaiser ¹⁶ and Bube.¹⁷)

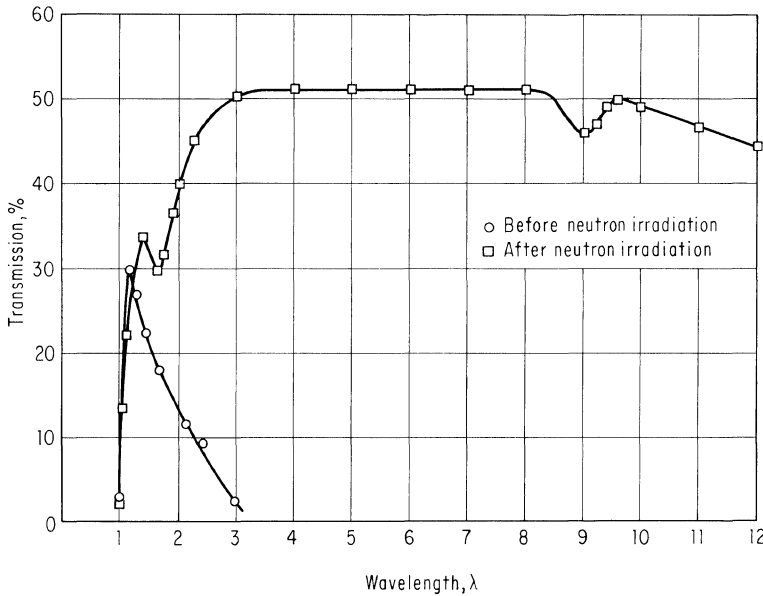


Fig. 9-17. Transmission versus wavelength for irradiated and unirradiated silicon. (Fan and Becker.⁷)

9-2. PHOTOCONDUCTIVITY

Three of the absorption processes result in photoconductivity. These are:

1. An electron is raised from the valence to the conduction band so that a free hole and a free electron are produced.
2. An electron is raised from the valence band to an un-ionized acceptor state so that a free hole is produced.
3. An electron is raised from a donor state to the conduction band so that a free electron is produced.

Process 1 occurs for incident wavelengths shorter than 1.1 microns and can be observed at room temperature. In order to extend the spectral response out to the longer wavelengths, the silicon may be doped with appropriate impurities so that process 2 or 3 above can occur. Since these impurity centers are usually already ionized at room temperature, it is necessary to cool the silicon before the effect can be observed. The shallower the level, the longer the wavelength response and the lower the temperature to which the material must be cooled. Table 9-1 is a tabulation of various doping elements and the long wavelength cutoff.¹⁷

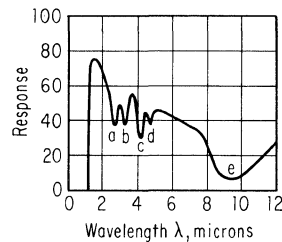


Fig. 9-18. A typical transmission curve of a crushed silicon disk taken at room temperature. The observed bands are: (a) 2.8 μ, (b) 3.3 μ, (c) 4.26 μ atmosphere CO₂ absorption, (d) 4.8 μ, and (e) 8 to 10 μ general absorption. (Hilton and Gamble.²¹)

Table 9-1*

Impurity	Donor or acceptor	Long-wavelength cutoff (calculated), microns
Au	A	2.3
Fe	D	2.3
Mn	D	2.3
Zn	A	2.3
Cu	D	2.5
Fe	D	3.1
Au	D	3.8
Zn	A	4.1
Cu	D	5.2
In	A	7.7
Ga	A	19
Al	A	22
As	D	25
B	A	28
P	D	28
Sb	D	32
Li	D	38

* From Richard H. Bube, "Photoconductivity of Solids," John Wiley & Sons, Inc., New York, 1960.

9-3. REFLECTION COEFFICIENT

Figure 9-19 shows the reflection coefficient in the range from 0.1 to 10 microns.² Figure 9-20 extends this out to much longer wavelengths and shows the effect of doping.^{6,22}

9-4. INDEX OF REFRACTION

Table 9-2 is a tabulation of room temperature refractive indices from 1.35 to 11.04 microns. Figure 9-21 includes this data, but extends it to a much shorter wavelength. The data for Table 9-2 were obtained by measuring the angle of minimum deviation of a silicon prism.²³ The extension to shorter wavelength, where silicon is nearly opaque, was calculated from the reflection coefficient.²

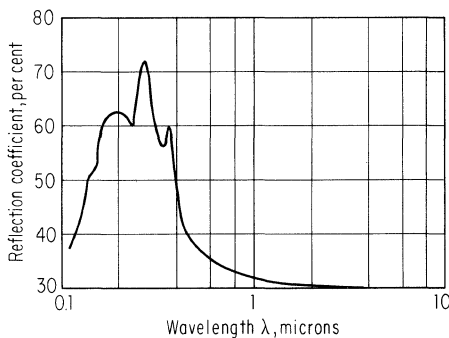


Fig. 9-19. Reflection coefficient versus wavelength for pure silicon. (Philipp and Taft² and Salzberg and Villa.²³)

Fig. 9-20. Reflectivity versus wavelength, n-type silicon. (Jones and Hilton⁶ and Albert and Combs.²²)

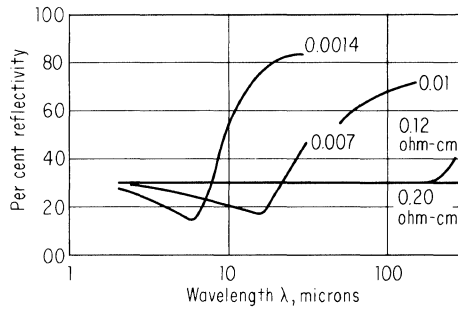


Table 9-2. Index of Refraction of Silicon*·†

Wavelength, microns	Index, <i>n</i>
1.357	3.4975
1.367	3.4962
1.395	3.4929
1.529	3.4795
1.660	3.4696
1.709	3.4664
1.813	3.4608
1.970	3.4537
2.152	3.4476
2.325	3.4430
2.437	3.4408
2.714	3.4358
3.000	3.4320
3.303	3.4297
3.418	3.4286
3.50	3.4284
4.00	3.4255
4.26	3.4242
4.50	3.4236
5.00	3.4223
5.50	3.4213
6.00	3.4202
6.50	3.4195
7.00	3.4189
7.50	3.4186
8.00	3.4184
8.50	3.4182
10.00	3.4179
10.50	3.4178
11.04	3.4176

* From C. D. Salzberg and J. J. Villa, Infrared Refractive Indexes of Silicon, Germanium, and Selenium Glass, *J. Opt. Soc. Am.*, vol. 47, p. 244, 1957.

† 5 ohm-cm, n-type.

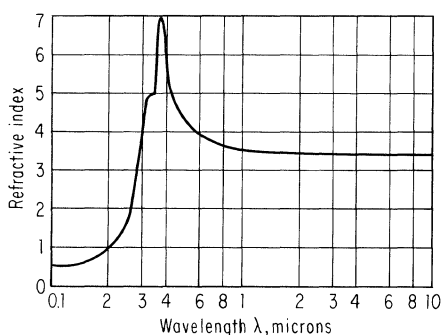


Fig. 9-21. Refractive index of silicon at room temperature. (Philipp and Taft² and Salzberg and Villa.²³)

9-5. EMISSIVITY

The data relating to silicon emissivity appear to have been taken for specialized uses and as such are somewhat sketchy. Figure 9-22 gives the spectral emissivity versus wavelength for several temperatures.^{24,25} Figure 9-23 shows emissivity at the lower temperatures from a heavily doped silicon surface (boron-diffused solar cell).²⁶ Table 9-3 gives the emissivity at 0.65 micron (the region used by optical pyrometers) versus temperature.²⁷

9-6. LIGHT EMISSION

When hole-electron recombination occurs, the excess energy must be dissipated. This may be done in three basic ways (see, for example, Ref. 17).

1. The emission of photons: the energy of each photon equals the energy difference between the two carriers before recombination.
2. The emission of several photons with their total energy equal to the excess energy.
3. By a three-body collision: the excess energy is imparted to a third carrier by Auger, or impact, recombination.

The light emitted is usually very weak because the probability of process 1's

Table 9-3. Spectral Emissivity at 0.65 Microns*

Temperature, °K	Spectral Emissivity
1000	0.64
1100	0.62
1200	0.60
1300	0.57
1400	0.54
1500	0.50
1600	0.48
1688	0.46

* From F. G. Allen, Emissivity at 0.65 Micron of Silicon and Germanium at High Temperatures, *J. Appl. Phys.*, vol. 101, pp. 1676-1678, 1956.

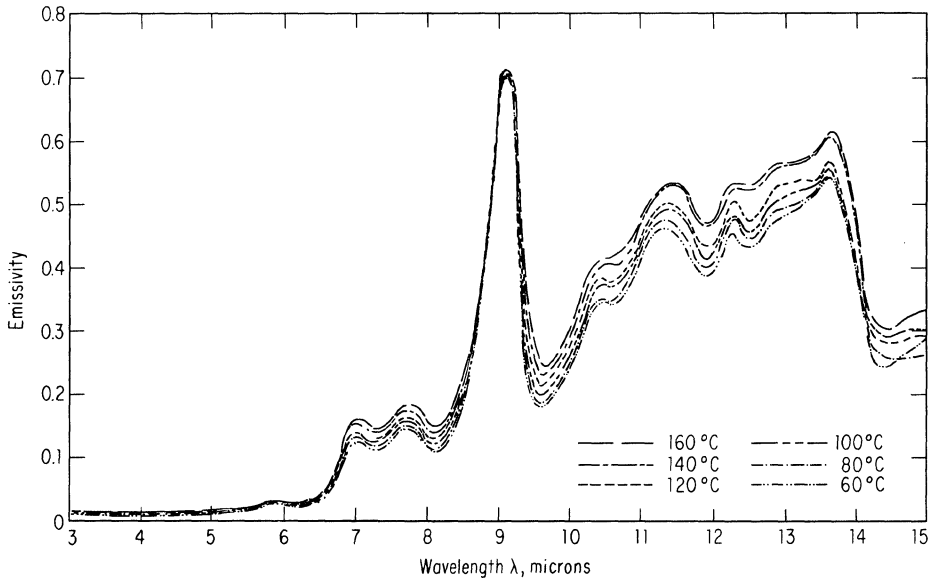
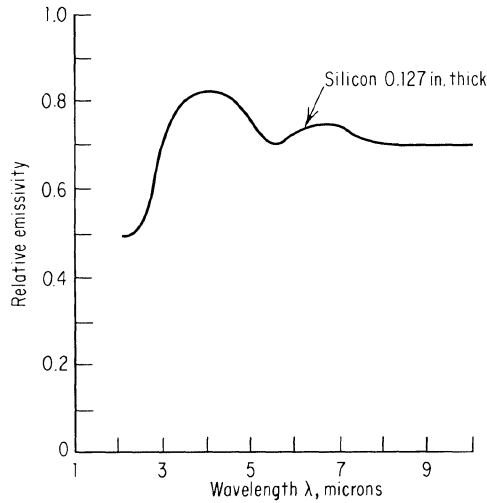


Fig. 9-22. Miscellaneous silicon emissivity data. The temperature of the sample of the top curve was 500°C. (Olt²⁴ and Stierwalt and Potter.²⁵)

occurring is small. However, radiation from several semiconductors, including silicon, has been observed.

The carriers may be generated in the material by higher-energy photons being absorbed by the silicon, may be injected at a forward-biased p-n junction, or may be generated during avalanche. In each case, since the light is being radiated in the bulk and not on the surface, the spectral response observed is affected by the transmission characteristic of the silicon (see Sec. 9-1). For light emitted from very shallow junctions, the correction will, however, be negligible.

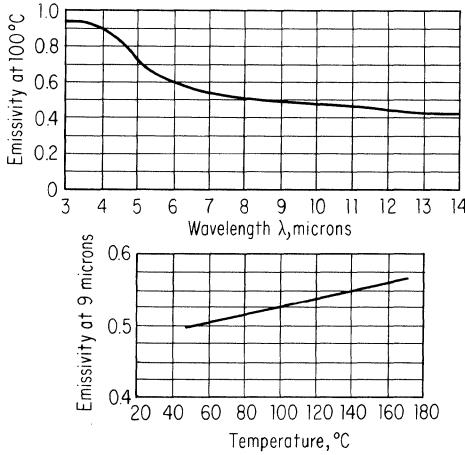


Fig. 9-23. Emissivity of a silicon solar cell versus wavelength.

Forward-biased p-n Junction. Figure 9-24 shows the silicon emission spectra observed when a p-n junction is forward-biased.²⁸ The curve marked “intrinsic” arises from the injected electrons recombining with holes in the conduction band and so has a wavelength corresponding to the band gap energy. If there are acceptor impurities in the material, and if the temperature is low enough that they are un-ionized, transitions can occur between the electrons and holes in these un-ionized acceptor centers. Since acceptor levels lie above the valence band, the energy difference between them and the injected electron is somewhat less than the band gap, so that the wavelength of the radiated light will be longer. The difference in wavelength for the various doping impurities reflects the different heights of the levels above the valence band.

Reverse-biased p-n Junction. If the junction is reverse-biased, visible light is emitted when avalanche occurs.²⁹ The spectral distribution of the light is continu-

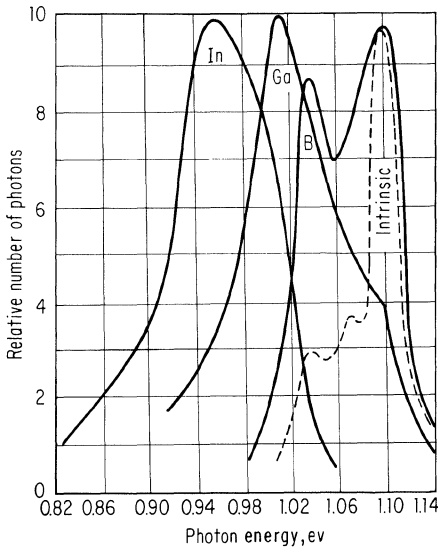


Fig. 9-24. Emission spectra from a forward-biased silicon p-n junction. (Haynes and Westphal.²⁸)

ous and is shown in Fig. 9-25. The short wavelengths apparently arise from free-electron-free-hole recombination, while the longer wavelengths are due to emission from intraband transitions.

The light from the reverse-biased junction has been used to study the character of the junction, and both varieties have been suggested as possible light sources for high-frequency choppers and as emitters for light amplifiers.

Triboluminescence. When some materials are rubbed or abraded, they emit light. This effect has been observed in silicon when it was sandblasted by such abrasives as Al₂O₃, SiC, and SiO₂ in atmospheres of H₂, N₂, and O₂. The emission appears in the orange and infrared although the observed intensities may have been considerably modified by the optical transmission properties of the silicon.³⁰

Electrochemiluminescence. A faint reddish glow has been observed during the anodic oxidation of single-crystal silicon.³¹

9.7. TYNDALL EFFECT

The Tyndall effect has been used to study the behavior of oxygen in silicon.^{32,33}

9-8. BIREFRINGENCE

If an optically isotropic material is subjected to stress, the index of refraction becomes dependent on the plane of polarization. For crystals of the diamond structure the behavior can be expressed as three stress optical coefficients: q_{1111} , q_{1122} , and q_{1212} . The constant q_{1111} relates the retardation of light polarized parallel to the [100] direction and traveling perpendicular to it to stress in the [100] direction. The constant q_{1122} relates the retardation of light polarized parallel to the [010] direction and traveling in the [001] direction to stress applied in the [100] direction. The constant q_{1212} describes the relationship between retardation and shear stress.³⁴ These constants have been measured for silicon as

$$q_{1111} - q_{1122} = -14.4 \times 10^{-14} \text{ cm}^2/\text{dyne} \equiv Q_1$$

$$2q_{1212} = -10 \times 10^{-14} \text{ cm}^2/\text{dyne} \equiv Q_2$$

by one investigator³⁵ and about 30 per cent less by others.³⁶ Experimentally Q is determined by the equation

$$Q = \frac{2h\lambda}{n_0^3 T d}$$

- where h = amount of retardation in units of wavelengths
- λ = wavelength in air
- n_0 = index of refraction of unstressed material
- T = applied stress
- d = crystal path length

This effect has been widely used to study residual stresses in silicon crystals after various growing and annealing cycles.³⁶⁻³⁹

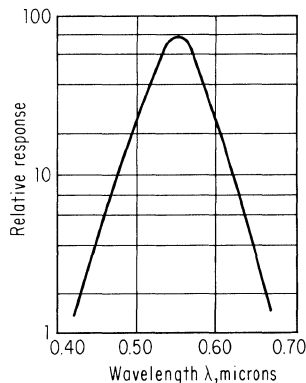


Fig. 9-25. Spectral response of light emitted from a silicon p-n junction back-biased to avalanche. (Chynoweth and McKay.²⁹)

9-9. OPTICAL ELEMENTS

While semiconductor-grade silicon is normally considered only as a starting material for transistors and rectifiers, its good transmission in the infrared has made it a major infrared optical material for both lenses and windows in the 3- to 5-micron region. For these applications silicon plates are available in diameters of over a foot and by appropriate segmenting procedures, windows even larger can be made. Figure 9-26 shows a 7.5-in.-diameter dome being bonded together from smaller pieces. By the proper choice of adhesive, dimensional stability can be maintained and the final grinding and polishing done after bonding.²⁰

Polycrystalline Material. When silicon was first being considered as an infrared optical material, it was assumed that single crystals would be required for good transmission and image quality. However, experiments were soon performed which showed that there was no measurable difference in the absorption coefficient of comparable purity single and polycrystalline silicon. In addition, the relative image quality was measured by constructing identical silicon lenses from single-crystal and grown polycrystalline ingots and examining the image formed when they were placed in parallel light. From this examination it was concluded that any differences were insignificant for normal optical usage.⁸ Figure 9-27 is a sketch of the equipment used and the results observed.

Grown polycrystalline silicon is characterized by having quite large single-crystal volumes (up to several cubic centimeters). However, some of the cast material that has since supplanted it for optical use has a very fine grain structure in which individual crystallites may be less than 1 mm across. Essentially the same experiments have been rerun for the cast variety and have again shown no significant dif-

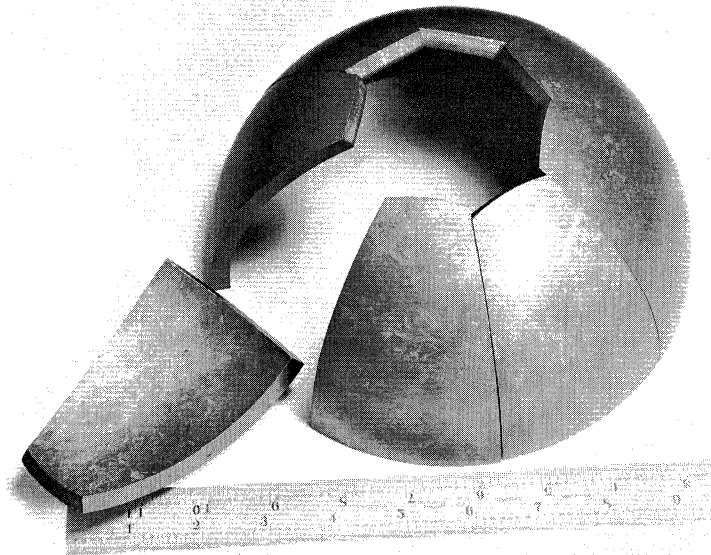


Fig. 9-26. Construction of a 8-in.-diameter silicon infrared dome from segments.

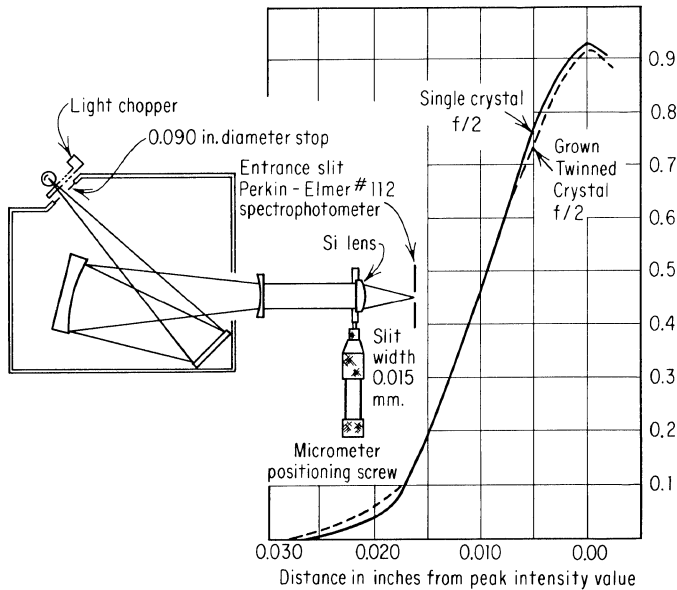


Fig. 9-27. Image profiling device and profile from single and grown twinned silicon lenses.

ferences of absorption coefficient or image quality from those of single-crystal silicon.^{40,41}

Modulators. With a suitable means of supplying electrons, for example a forward-biased p-n junction or an electron beam, the carrier concentration can be increased locally in a controlled fashion. This in turn increases the infrared absorption and allows infrared choppers to be constructed.^{42,43}

The absorption edge can be shifted to longer wavelengths by the application of a strong electric field. Thus, with proper choice of wavelength, infrared can also be modulated by this process.^{44,45}

9-10. OPTICAL COATINGS

Because of the high index of refraction, silicon to be used for refractive optics usually has coatings added to it to reduce the reflection losses at each surface. Similarly, silicon light sensors and energy converters normally use some sort of low-reflectance coating.

The most common type is a simple one-layer dielectric quarter-wave coating. In this case the criterion for zero reflection loss at some wavelength λ is for the coating to be $\lambda/4$ thick and have an index of refraction n_c given by

$$n_c = \left(\frac{n_{Si}}{n_{air}} \right)^{1/2}$$

This equation assumes that the silicon has negligible absorption. If this is not true, a more general derivation* can be used, but even with the relatively high

* For a complete derivation of both cases see Julius A. Stratton, "Electromagnetic Theory," chap. 9, McGraw-Hill Book Company, New York, 1941.

absorption coefficients encountered in solar cells, the change in value of n_c is small.

In practice it is of course difficult to find coatings that have the exact index required, so it is of interest to know how much deviation can be tolerated and still reduce reflections to a satisfactory level. This can be calculated by using the general equation from which the previous equation was derived:

$$R = \frac{(r_{12} + r_{23})^2 - 4r_{12}r_{23} \sin^2 (2\pi d/\lambda)}{(1 + r_{12}r_{23})^2 - 4r_{12}r_{23} \sin^2 (2\pi d/\lambda)}$$

where R = reflection coefficient of the combination

d = thickness of the layer

λ = wavelength in the layer

For a silicon coating to be used in air

$$r_{12} = \frac{n_{\text{air}} - n_{\text{film}}}{n_{\text{air}} + n_{\text{film}}}$$

$$r_{23} = \frac{n_{\text{film}} - n_{\text{Si}}}{n_{\text{film}} + n_{\text{Si}}}$$

Figure 9-28 is a plot of R for $\lambda/4$ coatings of various refractive indices at a wavelength of 4.5 microns (which is in a region where coated silicon optics are often used).⁸ For this specific case, losses of 1 per cent or less per surface would result from using materials with refractive indices of from 1.65 to 2.05. This same equation can also be used to calculate the reflective losses as a function of wavelength for a fixed layer thickness and index of refraction. Figure 9-29 shows the general character of $(1 - R)$, which will be proportional to the increased transmission through a plate with the coating. There is a multiplicity of peaks, representing higher-order reflections within the layer. Since silicon will not transmit wavelengths shorter than about 1.1 microns anyway, only the second-order peak would be observed in this case. The higher-order peaks get sharper and sharper and, in practice, usually show lower and lower transmission because of attenuation losses occurring in the layer as the energy is reflected back and forth. Figure 9-30 is a similar curve but plotted in terms of normalized wavelengths. The measured transmission curves of a coated and an uncoated piece of silicon are shown in Fig. 9-31. It should be remembered that all these data are for normal incidence.

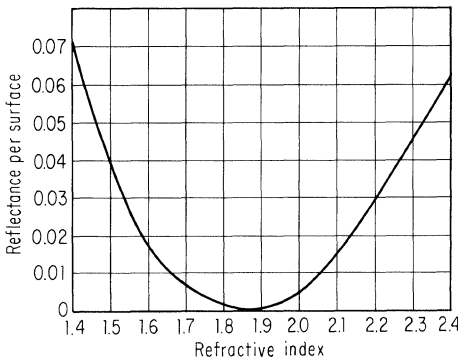
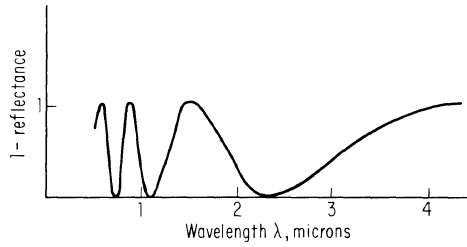


Fig. 9-28. Calculated reflectance per surface as a function of refractive index of coating material. (From data of Herrmann; Runyan, Herrmann, and Jones.⁸)

Fig. 9-29. Variation of $(1 - R)$ with wavelength for quarter-wave low-reflectance coating peaked for maximum transmission at 4.4 microns.



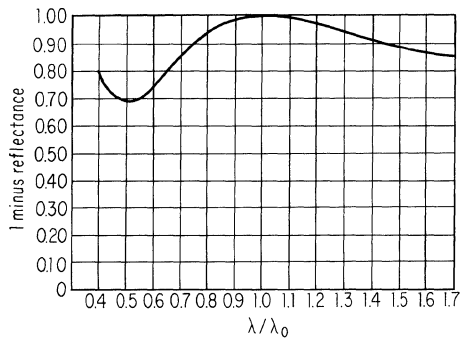
Deviations from normal will affect the wavelength at which minimum reflection occurs for a given thickness since the light path through the layer becomes longer.

As the temperature of the silicon and coating is increased, not only does the transmission decrease because of the increasing absorption coefficient, but also the wavelength for maximum transmission will shift because of the dependence of the indices of refraction on temperature. Experimental data for a plate originally peaked at 4.1 microns are shown in Fig. 9-32. If the temperature dependence of either the coating or the base material is known, it can be used to compute the temperature dependence of the other refractive index.

Vacuum evaporation techniques are normally used to produce the quarter-wave coatings for silicon optics, though painted-on organics and chemically formed films have also been used for reflection reduction on solar cells. Evaporated silicon monoxide, cerium oxide, and zinc sulfide all make acceptable coatings.⁴⁶⁻⁴⁸ In addition, titanium dioxide, aluminum oxide, and antimony oxide have been investigated, but are not recommended because of poor mechanical properties or difficulty in evaporation. Silicon monoxide is probably the most widely used coating since it is easy to deposit and possesses excellent mechanical properties. It does, however, have appreciable absorption at the longer wavelengths, so that if the coating is to be used beyond 7 or 8 microns, zinc sulfide is more appropriate. Complete coating information on these materials, including descriptions of the equipment necessary to maintain an even coating over large, flat or spherical sections, may be found in Refs. 8 and 46 to 48.

It is also possible to use multiple-layer films instead of the simple one-layer film just described and greatly broaden the first-order transmission peak. For example, a two-layer combination has been reported for silicon which gives transmittances of above 90 per cent from 1.5 to 4.1 microns. With three layers this can be further extended.⁴⁹

Fig. 9-30. Response of $\lambda/4$ coating of SiO on silicon.



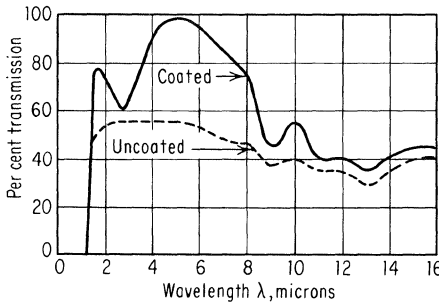


Fig. 9-31. Effect of an optical coating on transmission.

Instead of evaporating layers, silicon can be thermally oxidized or chemically stained. These layers are normally SiO₂, but chemical stains occasionally give an SiO layer. Either of these materials is satisfactory for short-wavelength coatings, e.g., solar cells, since the working range is from 0.5 to 1 micron, and, in that range, the indices of refraction of either are appropriate, and neither has a large attenuation coefficient.

If “thick” layers (several wavelengths) of a dielectric with an intermediate refractive index are added to the silicon, reflective losses can be reduced somewhat, but not as much as is possible with the quarter-wave coatings. For example, consider the effect of a clear plastic coating on the front surface of a solar cell.

1. The loss without any coating would be

$$R = \left(\frac{1 - 3.4}{1 + 3.4} \right)^2 = 0.3$$

i.e., only 70 per cent of the incident energy would be available for power conversion.

2. Assume the plastic layer has an index of refraction of 1.5. Then at the air-plastic interface

$$R = \left(\frac{1 - 1.5}{1 + 1.5} \right)^2 = 0.04$$

or 96 per cent of the incident energy passes on to the plastic-silicon interface.

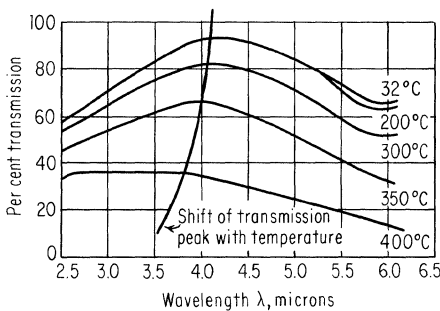


Fig. 9-32. Transmission through coated silicon plate as a function of wavelength for various temperatures. (From data of Herrmann; Runyan, Herrmann, and Jones.⁸)

3. For the plastic-silicon interface

$$R = \left(\frac{1.5 - 3.4}{1.5 + 3.4} \right)^2 = 0.14$$

or 86 per cent of the energy is transmitted into the silicon. From step 2, 4 per cent of the energy reflected from the silicon back to the plastic-air interface will be again reflected to the silicon surface, etc., but this is negligible so that 0.86×0.96 , or 83 per cent, of the original incident energy is available for conversion rather than 100 per cent (in theory) with a quarter-wave coating and 70 per cent without any coating. It should also be noted that since the quarter-wave coating actually has minimum loss only at discrete wavelengths (Fig. 9-29), the difference between the two coatings will be somewhat less than calculated.

Another suggested method of minimizing reflection losses, which is not a coating and which is not applicable to optical equipment but which could be used on solar cells, is to etch or cavitate myriads of tetrahedrons into the surface.⁵⁰ Then energy hitting the surface and being reflected will strike another surface before being lost. Thus 70 per cent of the originally reflected 30 per cent will be captured so that 91 per cent of the incident energy would be absorbed. This is illustrated in Fig. 9-33.

Rather than adding low-reflectance coatings, it is also possible to build up interference filters directly on the surface, so that the transmission range of the filter and silicon can be adjusted over a considerable range without the mechanical complication of a separate filter. In many instances, however, the more difficult task of putting the filter directly on the silicon may overshadow the advantages.

Coatings can also be applied to silicon to increase the emissivity at long wavelengths.^{26,51,52} This is particularly useful for solar cells since such coatings will help reradiate the unconverted incident energy. The general requirements for such coatings are that they produce negligible loss in the region where transmission is desired and have high emissivity in the wavelength region corresponding to the blackbody radiation peak for the temperature at which the silicon is to be maintained.

It is possible, for example, to bond a thin layer of glass to the front surface of the cell. The transmittance of the glass is good in the visible range, but becomes highly absorbent and thus highly emissive at longer wavelengths. By this technique the emissivity may be increased to about 0.8 in the 3- to 15-micron region. From a practical standpoint, however, this coating is hard to apply because of the difficulty of matching glass-silicon expansion coefficients over a wide range.

An alternate method that has been used is to vapor-deposit a thick layer of silicon monoxide (which also has high emissivity at long wavelengths) and then apply a quarter-wave coating of magnesium fluoride on top of the SiO. A much more sophisticated approach that shows promise involves building a multilayer filter which will meet the minimum reflection require-

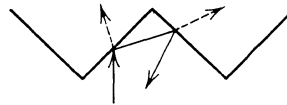


Fig. 9-33. Multiple reflections from a rough surface.

ment and will also have enough layers of SiO to raise the emissivity to a more desirable level.

9-11. OPTICAL GRINDING AND POLISHING PROCEDURES

Normal optical shop techniques used to grind and polish the fused silica are directly applicable to silicon. Roughing shapes from silicon can be accomplished using diamond wheel Blanchard grinders or curve generators at about the same rate as for fused silica. Diamond wheels are not necessary but the fabrication time of silicon optics (as well as fused-silica and soft glass optics) is substantially reduced by so doing.

Because of the high thermal conductivity of silicon, higher polishing tool pressures than normal are required to maintain proper surface temperature. The added pressure makes it more difficult to keep the shape of the polishing surface the same as the piece being polished. This in turn makes the polishing more time consuming so that to polish silicon to a good optical quality surface takes 30 to 50 per cent longer than for an equivalent fused-silica surface.

Polishing pitches such as coal tar and burgundy used with compounds such as barnsite, red rouge, cerox, and alumina are appropriate for silicon. For wafer polishing for device use, a combination of polishing cloth and low-thermal-conductivity polishing compound such as zirconium oxide will provide an adequate finish.

REFERENCES

1. Dash, W. C., and R. Newman: Intrinsic Optical Absorption in Single-crystal Germanium and Silicon at 77°K and 300°K, *Phys. Rev.*, vol. 99, pp. 1151–1155, 1955.
2. Philipp, H. R., and E. A. Taft: Optical Constants of Silicon in the Region 1 to 10 ev, *Phys. Rev.*, vol. 120, pp. 37–38, 1960.
3. Slykhouse, T. E., and H. G. Drickamer: The Effect of Pressure on the Optical Absorption Edge of Germanium and Silicon, *Phys. Chem. Solids*, vol. 7, pp. 210–213, 1958.
4. MacFarlan, G. G., T. P. McLean, J. E. Quarrington, and V. Roberts: Fine Structure in the Absorption Edge of Silicon, *Phys. Rev.*, vol. 111, pp. 1245–1254, 1958.
5. Spitzer, W., and H. Y. Fan: Infrared Absorption in n-type Silicon, *Phys. Rev.*, vol. 108, pp. 268–271, 1957.
6. Jones, C., and R. Hilton (Texas Instruments Incorporated): Personal communication.
7. Fan, H. Y., and M. Becker: Infrared Optical Properties of Silicon and Germanium, in H. K. Henisch (ed.), "Semiconducting Materials," Butterworth Scientific Publications, London, 1951.
8. Runyan, W. R., W. Herrmann, and L. Jones: "Crystal Development Program," Texas Instruments Incorporated, Final Report, AF33(600)-33736, 1958.
9. Johnson, F. A.: Lattice Absorption Bands in Silicon, *Proc. Phys. Soc. (London)*, vol. 73, pp. 265–272, 1959.
10. Kaiser, W., P. H. Keck, and C. F. Lange: Infrared Absorption and Oxygen Content in Silicon and Germanium, *Phys. Rev.*, vol. 101, pp. 1264–1268, 1956.
11. Hrostowski, H. J., and R. H. Kaiser: Infrared Absorption of Oxygen in Silicon, *Phys. Rev.*, vol. 107, pp. 966–972, 1957.

12. Green, G. W., C. A. Hogarth, and F. A. Johnson: Some Observations of the Effects of Oxygen on the Minority Carrier Lifetime and Optical Absorption of Silicon Crystals Pulled in Vacuo, *J. Electron. Control*, vol. 3, pp. 171–182, 1957.
13. Kaiser, W., and P. H. Keck: Oxygen Content of Silicon Single Crystals, *J. Appl. Phys.*, vol. 28, pp. 882–887, 1957.
14. Newman, R.: Concentration Effects on the Line Spectra of Bound Holes in Silicon, *Phys. Rev.*, vol. 103, pp. 103–106, 1956.
15. Newman, R.: Optical Properties of Indium-doped Silicon, *Phys. Rev.*, vol. 99, pp. 465–467, 1955.
16. Hrostowski, H. J., and R. H. Kaiser: Absorption Spectrum of Arsenic-doped Silicon, *Phys. Chem. Solids*, vol. 7, pp. 236–239, 1958.
17. Bube, R. H.: "Photoconductivity of Solids," John Wiley & Sons, Inc., New York, 1960.
18. Fan, H. Y., and A. K. Ramdas: Infrared Absorption and Photoconductivity in Irradiated Silicon, *J. Appl. Phys.*, vol. 30, pp. 1127–1134, 1959.
19. Corbett, J. W., G. D. Watkins, R. M. Chrenko, and R. S. McDonald: Defects in Irradiated Silicon. II. Infrared Absorption of the Si-A Center, *Phys. Rev.*, vol. 121, pp. 1015–1022, 1961.
20. "Development of Silicon Infrared Optical Components," Texas Instruments Incorporated, Final Report, AF33(600)-38085.
21. Hilton, A. Ray, and Fred Gamble: Infrared Absorption of Discs Made from Crushed Silicon, *J. Appl. Phys.*, vol. 33, p. 2398, 1962.
22. Albert, M. P., and J. F. Combs: Thickness Measurement of Epitaxial Films by the Infrared Interference Method, *J. Electrochem. Soc.*, vol. 109, pp. 709–713, 1962.
23. Salzberg, C. D., and J. J. Villa: Infrared Refractive Indexes of Silicon, Germanium, and Selenium Glass, *J. Opt. Soc. Am.*, vol. 47, p. 244, 1957.
24. Olt, R. D.: "Synthetic Sapphire, an Infrared Optical Material," Linde Industrial Crystals Bulletin, No. F-917, 1958.
25. Stierwalt, D. L., and R. F. Potter: Lattice Absorption Bands Observed in Silicon by Means of Spectral Emissivity Measurements, *J. Phys. Chem. Solids*, vol. 23, pp. 99–202, 1962.
26. "Efficiency Improvements of Silicon Solar Cells," Texas Instruments Incorporated, Final Report, Contract DA-23-072-012D-1435, 1960.
27. Allen, F. G.: Emissivity at 0.65 Micron of Silicon and Germanium at High Temperatures, *J. Appl. Phys.*, vol. 28, pp. 1510–1511, 1957.
28. Haynes, J. R., and W. C. Westphal: Radiation Resulting from Recombination of Holes and Electrons in Silicon, *Phys. Rev.*, vol. 101, pp. 1676–1678, 1956.
29. Chynoweth, A. G., and K. G. McKay: Photon Emission from Avalanche Breakdown in Silicon, *Phys. Rev.*, vol. 102, p. 376, 1956.
30. Jenny, D. A.: Triboluminescence in Semiconductors, *J. Appl. Phys.*, vol. 28, p. 1515 (L), December, 1957.
31. Gee, A.: Electrochemiluminescence at a Silicon Anode in Contact with an Electrolyte, *J. Electrochem. Soc.*, vol. 107, p. 787, September, 1960.
32. Kaiser, W.: Electrical and Optical Properties of Heat-treated Silicon, *Phys. Rev.*, vol. 105, pp. 1751–1756, 1957.
33. Schwuttke, G. H., O. A. Weinreich, and P. H. Keck: A Sensitive Method for Measuring Optical Scattering in Silicon, *J. Electrochem. Soc.*, vol. 105, pp. 706–709, 1960.
34. Poindexter, Edward: Piezobirefringence in Diamond, *Am. Mineralogist*, vol. 40, pp. 1032–1054, 1955.
35. Giardini, A. A.: Piezobirefringence in Silicon, *Am. Mineralogist*, vol. 43, pp. 249–262, 1958.

36. Hornstra, J., and P. Penning: Birefringence due to Residual Stress in Silicon, *Philips Res. Rept.*, vol. 14, pp. 237-249, 1959.
37. Dash, W. C.: Birefringence in Silicon, *Phys. Rev.*, vol. 48, p. 1536 (A), 1955.
38. Bond, W. L., and J. Andrus: Photographs of the Stress Field around Edge Dislocations, *Phys. Rev.*, vol. 101, p. 1211, 1956.
39. Lederhandler, S. R.: Infrared Studies of Birefringence in Silicon, *J. Appl. Phys.*, vol. 30, pp. 1631-1638, 1959.
40. Stello, P., and R. H. Griest: Optical Properties of Cast Polycrystalline Silicon, *Proc. IRIS*, vol. 4, pp. 101-107, 1959.
41. Runyan, W. R.: Use of Cast Silicon for Optics, *IRIS Late Development Paper*, April, 1959.
42. Lasser, M. E., P. H. Cholet, and R. B. Emmons: Electronic Scanning for Infrared Imaging, *Proc. IRE*, vol. 47, pp. 2069-2075, 1959.
43. Kruse, P. W., and L. D. McGlauchlin: Solid State Modulators for Infrared Communication, *Electronics*, vol. 34, pp. 177-181, Mar. 10, 1961.
44. Vavilov, V. S., and K. I. Britsyn: The Effect of a Strong Electric Field on the Absorption of Light by Si, *Soviet Phys.-Solid State*, vol. 2, pp. 1746-1747, February, 1961.
45. Britsyn, K. I., and V. S. Vavilov: The Effect of a High Frequency Electric Field on the Edge of the Main Band of Optical Absorption in Si, *Soviet Phys.-Solid State*, vol. 3, pp. 1816-1817, February, 1962.
46. Cox, T. J., and G. Hass: Antireflection Coatings for Germanium and Silicon in the Infrared, *J. Opt. Soc. Am.*, vol. 48, pp. 677-680, October, 1958.
47. Hass, G., and C. D. Salzberg: Optical Properties of Silicon Monoxide in the Wavelength Region from 0.24 to 14.0 Microns, *J. Opt. Soc. Am.*, vol. 44, pp. 181-187, March, 1954.
48. Hass, G.: "Properties, Oxidation, Decomposition and Applications of Thin Films of Silicon Monoxide," U.S. Army Corps of Engineers, ERDL, Report 1180, September, 1950.
49. Cox, J. T., G. Hass, and G. F. Jacobus: Infrared Filters of Antireflected Si, Ge, InAs and InSb, *J. Opt. Soc. Am.*, vol. 51, pp. 714-718, 1961.
50. Dale, Brian: "Research on Efficient Photovoltaic Solar Energy Converters," Transitron, Final Report, Contract AF19(604)5585, 1960.
51. Thelen, A.: The Use of Vacuum Deposited Coatings to Improve the Conversion Efficiency of Silicon Solar Cells in Space, paper presented at the American Rocket Society Space Power Systems Conference, September, 1960.
52. Escoffery, C. A., and Werner Luft: Optical Characteristics of Silicon Solar Cells and of Coatings for Temperature Control, *Solar Energy*, vol. 4, October, 1960.

Miscellaneous Physical Properties and Processes

For easy reference, many of the physical properties of silicon have been tabulated in Table 10-1. Curves and additional data on various of the properties, some of which are discussed in greater detail in the text, appear in Figs. 10-1 to 10-7 and Tables 10-2 and 10-3. In addition, for those interested, a short section devoted to elastic constants is included.

Table 10-1. Condensed Table of Physical Properties of Silicon

Density ¹	2.33 g/cc
Hardness ^{3,4}	7 Moh, 1,000 Vickers, 950–1,150 Knoop
Elastic constants ¹	c_{11} : 1.6740×10^{12} dynes/cm ² c_{12} : 0.6523×10^{12} dynes/cm ² c_{44} : 0.7959×10^{12} dynes/cm ²
Temperature coefficients of elastic constants ¹	$K_{c_{11}}$: $-75 \times 10^{-6}/^{\circ}\text{C}$ $K_{c_{12}}$: $-24.5 \times 10^{-6}/^{\circ}\text{C}$ $K_{c_{44}}$: $-55.5 \times 10^{-6}/^{\circ}\text{C}$
Young's modulus ⁵	1.9×10^{12} dynes/cm ² , [111] direction
Bulk modulus ⁶	7.7×10^{11} dynes/cm ²
Modulus of rupture (in bending) ^{2,5}	700–3,500 kg/cm ² *
Breaking strength (in compression) ²	4,900–5,600 kg/cm ²
Melting point ⁷	1412°C
Boiling point ⁷	3145°C
Heat of fusion ⁷	12.1 kcal/mole
Heat of vaporization ⁸	71 kcal/mole at boiling point
Specific heat ^{9–11}	0.18 (18–100°C) cal/g°C, 0.219 above melting point
Linear thermal coefficient of expansion ^{12,13}	$2.33 \times 10^{-6}/^{\circ}\text{C}$, room temperature†
Thermal conductivity ^{14–22}	0.3 cal/(sec)(cm)(°C) at 20°C‡
Expansion on freezing ²³	9% volume increase
Surface tension ²⁴	720 dynes/cm (freezing point)
Critical pressure ⁸	1,450 atm
Critical temperature ⁸	4920°C

* See text for further discussion.

† Refer to Fig. 10-5 for more complete data.

‡ Refer to Figs. 10-6 and 10-7 for more complete data.

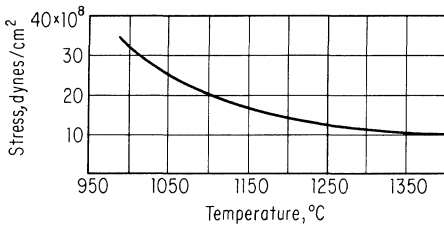


Fig. 10-1. Ultimate tensile stress. (Sylwestrowicz.²⁵)

10-1. ELASTIC CONSTANTS

The elastic behavior of solids is usually described by Hooke's law which relates the amount of deformation to the applied force which produced it. The one-dimensional Hooke's law for springs is the simplest example of this and is expressed as

$$F = KX \tag{10-1}$$

- where F = applied force
- X = displacement of the end of the spring
- K = elastic constant of the spring

In the completely general case of forces applied to an anisotropic medium, the simple equation just discussed expands into a set of six equations with 36 elastic constants.^{26,*} These equations are:

$$\begin{aligned} T_1 &= c_{11}S_1 + c_{12}S_2 + c_{13}S_3 + c_{14}S_4 + c_{15}S_5 + c_{16}S_6 \\ &\vdots \\ T_6 &= c_{61}S_1 \dots \dots \dots c_{66}S_6 \end{aligned} \tag{10-2}$$

- where T_i = applied stress
- S_j = strain
- c_{ij} = elastic constants

In matrix notation, Eq. (10-2) becomes

$$(T_1, T_2, T_3, T_4, T_5, T_6) = \begin{pmatrix} c_{11} & c_{12} & c_{13} & c_{14} & c_{15} & c_{16} \\ \vdots & & & & & \\ c_{61} & \dots & \dots & \dots & \dots & c_{66} \end{pmatrix} (S_1, S_2, S_3, S_4, S_5, S_6) \tag{10-3}$$

* Superscript numbers indicate items listed in References at the end of the chapter.

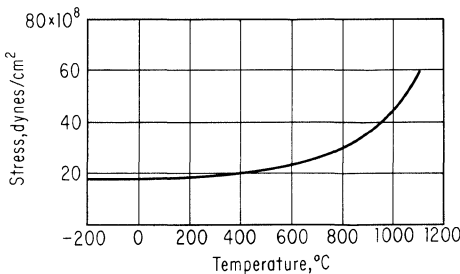


Fig. 10-2. Fracture stress. (From Sylwestrowicz.²⁵)

Table 10-2*

A. Heat Capacity and Debye Temperature		
T , °K	Debye Temp, °K	C_p cal/mole deg
2.5	...	0.000 027 1
5	640	0.000 219
10	...	0.001 845
20	540	0.022 65
30	470	0.114 9
40	460	0.295 7
50	475	0.527 2
70	...	1.019
100	575	1.739
140	630	2.650
200	640	3.735
240	645	4.246
300	640	4.796

B. Heat Content $H_T - H_{298.16}$	
T , °K	cal/mole
400	515
500	1060
600	1640
700	2230
800	2830
900	3440
1000	4060
1100	4690
1200	5340

Over this temperature range $C_p = 5.79 + 0.56 \times 10^{-3}T - 1.09 \times 10^{-5}T^2$

C. Heat of Sublimation at 298°K	
Si ₂₈	107 kcal/mole
Si ₂₉	140 kcal/mole
Si ₃₀	146 kcal/mole

* Compiled from R. E. Honig, Vapor Pressure Data for the Solid and Liquid Elements, *RCA Rev.*, vol. 23, pp. 567-586, 1962; P. Flubacher, A. J. Leadbetter, and J. A. Morrison, The Heat Capacity of Pure Silicon and Germanium and Properties of Their Vibrational Frequency Spectra, *Phil. Mag.*, ser. 8, vol. 4, pp. 273-294, 1959; and K. K. Kelly, "Contributions to the Data on Theoretical Metallurgy," p. 476, Bureau of Mines Bulletin, 1949.

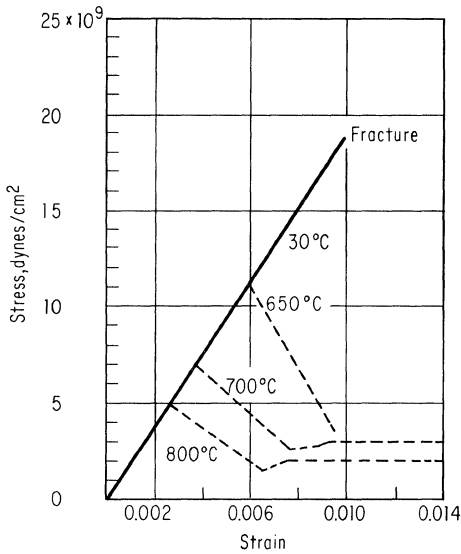


Fig. 10-3. Silicon stress-strain curves for various temperatures. (Pearson, Read, and Feldman.⁵)

The need for six components of stress may be seen by visualizing a little cube acted on by the most general possible set of forces. These can all be expressed as a combination of the following:

1. Three sets of compressive forces normal to the faces of the cube as illustrated in Fig. 10-8a.
2. Three sets of couples acting parallel to the cube faces and tending to twist it. This is shown in Fig. 10-8b.

These six stresses then produce six components of strain. Three of these are simple compression or tension along each axis, and the other three are the angular displacement of line elements due to the couples T_4 , T_5 , and T_6 .

The most general anisotropic solid requires 36 elastic constants, but if the material has a high degree of symmetry and many of the c 's are identical or zero, the number is radically reduced. For cubic crystals, there are only three independent constants. In the case of an isotropic solid, the number of constants reduces to two.

The three constants for the cubic crystal are c_{11} , c_{12} , and c_{44} . For this case Eq. (10-3) becomes

$$(T_1, T_2, T_3, T_4, T_5, T_6) = \begin{pmatrix} c_{11} & c_{12} & c_{12} & 0 & 0 & 0 \\ c_{12} & c_{11} & c_{12} & 0 & 0 & 0 \\ c_{12} & c_{12} & c_{11} & 0 & 0 & 0 \\ 0 & 0 & 0 & c_{44} & 0 & 0 \\ 0 & 0 & 0 & 0 & c_{44} & 0 \\ 0 & 0 & 0 & 0 & 0 & c_{44} \end{pmatrix} (S_1, S_2, S_3, S_4, S_5, S_6) \tag{10-4}$$

where T_1 , T_2 , and T_3 are stresses applied in the direction of the crystallographic axes x , y , and z , respectively.

Sometimes, the stress-strain relationship is written as

$$\begin{aligned}
 S_1 &= s_{11}T_1 + s_{12}T_2 + s_{13}T_3 + s_{14}T_4 + s_{15}T_5 + s_{16}T_6 \\
 &\vdots \\
 S_6 &= s_{61}T_1 \dots \dots \dots s_{66}T_6
 \end{aligned}
 \tag{10-5}$$

In this case s_{ij} is referred to as a compliance coefficient. For the cubic case the c 's and s 's are related by

$$\begin{aligned}
 s_{11} &= \frac{c_{11} + c_{12}}{(c_{11} - c_{12})(c_{11} + 2c_{12})} \\
 s_{12} &= \frac{-c_{12}}{(c_{11} - c_{12})(c_{11} + 2c_{12})} \\
 s_{44} &= \frac{1}{c_{44}}
 \end{aligned}
 \tag{10-6}$$

c_{ij} may be expressed in terms of s_{ij} simply by interchanging the c 's and s 's of

Table 10-3. Thermal Expansion of Silicon*

$T, ^\circ\text{K}$	$a = \frac{1}{\ell} \frac{d\ell}{dT} \times 10^6$
40	-0.05
50	-0.20
60	-0.41
70	-0.59
80	-0.77
90	-0.51
100	-0.31
110	-0.15
120	+0.01
130	+0.16
140	+0.31
150	+0.47
160	+0.65
170	+0.84
180	+1.05
190	+1.28
200	+1.49
210	+1.67
220	+1.83
230	+1.97
240	+2.07
250	+2.16
260	+2.22
270	+2.27
280	+2.30
290	+2.31
300	+2.33

* From D. F. Gibbons, Thermal Expansion of Some Crystals with the Diamond Structure, *Phys. Rev.*, vol. 103, pp. 569-571, 1956.

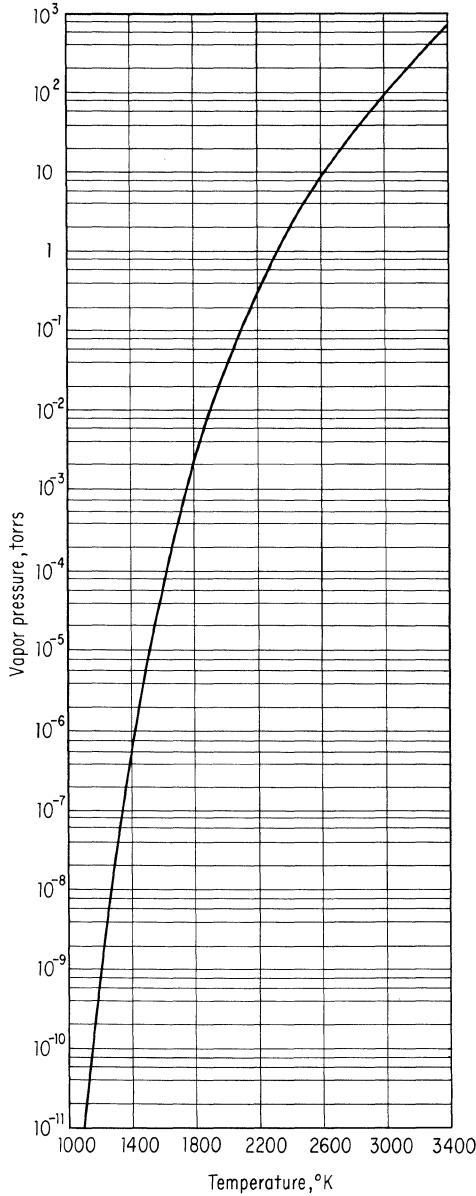


Fig. 10-4. Silicon vapor pressure versus temperature. (Honig.⁷)

Eq. (10-6).²⁷ All the various elastic moduli are expressible in terms of these elastic constants so that a determination of these constants will allow their calculation.

Young's Modulus. If a tension or compression is applied in one direction only, and the sides of the body are free to expand or contract, then the applied stress equals Young's modulus times the strain, e.g.,

$$T_1 = ES_1 \tag{10-7}$$

where E is Young's modulus and depends on the direction of applied forces.

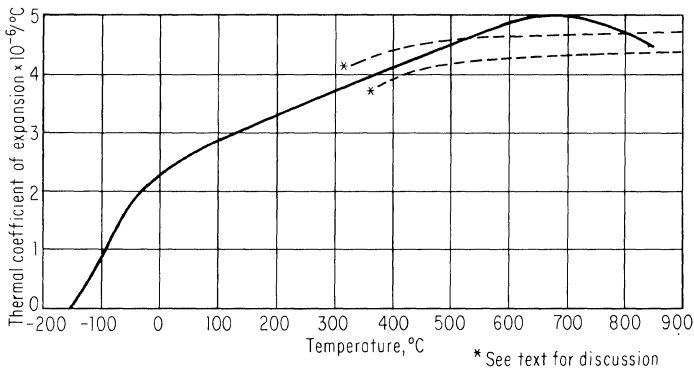


Fig. 10-5. Thermal expansion coefficient versus temperature. (Compiled primarily from Refs. 12 and 13.)

Poisson's Ratio. During the application of the simple tension or compression just described, the cross section of the body will either contract or expand. Poisson's ratio is the ratio of the amount of strain perpendicular to the applied stress to the amount of strain in the direction of the stress. The ratio then depends not only on the direction of applied stress, but also on the direction of contraction desired.

Modulus of Compression. If $T_1 = T_2 = T_3$ and all other stresses equal zero, then the body is being subjected to hydrostatic pressure, and the relation between

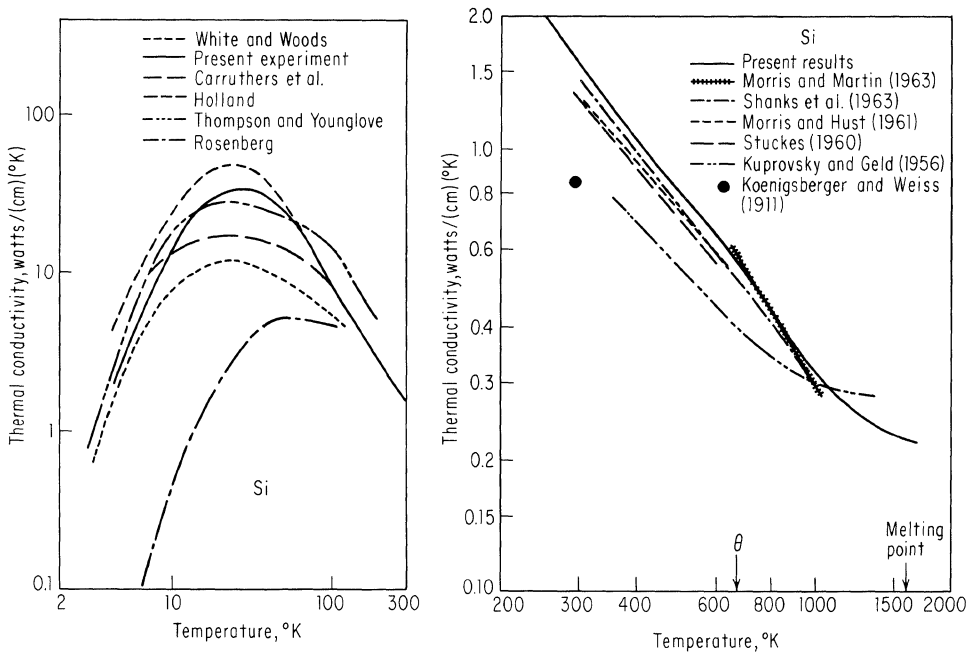


Fig. 10-6. A comparison of thermal conductivity data. (Glassbrenner and Slack.²²)

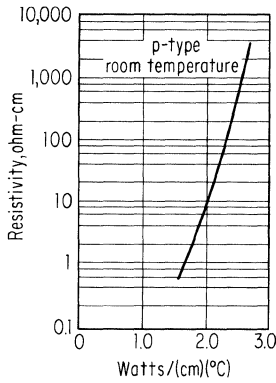


Fig. 10-7. Resistivity versus thermal conductivity. (Adapted from Ref. 16.)

the applied pressure P and the volume reduction δ is given by

$$P = K\delta \tag{10-8}$$

where K is the modulus of compression.

Shear Modulus or Modulus of Rigidity. If a single couple is acting on the body, then the angular displacement times the shear modulus equals the torsional stress, e.g.,

$$T_4 = \mu S_4 \tag{10-9}$$

EXAMPLE 10-1. Solve for Young's modulus for a silicon single crystal with tension applied in the [010] direction.

Since the only force applied is in the y direction, $T_1, T_3, T_4, T_5,$ and $T_6,$ are all zero. Equation (10-1), combined with the reduced number of c 's required for the cubic case, becomes

$$\begin{aligned} 0 &= c_{11}S_1 + c_{12}S_2 + c_{12}S_3 \\ T_2 &= c_{12}S_1 + c_{11}S_2 + c_{12}S_3 \\ 0 &= c_{12}S_1 + c_{12}S_2 + c_{11}S_3 \\ 0 &= c_{44}S_4 \\ 0 &= c_{44}S_5 \\ 0 &= c_{44}S_6 \end{aligned} \tag{10-10}$$

Now, using determinants, solve for S_2 .

$$S_2 = \frac{\begin{vmatrix} c_{11} & 0 & c_{12} \\ c_{12} & T_2 & c_{12} \\ c_{12} & 0 & c_{11} \end{vmatrix}}{\begin{vmatrix} c_{11} & c_{12} & c_{12} \\ c_{12} & c_{11} & c_{12} \\ c_{12} & c_{12} & c_{11} \end{vmatrix}} = \frac{T_2(c_{11}^2 - c_{12}^2)}{\Delta} \tag{10-11}$$

where Δ is the determinant in the denominator.

Since Young's modulus is defined as stress/strain

$$E_{[100]} = \frac{\Delta}{c_{11}^2 - c_{12}^2} \tag{10-12}$$

Effect of Direction on Moduli. In case the applied stresses are not parallel to the crystallographic axes, a more general set of equations [rather than Eq. (10-2)] must be used in order to solve for the various moduli in terms of the three elastic constants. There is little variation of Poisson's ratio with direction, and it will usually be just a little over $1/4$. Young's modulus, however, is sensitive to direction.

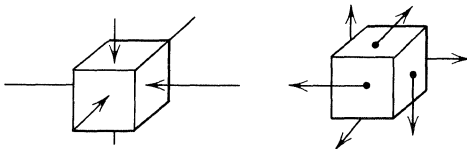


Fig. 10-8. The six components of stress.

Equation (10-13) gives the general expression for it in terms of the elastic constants and the direction cosines of the applied force.²⁷

$$\frac{1}{E} = s_{11} - 2 \left(s_{11} - s_{12} - \frac{s_{44}}{2} \right) (\alpha^2 \beta^2 + \alpha^2 \gamma^2 + \beta^2 \gamma^2) \quad (10-13)$$

where α , β , and γ are the direction cosines.

As a special case, it can be shown that as long as the stress direction lies in the (111) plane, Young's modulus and Poisson's ratio do not change. They are given by²⁸

$$E_{(111)} = \frac{4}{2s_{11} + 2s_{12} + s_{44}}$$

$$\sigma_{(111)} = \frac{1}{6} \left(5s_{12} + s_{11} - \frac{s_{44}}{2} \right) E_{(111)} \quad (10-14)$$

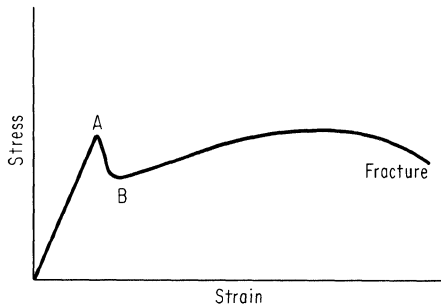
Most silicon devices are made from wafers cut parallel to (111) planes so that Eq. (10-14) is particularly useful in analyzing the stress induced in the wafers during transistor fabrication.

10-2. SOME TENSILE TESTING DEFINITIONS*

Tensile testing is usually accomplished by clamping one end of a rod-shaped test specimen to a fixed point and the other to a movable "crosshead." The crosshead is then driven at a constant rate, i.e., it applies a uniform strain per unit time to the sample. Simultaneously, the stress required to produce this uniform rate of strain is recorded so that a stress-strain curve such as that shown in Fig. 10-9 is obtained. Brittle materials are also often tested by "three-point loading" in which the test member is supported at each end on knife edges, and loading is applied in the middle of the sample. Failure of the sample occurs when the outer fiber, which is in tension, reaches its limit. Variations of this method include simple cantilever loading, and the rupture of uniformly loaded disks. "Ultimate tensile strength" is defined as the stress obtained by dividing the maximum load reached before breaking by the initial cross section. The "yield point" has been reached when appreciable

* See for example, S. Timoshenko and G. H. MacCullough, "Elements of Strength of Materials," D. Van Nostrand Company, Inc., Princeton, 1949.

Fig. 10-9. Stress-strain curve showing upper and lower yield points.



elongation occurs without additional stress being applied. If the yielding is accompanied by an abrupt decrease in stress, point *A* of Fig. 10-9 is the “upper yield point” and *B* is the “lower yield point.” The upper yield point is often, and certainly in the case of silicon, dependent on subtle variations of the material, while the lower one is relatively constant for a given material. Thus when designing structural members, the lower yield point is of most concern. “Fracture stress” is found by dividing the load at time of fracture by the final cross section. The “elastic limit” is the highest stress to which the material may be subjected without permanent deformation. After plastic flow begins, the sample will begin to lengthen appreciably and reduce its cross section. “True stress” is obtained by dividing the load by the cross section in the neck of the sample. If the normal stress-strain curve is converted to true stress-strain, then the new curve will show the effects of strain hardening.

10-3. PLASTIC FLOW

During World War II it was observed in Germany that if silicon were heated red hot and hit with a hammer, there would be some plastic flow before shattering.²⁹ In 1951 more elaborate experiments were performed,^{30,31} and showed that silicon heated above approximately 800°C showed plastic flow and would also work harden as it flowed. The plastic deformation occurs by slip between (111) planes in a [110] direction.⁵ Figure 10-10 shows the shapes of some silicon cylinders after pressing and nicely illustrates the effect of slip in the [110] direction.³² Later experiments have shown that appreciable plastic deformation starts at about 600°C. Below this temperature there is little plastic flow, so usually the silicon deflects elastically until fracture stress is reached. That plastic flow would be difficult to

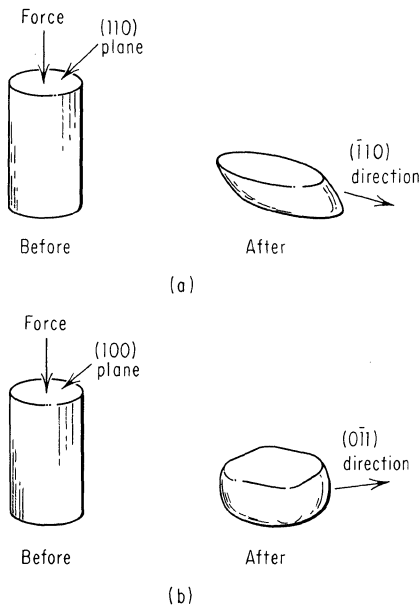


Fig. 10-10. Effect of orientation on single-crystal-silicon pressing characteristics.

observe at lower temperatures is not unexpected since stress concentrations usually cause failure long before the main body of the silicon is close to the breaking stress. Room-temperature flow can be observed, however, during microhardness measurements and occasionally during scribing.

The fact that silicon can be stressed to the fracture point without appreciable plastic flow or creep makes it a good material for piezoresistive transducer elements since it can operate over wide ranges of stress without fear of shift in the zero point due to stress relief. Even though negligible plastic flow occurs at low temperatures, it is quite possible to damage silicon so that if its temperature is subsequently raised, the stored elastic energy can cause plastic flow. By this mechanism very small surface damage may, during diffusion, for example, propagate slip quite deeply into the crystal.³³ Plastic flow caused by excessive stress from thermal shock is responsible for the familiar star pattern of dislocations seen in improperly annealed silicon crystals.³⁴

In the range from -196 to 600°C the fracture stress is independent of temperature. Above 600°C it appears to increase with increasing temperature (Fig. 10-2). This is contrary to expectations if it is assumed that throughout the range fracture stress should be proportional to the shear modulus. Since the fracture stress is always considerably below theoretical estimation, it is likely that increased temperatures reduce the possibility of localized, excessive stress concentration occurring. Ultimate strength however, decreases with temperature and is shown in Fig. 10-1. The original number of dislocations appears to have little effect on the lower yield point and on fracture stress, presumably because the very early stages of deformation introduce far more new dislocations than were there originally. Oxygen in the crystal in excess of about 10^{15} atoms/cm³ does not appear to affect the ultimate strength, but does cause an upper yield point in the temperature ranges from 600 to 1100°C and above 1300°C .²⁵ The initial number of dislocations (Fig. 10-11), as well as the rate of strain, changes the upper yield point considerably.³⁵

10-4. DISTRIBUTION OF BREAKING STRENGTHS

Since silicon is a brittle material at room temperature, breaking strength measurements have in general been made by methods developed for use in ceramics. The most common of these is the standard three-point beam loading technique,³⁶ though by using jaws carefully designed to minimize shear forces, standard tensile-testing machines can be used.^{25,35} A somewhat simpler system, but one which is subject to larger errors primarily because of clamping difficulties, involves end loading of a cantilever beam. Another method reported, but not particularly recommended, is to uniformly load a thin disk of silicon until it ruptures.² The combined results of these measurements show three separate ranges of breaking strengths.

At the low end of the scale, large samples with relatively little surface preparation other than sawing and perhaps a light etch give values in the range of 10,000 to 20,000 psi. If relatively small samples (0.25-in. by 0.025-in. cross section) are prepared with etched surfaces, then the middle range of from 25,000 to 60,000 psi,

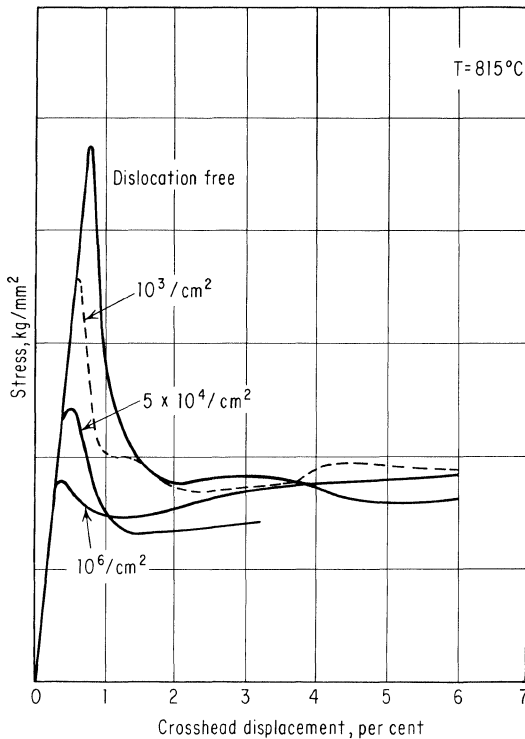


Fig. 10-11. Influence of dislocation density on upper yield point. (Patel and Chaudhuri.³⁵)

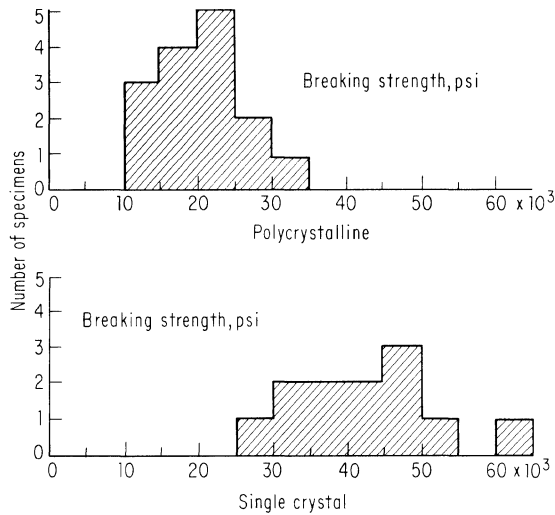
with a distribution of breaking strengths such as is shown in Fig. 10-12, is observed. It should be understood that these curves are only approximate and are based on a small number of samples, but they can be used to estimate breaking strength ranges to be expected for different surface preparations. Small silicon whiskers, which should be expected to have a surface free of cracks and chips have breaking strengths in excess of 200,000 psi (2×10^{10} dynes/cm²).

Investigators making single-crystal-silicon strain gauges have found similar breaking strengths on samples of conventionally grown material etched to thicknesses of a few mils. Measurements of polycrystalline samples in the intermediate size range have in general given somewhat lower breaking strengths than single crystals, but this is apparently due to the greater difficulty of obtaining a surface free from grooves and pits that could produce stress concentrations.²

10-5. IMPACT TESTING

A series of samples, consisting of single-crystal and grown polycrystalline material was subjected to a standard Izod test. In this test a $\frac{3}{8}$ -in. by $\frac{3}{4}$ -in. by $2\frac{3}{8}$ -in. long sample is clamped between jaws of a vise so that $1\frac{1}{8}$ -in. of the sample extends above the jaws. A pendulum mounted hammer then strikes the sample 1 in. from the vise jaws. This gives a cantilevered specimen length of 1 in. Typical breaking energies for both single-crystal and grown polycrystalline material are between 0.08 and 0.09 ft-lb.³⁷

Fig. 10-12. Distribution of breaking strength of silicon; large samples, three-point loading. The low values reflect difficulty in obtaining smooth surfaces. These values are however to be expected from the types of surface preparation that a transistor wafer, for example, might receive.



10-6. HARDNESS

Microhardness measurements (Vickers and Knoop) can be made on silicon and silicon-germanium alloys by using a very low force (few grams) on the diamond point. The use of greater force on test fixtures with blunt indenters (such as Brinell or Rockwell) produces large-scale sample fracture. The relative hardness in different crystallographic directions has been investigated both by the Knoop indenter and by measuring the amount of abrasion from the rims of rotating silicon disks. The results of some of these measurements are shown in Tables 10-4 and 10-5.⁴ Increasing temperature, infrared radiation, and current flow through the sample all tend to reduce the hardness. The effects of temperature and current are illustrated by the data of Table 10-6.³⁸ Under a strong source of near infrared the apparent hardness may be reduced by 20 to 50 per cent.³⁹

10-7. THERMAL EXPANSION COEFFICIENT

The solid curve of Fig. 10-5 is a composite constructed from published data.^{12,13} In addition, the dotted lines show some sparse data indicating that impurity con-

Table 10-4. Effect of Crystal Orientation on Hardness (Knoop Indenter, 100-g load)*

Face	Average	Range (depending on direction of long axis of indenter)
(111)	948	935-970
(110)	964	940-980
(100)	964	950-980

* From A. A. Giardini, A Study of the Directional Hardness in Silicon, *Am. Mineralogist*, vol. 43, pp. 957-969, 1958.

Table 10-5. Effect of Grinding Direction on Comparative Hardness*

Grinding on plane	In the direction toward	Comparative hardness
(101)	(001)	2
(001)	(101)	1.95
(112)	(101)	1.55
(101)	(112)	1.50
(001)	(111)	1.50
(111)	(001)	1.5
(101)	(111)	1.2
(111)	(101)	1.05

* From A. A. Giardini, A Study of the Directional Hardness in Silicon, *Am. Mineralogist*, vol. 43, pp. 957-964, 1958.

centration may appreciably affect α . The upper curve is for 6 to 10 ohm-cm arsenic-doped material; the bottom one is for 0.01 ohm-cm antimony-doped material.

Thermal Shock. Failure by thermal shock occurs when nonuniform temperatures through the body causes nonuniform expansion or contraction which, in turn, results in localized stresses that exceed the breaking strength of the material. Thus, if a material were relatively weak but still had a negligible coefficient of expansion, it would have good shock resistance. A high thermal conductivity minimizes thermal gradients and enhances shock resistance. High breaking strength or the ability to flow plastically likewise reduces thermal-shock breakage.

All these factors have been combined into two "resistance factors" or figures of merit R and R' defined as follows:

$$R = \frac{S(1 - \sigma)}{\alpha E}$$

$$R' = \frac{S(1 - \sigma)k}{\alpha E}$$

where S = breaking stress
 σ = Poisson's ratio
 α = thermal expansion coefficient
 E = Young's modulus
 k = thermal conductivity⁴⁰

The requirements for two factors may be visualized by considering two sets of circumstances. If the heat transfer coefficient is low, then a high thermal conductivity would minimize thermal gradients. Conversely, if the heat transfer mechanism were very good, then thermal conductivity of the sample would become relatively unimportant. The correct choice of a breaking strength number is difficult. Some have even gone so far as to derive shock resistance parameters based on the expected statistical behavior of breaking measurements.⁴¹

There have been numerous tests devised for measuring thermal-shock resistance

Table 10-6. Effect of Temperature and Current Flow on Hardness (Knoop Indenter, 10-g load)*

Temperature, °C	Hardness without current flow	Hardness with current flow
-196	764	479
25	675	545
200	575	575

* From J. H. Westbrook and J. J. Gilman, An Electrochemical Effect in Semiconductors, *J. Appl. Phys.*, vol. 33, pp. 2360-2369, 1962.

of brittle materials, i.e., those which have negligible plastic flow before rupture, but they are all dependent on geometry and usually fall into two categories. One is designed to give values of R and R' independent of the individual measurements and would thus use simple shapes in order not to unduly complicate calculations. The other is strictly a comparative test and may use any desired shape. A fairly common version of this is to use a single thermal-shock cycle of increasing severity until fracture occurs. In this sort of test, tiny fractures may occur which materially weaken the sample but may be hardly detectable visually. Probably the best way to detect such cracks is to load the sample to something less than its usual breaking stress after each cycle.

A test such as this was performed on silicon bars approximately 1 cm by 1 cm by 4 cm long. They fracture after quenching in ice water from 350°C but not from 300°C. Tests performed on single-crystal, grown polycrystalline, and cast silicon gave similar results. Since no differences in any of the parameters affecting R and R' have been observed, this is not surprising.

Calculation of Thermally Induced Stresses. Thermal stress may be caused either by externally constraining the body so that it cannot expand or contract with temperature changes, or by unequal temperatures within the body which in turn causes it to expand or contract unevenly.

In order to compute such stresses, first determine how much the various dimensions would normally change over the desired temperature range, then calculate how much force is required to return them to their constrained value. The total amount of linear deformation δ due to temperature change is given by

$$\delta = \alpha L \Delta T \quad (10-15)$$

where α = linear thermal expansion coefficient

L = length of body

ΔT = temperature change

From this, the strain S (deformation per unit length) is given by

$$S = \alpha \Delta T \quad (10-16)$$

EXAMPLE 10-2. Suppose a silicon bar of length L cut with the long dimension in the [111] direction is clamped at room temperature as shown in Fig. 10-13. Assume that there is no

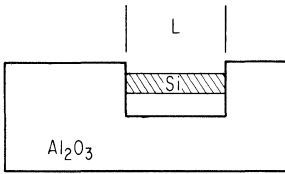


Fig. 10-13. Silicon bar constrained by aluminum oxide clamp.

deformation of the clamp and that it is made of sintered aluminum oxide. Further assume that no flexing of the silicon bar occurs. What is the stress on the bar when the temperature of the whole assembly is raised to 425°C?

1. Refer to Fig. 10-5 and estimate the average thermal expansion coefficient of silicon over the 25 to 400°C range. Call it α_s .
2. Refer to a ceramics handbook and determine the same thing for aluminum oxide. Call it α_a .

Since the aluminum oxide block does expand also, the total amount of silicon deformation will be given by

$$\delta = L \Delta T (\alpha_s - \alpha_a) \quad (10-17)$$

or the strain will be

$$S_{111} = (\alpha_s - \alpha_a) \Delta T \quad (10-18)$$

Now, from the definition of Young's modulus, the stress required to produce that amount of strain is just Young's modulus times S_{111} and is independent of the length L .

E_{111} may be calculated from Eq. (10-13) or obtained from Table 10-1. In making computations involving stresses caused by uneven heating or cooling, one of the major problems is determining the thermal gradient within the sample. This will depend not only on the geometry of the sample but also on the method of heat removal or addition. Also, the expansion coefficient, thermal conductivity, and specific heat all vary with temperature so that normally only qualitative results are obtained.*

10-8. THERMAL CONDUCTIVITY

There have been a number of measurements made in the temperature range from a few degrees Kelvin to the melting point. At the low-temperature end agreement is rather poor and is attributed to variations in sample size (boundary scattering) and scattering from impurities and other defects. Above 1000°K there are some data that indicate no further decrease in conductivity and other that show a continuous decrease until the melting point is reached. These data are all shown in Fig. 10-6*a* and *b*. Most of the thermal conductivity contribution comes from the lattice, even at elevated temperatures. The other important mechanism is electronic thermal conductivity, most of which comes from thermally generated hole-electron pairs. Table 10-7 gives the calculated $K_{\text{electronic}}$ for several temperatures. Because this effect is small, the added carriers produced by heavy doping would be expected to contribute little to the overall thermal conductivity. In fact, their effect is apparently to reduce the lattice conductivity considerably more than the electronic portion is increased. Figure 10-7 is a curve which indicates this reduction.†

* For the more complicated and, unfortunately, more useful configurations, the reader is referred to standard texts on strength of materials.

† This decrease is probably quite dependent on the amount of strain introduced by the particular impurity used.

10-9. SURFACE ENERGY⁴²

The surface energy of silicon has been determined by cleavage techniques for {111} planes. From this and the bond density, values for the {100} and {110} planes are calculated. Preferred numbers are:

Plane	Energy, ergs/cm ²
{111}	1,230
{110}	1,510
{100}	2,130

The Si-Si bond strength is calculated to be approximately 45.5 kcal/mole.

10-10. HOT FORMING

With the advent of silicon infrared optics, which require thin-walled domes, and silicon solar cells, which require very thin sheets, there has been considerable impetus to develop hot-working techniques. Two approaches have been used. In the older of the two, and the one directed toward dome applications, the silicon was formed directly in suitable dies.³² A later innovation, used primarily for the rolling of thin sheets, involved encasing the silicon in a refractory metal and then using standard hot rolling equipment and techniques.⁴³ In the first method both the ingot to be formed and the dies are heated in an inert atmosphere to the required temperature. This requires that the dies have the necessary strength at elevated temperature and that they not seriously react with the silicon at those temperatures. The recommended die material is graphite and the temperature should be above 1250°C. The pressure required will, of course, depend on the radius and thickness, but, typically, with an arrangement as shown in Fig. 10-14, a total force of 5,000 to 10,000 lb will be required to produce a 2-in. radius full hemisphere.

Figure 10-15 shows two hemispherical domes of wall thickness in the order of 0.1 in. and radius of 2 in. that were formed from plates of comparable thickness. Curved sections of larger radius and greater thickness are also feasible and have been made.

In some of the early stages of development it was hoped that an ingot could be

Table 10-7. The Theoretical Electronic Thermal Conductivity for Several Temperatures*

T , °K	ohm-cm	k_e , watts/cm-deg
800	0.25	0.0014
1000	0.045	0.0065
1200	0.013	0.017
1400	0.006	0.035
1600	0.003	0.058
1681	0.0026	0.068

* From C. J. Glassbrenner and G. A. Slack, Thermal Conductivity of Silicon and Germanium from 3°K to the Melting Point, *Phys. Rev.*, vol. 134, pp. A1058-A1069, 1964.

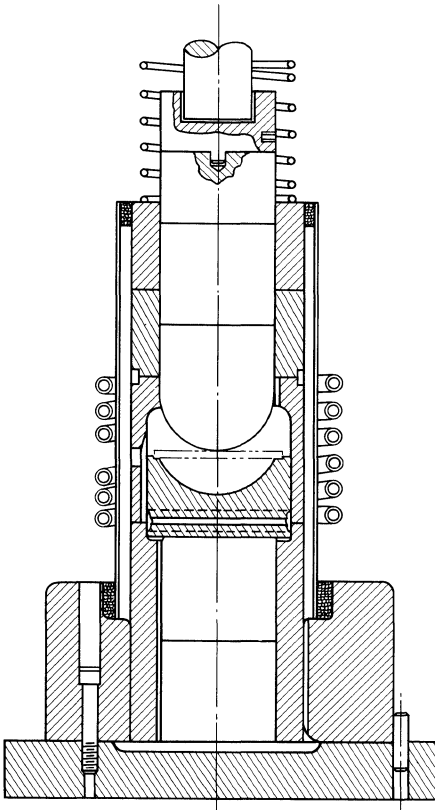


Fig. 10-14. Silicon hot press.

hot formed into flats and then to domes, but the pressures involved were too large to be practical; for example, 20,000 psi only caused a 66 per cent reduction of $\frac{1}{2}$ -in.-long by $\frac{3}{8}$ -in.-diameter slugs. In the second procedure the silicon is protected by a molybdenum sheath and is then rolled or extruded in a standard manner. The goal of this approach is to obtain large thin sheets of polycrystalline silicon which can then be fabricated into devices (in particular, solar cells).

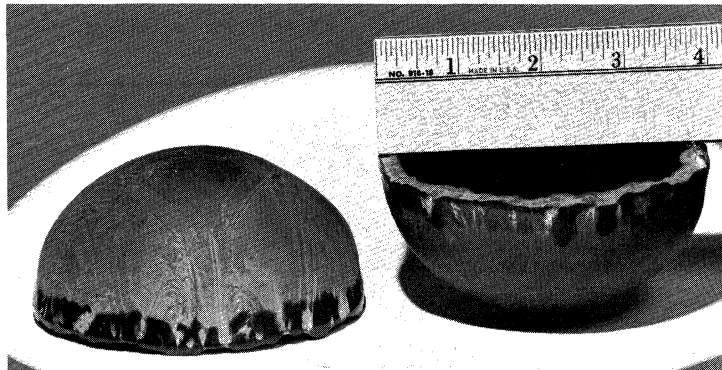


Fig. 10-15. Hot-formed 4-in.-diameter silicon domes.

Sheets of several square inches area have been made this way, but thus far the poor quality of material has prevented its use in device fabrication.

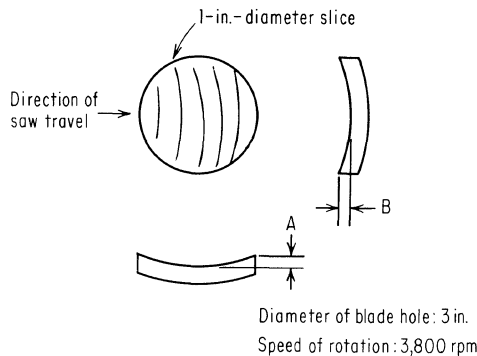
Deformation occurs by slip between (111) planes and results in areas of high dislocation densities. In the case of the rolling experiments just mentioned, it is presumably an excess of these dislocations which makes etching of the surface erratic and gives high reverse currents and low lifetimes in diodes made from such material.

Sintering. 225-mesh silicon has been compacted to about 20 per cent porosity by applying 20,000 psi at a temperature of 1300°C.² Gaulé, Braslin, and Pastore have used relatively low pressures, coupled with heating from an r-f coil to compact silicon chunks up to several millimeters in diameter and confined in a fused quartz tube into rods suitable for float zoning.⁴⁴

10-11. SAWING AND LAPPING*

Diamond-impregnated wheels are usually used for slicing silicon, and while there seems to have been no comprehensive study made of the cutting characteristics versus grit size, peripheral speed, feed speed, etc., some general observations can be made. Excessive feed speeds cause the slices to be cut dish-shaped on an I/D saw and wedge-shaped on a normal saw. Some data illustrating this effect are shown in Fig. 10-16. The blade peripheral speed is not particularly critical, but should be in the range of 3,000 to 4,500 ft/min for best results.

* For a short discussion of polishing procedures, refer to Sec. 9-11.



Feed speed, in./min	A, mils	B, mils
0.5	≈0.2	≈0.1
1.5	≈0.2	≈0.1
2.5	≈0.2	≈0.1
3.5	0.3-0.4	≈0.1
5.0	0.7	≈0.2
6.0	0.9	≈0.4

Fig. 10-16. Amount of cupping produced during slicing for I/D saw. (J. B. Sherer, unpublished work.)

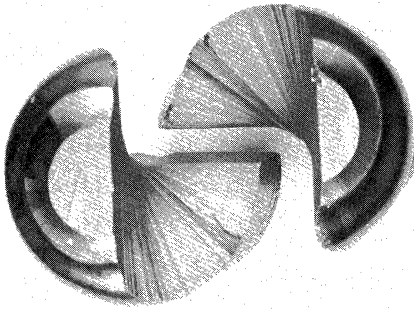


Fig. 10-17. Silicon crystal cut in corkscrew fashion by a wire saw.

Reciprocating saws, using either smooth steel blades and an abrasive slurry or blades plated with diamonds, are sometimes used in special applications. Cutting speed per blade is much slower, but up to several hundred blades per saw can be used. The use of wires, both as belts and as reciprocating elements, has been examined, but excessive wear leads to very short wire life. Figure 10-17 shows a wire cut through a 1.3-in.-diameter silicon crystal that would have been difficult to achieve with any other equipment. Band saws with diamond-plated blades are occasionally used for rough cutting, but seldom for precision work. Silicon can also be electrolytically shaped, but control problems have made it difficult to cut uniform thickness slices.⁴⁵

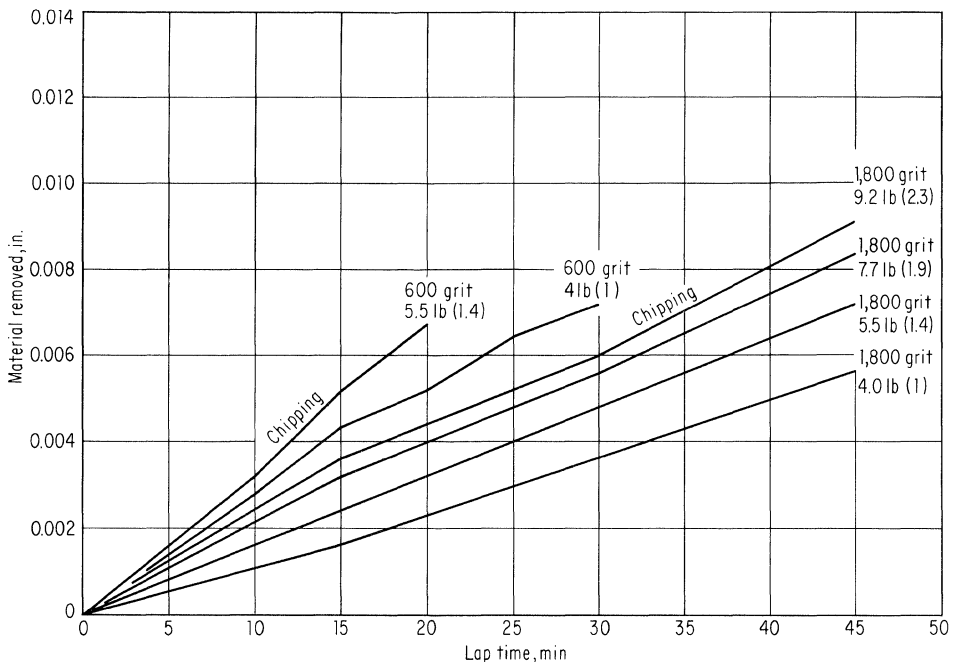


Fig. 10-18. Curves for lapping plate weight versus material removed using planetary lap with four 1-in.-diameter slices per block. (J. B. Sherer, unpublished work.)

Lapping may be done either free, i.e., the slice "floats" between two lapping plates, or from one side only. Since bowed slices will usually be somewhat straightened when fastened to a block for single-side lapping, after lapping and release, they will still be bowed. This is a major disadvantage of such lapping, but the use of diamond stops on the blocks allows thickness to be controlled more easily than on free lapping. The lapping rate increases with both an increase in weight on the slice and with grit size. This is shown in Fig. 10-18. Results comparable to lapping can be obtained from various diamond grinders. One of the more successful is the Blanchard grinder widely used in the optical industry.

Damage. When slices are cut or lapped there is usually considerable damage introduced into the slice. After any of these cutting or lapping processes the surface is left under tension as has been verified both by observing the direction of bending after lapping one side of a polished slice (or polishing one side of a lapped slice) and by birefringence measurements.^{46-48,*} Minimum damage depth seems to be comparable to the lapping compound diameter, but it may be as great as several mils. The character of the damage seems to range from dislocations in the case of very light abrasion to a combination of cracks and dislocations for heavy abrasions.⁴⁹

REFERENCES

1. McSkimin, H. J., W. L. Bond, E. Buehler, and G. K. Teal: Measurement of the Elastic Constants of Silicon Single Crystals and Their Thermal Constants, *Phys. Rev.*, vol. 83, p. 1080 (L), 1951.
2. Runyan, W. R., J. M. Willmore, and L. E. Jones: Growth Techniques and Mechanical Properties of Optical-quality Silicon, *Proc. IRIS*, vol. 3, pp. 49-58, 1958.
3. Wang, C. C., and B. H. Alexander: Hardness of Germanium-Silicon Alloys at Room Temperatures, *Acta Met.*, vol. 3, pp. 515-516 (L), 1955.
4. Giardini, A. A.: A Study of the Directional Hardness in Silicon, *Am. Mineralogist*, vol. 43, pp. 957-969, 1958.
5. Pearson, G. L., W. T. Read, Jr., and W. L. Feldman: Deformation and Fracture of Small Silicon Crystals, *Acta Met.*, vol. 5, pp. 181-191, 1957.
6. Conwell, E. M.: Properties of Silicon and Germanium, *Proc. IRE*, vol. 40, pp. 1327-1337, 1952.
7. Honig, R. E.: Vapor Pressure Data for the Solid and Liquid Elements, *RCA Rev.*, vol. 23, pp. 567-586, 1962.
8. Hampel, C. A. (ed.): Rare Metals Handbook, Reinhold Publishing Corporation, New York, 1954.
9. Flubacher, P., A. J. Leadbetter, and J. A. Morrison: The Heat Capacity of Pure Silicon and Germanium and Properties of Their Vibrational Frequency Spectra, *Phil. Mag.*, ser. 8, vol. 4, pp. 273-294, 1959.
10. Kelly, K. K.: "Contributions to the Data on Theoretical Metallurgy," p. 476, Bureau of Mines Bulletin, 1949.
11. Pearson, G. L., and R. G. Treuting: Surface Melt Patterns on Silicon, *Acta Cryst.*, vol. 2, pp. 397-399, 1958.
12. Gibbons, D. F.: Thermal Expansion of Some Crystals with the Diamond Structure, *Phys. Rev.*, vol. 112, pp. 136-140, 1958.

* This effect is also observed in glass during optical polishing and is sometimes referred to as the Twyman effect after F. Twyman, who reported it in 1905.

13. Maissel, L.: Thermal Expansion of Silicon, *J. Appl. Phys.*, vol. 31, p. 211 (L), 1960.
14. White, G. K., and S. B. Woods: Thermal Conductivity of Germanium and Silicon at Low Temperatures, *Phys. Rev.*, vol. 103, pp. 569–571, 1956.
15. Stuckes, A. D.: The Thermal Conductivity of Germanium, Silicon, and Indium Arsenide from 40 to 425°C, *Phil. Mag.*, ser. 8, vol. 5, pp. 84–99, 1960.
16. Younglove, B. A.: “Thermal Conductivity of Silicon at Low Temperatures,” Ph.D. thesis, University of Texas, Austin, 1961.
17. Thompson, J. C., and B. A. Younglove: Thermal Conductivity of Silicon at Low Temperatures, *J. Phys. Chem. Solids*, vol. 20, pp. 146–149, 1961.
18. Morris, Robert G., and Jerome G. Hust: “Thermal Conductivity Measurements in Silicon from 30 to 425°C,” paper presented at the American Physical Society Meeting, March, 1961.
19. Carruthers, J. A., T. H. Gabelle, A. M. Rosenberg, and J. M. Ziman: The Thermal Conductivity of Ge and Si between 2 and 300°K, *Proc. Roy. Soc. (London)*, ser. A, vol. 238, pp. 502ff., 1957.
20. Shanks, H. R., P. D. Maycock, P. H. Sidles, and G. C. Danielson: Thermal Conductivity of Silicon from 300 to 1400°K, *Phys. Rev.*, vol. 130, pp. 1743–1748, 1963.
21. Morris, Robert G., and Joel J. Martin: Thermal Conductivity Measurements of Silicon from 680 to 1000°K, *J. Appl. Phys.*, vol. 34, pp. 2388–2389, 1963.
22. Glassbrenner, C. J., and G. A. Slack: Thermal Conductivity of Silicon and Germanium from 3°K to the Melting Point, *Phys. Rev.*, vol. 134, pp. A1058–A1069, 1964.
23. Logan, R. A., and W. L. Bond: Density Change in Silicon on Melting, *J. Appl. Phys.*, vol. 30, p. 322, 1959.
24. Keck, P. H., and W. Van Horn: The Surface Tension of Liquid Silicon and Germanium, *Phys. Rev.*, vol. 91, pp. 512–513, 1953.
25. Sylwestrowicz, W. D.: Mechanical Properties of Single Crystals of Silicon, *Phil. Mag.*, ser. 8, vol. 7, pp. 1825–1845, 1962.
26. Love, A. E. H.: “A Treatise on the Mathematical Theory of Elasticity,” Dover Publications, Inc., 1944.
27. Menzel, D. H. (ed.): “Fundamental Formulas of Physics,” Prentice-Hall, Inc., Englewood Cliffs, N.J., 1955.
28. Riney, T. D.: Residual Thermoelastic Stresses in Bonded Silicon Wafers, *J. Appl. Phys.*, vol. 32, pp. 454–460, 1961.
29. Smotko, J. S.: “Experiments to Produce Ductile Silicon,” FIAT, Final Report 789, 1946.
30. Gallagher, C. J.: Plastic Deformation of Germanium and Silicon, *Phys. Rev.*, vol. 88, pp. 721–722, 1952.
31. Seitz, F.: The Plasticity of Silicon and Germanium, *Phys. Rev.*, vol. 88, pp. 722–724, 1952.
32. Runyan, W. R., W. Herrmann, and L. Jones: “Crystal Development Program,” Texas Instruments Incorporated, Final Report, AF33(600)-33736, 1958.
33. Dash, W. C.: Dislocations in Silicon and Germanium Crystals in “Properties of Elemental and Compound Semiconductors,” pp. 195–209, Interscience Publishers, Inc., New York, 1960.
34. Billig, E.: Some Defects in Crystals Grown from the Melt. I. Defects Caused by Thermal Stresses, *Proc. Roy. Soc. (London)*, ser. A, vol. 235, pp. 37–55, 1956.
35. Patel, J. R., and A. R. Chaudhuri: Macroscopic Plastic Properties of Dislocation-free Germanium and Other Semiconductor Crystals. I. Yield Behavior, *J. Appl. Phys.*, vol. 34, pp. 2788–2799, 1963.
36. Duckworth, W. H.: Precise Tensile Properties of Ceramic Bodies, *J. Am. Ceram. Soc.*, vol. 34, pp. 1–9, 1951.
37. Oliphint, J. B. (University of Texas): Private communication.

38. Westbrook, J. H., and J. J. Gilman: An Electromechanical Effect in Semiconductors, *J. Appl. Phys.*, vol. 33, pp. 2360–2369, 1962.
39. Kuczynski, G. C., and R. F. Hochman: Light-induced Plasticity in Semiconductors, *Phys. Rev.*, vol. 108, pp. 946–948, 1957.
40. Kingery, W. D.: Factors Affecting Thermal Stress Resistance of Ceramic Bodies, *J. Am. Ceram. Soc.*, vol. 38, pp. 3–13, 1955.
41. Manson, S. S., and R. W. Smith: Theory of Thermal Shock Resistance of Brittle Materials Based on Weibull's Statistical Theory of Strength, *J. Am. Ceram. Soc.*, vol. 38, pp. 18–27, 1955.
42. Jaccodine, R. J.: Surface Energy of Germanium and Silicon, *J. Electrochem. Soc.*, vol. 110, pp. 524–527, 1963.
43. Elliott, J. F., R. E. Hysell, and C. L. Kolbe: "Investigation of Large Area Photovoltaic Solar Energy Converters," General Electric Company, Final Report, DA-36-039-56-85286.
44. Gaulé, G., J. Braslin, and J. Pastore: "A Silicon Sintering Process," paper presented at the Fall Meeting of the Electrochemical Society, Oct. 7, 1957.
45. Uhler, A.: Electrolytic Shaping of Silicon and Germanium, *Bell System Tech. J.*, vol. 35, pp. 333–347, 1956.
46. Dash, William C.: Distorted Layers in Silicon Produced by Grinding and Polishing, *J. Appl. Phys.*, vol. 29, pp. 228–229 (L), 1958.
47. Lederhandler, S. R.: Infrared Studies of Birefringences in Silicon, *J. Appl. Phys.*, vol. 30, pp. 1631–1638, 1959.
48. Prussin, S. A.: The Influence of Surface Damage on the Generation of Dislocations in Lapped Silicon Wafers, in John B. Schroeder (ed.), "Metallurgy of Semiconductors," Interscience Publishers, Inc., New York, 1962.
49. Stickler, R., and G. R. Booker: Surface Damage on Abraded Specimens, *Phil. Mag.*, vol. 8, p. 859, May, 1963.

11

Metallurgy

11-1. REVIEW OF BINARY PHASE SYSTEMS^{1,*}

Isomorphous. The simplest system is binary isomorphous and occurs when the two metals are mutually soluble in all proportions, both as a liquid and as a solid. For such cases, the solution must be substitutional, and both components must have the same crystal structure and similar lattice spacings, otherwise a phase change would occur as one element is progressively replaced by the other. Figure 11-1 shows the phase diagram of such a system.

If the melt is initially of composition X , it will remain fixed until the liquidus line is reached. At the point (T_1, X) , material of composition Y will begin freezing.† Similarly, if a solid of composition X is heated, nothing will happen until the solidus curve is reached, at which time melting starts. The liquid would then have an initial composition Z . The isothermal line between the liquidus and solidus

* Superscript numbers indicate items listed in References at the end of the chapter.

† Thus, $(100 - Y)/(100 - X)$ is the ratio of impurity concentration in the solid to that in the melt and is the familiar segregation coefficient. It should be further observed that the liquidus and solidus lines are curved and would thus imply a segregation coefficient dependent on concentration. Over the very small range of interest in doping, however, the two curves are quite straight.

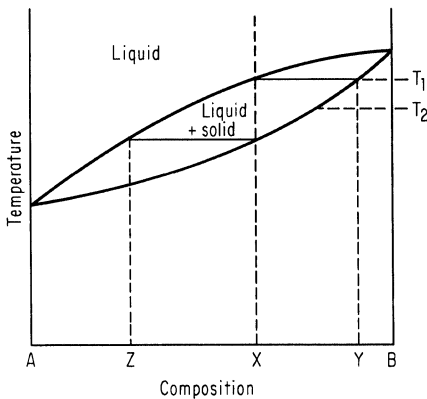
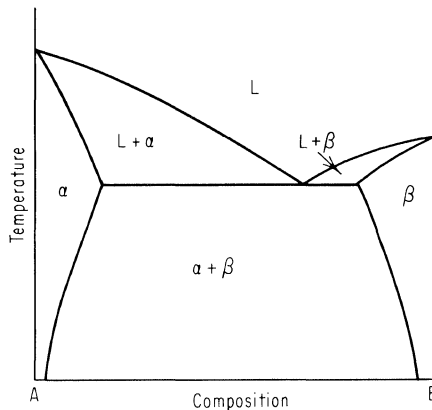


Fig. 11-1. Isomorphous system phase diagram.

Fig. 11-2. Eutectic system phase diagram.



curve is called a tie line and joins the composition points of the two phases that can coexist at a given temperature and pressure. The silicon-germanium system is an example of this type (Fig. 11-24).

When the temperature is T_1 , a solid of composition Y is crystallizing, but as soon as the temperature drops to T_2 , a new composition is in equilibrium with the melt. A solid of uniform composition can be realized only by the diffusion of more of component A into the previously crystallized solid. Thus, if freezing takes place too rapidly for diffusion to occur, the composition will vary throughout the solid, and coring will usually occur.

Eutectic. The somewhat more complicated binary eutectic system is illustrated in Fig. 11-2. The silicon-aluminum system (Fig. 11-12) has this type behavior. In this system, the addition of either component to the other lowers the melting point. Thus, the liquidus line has a minimum which is called the eutectic point. There are two terminal solid phases, α and β , rather than only one as in the binary isomorphous system; and the liquid composition at the eutectic point is the only composition that can simultaneously be in equilibrium with both solids. When a eutectic alloy is cooled through the eutectic temperature, the liquid freezes isothermally, and apparently the two phases deposit simultaneously.

When liquid of composition different from the eutectic is cooled, for example, X_1 of Fig. 11-3, metal of composition α_1 first freezes. Then as the temperature is dropped further, the composition changes to α_2 to α_3 and the liquid composition changes from L_1 to L_2 to L_3 until finally the liquid composition reaches the eutectic composition. At that point, the remainder of the liquid freezes isothermally to produce a solid mixture of $\alpha + \beta$.

Alloys of composition different from the eutectic are called “hypoeutectic” or “hypereutectic” alloys, depending on which side of the eutectic point they occur. Normally, hypoeutectic denotes the alloy richer in the more common metal.

The composition range of the terminal solid solution may be so narrow that it cannot be seen on a normal diagram as being any different from the pure metal. For this case the diagram degenerates into one such as Fig. 11-4a. An example of this is the gold-silicon system of Fig. 11-25. There are many systems in which the eutectic composition occurs extremely close to one of the components. This will

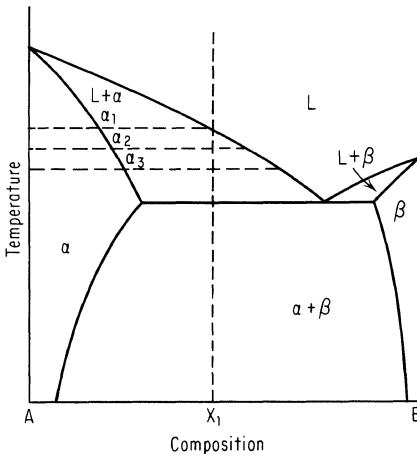


Fig. 11-3. Temperature versus composition for the eutectic system.

look like Fig. 11-4b. In the event that the solubility of *A* in *B* is very small, then the range of *B* might also be very narrow so that the diagram further reduces to Fig. 11-4c. (See, for example, the antimony-silicon diagram in Fig. 11-13.)

Eutectoid. If, instead of the liquid phase shown in Fig. 11-2, there is another solid phase α , and then some sort of transition from the third solid phase to the liquid, the reaction involving the three solid phases is called a eutectoid reaction. This is illustrated in Fig. 11-5.

Monotectic. In this reaction, one liquid phase decomposes with decreasing temperature into a solid phase and a new liquid phase. This is shown in Fig. 11-6. For temperatures above the critical point, the liquid phases L_1 and L_2 are indistinguishable. However, below that they are immiscible, so that if the composition is between X and Y , the two liquids will both be present. The two may be layered or intimately mixed, such as in emulsion. If the terminal solubility is very small, then as a limiting case the monotectic system becomes that shown in Fig. 11-7.

The bismuth-silicon system (Fig. 11-16) is monotectic and is intermediate between those of Figs. 11-6 and 11-7. The monotectic system is of interest because

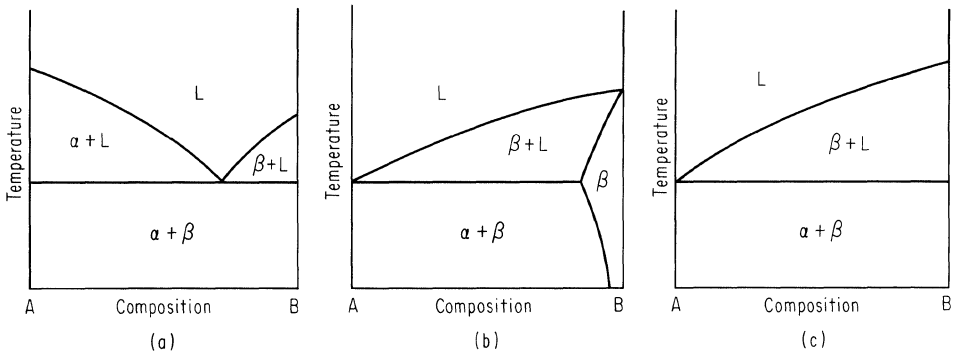
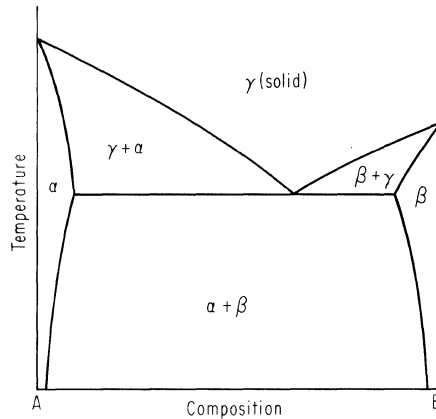


Fig. 11-4. The effect of terminal solid solution range on eutectic phase diagram.

Fig. 11-5. Eutectoid phase diagram.

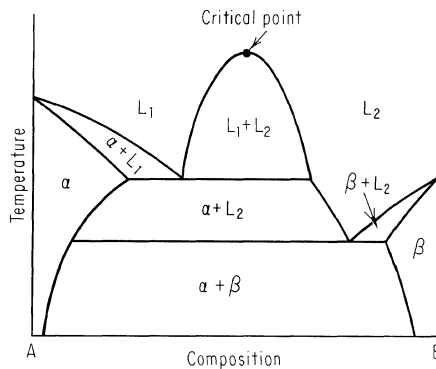


it suggests the possibility of floating molten silicon on a pool of higher-density liquid in order to allow crystal growing² or casting with a minimum of container restraint.

Syntectic. This system is shown in Fig. 11-8. The complete diagram is not drawn because it could be terminated by any of several other systems, none of which would affect the behavior in the region shown. It differs from the previously described monotectic system in that at the syntectic composition, the two immiscible liquids transform into a solid phase only, rather than into a solid phase and another liquid phase. This system is rare and not known to occur in any of the silicon alloys.

Peritectic. In the peritectic reaction, a solid phase decomposes into a liquid phase and a new solid phase as the temperature is increased. A phase diagram illustrating this is shown in Fig. 11-9. If the liquid has a composition Y , corresponding to the peritectic point P , then as the temperature is decreased from T_Y to T_P , solid phase α will freeze. At temperature T_P , the liquid and α react to form the β phase. If the composition were X , rather than Y , then the transformation at temperature T_P would not require all of the α phase so that both α and β would be present in the final solid. The β phase forms at the interface between the liquid and the α phase and in general reduces the diffusion and greatly slows down the

Fig. 11-6. Monotectic phase diagram.



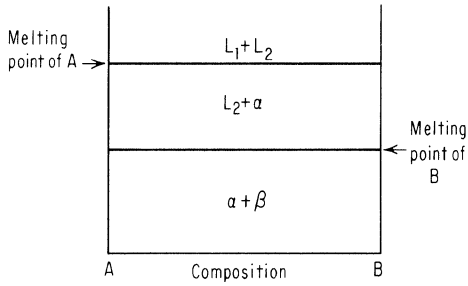


Fig. 11-7. Limiting case of the monotectic system.

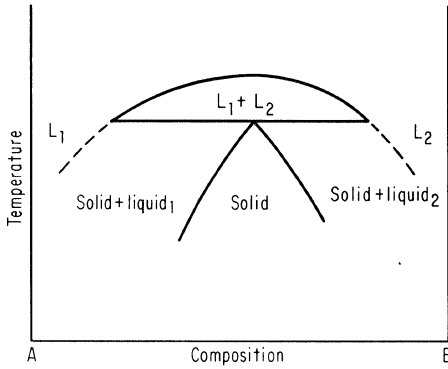


Fig. 11-8. Syntectic phase diagram.

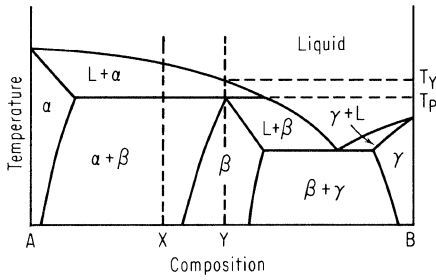


Fig. 11-9. Peritectic phase diagram.

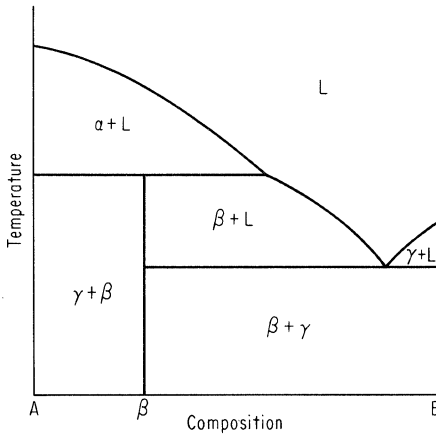


Fig. 11-10. Peritectic system with narrow terminal and β phases.

$\alpha + \text{liquid} \longrightarrow \beta$ reaction. For this reason the departure from equilibrium in the natural freezing of peritectic alloys is normally very large.

When the solid solubility range of the β phase becomes very narrow, it will appear on the phase diagram as a single line. Likewise, the terminal phase may become quite narrow so that instead of Fig. 11-9 the phase diagram may appear as Fig. 11-10. This combination is more appropriate for silicon than Fig. 11-9. (See, for example, Fig. 11-49 which is the diagram for SiZr.)

Peritectoid. In this system (which is analogous to the eutectoid system shown in Fig. 11-11) the β phase transforms at the peritectoid composition in an $\alpha + \gamma$ solid phase. An example of this is to be found in the manganese-silicon system of Fig. 11-31 in the vicinity of 20 atomic per cent manganese.

Congruent Transformations. If a phase changes directly into another phase without any alteration in composition, then the phase change is congruent. For example, if a congruent component melts, the liquid has the same composition as the solid phase. This is in contrast to, e.g., the peritectic system just described, where raising the temperature of the β phase gives a liquid and another solid phase. Solid phases which exhibit congruent transformations are often found in binary systems and are usually considered to be intermetallic compounds. (An example of this is Mg_2Si of Fig. 11-30.) When such a congruent phase occurs it effectively isolates the systems on each side of it. Thus, in the case of the Mg-Si system, the Mg_2Si splits the diagram into two parts, each of which is simple eutectic. In the case of more complex systems such as manganese-silicon (Fig. 11-31) there are many congruent phases so that one diagram may contain several of the systems such as have been described.

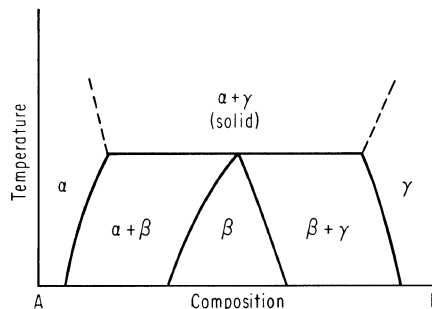
11-2. PHASE DIAGRAMS²⁻⁶

Figures 11-12 to 11-49 are a collection of silicon phase diagrams.

11-3. LIMITS OF SOLUBILITY⁷

Because the limits of solubility of many of the elements of interest in silicon are so small, little such information can be read from standard phase diagrams because of the scale normally used. Figure 11-50 shows on a greatly expanded scale the composition of the terminal solid solution for several metals in silicon.

Fig. 11-11. Peritectoid phase diagram.



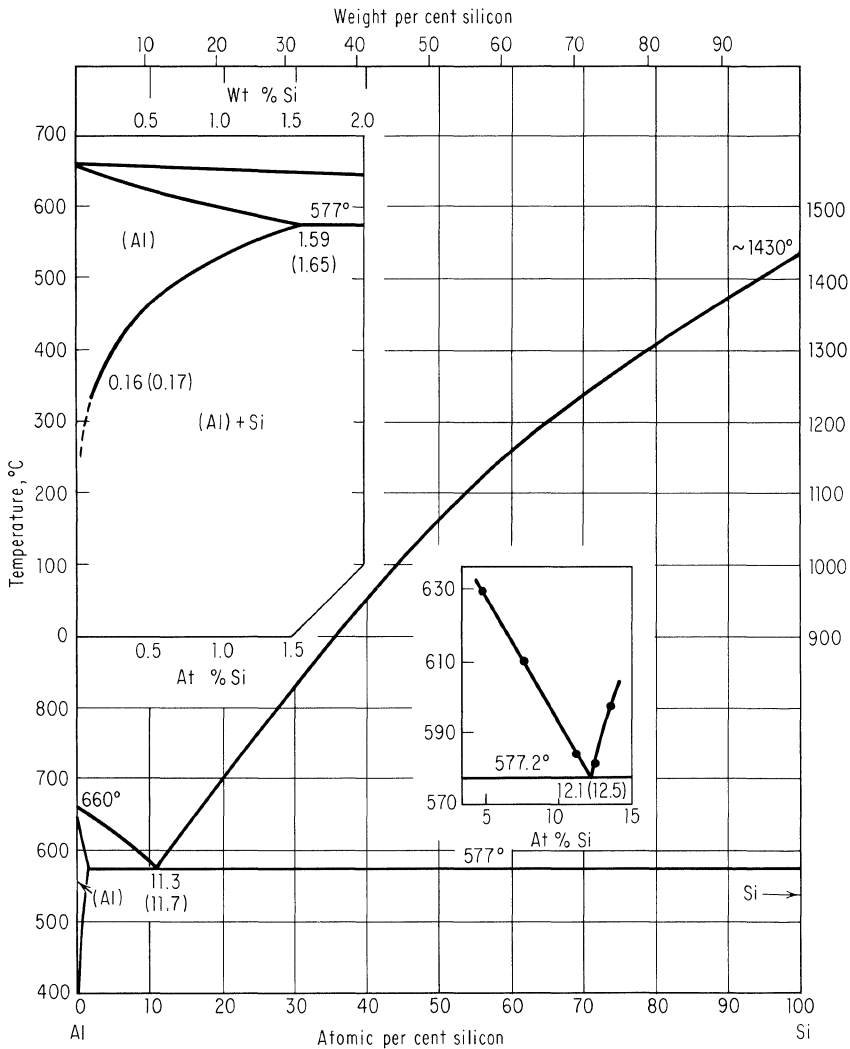


Fig. 11-12. Aluminum-silicon phase diagram. (From "Constitution of Binary Alloys" by Max Hansen. Copyright, 1958. McGraw-Hill Book Company. Used by permission.)

11-4. SEGREGATION COEFFICIENTS

It was mentioned earlier that the segregation coefficient for Ge in Si could be read from the silicon-germanium phase diagram. In principle the segregation for any other element can also be obtained from the appropriate phase diagram. Thus, in Fig. 11-51, which shows a portion of a silicon phase diagram on expanded scale, $k = BC/AC$. But since the terminal phase is so narrow, BC cannot be seen in most phase diagrams. However, the solubility curves of Fig. 11-50 are really plots of the boundary of the silicon terminal phase boundary, so that by reading AC from the phase diagram, and BC from the solubility curves, k can still be determined.

EXAMPLE 11-1. Find k for gallium in silicon:

1. Assume terminal solidus curve linear from 1400° to melting point (assume 1410°).
2. Determine BC from Fig. 11-50 as 7×10^{18} atoms/cm³.
3. Examination of the silicon-gallium phase diagram of Fig. 11-23 shows that because of the scale, AC for a temperature 10 to 20° from the melting point could not be read, and further, that because of differences in determining the silicon melting point, that particular curve does not even extend to 1400° , where BC was read. Accordingly, consider that the liquidus curve is linear to 1200°C . Then determine AC for that temperature. This gives 50 atomic per cent. By similar triangles (see Fig. 11-52) an AC for a temperature of 10° below the melting point can be determined by $AC_{-10} = 10/196 \times 50$ atomic per cent = 2.5 atomic per cent.
4. Since these units are in atomic per cent, and those for BC as read from the solubility chart are impurities per cubic centimeter, convert from atomic per cent to atoms per cubic centimeter. There are 5×10^{22} silicon atoms/cm³ (from Chap. 6), so 2.5 atomic per cent = $5 \times 10^{22} \times 0.025 = 1.25 \times 10^{21}$ atoms/cm³.
5. $k = BC/AC = (7 \times 10^{18}) / (1.25 \times 10^{21}) = 5.6 \times 10^{-3}$ which compares favorably with the value of 8×10^{-3} given in Table 6-1.

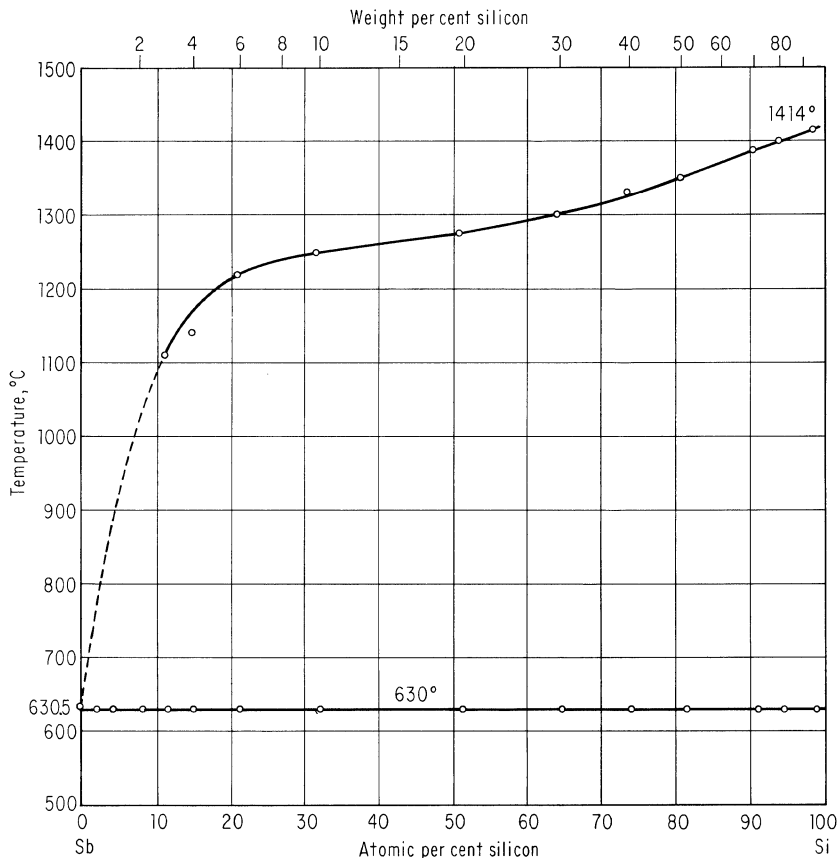


Fig. 11-13. Antimony-silicon phase diagram. (From "Constitution of Binary Alloys" by Max Hansen. Copyright, 1958. McGraw-Hill Book Company. Used by permission.)

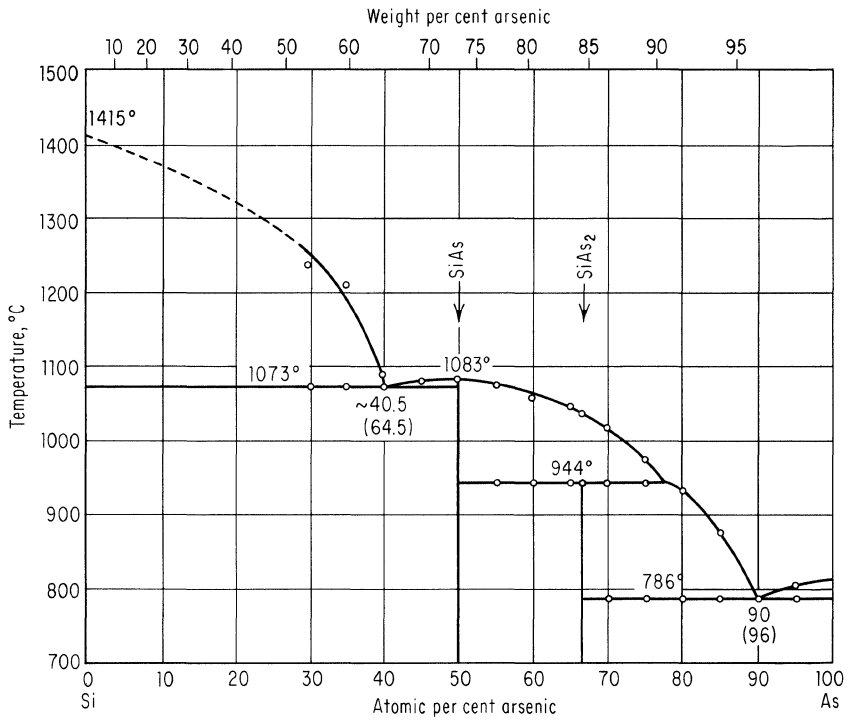


Fig. 11-14. Arsenic-silicon phase diagram. (From "Constitution of Binary Alloys" by Max Hansen. Copyright, 1958. McGraw-Hill Book Company. Used by permission.)

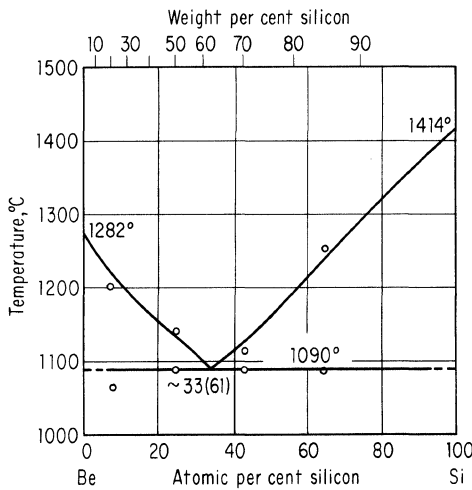


Fig. 11-15. Beryllium-silicon phase diagram. (From "Constitution of Binary Alloys" by Max Hansen. Copyright, 1958. McGraw-Hill Book Company. Used by permission.)

Fig. 11-16. Bismuth-silicon phase diagram. (From "Constitution of Binary Alloys" by Max Hansen. Copyright, 1958. McGraw-Hill Book Company. Used by permission.)

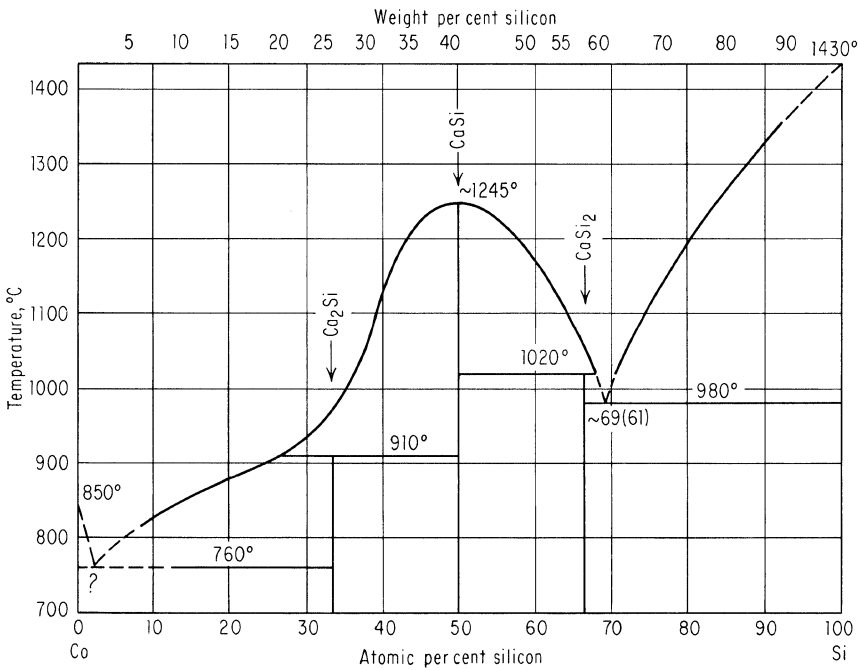
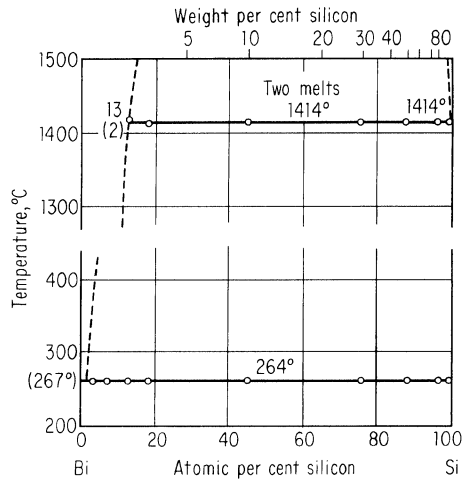


Fig. 11-17. Calcium-silicon phase diagram. (From "Constitution of Binary Alloys" by Max Hansen. Copyright, 1958. McGraw-Hill Book Company. Used by permission.)

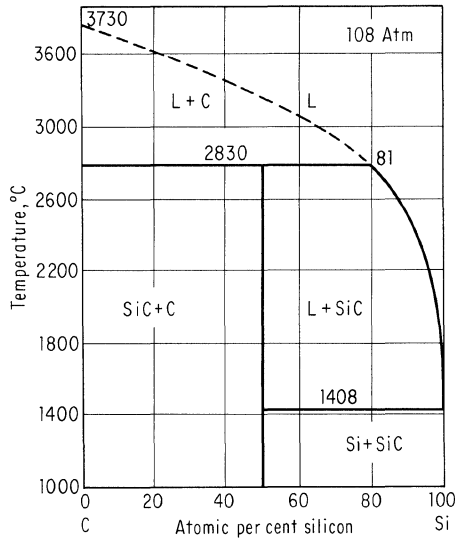
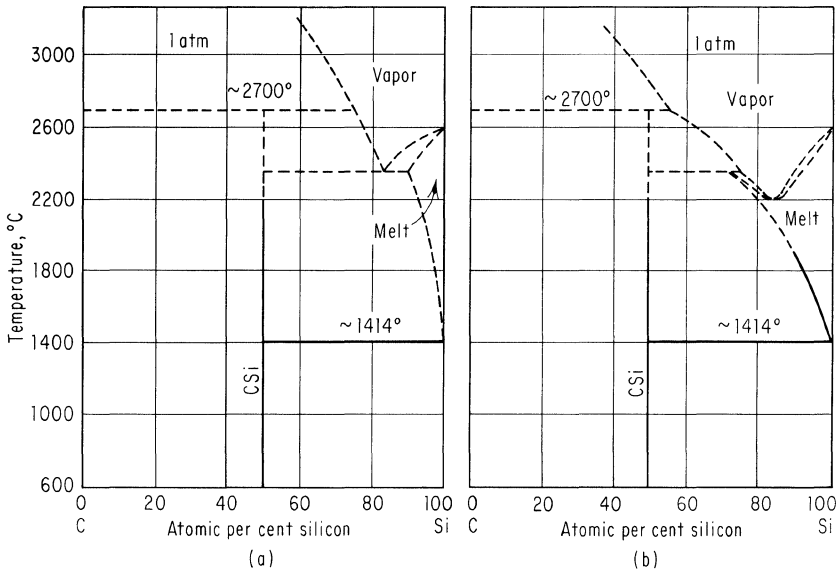


Fig. 11-18. Carbon-silicon phase diagram. (From "Constitution of Binary Alloys" by Max Hansen. Copyright, 1958. McGraw-Hill Book Company. Used by permission; and from "The Si-C and Ge-C Phase Diagrams" by R. I. Scace and G. A. Slack in "Silicon Carbide," copyright, 1960, Pergamon Press, used by permission.)

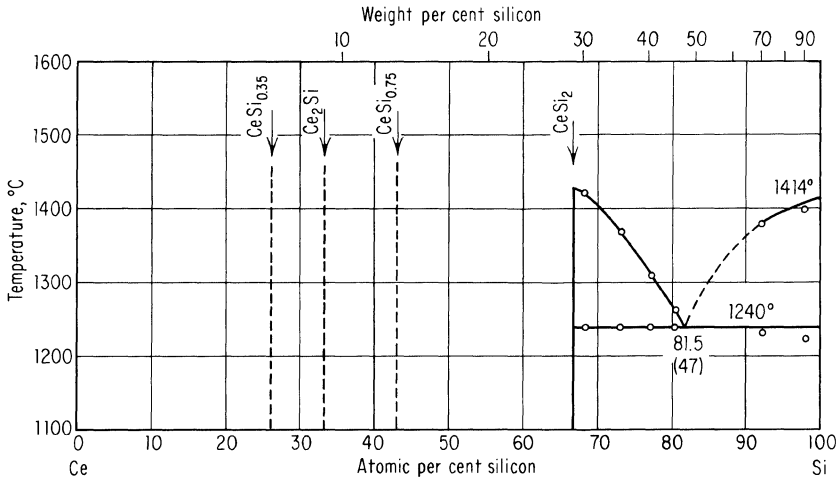


Fig. 11-19. Cerium-silicon phase diagram. (From "Constitution of Binary Alloys" by Max Hansen. Copyright, 1958. McGraw-Hill Book Company. Used by permission.)

11-5. SILICON-GERMANIUM ALLOYS

Since silicon and germanium are miscible in all proportions, it is possible in principle to form a whole series of alloys of varying composition that have band gaps covering the range between the two elements and which would be useful for a variety of other studies. In practice, however, it is difficult by conventional means to form the alloys, probably because low diffusion coefficients prevent equilibrium conditions from being met in reasonable times. Codepositing the silicon and germanium from the vapor phase apparently obviates the need for a diffusion to produce equilibrium and allows a straightforward method of producing composition alloys.^{9,10}

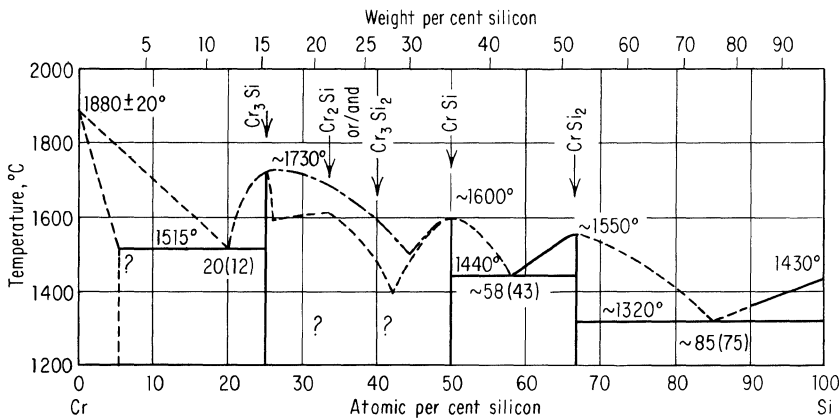


Fig. 11-20. Chromium-silicon phase diagram. (From "Constitution of Binary Alloys" by Max Hansen. Copyright, 1958. McGraw-Hill Book Company. Used by permission.)

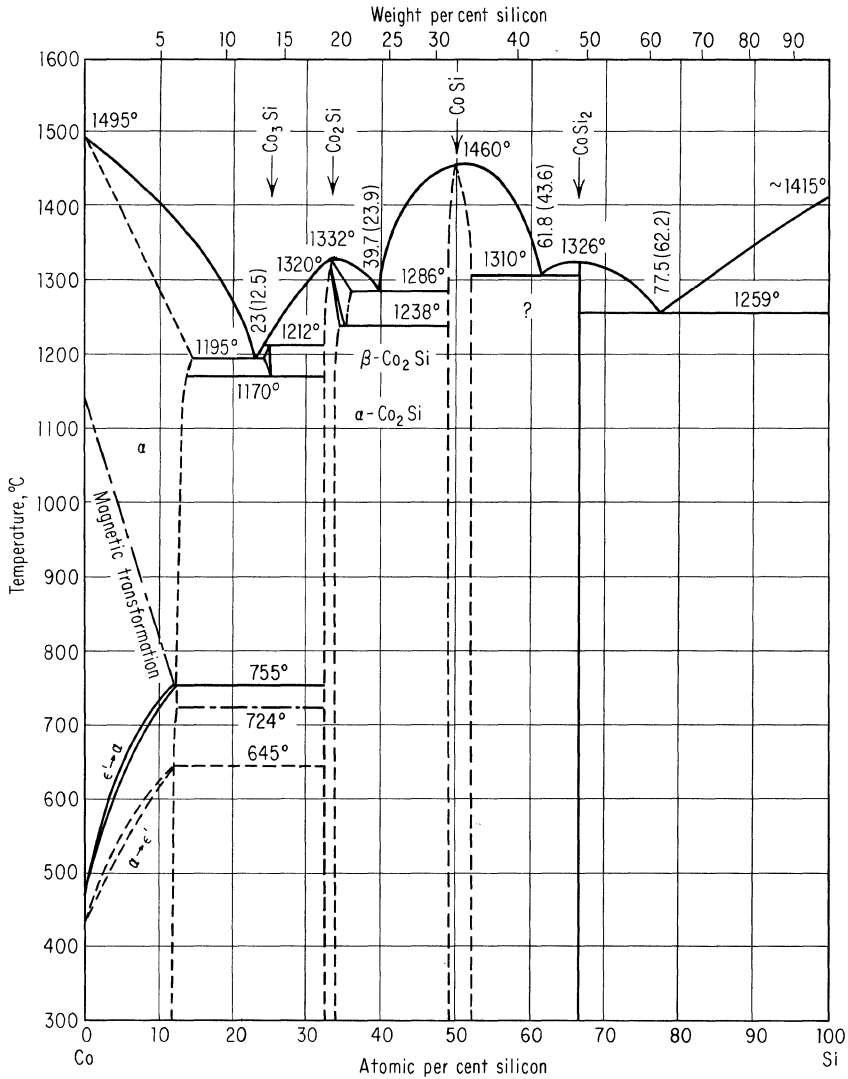


Fig. 11-21. Cobalt-silicon phase diagram. (From "Constitution of Binary Alloys" by Max Hansen. Copyright, 1958. McGraw-Hill Book Company. Used by permission.)

11-6. SOLUBILITIES AND FORMATION OF PRECIPITATES

Most elements have a maximum solubility in silicon in the temperature region of from about 1200 to 1300°C. Because of this, if a high concentration of impurity is introduced at elevated temperatures, e.g., by diffusion, or during crystal growing, it is possible for a second phase to precipitate during cooling.¹¹ In order for this to occur, the cooling must be slow enough or the diffusion rate of the impurity high enough to allow coagulation. In most instances the diffusion rate is quite low at temperatures below 900°C, so any reasonable cooling rate will preclude precipitation. On the other hand, some of the faster diffusers, such as copper

and gold, have high diffusion coefficients at much lower temperatures, so that it is possible to cool at rates of a few degrees per minute and cause much of the copper or gold to precipitate. Most of the fast diffusers are “lifetime killers” when distributed through the lattice. They also usually have a very low solubility at low temperatures so that slow cooling to allow them to precipitate as separate phases will reduce lifetime degradation.

The following discussions summarize the behavior of several of the more common elements.

Aluminum. Crystals heavily doped with aluminum, which also contain oxygen, often have precipitates which are apparently caused by the aluminum combining with the oxygen to form alumina.¹²

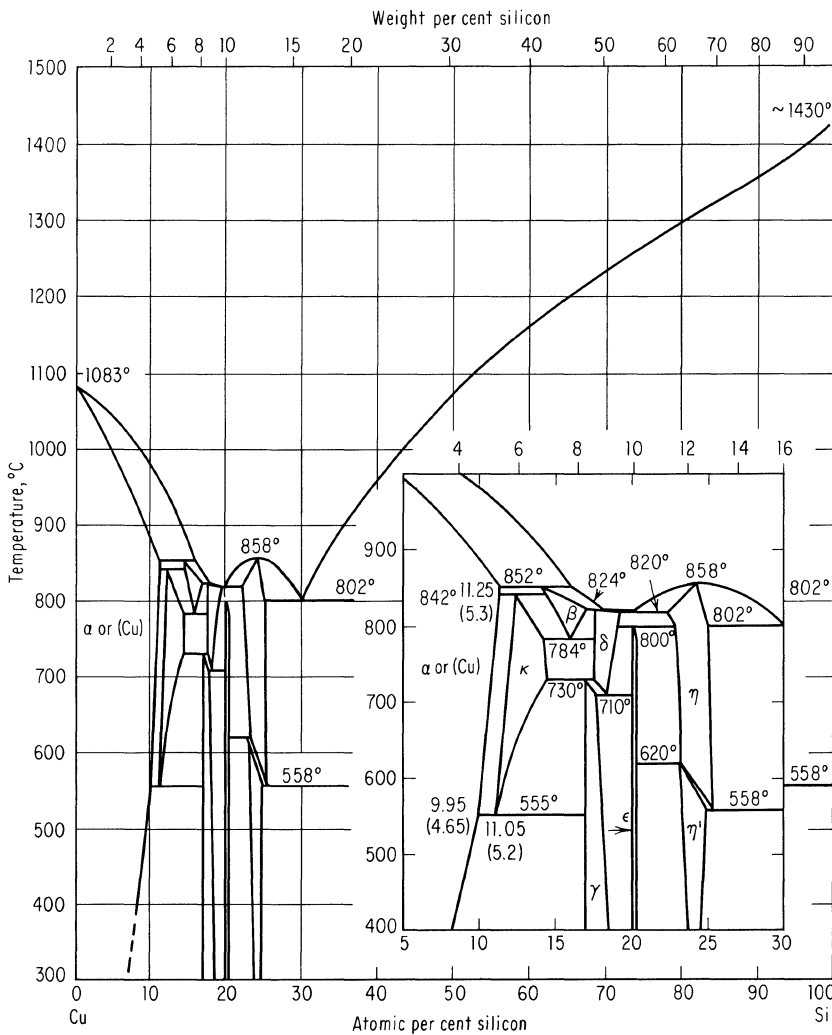


Fig. 11-22. Copper-silicon phase diagram. (From “Constitution of Binary Alloys” by Max Hansen. Copyright, 1958. McGraw-Hill Book Company. Used by permission.)

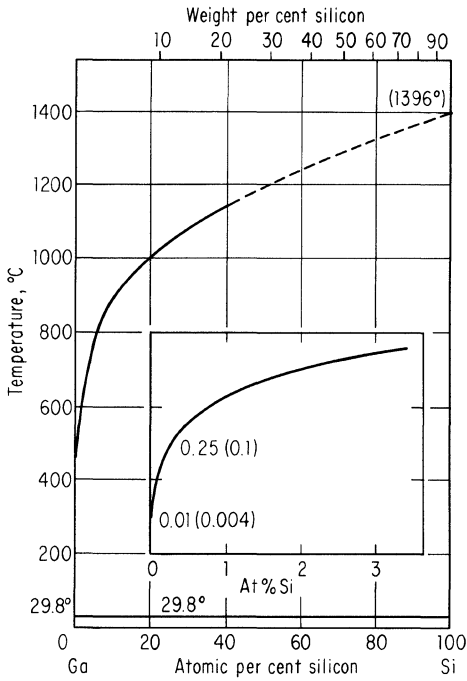


Fig. 11-23. Gallium-silicon phase diagram. (From "Constitution of Binary Alloys" by Max Hansen. Copyright, 1958. McGraw-Hill Book Company. Used by permission.)

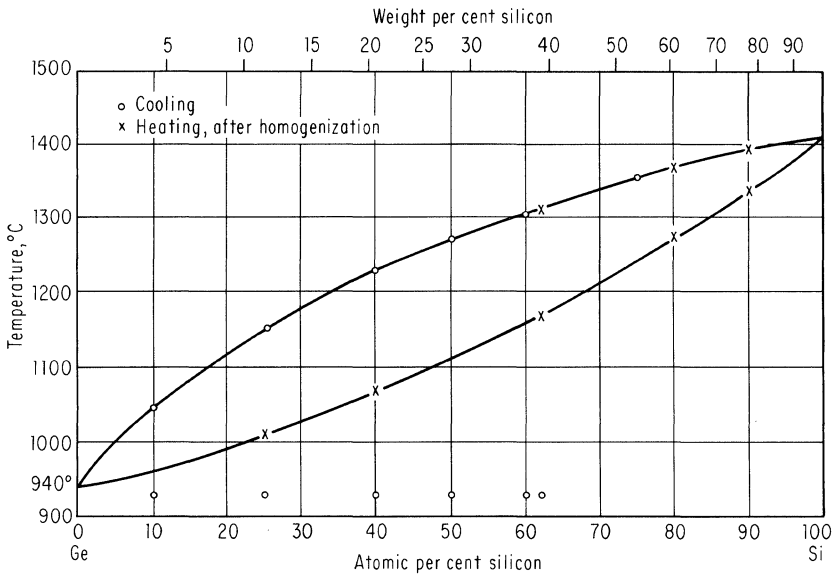


Fig. 11-24. Germanium-silicon phase diagram. (From "Constitution of Binary Alloys" by Max Hansen. Copyright, 1958. McGraw-Hill Book Company. Used by permission.)

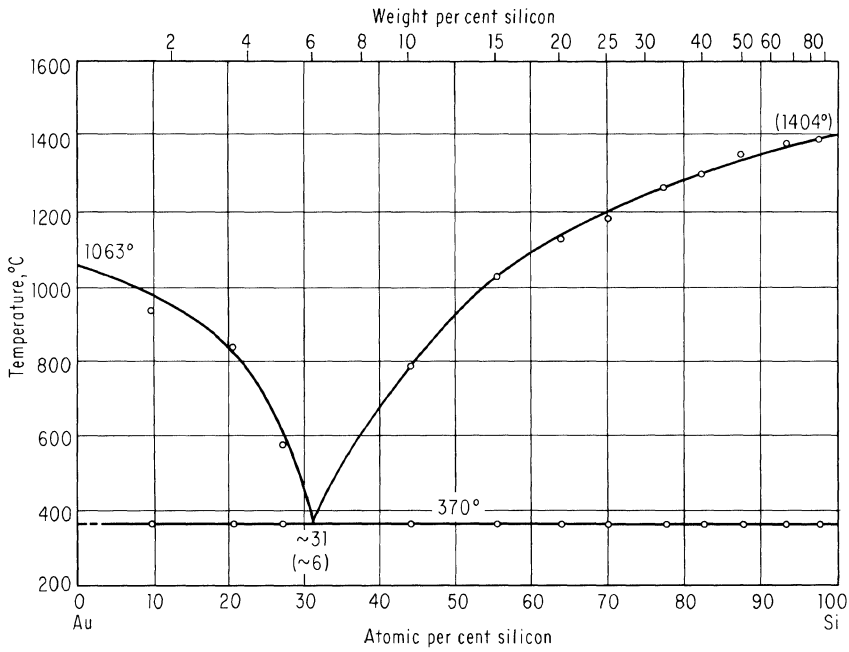


Fig. 11-25. Gold-silicon phase diagram. (From "Constitution of Binary Alloys" by Max Hansen. Copyright, 1958. McGraw-Hill Book Company. Used by permission.)

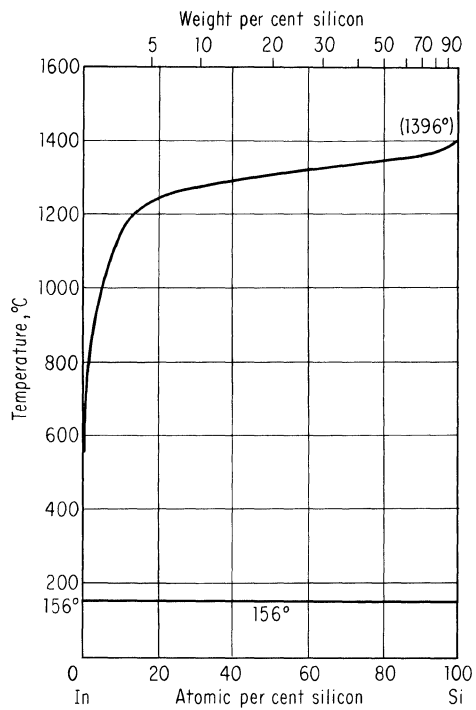


Fig. 11-26. Indium-silicon phase diagram. (From "Constitution of Binary Alloys" by Max Hansen. Copyright, 1958. McGraw-Hill Book Company. Used by permission.)

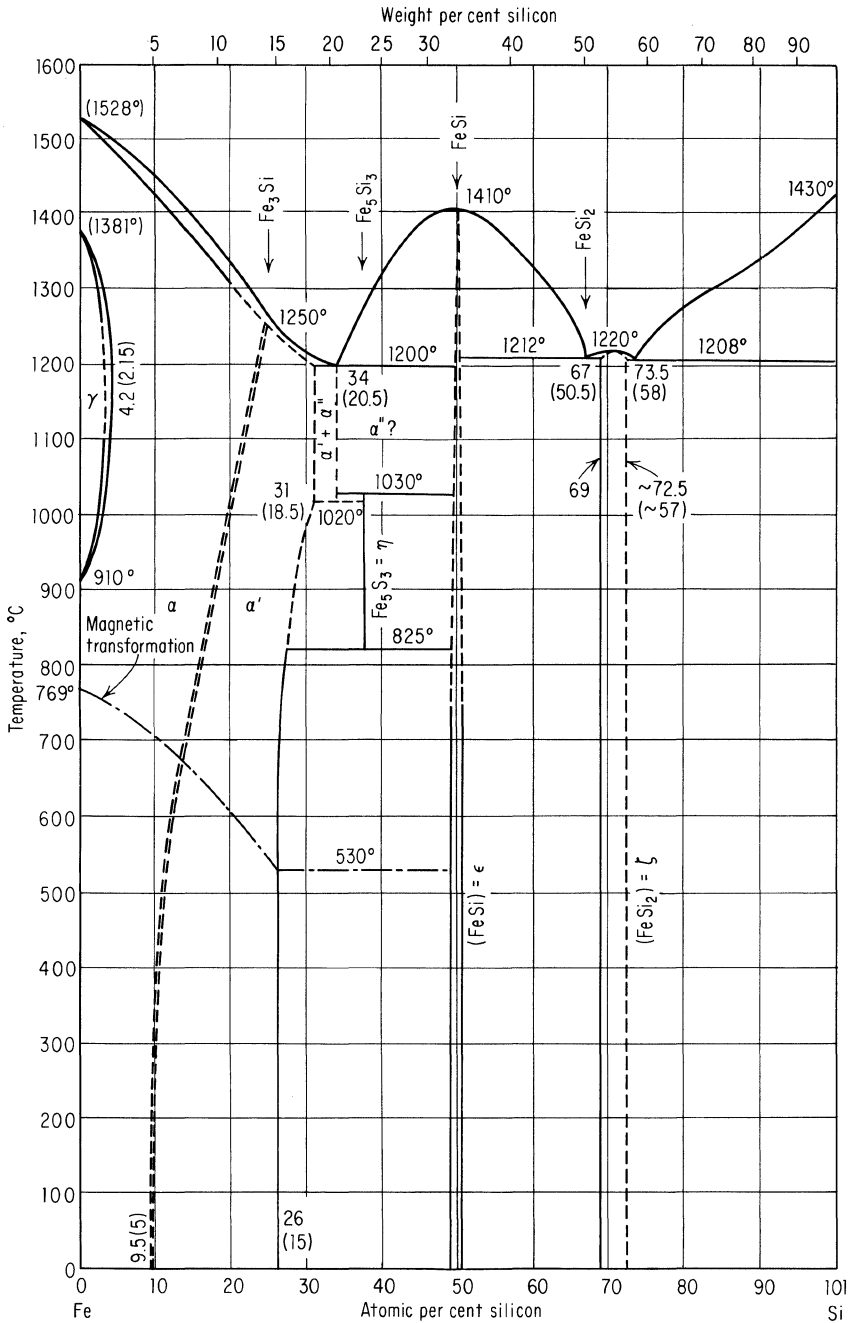
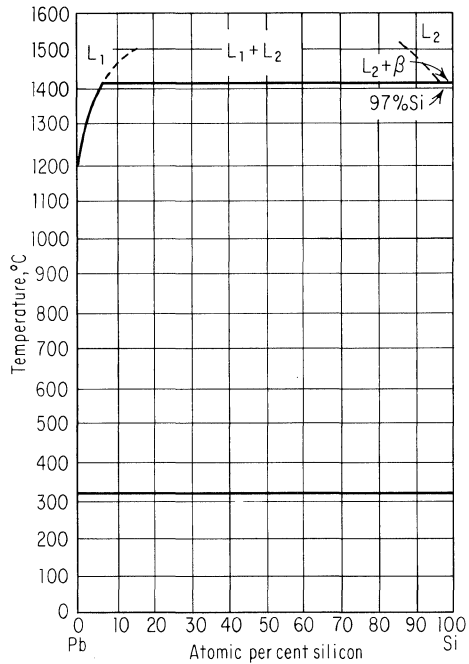


Fig. 11-27. Iron-silicon phase diagram. (From "Constitution of Binary Alloys" by Max Hansen. Copyright, 1958. McGraw-Hill Book Company. Used by permission.)

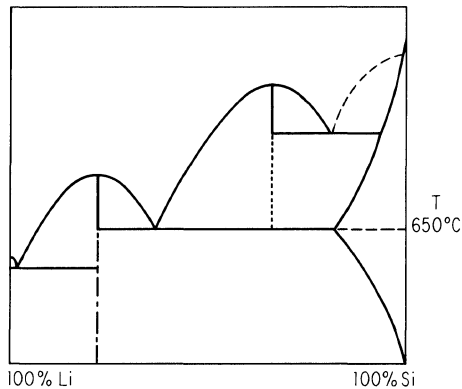
Fig. 11-28. Lead-silicon phase diagram. (From "Investigation of Thin Sheets of High-quality Single Crystal Silicon" by F. T. Fitch, W. R. Grace & Co. final technical summary report, contract DA 36-039-SC 85242, September, 1960. Used with permission.)



Antimony. Antimony precipitates have been observed in heavily doped crystals grown from the melt when the antimony concentration in the crystal approached 10^{19} atoms/cm³ (as determined by resistivity measurements).¹³

Carbon. The solubility of carbon in silicon increases with temperature and very near the melting point is about 10^{18} atoms/cm³.¹⁴ Crystals saturated at a high temperature and then cooled usually show carbon precipitation quite independent of the cooling rates. The precipitates are beta silicon carbide and apparently are formed during the diffusion. It is also observed that some crystals as grown are saturated with carbon,^{14,15} and while there are many possible sources (e.g., hydrocarbons in the hydrogen used in manufacture, hydrocarbons in the inert gas used

Fig. 11-29. Lithium-silicon phase diagram. (After Thurmond, in "Solubility of Lithium in Doped and Un-doped Silicon: Evidence for Compound Formation," by H. Reiss, C. S. Fuller, and A. J. Pietruskiewicz, *J. Chem. Phys.*, vol. 25, pp. 650-655, 1956. Used by permission.)



for growing, and transport of carbon from crucible to the silicon melt), the presumed low segregation coefficient of carbon in silicon makes it difficult to understand how incorporation occurs.

Copper.¹⁶ In intrinsic silicon most of the dissolved copper is interstitial and singly charged with the ratio of substitutional to interstitial solubility being about 10^{-4} at 700°C . Because of the electronic interaction between copper and any shallow donors or acceptors which may be present, the solubilities will be different in extrinsic material.* For p-type, the interstitial solubility (the substitutional values

*For a comprehensive survey of such effects the reader is referred to Howard Reiss, C. S. Fuller, and F. J. Morin, *Chemical Interaction among Defects in Ge and Si*, *Bell System Tech. J.*, vol. 35, pp. 535-636, 1956, and W. Shockley and J. L. Moll, *Solubility of Flaws in Heavily Doped Semiconductors*, *Phys. Rev.*, vol. 119, pp. 1480-1483, 1960.

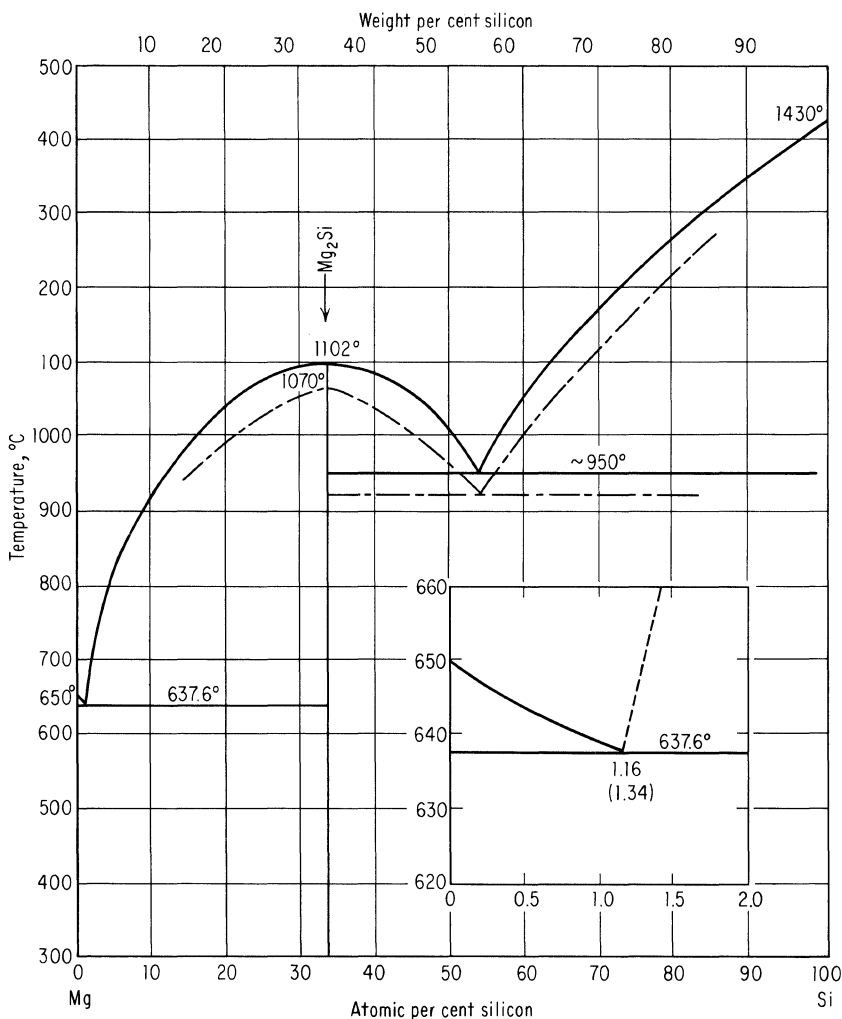


Fig. 11-30. Magnesium-silicon phase diagram. (From "Constitution of Binary Alloys" by Max Hansen. Copyright, 1958. McGraw-Hill Book Company. Used by permission.)

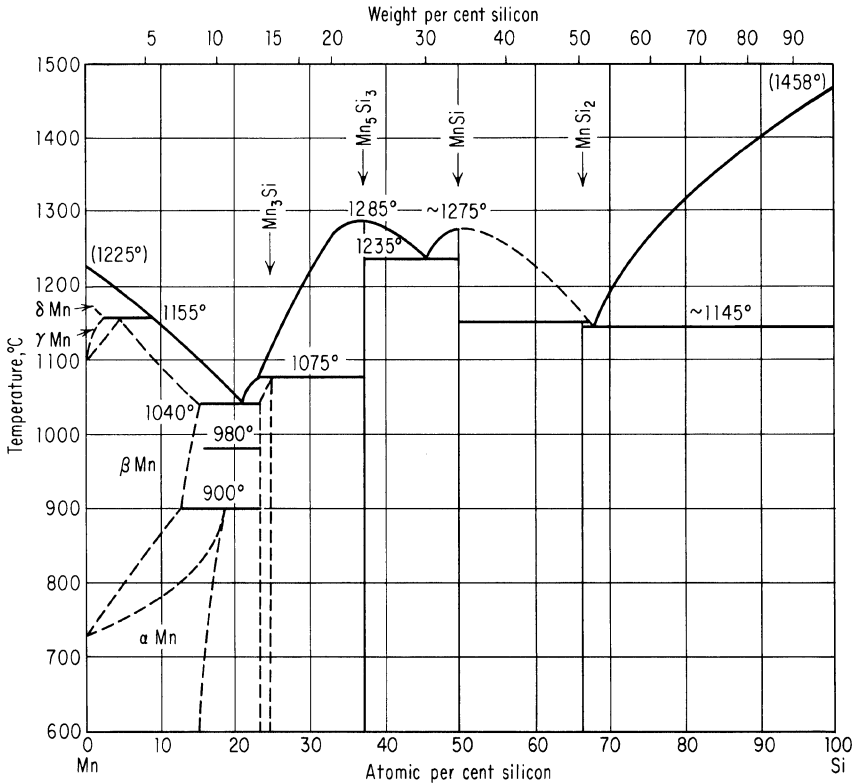


Fig. 11-31. Manganese-silicon phase diagram. (From "Constitution of Binary Alloys" by Max Hansen. Copyright, 1958. McGraw-Hill Book Company. Used by permission.)

are depressed) is given by

$$C^i = C_i^i \frac{P}{n_i}$$

For n-type,

$$C^{total} = C_i^i \frac{n_i}{n} + C_{i,sub} \left(\frac{n}{n_i}\right)^{3*}$$

$$C_i^i = 6 \times 10^{15} \text{ atoms/cm}^3 \quad \text{at } 700^\circ\text{C}$$

$$C_i^i = 7 \times 10^{14} \text{ atoms/cm}^3 \quad \text{at } 600^\circ\text{C}$$

where the subscript i refers to intrinsic, the superscript i to interstitial, and n_i is defined in Eq. (8-2). From these equations it can be seen that the total solubility increases monotonically for p-type material as the doping level increases, but that for n-doping, a decrease will first be observed as the interstitial solubility is depressed, and then as the substitutional contribution becomes appreciable, additional increases in doping cause rapid increases in solu-

*The third power is involved because substitutional copper is a triple acceptor.

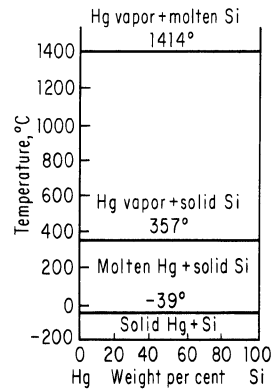


Fig. 11-32. Mercury-silicon phase diagram. (From "Silicon and Its Binary Systems" by A. S. Bereznoi. Copyright, 1960. Consultants Bureau. Used by permission.)

bility. At 700°C the minimum occurs at slightly less than 10^{19} donor atoms/cm³.

Because of this greatly enhanced solubility in heavily doped regions, such regions in device structures can act as sinks and accumulate excessive amounts of copper which may then precipitate upon cooling and cause device degradation.

Gold.¹⁷ Gold may occupy either substitutional or interstitial sites but, in contrast to copper, below 1200°C the substitutional solubility is higher than the interstitial solubility. The two values are given by

$$C_{\text{sub}} = 8.2 \times 10^{22} e^{-40.6\text{kcal}/RT}$$

$$C_{\text{interstitial}} = 6 \times 10^{24} e^{-58 \pm 10\text{kcal}/RT}$$

Lithium.¹⁸ Lithium solubility is affected not only by interaction with holes and electrons, but also by the formation of complexes with acceptor ions.

Oxygen. When oxygen is introduced into a silicon crystal during growth or diffusion at high temperatures, it apparently occupies interstitial positions, has a maximum solubility of about 2×10^{18} atoms/cm³, and is un-ionized.¹⁹⁻²¹ In the interstitial position it forms SiO bonds which give a strong infrared absorption band at 9.1 microns. Heating the silicon for extended periods of time in the range of 450°C causes aggregates of complexes of the type SiO₂, SiO₃, and SiO₄ to form.

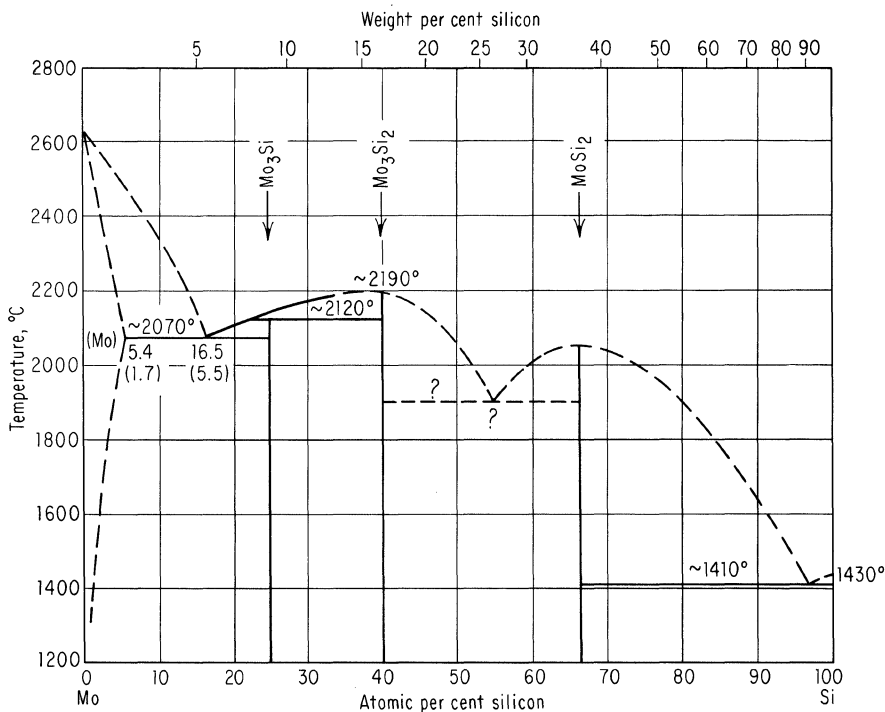


Fig. 11-33. Molybdenum-silicon phase diagram. (From "Constitution of Binary Alloys" by Max Hansen. Copyright, 1958. McGraw-Hill Book Company. Used by permission.)

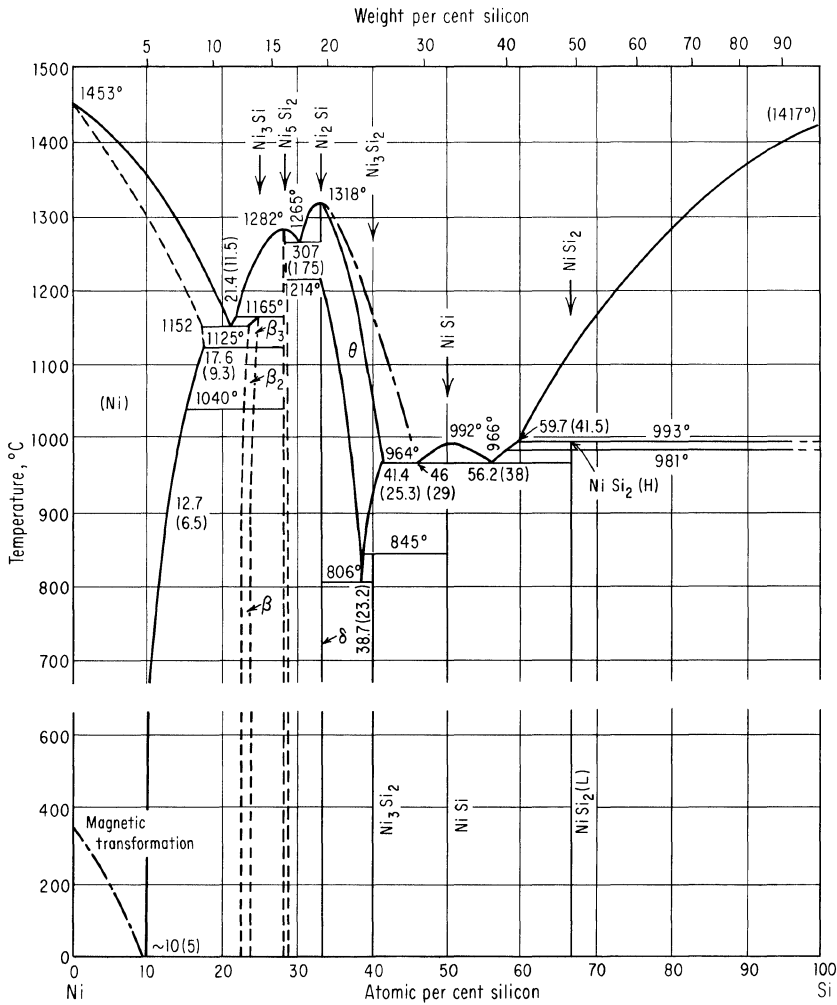


Fig. 11-34. Nickel-silicon phase diagram. (From "Constitution of Binary Alloys" by Max Hansen. Copyright, 1958. McGraw-Hill Book Company. Used by permission.)

These complexes no longer have a 9-micron absorption band, but some of them are electrically active. As the heat treatment progresses, the 9-micron absorption band decreases, and the donor concentration first increases and then decreases. This decrease can be explained by considering that for polymers involving more than four oxygen atoms there are no available donors, and that as the chains continue to grow the supply of individual SiO_{2-4} complexes is depleted. If the temperature is raised to near the silicon melting point, the SiO bond is the more stable, the SiO_x groups dissolve, and the oxygen returns to its original state. Heat treatment at 1000°C reduces the absorption, but does not produce appreciable donors, presumably because only the longer oxygen chains are formed.²² It is also observed that at 1000°C, the rate of aggregate formation is structure-dependent,

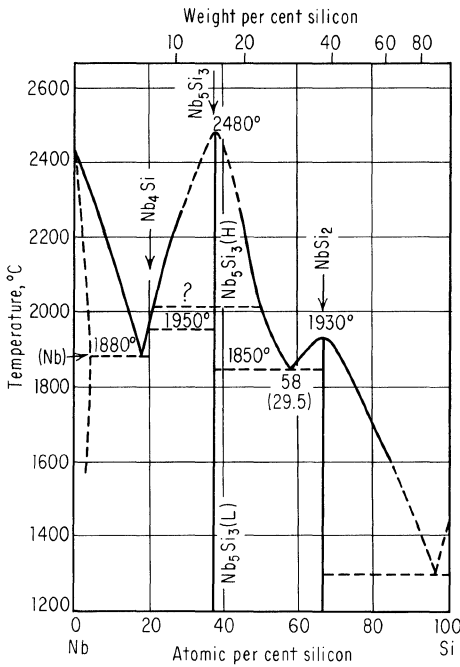


Fig. 11-35. Niobium (Columbium)-silicon phase diagram. (From "Constitution of Binary Alloys" by Max Hansen. Copyright, 1958. McGraw-Hill Book Company. Used by permission.)

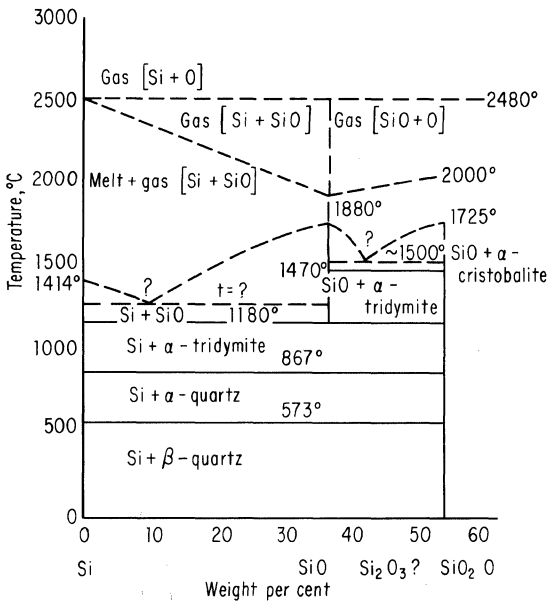


Fig. 11-36. Oxygen-silicon phase diagram (hypothetical). (From "Silicon and Its Binary Systems" by A. S. Berezhnoi. Copyright, 1960, Consultants Bureau. Used by permission.)

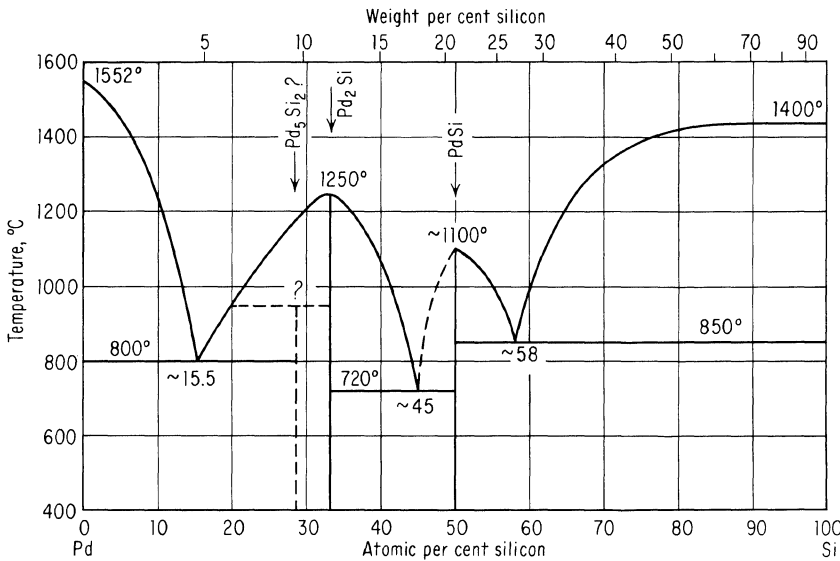


Fig. 11-37. Palladium-silicon phase diagram. (From "Constitution of Binary Alloys" by Max Hansen. Copyright, 1958. McGraw-Hill Book Company. Used by permission.)

i.e., the more dislocations present in the crystal, the shorter the annealing time required to reach equilibrium.²³

11-7. EFFECT OF HIGH-IMPURITY CONCENTRATION

Those impurities which have high solubilities are less likely to precipitate than the lower solubility elements just discussed, but they can nevertheless produce damage when present in high concentration. A silicon phosphide separate phase has, for example, been observed in the surface layers of heavily phosphorus-doped diffused layers.²⁴ In addition, the lattice strain due to the impurities may be considerable.

Table 11-1. Values of Misfit Ratio for Substitutional Impurities in Silicon*

Impurity	Γ
B	0.746
Al	1.068
Ga	1.068
P	0.932
As	1.000
Sb	1.150
Sn	1.186

* From J. R. Carruthers, R. B. Hoffman, and J. D. Ashner, X-ray Investigation of the Perfection of Silicon, *J. Appl. Phys.*, vol. 34, pp. 3389-3393, 1963.

This strain ϵ can be calculated from ²⁵

$$\epsilon = [1 + f(\Gamma^3 - 1)]^{1/3} - 1$$

where f = atom fraction

Γ = ratio of the Pauling covalent radius of solute to silicon atoms

Values for Γ are given in Table 11-1. A substitution of these numbers shows that 4×10^{18} , 8×10^{19} , and 2.5×10^{19} atoms/cm³ of antimony, boron, and phosphorus respectively will produce a strain of 10^{-6} . As an example of the severity of this effect, if boron is diffused locally, as is normal in making planar devices, it is pos-

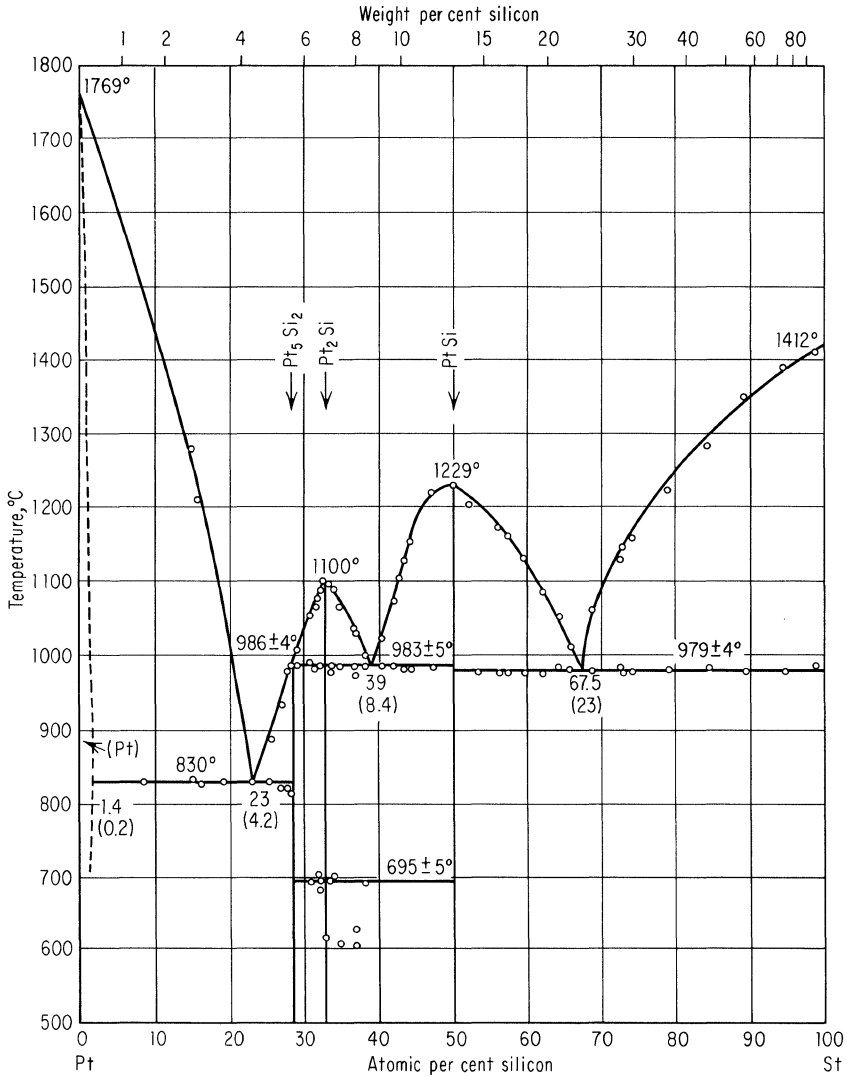


Fig. 11-38. Platinum-silicon phase diagram. (From "Constitution of Binary Alloys" by Max Hansen. Copyright, 1958. McGraw-Hill Book Company. Used by permission.)

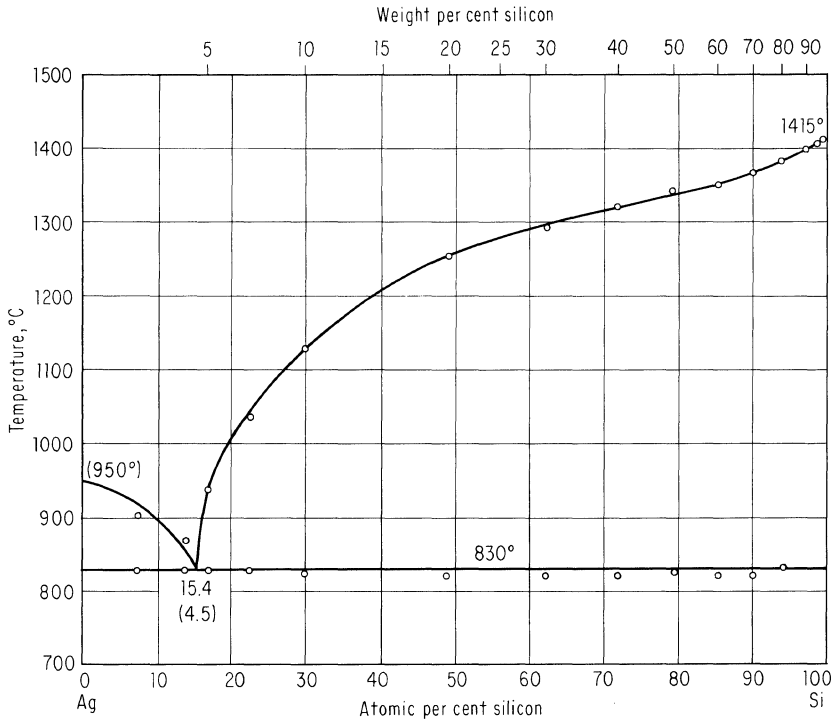


Fig. 11-39. Silver-silicon phase diagram. (From "Constitution of Binary Alloys" by Max Hansen. Copyright, 1958. McGraw-Hill Book Company. Used by permission.)

sible to change the lattice spacing enough for stress relief via slip to occur.^{26,27} By way of comparison, birefringence and X-ray investigations show the strain in as-grown crystals is often as much as 10^{-5} .

11-8. COPPER DECORATIONS^{28,29}

Precipitates such as just described often occur on dislocations and other structural defects. Because of this it is possible to deliberately saturate silicon with (for example, copper) precipitate, and by viewing with infrared, directly observe the various defects. Decoration can be accomplished by allowing a thin film of copper nitrate solution to dry on the surface, diffusing for the order of an hour at a relatively high temperature (approximately 1000° or above), and then quenching. Viewing can be done on an infrared imaging device sensitive to wavelengths longer than 1.1 microns.

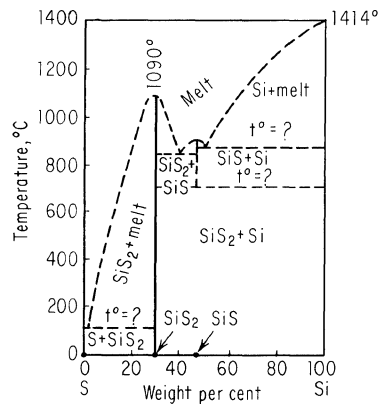


Fig. 11-40. Sulfur-silicon phase diagram (hypothetical). (From "Silicon and Its Binary Systems" by A. S. Bereznoi. Copyright, 1960, Consultants Bureau. Used by permission.)

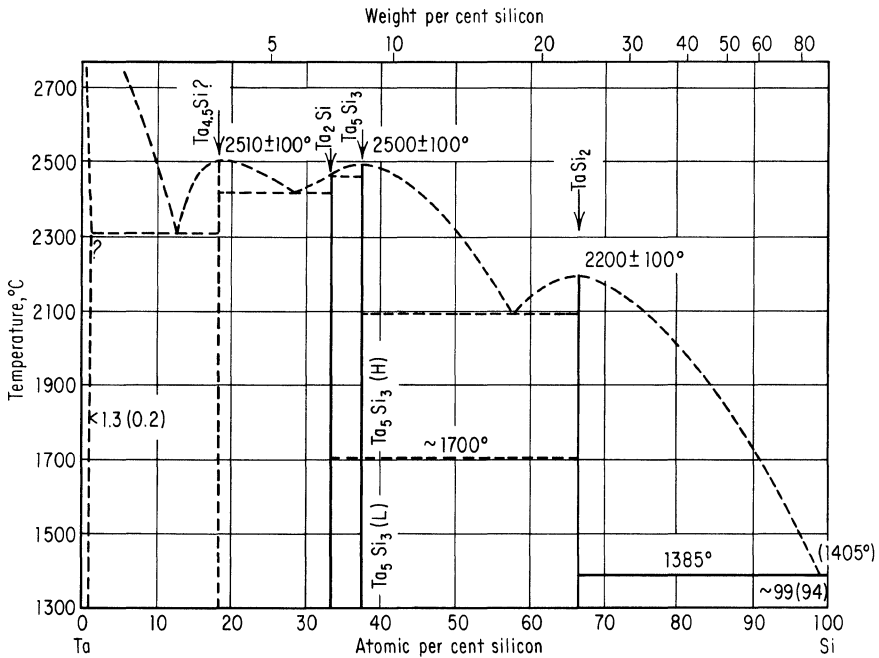


Fig. 11-41. Tantalum-silicon phase diagram. (From "Constitution of Binary Alloys" by Max Hansen. Copyright, 1958. McGraw-Hill Book Company. Used by permission.)

11-9. GETTERING TECHNIQUES

In a few instances, metal precipitates are useful, but usually they are deleterious to device performance and should be avoided.³⁰ In addition, the presence of transition metals, even as isolated atoms, often produces unwanted carrier lifetime degradation.^{31,32} The small quantities of metals necessary to cause trouble make it very difficult to prevent their introduction into the silicon during manufacturing, surface preparation, diffusion, etc. In general it has proven more advantageous to use getters to remove them during the last high-temperature operation. The most successful of these are glassy layers on the surface, such as phosphorus oxide-silicon oxide, or boric oxide-silicon oxide compounds. Liquid metal-silicon eutectic layers on the surface apparently behave similarly, though are not as effective as the glasses.^{30,32-34} It has also been reported that mechanical damage on the surface will satisfactorily trap various metal contaminants. The use of high-tempera-

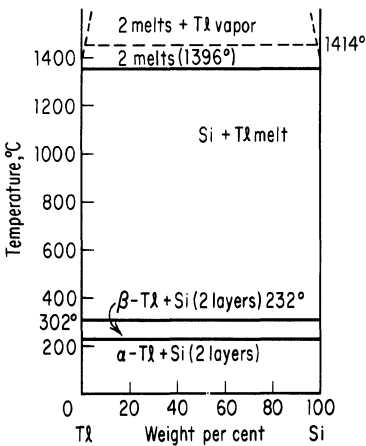


Fig. 11-42. Thallium-silicon phase diagram. (From "Silicon and Its Binary Systems" by A. S. Berezhnoi. Copyright, 1960, Consultants Bureau. Used by permission.)

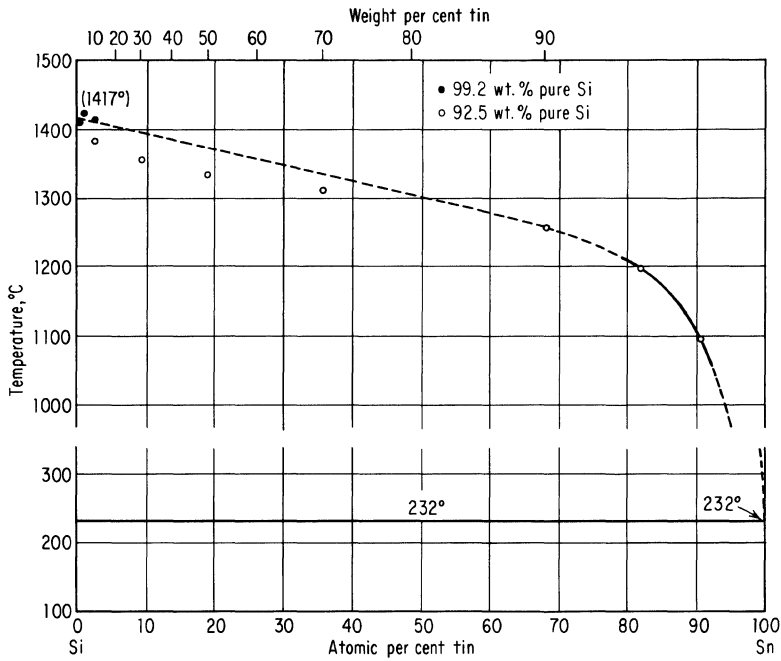


Fig. 11-43. Tin-silicon phase diagram. (From "Constitution of Binary Alloys" by Max Hansen. Copyright, 1958. McGraw-Hill Book Company. Used by permission.)

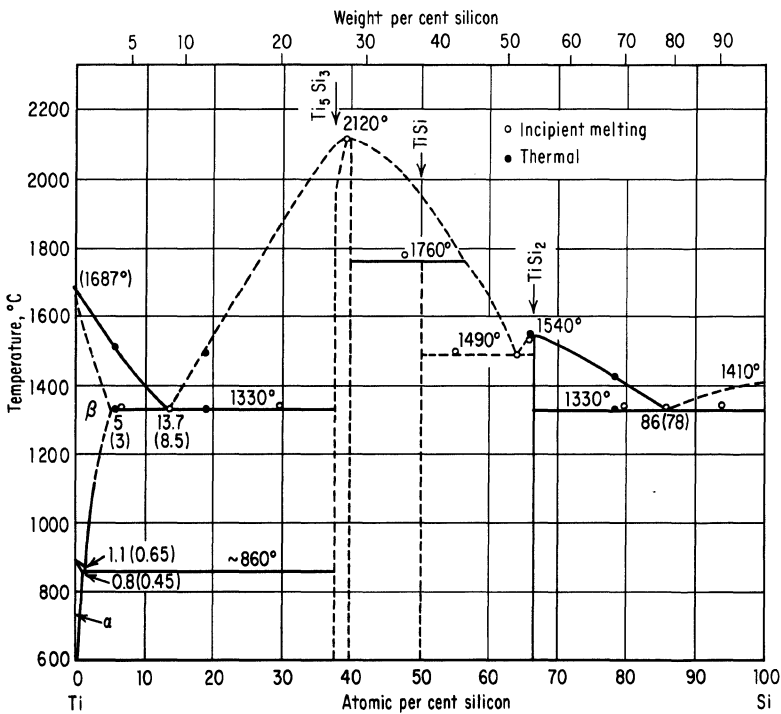


Fig. 11-44. Titanium-silicon phase diagram. (From "Constitution of Binary Alloys" by Max Hansen. Copyright, 1958. McGraw-Hill Book Company. Used by permission.)

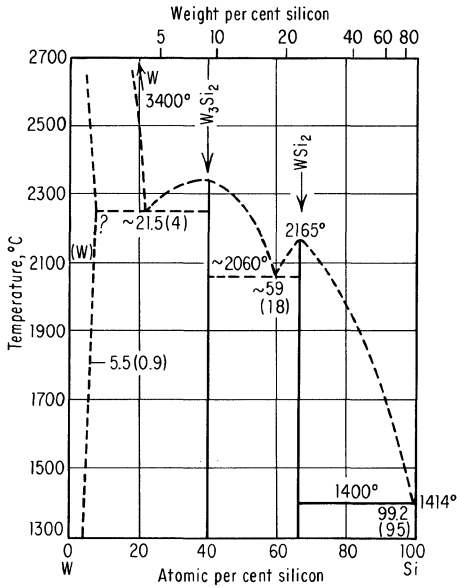


Fig. 11-45. Tungsten-silicon phase diagram. (From "Constitution of Binary Alloys" by Max Hansen. Copyright, 1958. McGraw-Hill Book Company. Used by permission.)

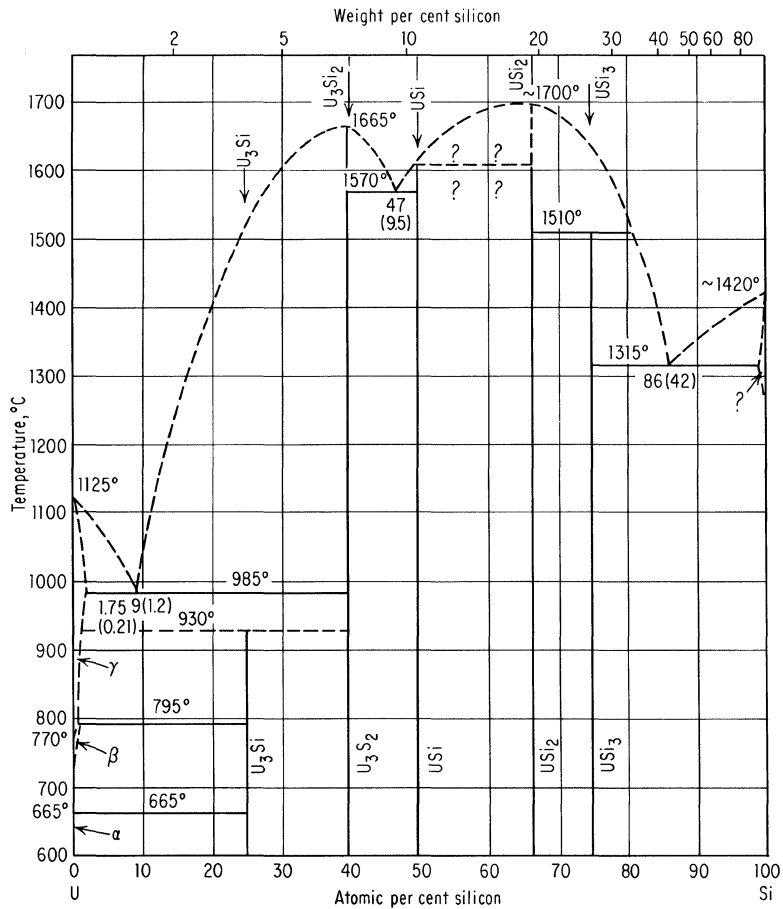


Fig. 11-46. Uranium-silicon phase diagram. (From "Constitution of Binary Alloys" by Max Hansen. Copyright, 1958. McGraw-Hill Book Company. Used by permission.)

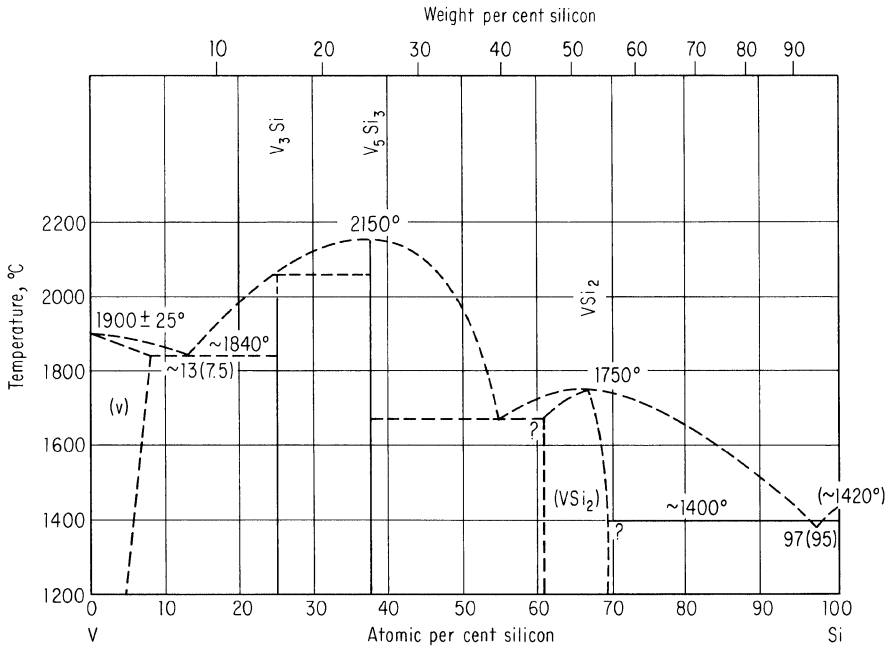


Fig. 11-47. Vanadium-silicon phase diagram. (From "Constitution of Binary Alloys" by Max Hansen. Copyright, 1958. McGraw-Hill Book Company. Used by permission.)

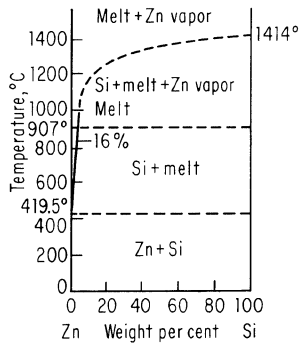


Fig. 11-48. Zinc-silicon phase diagram. (From "Silicon and Its Binary Systems" by A. S. Berezhnoi. Copyright, 1960. Consultants Bureau. Used by permission.)

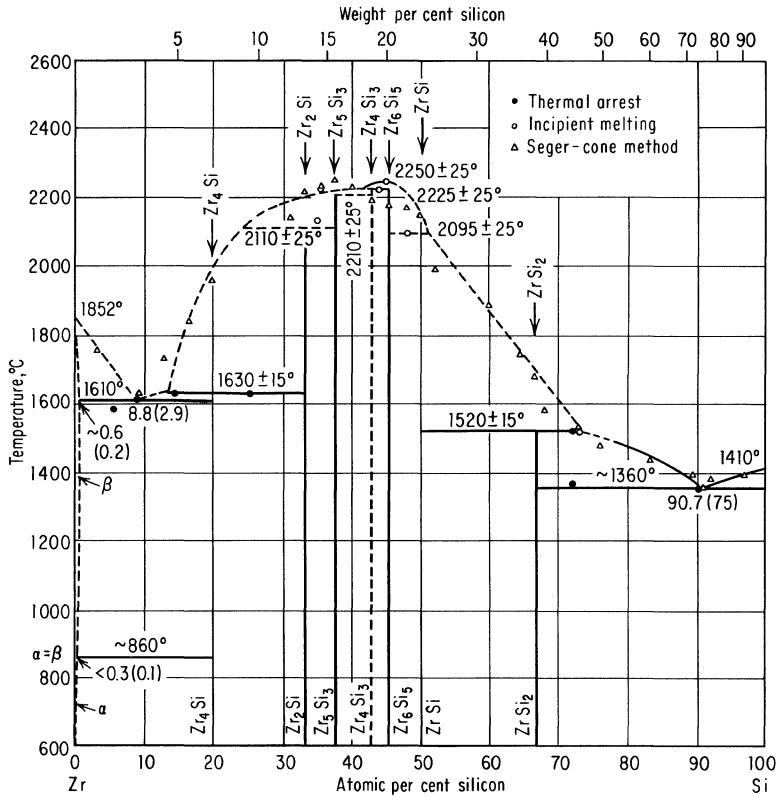


Fig. 11-49. Zirconium-silicon phase diagram. (From "Constitution of Binary Alloys" by Max Hansen. Copyright, 1960. McGraw-Hill Book Company. Used by permission.)

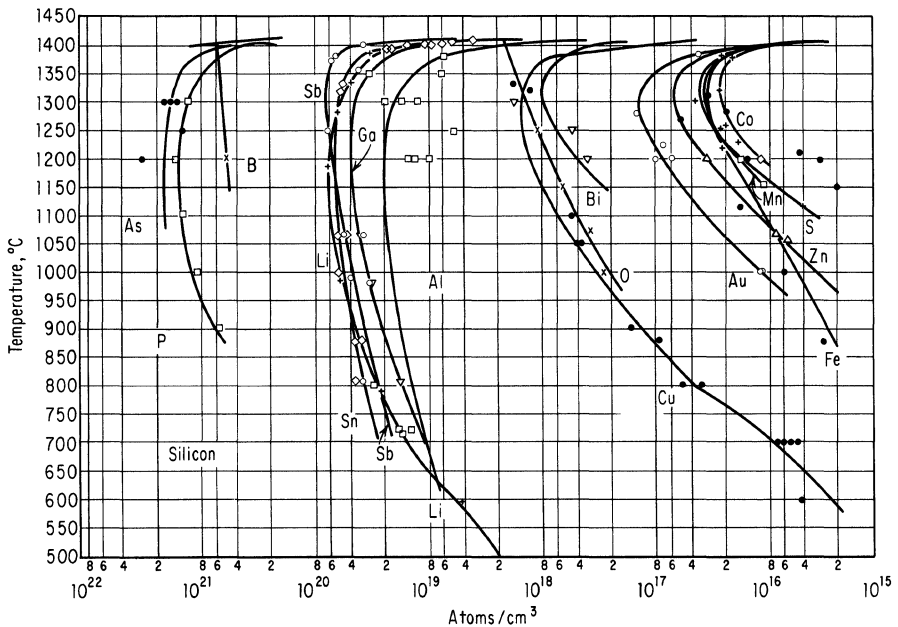


Fig. 11-50. Solid solubilities of impurity elements in silicon. (From "Solid Solubilities of Impurity Elements in Germanium and Silicon" by F. A. Trumbore, Bell System Tech. J., vol. 39, pp. 205-233, 1960. Used with permission.)

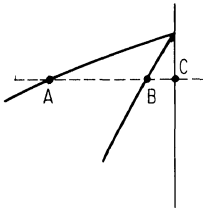


Fig. 11-51. Portion of a phase diagram.

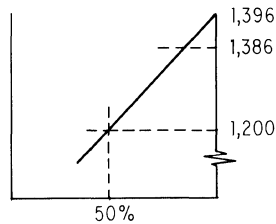


Fig. 11-52. Determination of the slope of the liquidus line.

ture gas ambients that form volatile compounds with the impurities has also been suggested, but has not been used as widely as the other methods.³⁵

REFERENCES

1. Rhines, Frederick N.: "Phase Diagrams in Metallurgy," McGraw-Hill Book Company, New York, 1956.
2. Fitch, F. T.: Investigation of Thin Sheets of High-quality Single Crystal Silicon, W. R. Grace & Co., Final Technical Summary Report, Contract DA36-039-SC85242, September, 1960.
3. Hansen, Max: "Constitution of Binary Alloys," McGraw-Hill Book Company, New York, 1958.
4. Scace, R. I., and G. A. Slack: The Si-C and Ge-C Phase Diagrams, "Silicon Carbide," Pergamon Press, New York, 1960.
5. Reiss, H., C. S. Fuller, and A. J. Pietruszkiewicz: Solubility of Lithium in Doped and Un-doped Silicon: Evidence for Compound Formation, *J. Chem. Phys.*, vol. 25, pp. 650-655, October, 1956.
6. Bereznoi, A. S.: "Silicon and Its Binary Systems," translated from Russian, Consultants Bureau, New York, 1960.
7. Trumbore, F. A.: Solid Solubilities of Impurity Elements in Germanium and Silicon, *Bell System Tech. J.*, vol. 39, pp. 205-233, 1960.
8. Pfann, W. G.: Principles of Zone Melting, *Trans. AIME*, vol. 194, p. 747, 1952.
9. Miller, K. J., and M. J. Grieco: Epitaxial Silicon-Germanium Alloy Films on Silicon Substrates, *J. Electrochem. Soc.*, vol. 109, pp. 70-71, 1962.
10. Oda, Jyoji: Vapor Growth of Silicon-Germanium Crystals, *J. Appl. Phys. (Japan)*, vol. 1, pp. 131-132, 1962.
11. Burton, J. A.: Impurity Centers in Ge and Si, *Proc. Intern. Conf. Semicond., Amsterdam, Physica*, vol. 20, pp. 845-854, 1954.
12. Bullough, R., R. C. Newman, J. Wakefield, and J. B. Willis: Precipitation in Silicon Crystals Containing Aluminum, *J. Appl. Phys.*, vol. 31, pp. 707-714, 1960.
13. Miller, D. P., and Kent Howard: Unpublished work.
14. Newman, R. C., and J. Wakefield: Diffusion and Precipitation of Carbon in Silicon, in J. V. Schroeder (ed.), "Metallurgy of Semiconductor Materials," Interscience Publishers, Inc., New York, 1962.
15. Booker, G. R., and R. Stickler: "Small Particles in Silicon," Late News Paper, Spring Meeting of the Electrochemical Society, 1964.
16. Hall, R. N., and J. H. Racette: Diffusion and Solubility of Copper in Extrinsic and

- Intrinsic Germanium, Silicon, and Gallium Arsenide, *J. Appl. Phys.*, vol. 35, pp. 379–397, 1964.
17. Wilcox, W. R., and T. J. La Chapelle: Mechanism of Gold Diffusion into Silicon, *J. Appl. Phys.*, vol. 35, pp. 240–246, 1964.
 18. Reiss, Howard, C. S. Fuller, and F. J. Morin: Chemical Interaction among Defects in Ge and Si, *Bell System Tech. J.*, vol. 35, pp. 535–636, 1956.
 19. Kaiser, W., and P. H. Keck: Oxygen Content of Silicon Single Crystals, *J. Appl. Phys.*, vol. 28, pp. 882–887, 1957.
 20. Kaiser, W., P. H. Keck, and C. F. Lange: Infrared Absorption and Oxygen Content in Silicon and Germanium, *Phys. Rev.*, vol. 101, pp. 1264–1268, 1956.
 21. Hrostowski, H. J., and R. H. Kaiser: Infrared Absorption of Oxygen in Silicon, *Phys. Rev.*, vol. 107, pp. 966–972, 1957.
 22. Kaiser, W., H. L. Frisch, and H. Reiss: Mechanism of the Formation of Donor States in Heat-treated Silicon, *Phys. Rev.*, vol. 112, pp. 1546–1554, 1958.
 23. Lederhandler, S., and J. R. Patel: Behavior of Oxygen in Plastically Deformed Silicon, *Phys. Rev.*, vol. 108, pp. 239–242, 1957.
 24. Schmidt, P. F., and R. Stickler: "Silicon Phosphide in Diffused Silicon," Late News Paper, Spring Meeting of the Electrochemical Society, 1964.
 25. Carruthers, J. R., R. B. Hoffman, and J. D. Ashner: X-ray Investigation of the Perfection of Silicon, *J. Appl. Phys.*, vol. 34, pp. 3389–3393, 1963.
 26. Queisser, H. J.: Slip Patterns on Boron-doped Silicon Surfaces, *J. Appl. Phys.*, vol. 32, pp. 1776–1780, 1961.
 27. Miller, D. P., J. E. Moore, and C. R. Moore: Boron Induced Dislocations in Silicon, *J. Appl. Phys.*, vol. 33, pp. 2648–2652, 1962.
 28. Dash, W. C.: Copper Precipitation on Dislocations in Silicon, *J. Appl. Phys.*, vol. 27, pp. 1193–1195, 1956.
 29. Schwuttke, G. H.: Study of Copper Precipitation Behavior in Silicon Single Crystals, *J. Electrochem. Soc.*, vol. 108, pp. 163–167, 1961.
 30. Goetzberger, A., and W. Shockley: Metal Precipitates in p-n Junctions, *J. Appl. Phys.*, vol. 31, pp. 1821–1824, 1960.
 31. Bemski, G.: Recombination Properties of Gold in Silicon, *Phys. Rev.*, vol. 111, pp. 1515–1518, 1958.
 32. Silverman, S. J., and J. B. Singleton: Technique for Preserving Lifetime in Diffused Silicon, *J. Electrochem. Soc.*, vol. 106, pp. 591–594, 1958.
 33. Ing, S. W., Jr., R. E. Morrison, L. L. Alt, and R. W. Aldrich: Gettering of Metallic Impurities from Planar Silicon Diodes, *J. Electrochem. Soc.*, vol. 110, pp. 533–537, 1963.
 34. Adamic, J. W., and J. E. McNamara: A Study of the Removal of Gold from Silicon Using Phosphorus and Boron Glass Getters, paper presented at the October, 1964, meeting of the Electrochemical Society.
 35. Waldner, M., and L. Sivo: Lifetime Preservation in Diffused Silicon, *J. Electrochem. Soc.*, vol. 107, pp. 298–301, 1960.

Author Index

In the following index the superscript number following the page number is the number of the reference in the list of references at the end of each chapter. Thus the entry Mellor, J. W., ²²³ indicates that J. W. Mellor is the author referred to on page 2 where the reference number occurs. The page numbers without superscript numbers are pages on which the author's name explicitly appears. Page numbers in italics are those of the list of references at the end of each chapter.

- Adamic, J. W., 262³⁴, 268
 Adcock, W. A., 125¹², 160
 Albert, M. P., 198²², 199, 211
 Aldrich, R. W., 262³³, 268
 Alexander, B. H., 213³, 233
 Alimbarashvili, N. A., 136³¹, 161
 Allen, F. G., 200²⁷, 200, 211
 Allen, R. B., 130¹⁷, 160
 Allen, T. B., 2⁶, 4, 17², 21–22¹⁴, 27
 Alt, L. L., 262³³, 268
 Amick, J. A., 62⁵², 77⁵², 80
 Anderson, H. C., 7²⁷, 10²⁷, 14²⁷, 15
 Anderson, R. E., 127¹³, 160, 185²⁹, 186
 Andrus, J., 203³⁸, 212
 Arayama, H., 10⁴⁹, 16
 Aries, R. S., 6²⁰, 15
 Armstrong, W. J., 146, 161
 Ashner, J. D., 259, 260²⁵, 268
 Atalla, M. M., 132–133, 160
 Austin, A. E., 135, 160
 Austin, L. W., 2, 4
- Baldrey, J. A., 76⁹⁵, 82
 Balluffi, R. W., 153⁶⁹, 162
 Bardeen, J., 136³², 161, 167–168, 185
 Barrier, R. M., 117², 159
 Bartlett, B. E., 58³⁴, 80
 Baruch, P., 154, 163
 Batdorf, R. L., 129¹⁶, 160
 Batsford, K. O., 75^{91,93}, 82
 Bean, K. E., 73, 82
 Becker, M., 27, 4, 188⁷, 191, 194⁷, 197, 210
 Belanovski, A. S., 158⁷⁵, 162
 Bemski, G., 262³¹, 268
 Bereznoi, A. S., 2⁵, 3, 9³⁹, 15, 241⁶, 255, 258, 261–262, 265, 267
 Berkova, A. V., 57³³, 80
 Bernstein, H., 130¹⁷, 160
 Bertrand, L., 13⁵⁹, 16
 Berzelius, J. J., 1, 5
 Bholá, S. R., 69⁸², 82
 Bicknell, R. W., 75⁹⁵, 78¹⁰⁵, 82–83
- Billig, E., 41²⁰, 79, 223³⁴, 234
 Bittmann, C. A., 64⁶³, 81
 Blackwell, G. R., 63⁵⁹, 81
 Blanc, J., 149, 161
 Bolger, D. E., 9³⁵, 15
 Bolling, G. F., 31³, 79
 Boltaks, B. I., 151⁶⁰, 157⁶⁰, 162, 166³, 169, 177, 185
 Boltzmann, L., 159
 Bond, W. L., 203³⁸, 212, 213^{1,23}, 233–234
 Booker, G. R., 233⁴⁹, 235, 253¹⁵, 267
 Borgeaud, P., 97
 Bose, J. C., 2, 4
 Bradley, R. R., 69, 82
 Bradshaw, 21¹⁸, 27
 Braslin, J., 231, 235
 Brattain, W. H., 3¹⁵, 4, 136³², 161
 Braun, I., 53²⁷, 54, 80
 Bridgeman, 33
 Britsyn, K. I., 205^{44,45}, 212
 Brixey, J., 148⁴⁴, 161
 Brockbank, C. J., 6¹⁴, 15
 Broder, 34⁸, 79
 Brooks, H., 166, 167, 177, 182³¹, 185–186
 Bube, R. H., 169, 189¹⁷, 196, 197¹⁷, 198, 200¹⁷, 211
 Buckley, H. E., 33–34⁵, 36–37⁵, 79
 Buehler, E., 3, 4, 23²⁴, 28, 62⁵⁴, 81, 115⁴, 116, 213¹, 233
 Buerger, M. J., 98¹¹, 102
 Bullis, W. M., 170
 Bullough, R., 249¹², 267
 Burton, J. A., 54²⁸, 80, 248¹¹, 267
 Bush, E. L., 10^{44,45}, 16
 Butler, K. H., 7–8³³, 15
 Bylander, E. G., 65⁷², 78^{109,110}, 81, 83
- Cahn, R. W., 98¹⁰, 102
 Carlson, R. O., 149, 151, 157⁷⁴, 161–162, 169
 Carmen, J. N., 64⁶³, 81
 Carruthers, J. A., 213¹⁹, 219, 234
- Carruthers, J. R., 259, 260²⁵, 268
 Carslaw, H. S., 117⁴, 159
 Caswell, E. G., 9⁴³, 16
 Cate, G., 60³⁹, 80
 Celmer, P. R., 21²⁰, 27
 Cerness, J. F., 21¹⁹, 27
 Chalmers, B., 59³⁷, 80
 Chapman, P. W., 167–168, 179, 185
 Charig, J. M., 68, 75⁹⁴, 78¹⁰⁵, 82–83
 Chaudhuri, A. R., 223³⁵, 224, 234
 Cholet, P. H., 205⁴², 212
 Chrenko, R. M., 191¹⁹, 211
 Christensen, H., 3²², 4, 37¹⁷, 65^{17,67}, 79, 81
 Chu, T. L., 75⁸⁹, 82
 Chynoweth, A. G., 202²⁹, 203, 211
 Clark, J. C., 97⁵, 102
 Cline, C. F., 149⁴⁷, 161
 Cline, J. E., 145³⁷, 148, 161
 Cole, R. L., 17⁵, 19⁹, 24^{5,25}, 27–28
 Collins, C. B., 149⁵², 161
 Collins, F. M., 77, 78⁹⁷, 82
 Combs, J. F., 198²², 199, 211
 Comrie, L. J., 142–143
 Conn, J. B., 7²⁹, 15
 Constantin, C., 154⁸¹, 163
 Conwell, E. M., 166, 185–186, 213⁶, 233
 Corbett, J. W., 191¹⁹, 211
 Cornelison, B., 125¹², 160
 Cowland, F. C., 10⁴⁶, 16
 Cox, T. J., 207^{46,49}, 212
 Cronmeyer, D. C., 179, 186
 Crouch, M. L., 3²⁰, 4, 7²⁸, 15, 37¹⁹, 65¹⁹, 68¹⁹, 79
 Czochralski, 34–35
- Dale, B., 209⁵⁰, 212
 Danielson, G. C., 422¹, 79, 213²⁰, 234
 D'Asaro, L. A., 146⁴⁰, 148⁴⁰, 161
 Dash, W. C., 3²¹, 4, 61⁴⁶, 62, 80, 187¹, 188, 203³⁷, 210, 212, 223³³, 233⁴⁶, 234–235, 261²⁸, 268

270 Author Index

- Davies, E. A., 172¹⁹, 180, 186
 Deal, B. E., 657³, 81
 Debye, P. P., 166⁷, 179¹⁴, 185–186
 De Chalmot, G., 6⁴, 14
 Dempster, J. T. H., 61³, 14
 Derick, L., 146, 149³⁹, 161
 Deville, S.-C., 2
 Dikhoff, J. A. M., 57³², 60³⁸, 80
 Ditzzenberger, J. A., 145^{36,38}, 146, 147, 148³⁸, 149, 151, 155–156, 161
 Donovan, R. P., 150, 152, 162
 Drickamer, H. G., 176²², 181, 186, 187³, 188, 210
 Duckworth, W. H., 223³⁶, 234
 Dunwoody, H. H. C., 2, 4
- Ebsworth, E. A. V., 7²⁶, 9²⁶, 15
 Egli, P. H., 33⁶, 79
 Elliott, J. F., 229⁴³, 235
 Ellis, R. C., 21¹⁵, 27
 Ellis, W. C., 65⁶⁵, 81, 100^{15,16,17}, 103
 Emeis, 3
 Emmons, R. B., 205⁴², 212
 Eringer, J., 6², 14
 Escoffery, C. A., 209⁵², 212
- Fabricius, E. D., 121⁸, 160
 Fageant, J., 100¹⁷, 103
 Fahrig, R. H., 35¹¹, 79
 Fan, H. Y., 2⁷, 4, 187⁵, 188⁷, 189^{5,18}, 190–191, 194⁷, 197, 210–211
 Faust, J. W., Jr., 97⁸, 102
 Feldman, W. L., 213³, 216, 222⁵, 233
 Fischer, J. L., 60⁴⁰, 80
 Fisher, J. C., 133²², 134, 160
 Fitch, F. T., 239², 241², 253, 267
 Flores, J. M., 179, 186
 Flubacher, P., 213⁹, 215, 233
 Flynt, W. E., 78¹⁰³, 83
 Forst, J. J., 182³⁰, 186
 Franchoy, R., 6⁵, 14
 Frisch, H., 257²², 268
 Frosch, D. J., 146, 149³⁹, 161
 Fuller, C. S., 136³⁰, 145^{36,38}, 146–147, 148³⁸, 149, 151, 155–156, 157^{72,73}, 159³⁰, 160–162, 241⁵, 253–254, 256¹⁸, 267–268
- Gallagher, C. J., 136²⁹, 160, 222³⁰, 234
 Gamble, F., 194²¹, 197, 211
 Gaulé, G. K., 48²⁴, 79, 231, 235
 Gavalier, J. R., 75⁸⁹, 82
 Gay-Lussac, J. L., 1, 5
 Geballe, T. H., 185, 186, 213¹⁹, 234
 Gee, A., 203³¹, 211
 Geld, 219
 Giardini, A. A., 203³⁵, 211, 213⁴, 225–226, 233
- Gibbons, D. F., 213¹², 217, 219¹², 225¹², 233
 Gilman, J. J., 225³⁸, 227, 235
 Giusto, M. B., 9–10⁴¹, 16
 Glang, R., 37, 68⁸⁰, 79, 82
 Glassbrenner, C. J., 213²², 219, 229, 234
 Gleim, P. S., 73, 82
 Goetzberger, A., 136²⁸, 149, 155, 160, 262³⁰, 268
 Goldberg, C., 97⁷, 102
 Golovin, B. I., 48²³, 79
 Gosling, D. S., 172¹⁹, 180, 186
 Gravel, C. L., 149, 161
 Green, G. W., 189¹², 193, 211
 Grieco, M. J., 68⁷⁹, 82, 247⁹, 267
 Griest, R. H., 17³, 27, 205⁴⁰, 212
 Gummel, H. K., 121⁷, 160
 Gupta, D. C., 166
- Haas, C., 159⁷⁷, 163
 Hale, A. P., 77⁹⁹, 82
 Hall, R. N., 57³⁰, 62⁵⁵, 80–81, 153⁶⁶, 157^{66,74}, 162, 164², 165, 169, 185, 254¹⁶, 267
 Hampel, C. A., 17¹, 27, 149⁴⁶, 161, 213⁸, 233
 Handelman, E. T., 78¹⁰², 83
 Hannay, N. B., 62⁵⁶, 81, 157⁷⁸, 159⁷⁸, 163, 182²⁸, 183–184, 186
 Hansen, M., 241³, 242–252, 254–267
 Hass, G., 207^{46,47,48,49}, 212
 Haus, J., 62⁴⁸, 80
 Hauskrecht, T., 7³¹, 15
 Haynes, J. R., 202, 211
 Heaps, J. D., 78¹⁰⁸, 83
 Heldt, L. A., 153⁶⁸, 162
 Herrick, C. S., 105^{2,53}, 136², 16
 Herring, 166–167, 177
 Herrmann, W., 188⁸, 204⁸, 206, 207⁸, 208, 210, 222³², 229³², 234
 Hicks, J., 17⁵, 24⁵, 27
 Hillegas, W. J., Jr., 76⁹⁶, 82
 Hilton, A. R., 188⁶, 190, 194²¹, 197, 198⁶, 199, 210–211
 Hino, J., 19⁷, 27
 Hobstetter, J. N., 153⁶⁸, 162
 Hochman, R. F., 225³⁹, 235
 Hoffman, R. B., 259, 260²⁶, 268
 Hogarth, C. A., 189¹², 193, 211
 Homan, C. H., 61⁵, 15
 Honess, A. P., 97⁹, 102
 Honig, R. E., 213⁷, 215, 218, 233
 Horiuchi, S., 132²⁰, 160
 Horn, F. H., 62^{49,50}, 63⁴⁹, 80
 Hornstra, J., 203³⁹, 212
 Howard, B. T., 155⁸³, 163
 Howard, K., 253¹³, 267
 Hrostowski, H. J., 189^{11,16}, 196, 210–211, 256²¹, 268
 Hsüeh Shih-yin, 151⁶⁰, 157⁶⁰, 162, 166⁵, 169, 177, 185
 Hubner, K., 135, 160
 Hull, G. W., 185, 186
- Hulme, K. F., 57³¹, 80
 Hunt, W. F., 84¹, 85, 102
 Hurler, D. T. J., 58³⁵, 80
 Hust, J. G., 213¹⁸, 219, 234
 Hysell, R. E., 229⁴³, 235
- Ing, S. W., Jr., 262³³, 268
 Irvin, J. C., 105¹, 106–107, 116, 158, 163
 Irvine, J. W., Jr., 12⁵⁵, 16
- Jaccodine, R. J., 154, 163, 229⁴², 235
 Jackson, K. A., 59³⁷, 80
 Jackson, W. B., 11⁵⁴, 16
 Jacobus, G. F., 207⁴⁹, 212
 Jaeger, J. C., 117⁴, 159
 James, W. J., 97
 Jenny, D. A., 203³⁰, 211
 Jensen, R. V., 21²⁰, 27
 Johnson, F. A., 188⁹, 189¹², 192–193, 210–211
 Johnson, L. R., 33⁶, 79
 Johnson, S., 9–10⁴¹, 16
 Jones, C., 188⁶, 190, 198⁶, 199, 210
 Jones, L., 229³², 231², 233–234
 Jones, R. V., 62⁵¹, 80
 Jost, W., 117–118³, 121–122³, 124³, 136³, 141³, 154³, 159
 Joyce, B. A., 68–69, 75⁸⁴, 78¹⁰⁵, 82–83
 Joyce, B. D., 76⁹⁵, 82
- Kahng, D., 69–70⁸⁴, 82
 Kaiser, R. H., 189^{11,16}, 196, 210–211, 256²¹, 268
 Kaiser, W., 18, 27, 189^{10,13}, 193–194, 203³², 210–211, 256^{19,20}, 257²², 268
 Kataoka, Y., 77⁹⁸, 82
 Keck, P. H., 3, 18, 27, 34⁸, 35, 79, 189^{10,13}, 193–194, 203³³, 210–211, 213²⁴, 234, 256^{19,20}, 268
 Kelly, K. K., 213¹⁰, 215, 233
 Kesperis, J. S., 148, 161
 Kessler, J. O., 149, 161
 Kilgore, B. F., 77¹⁰¹, 83
 Killoran, D. R., 140³⁵, 161
 King, G., 9⁴⁰, 15
 Kingery, W. D., 226⁴⁰, 235
 Kleimack, J. J., 3²², 4, 65⁶⁷, 81
 Klein, C. A., 179, 186
 Kodera, H., 56, 57, 59, 80
 Koenigsberger, 219
 Kohane, T., 179, 186
 Kolbe, C. L., 229⁴³, 235
 Krag, W. E., 179, 186
 Kraus, E. H., 84¹, 85, 102
 Krchma, I. J., 9^{36,38}, 15
 Kriebler, J. G., 10⁵³, 16
 Kruse, P. W., 205⁴³, 212
 Kucher, T. I., 129¹⁵, 160
 Kuczynski, G. C., 225³⁹, 235
 Kuprovsky, 219
 Kurtz, A. D., 130¹⁷, 149, 156⁸⁴, 160–161, 163

- Kushner, L. M., 35¹², 79
 Kyropoulas, 34
- La Chapelle, T. J., 153⁶⁵, 157–158⁶⁵, 162, 256¹⁷, 268
 Lang, G. A., 73, 82
 Lange, C. F., 189¹⁰, 193, 210, 256²⁰, 268
 Lange, L. F., 18⁶, 27
 Larrabee, G., 20
 Lasser, M. E., 205⁴², 212
 Lavoisier, A. L., 1
 Leadbetter, A. J., 213⁹, 215, 233
 Lederhandler, S. R., 203³⁹, 212, 233⁴⁷, 235, 259²³, 268
 Lenusky, 88
 Leverton, W. F., 63^{57,58}, 81
 Levin, 34⁸, 79
 Lewis, C. H., 9–10⁴¹, 16
 Lewis, E. D., 7²³, 15
 Li, C. H., 65⁷¹, 81
 Lieberman, 34⁸, 79
 Lindberg, O., 169
 Little, J. B., 3, 31, 34⁷, 79
 Litton, F. B., 7²⁷, 10²⁷, 14²⁷, 15
 Loar, H. H., 3²², 4, 65⁶⁷, 81
 Logan, R. A., 213²³, 234
 Long, D., 167–168, 179, 185–186
 Lothrop, R. P., 149, 161
 Luft, W., 209⁵², 212
 Lyon, D. W., 7²³, 15
- McAleer, W. J., 65⁷⁷, 81
 MacCullough, G. H., 221
 McDonald, R. S., 191¹⁹, 211
 MacFarlane, G. G., 187⁴, 189, 210
 McGlauchlin, L. D., 205⁴³, 212
 MacHalske, F. J., 61⁶, 15
 McKay, K. G., 202²⁹, 203, 211
 Mackintosh, I. M., 151, 155, 162
 McLaughlin, W. A., 63⁶², 81
 McLean, T. P., 187⁴, 189, 210
 McNamara, J. E., 262³⁴, 268
 Macphee, M., 9³⁵, 15
 McSkimin, H. J., 213¹, 233
 Maekawa, S., 151, 162
 Maissel, L., 213¹³, 219¹³, 225¹³, 234
 Maita, J. P., 164¹, 165, 179, 185
 Malkovich, R. Sh., 136³¹, 161
 Mamasevity, H. M., 78¹⁰⁴, 83
 Manson, S. S., 226⁴¹, 235
 Manz, R. C., 69–70⁸⁴, 82
 Marcel, P., 13⁶¹, 16
 Margerum, E. A., 62⁵², 77⁵², 80
 Mark, A., 65⁶⁹, 81
 Martin, J. J., 213²¹, 219, 234
 Mason, R. W., 8³⁴, 15
 Mason, W. P., 182³⁰, 186
 Matano, 159
 Matare, H. F., 63⁶⁰, 81
 Maverick, E. F., 3²⁰, 4, 7²⁸, 15, 37¹⁹, 65¹⁹, 68¹⁹, 79
 Maycock, P. D., 42²¹, 79, 213²⁰, 234
- Mayer, A., 69⁸², 82
 Mayer, S. E., 69–70⁸³, 82
 Medcalf, W. E., 35¹¹, 79
 Mellor, J. W., 2²³, 4, 5¹, 7¹, 14
 Mendelson, S., 75⁹⁰, 82
 Menzel, D. H., 218²⁷, 221²⁷, 234
 Messier, J., 179, 186
 Milford, F. J., 135, 160
 Miller, D. P., 75⁸⁸, 82, 253¹³, 261²⁷, 267–268
 Miller, K. J., 68⁷⁹, 82, 247⁹, 267
 Miller, R. C., 123¹¹, 124, 146, 156, 160–161, 163
 Mil'vidskii, M. G., 48²³, 57³³, 79–80
 Minamiya, J., 10⁴⁹, 16
 Minomura, S., 176²², 181, 186
 Mitchell, G. A., 17⁵, 24^{5,25}, 27–28
 Mitchell, M. M., 78¹⁰⁹, 83
 Moats, G. H., 11⁵⁴, 16
 Moll, J. L., 254
 Monchamp, R. R., 65⁷⁷, 81
 Moore, C. R., 75⁸⁸, 82, 261²⁷, 268
 Moore, J. E., 261²⁷, 268
 Morin, F. J., 157⁷², 162, 164¹, 165, 179, 185, 254, 256¹⁸, 268
 Morris, R. G., 213^{18,21}, 219, 234
 Morrison, J. A., 213⁹, 215, 233
 Morrison, R. E., 262³³, 268
 Mortimer, G. D., 61⁴², 80
 Moss, T. S., 176²¹, 185²¹, 186
 Mullin, J. B., 57³¹, 80
 Murphy, R. J., 78¹¹⁰, 83
 Myers, J., 179, 186
 Mytton, R. W., 21¹⁶, 27
- Nacken, 34
 Nasby, R., 170
 Nelson, H., 64⁶⁴, 81
 Newman, R. C., 78¹⁰⁶, 83, 149, 158⁴⁸, 161, 187–188, 189^{14,15}, 195, 210–211, 249¹², 253¹⁴, 267
 Nicholson, K. C., 21¹⁷, 27
 Nussbaum, A., 78¹⁰⁸, 83
 Nuttall, R., 70⁸⁵, 82
- O'Connor, J. R., 63⁶², 81
 Oda, J., 247¹⁰, 267
 Ohl, R. S., 3¹⁶, 4
 Okura, K., 10⁴⁹, 16
 Oliphint, J. B., 224³⁷, 234
 Olson, C. M., 7²³, 7–8³³, 93^{6,37}, 13⁵⁹, 15–16
 Olt, R. D., 200²⁴, 201, 211
 Oualline, C. M., 24²⁵, 28
 Owen, A. E., 151, 162
- Parker, R. L., 35¹², 79
 Pastore, J. R., 48²⁴, 79, 231, 235
 Patel, J. R., 223³⁵, 224, 234, 259²³, 268
 Pauls, G., 13⁵⁸, 16
 Pearson, G. L., 3¹⁵, 4, 167–168, 185, 213^{5,11}, 216, 222⁵, 233
 Peavler, 88
- Pell, E. M., 157⁷⁴, 162, 169
 Penhale, L. G., 10⁴⁶, 16
 Penning, P., 203³⁶, 212
 Petritz, R. L., 3¹⁹, 4, 35¹⁰, 79
 Petrow, D. A., 158⁷⁵, 162
 Pfann, W. G., 34–35, 38, 50²⁶, 51–53, 64⁹, 79–80, 108³, 109, 116, 182²⁴, 186, 242⁸, 267
 Pfister, J. C., 154⁸¹, 163
 Philipp, H. R., 187, 198, 200, 210
 Phillips, C. J., 1², 3
 Pickard, G. W., 2, 4
 Pietenpol, W. J., 3¹⁸, 4
 Pietruszkiewicz, A. J., 241⁵, 253, 267
 Pohl, F. A., 7³¹, 15
 Poindexter, E., 203³⁴, 211
 Pollak, P. I., 65⁷⁷, 81
 Potter, H. N., 6^{8,19}, 14–15
 Potter, R. F., 200²⁵, 201, 211
 Povilonis, E. I., 78¹⁰², 83
 Prim, R. C., 54²⁸, 80
 Prussin, S. A., 233⁴⁸, 235
- Quarrington, J. E., 187⁴, 189, 210
 Queisser, H. J., 135, 136^{26,27}, 149, 155, 160, 261²⁶, 268
- Racette, J. H., 153⁶⁶, 157⁶⁶, 162, 164², 165, 185, 254¹⁶, 267
 Ramdas, A. K., 189¹⁸, 211
 Ramsdell, L. S., 84¹, 85, 102
 Rasmanis, E., 78^{111,112}, 83
 Ratcliff, G., 120⁹, 160
 Read, W. T., Jr., 213⁵, 216, 222⁵, 233
 Reiss, H., 241⁵, 253–254, 256¹⁸, 257²², 267–268
 Rhines, F. N., 236¹, 267
 Rice, W. R., 127¹⁴, 128, 160
 Richard, M., 77¹⁰⁰, 82
 Riney, T. D., 221²⁸, 234
 Riser, H., 165–167
 Roberts, R. W., 77¹⁰¹, 83
 Roberts, V., 187⁴, 189, 210
 Rosenberg, A. M., 213¹⁹, 219, 234
 Rosenberger, G., 7³², 15
 Ross, J. W., 60⁴⁰, 80
 Roth, E. A., 62⁵², 77⁵², 80
 Royer, M. L., 3
 Rubin, B., 11⁵⁴, 16
 Rummel, T., 13⁹⁴, 16
 Runyan, W. R., 17⁴, 24^{4,26}, 27–28, 43²², 46, 60⁴⁰, 70⁷⁴, 79–81, 229³², 231², 233–234
 Ruoff, A. L., 153⁶⁹, 162
 Rusler, G. W., 61⁴¹, 80
 Rutter, J. W., 59³⁷, 80
- Sah, C. T., 130¹⁸, 132¹⁸, 160
 Saintesprit, R., 154⁸¹, 163
 Salkowitz, E. I., 100¹⁴, 103
 Salzberg, C. D., 198, 199, 200, 207⁴⁷, 211–212
 Sangster, R. C., 3, 4, 7²⁸, 14⁶⁵, 15–16, 37¹⁹, 65¹⁹, 68¹⁹, 79

272 Author Index

- Saratovkin, D. D., 291, 78
 Sargeant, 211⁸, 27
 Sauveur, 36
 Savage, A., 146, 161
 Scace, R. I., 201³, 27, 241⁴, 246, 267
 Scaff, 3
 Schaefer, H., 146⁶, 16
 Schaschkow, J. M., 158⁷⁵, 162
 Scheid, B., 61¹, 14
 Schmidt, P. F., 151, 162, 259²⁴, 268
 Schmidt, W., 6³, 14
 Schnable, G. L., 76⁹⁶, 82
 Schweickert, H., 62^{47,48}, 80
 Schwuttke, G. H., 75⁹², 82, 97⁶, 102, 203³³, 211, 261²⁹, 268
 Scott, T. R., 94⁰, 15
 Seed, R. G., 145³⁷, 148, 161
 Seitz, F., 222³¹, 234
 Selker, M. L., 211⁹, 27
 Sello, H., 130¹⁸, 132¹⁸, 160
 Severiens, J. C., 136³⁰, 157⁷³, 159³⁰, 160, 162
 Shanks, H. R., 422¹, 79, 213²⁰, 219, 234
 Shea, D. E., 69–70⁸³, 82
 Shepherd, W. H., 222¹, 27
 Sherer, J. B., 231–232
 Shewmon, P. G., 117¹, 134, 153–154¹, 159
 Shields, J., 174²⁰, 180, 186
 Shockley, W., 201¹, 27, 49²⁵, 62⁵¹, 79–80, 88⁴, 90, 102, 135, 136^{32,33}, 160–161, 254, 262³⁰, 268
 Shortes, S. R., 151, 162
 Sidles, P. H., 422¹, 79, 213²⁰, 234
 Sils, V., 75⁹², 82
 Silverman, S. J., 262³², 268
 Simpson, W. I., 78¹⁰⁴, 83
 Singleton, J. B., 262³², 268
 Sivo, L., 267³⁵, 268
 Slack, G. A., 201³, 27, 213²², 219, 229, 234, 241⁴, 246, 267
 Slawson, C. B., 99–100¹², 102
 Slichter, W. P., 54²⁸, 80
 Slykhouse, T. E., 187³, 188, 210
 Smith, A. M., 150, 152, 162
 Smith, C. S., 179²³, 186
 Smith, R. A., 167⁹, 169¹⁰, 184, 185²⁷, 186
 Smith, R. C. T., 123, 144, 160
 Smith, R. W., 226⁴¹, 235
 Smith, W. E., 62¹, 15
 Smits, F. M., 118⁵, 123¹¹, 124, 129¹⁶, 155⁵, 160, 163
 Smotko, J. S., 72⁴, 15, 222²⁹, 234
 Smythe, R. L., 148⁴⁴, 161
 Sobey, A. E., 182, 186
 Sosman, R. B., 1³, 3
 Sparks, M., 61⁴³, 80
 Spitzer, W., 187⁵, 189⁵, 190, 210
 Sproul, W. T., 94
 Star, N., 135⁹, 16
 Stauffer, R. A., 125⁶, 16
 Stavish, T., 73, 82
 Steinmaier, W., 65⁷⁶, 81
 Stello, P. E., 17³, 21¹⁶, 27, 64⁶³, 81, 205⁴⁰, 212
 Sterling, H. F., 104^{44,45}, 16, 22²³, 28, 61⁴⁵, 62, 80–81
 Stickler, R., 233⁴⁹, 235, 253¹⁵, 259²⁴, 267–268
 Stierwalt, D. L., 200²⁵, 201, 211
 Stirland, D. J., 75⁹⁴, 78¹⁰⁵, 82–83
 Stock, A. E., 7²⁵, 15
 Stockbarger, D. C., 191⁰, 27, 33
 Storks, K. H., 37¹⁶, 79
 Strack, H., 154⁷⁰, 162
 Stratton, J. A., 205
 Straub, W. D., 179, 186
 Straumanis, M. E., 97
 Strauss, H. E., 197, 27
 Struthers, J. D., 149^{49,50}, 157⁵⁰, 161
 Stuckes, A. D., 213¹⁵, 219, 234
 Sutton, J. R., 100¹³, 103
 Swalin, R. A., 153⁶³, 162
 Sylwestrowicz, W. D., 214, 223, 234
 Szekely, G., 10⁵¹, 16
 Taft, E. A., 187, 198, 200, 210
 Tammann, 33
 Tanenbaum, M., 61⁴⁴, 80
 Tannenbaum, E., 132–133, 155–156, 160, 162
 Teal, G. K., 3, 4, 31, 34, 37^{18,17}, 62⁵⁴, 63⁶¹, 65¹⁷, 79, 81, 115⁴, 116, 213¹, 233
 Thelen, A., 209⁵¹, 212
 Thénard, 1, 5
 Theuerer, H. C., 3, 4, 7³⁰, 15, 19⁸, 27, 65^{67,68}, 81
 Thomas, C. O., 69–70⁸⁴, 82
 Thomas, D. J. D., 75^{91,93}, 82
 Thompson, J. C., 213¹⁷, 219, 234
 Thornton, C. G., 76⁹⁶, 82
 Thur, R. E., 36¹⁴, 77¹⁴, 79
 Thurmond, C. D., 7²², 15, 253
 Thurston, N., 182²⁴, 186
 Tiller, W. A., 31³, 59³⁷, 79–80
 Tompkins, B. E., 149, 161
 Tone, F. J., 6^{8,10,12}, 14
 Tornillo, L. M., 182³⁰, 186
 Torrey, H. C., 31⁴, 4, 61⁷, 15
 Trainor, A., 58³⁴, 80
 Tremere, D. A., 130¹⁸, 132¹⁸, 160
 Treuting, R. G., 31⁴, 79, 100¹⁸, 103, 213¹¹, 233
 Trumbore, F. A., 18, 108², 116, 241⁷, 266–267
 Tsai, J. C. C., 131, 132¹⁹, 146¹⁹, 160
 Tuft, O. N., 167–168, 179³, 185
 Tung, S. K., 65^{70,75}, 67⁷⁵, 81
 Tuttle, O. N., 78¹⁰⁸, 83
 Twyman, F., 233
 Udy, M. J., 6⁹, 14
 Uhler, A., 232⁴⁵, 235
 Unvala, B. A., 36¹³, 77¹³, 79
 Van Arkel, A. E., 37, 79
 Van Horn, W., 213²⁴, 234
 Vavilov, V. S., 205^{44,45}, 212
 Verneuil, 34–35
 Via, G. G., 361⁴, 77¹⁴, 79
 Villa, J. J., 198, 199, 200, 211
 Von Batchelder, F. W., 100¹⁴, 103
 Voos, W., 61⁸, 15
 Wackwitz, R. C., 123⁹, 139–140³⁴, 160–161, 166
 Wagner, R. S., 31⁴, 65⁶⁵, 79, 81
 Wajda, E. S., 37, 68⁸⁰, 79, 82
 Wakefield, J., 78¹⁰⁶, 83, 149, 158⁴⁸, 161, 249¹², 253¹⁴, 267
 Waldner, M., 267³⁵, 268
 Wang, C. C., 213³, 233
 Wang, E. Y., 53²⁷, 54, 80
 Ware, R. M., 222², 27
 Warmoltz, N., 159⁷⁶, 162
 Warren, R. W., 22²³, 28, 62⁵³, 81
 Watelski, S. B., 75⁸⁸, 82, 136²⁸, 160, 165–167, 181
 Watkins, G. D., 191¹⁹, 211
 Weinreich, O. A., 203³³, 211
 Weiser, K., 153⁶⁴, 162
 Weiss, 219
 Weisskopf, V. F., 166, 186
 Westbrook, J. H., 225³⁸, 227, 235
 Westphal, W. C., 202, 211
 Whipple, R. T. P., 133²³, 134–135, 160
 White, G. K., 213¹⁴, 219, 234
 Whitmer, C. A., 31⁴, 4, 61⁷, 15
 Widmer, H., 153⁶⁷, 162
 Wieringen, A. V., 159⁷⁶, 162
 Wilbur, J. M., Jr., 97⁵, 102
 Wilcox, W. R., 153⁶⁵, 157–158⁶⁵, 162, 256¹⁷, 268
 Williams, E. L., 147, 156, 161
 Willis, J. B., 249¹², 267
 Willmore, J. M., 213², 223–224², 231², 233
 Wilson, J. M., 94⁰, 15
 Wolff, G. A., 97⁵, 102
 Wolfstirn, K. B., 149⁴⁹, 161, 179, 186
 Wood, E. A., 86³, 88³, 102
 Wood, V. E., 135²⁵, 160
 Woods, S. B., 213¹⁴, 219, 234
 Wurst, E. C., 151, 162
 Wyckoff, R. W. G., 86², 87, 88², 102
 Wynne, R. H., 97⁷, 102
 Yamaguchi, J., 132²⁰, 160
 Yatsko, R. S., 148, 161
 Yee, R., 156, 163
 Yodis, A. W., 83⁴, 136⁰, 15–16
 Younglove, B. A., 213^{16,17}, 219, 220¹⁶, 234
 Zeffoss, S., 33⁶, 79
 Ziegler, G., 115⁵, 116
 Ziman, J. M., 213¹⁹, 234
 Zook, J. D., 167–168, 179³, 185

Subject Index

- Absorption coefficient, 187
 - near band edge, 189
 - effect of neutrons on, 197
 - lattice, 192
 - due to mechanical damage, 194, 197
 - for n-type, 190
 - due to n-type impurities, 196
 - due to oxygen, 194
 - for p-type, 191
 - due to p-type impurities, 195
 - of polycrystalline material, 204
 - due to radiation damage, 189
 - vs. temperature, 191–192
 - vs. wavelength, 188–192
- Acceptor levels, 169
- Activation energy, 169
- Alloys (*see* Phase diagrams; also individual elements)
- Aluminum, activation energy, 169
 - diffusion coefficient, 156
 - methods for adding to melt, 112
 - methods for diffusing, 146
 - misfit ratio, 259
 - optical absorption spectrum, 195
 - precipitates, 249
 - as reducing agent, 6
 - segregation coefficient, 108
 - silicon phase diagram, 242
 - solid solubility of, 266
- Aluminum oxide, 249
- Ambit casting, 24
- Amorphous silicon, 2, 5
- Antimony, activation energy, 169
 - diffusion coefficient, 155
 - methods for adding to melt, 113
 - methods for diffusing, 146
 - misfit ratio, 259
 - optical absorption spectrum, 196
 - precipitates, 253
 - segregation coefficient, 108
 - silicon phase diagram, 243
 - solid solubility of, 266
 - strain produced by, 260
- Antireflectance coatings, 205
- Arsenic, activation energy, 169
 - diffusion coefficient, 155
 - methods for adding to melt, 114
 - methods for diffusing, 146
 - misfit ratio, 259
 - optical absorption spectrum, 196
- Arsenic, segregation coefficient, 108
 - silicon phase diagram, 244
 - solid solubility, 266
- Autodoping, 69
- Avalanche, 173
- Avalanche breakdown voltage, 174, 180–181
- Beryllium, 20
 - silicon phase diagram, 244
- Birefringence, 203, 233
- Bismuth, diffusion coefficient, 155
 - methods for diffusing, 147
 - optical absorption spectrum, 196
 - segregation coefficient, 108
 - silicon phase diagram, 245
 - solid solubility, 266
- Boiling point, 213
- Boltzmann-Matano method, 159
- Bond strength, 229
- Boron, activation energy, 169
 - diffusion coefficient, 153, 156
 - effect on resistivity, 110
 - as getter, 262
 - lattice damage, 260
 - methods for adding to melt, 113
 - methods for diffusing, 147
 - misfit ratio, 259
 - optical absorption spectrum, 195
 - segregation coefficient, 108
 - solid solubility, 266
 - strain produced by, 260
- Boron nitride, 21
- Box diffusion, 146
- Breaking strength, 213, 223
- Bulk modulus, 213
- Calcium-silicon phase diagram, 245
- Carbon, diffusion coefficient, 158
 - in epitaxial layers, 75
 - methods for diffusing, 149
 - precipitates, 253
 - segregation coefficient, 20
 - silicon phase diagram, 246
 - solubility, 253
- Carriers, absorption due to, 187
 - intrinsic concentration, 165
 - table of terminology, 166
 - (*See also* Mobility; Resistivity)
- Casting, ambit, 24
 - perfection, 17

274 Subject Index

- Casting, techniques, 17
 - Cerium-silicon phase diagram, 247
 - Chromium-silicon phase diagram, 247
 - Closed-tube diffusion, 145
 - Coatings, high-emissivity, 209
 - low-reflectance, 205
 - optical, 205
 - Cobalt, segregation coefficient, 108
 - silicon phase diagram, 248
 - solid solubility, 266
 - Columbium (*see* Niobium-silicon phase diagram)
 - Compensation, 65, 105, 166
 - Complexing agents, 7
 - Compliance coefficient, 217
 - Conduction (*see* Mobility; Resistivity; Thermal conductivity)
 - Congruent transformations, 241
 - Constitutional supercooling, 58
 - Conversion tables, 183, 195
 - Copper, activation energy, 169
 - decoration with, 256, 261
 - diffusion coefficient, 157
 - gettering, 262
 - interstitial solubility, 255
 - methods for diffusion, 149
 - precipitation, 256, 261
 - segregation coefficient, 108
 - silicon phase diagram, 249
 - solid solubility, 266
 - substitutional solubility, 254
 - Critical pressure, 213
 - Critical temperature, 213
 - Crystal growth, categories, 29
 - closed-tube, 37
 - Czochralski, 34
 - distribution of impurities during, 50
 - effect on, of spin, 46
 - of surface tension, 48
 - epitaxial, 3, 65
 - float zone, 35
 - Kyropoulas, 34
 - from melt, 32
 - solution epitaxy, 63
 - by strain, 36
 - Teal-Little, 38
 - Van Arkel, 37
 - from vapor, 65
 - Verneuil, 34
 - VLS, 65
 - zone leveling, 34
 - Crystal systems, 84

 - Debye temperature, 215
 - Defects, decoration of, 261
 - dislocations, 75, 153, 223, 233
 - during epitaxial growth, 75
 - grain boundaries, 101
 - lineage, 102
 - slip, 223, 261
 - stacking faults, 75, 136
 - twins, 101
 - Deformation, plastic, 222
 - Dendrites, 8, 12, 31
 - Density, 213
 - Deposition, electrolytic, 37
 - Dielectric constant, 185

 - Diffusion, box, 146
 - closed-tube, 145
 - from concentration step, 124
 - during epitaxial growth, 128
 - along grain boundaries, 133
 - graphical solutions, 137
 - from infinite source, 118
 - under influence of field, 136
 - from limited source, 122
 - mechanisms, 151
 - with moving boundary, 127, 129
 - multiple, 120, 123, 126
 - open-tube, 145
 - through oxide, 131
 - processes, 141
 - with rate limitation, 123
 - into thin section, 121
 - Diffusion coefficients, carbon, 158
 - copper, 157
 - effect on, of dislocations, 153
 - of orientation, 154
 - of vacancies, 153
 - germanium, 158
 - helium, 159
 - hydrogen, 159
 - interstitial gold, 157
 - iron, 157
 - lithium, 157
 - measurement of, 154
 - n-type, 155
 - oxygen, 159
 - p-type, 156
 - phosphorus, 156
 - silicon self-diffusion, 158
 - silver, 157
 - substitutional gold, 158
 - sulfur, 157
 - zinc, 157
- Dislocations, 75, 153, 223, 233
- Donor levels, 169
- Doping, 110
 - by aluminum, 112
 - from aluminum oxide, 20
 - by antimony, 113
 - by arsenic, 114
 - auto-, 69
 - from beryllium oxide, 20
 - by bismuth, 113
 - by boron, 113
 - from boron nitride, 21
 - effect of residual boron, 110
 - by gallium, 110
 - by indium, 110
 - by oxygen, 18
 - by phosphorus, 114
 - from silicon nitride, 21
 - (*See also* Impurities; Segregation coefficients)
- Drift mobility, 168
-
- Effective mass, 183
- Elastic constant, 213–214
- Electrochemiluminescence, 203
- Electrolytic deposition, 37
- Electron mobility, 177, 179
- Electrons (*see* Carriers)

- Emission, light, 200
 Emisivity, 200
 Emitter push, 154
 Energy bands, 182
 Epitaxy, 3, 64–65, 78
 Error function, 141–142
 Etching, 72, 98, 101
 Eutectic system, 237
 Eutectoid system, 238
- Faceting, 57
 Ferrosilicon, 2, 5
 Fick's law, 117
 Float-zone method, 3, 35
 Fracture stress, 214, 222
 Fusion, heat of, 2, 40, 213
- Gallium, activation energy, 169
 diffusion coefficient, 156
 methods for adding to melt, 110
 methods for diffusing, 149
 misfit ratio, 259
 optical absorption spectrum, 195
 segregation coefficient, 108
 -silicon phase diagram, 250
 solid solubility, 266
 as solvent, 63
- Gettering, 262
 Germanium-silicon, alloys, 247
 epitaxy, 78
 phase diagram, 250
- Glassy layer, 122
 Glassy source, 118
- Gold, activation energy, 169
 diffusion coefficient, 157–158
 effect on resistivity, 166
 interstitial solubility, 256
 methods for diffusion, 149
 methods for gettering, 262
 segregation coefficient, 108
 -silicon phase diagram, 251
 solid solubility, 266
 as solvent, 65
 substitutional solubility, 256
- Gradient freezing, 3
 Grain boundary, 101, 133
 Grinding, 210, 232
 Blanchard, 210
 optical, 210
 (*See also* Lapping; Polishing)
- Growth rate, maximum, 41
 Gummel number, 121
- Hall coefficient, 169
 Hall mobility, 169, 180
 Hardness, 213, 225
 Heat, of fusion, 2, 40, 213
 of sublimation, 215
 of vaporization, 213
 Heat capacity, 215
 Heat content, 215
 Helium, diffusion coefficient, 159
 Hole mobility, 177, 179
 Holes (*see* Carriers)
 Hot forming, 229
 Hydrogen, diffusion coefficient, 159
- Hydrogen, as reducing agent, 12, 65
 Hypereutectic, 237
 Hypoeutectic, 237
- Impact testing, 224
 Impurities, compensation of, 65, 105, 166
 conduction due to, 104, 164
 distribution of, after normal freeze, 50
 after zone pass, 51
 effect on mobility, 166
 limiting distribution, 51
 mobility of, 136
 (*See also* Doping; Segregation coefficient)
- Impurity striations, 59
 Index of refraction, 198–200
 Indium, activation energy, 169
 diffusion coefficient, 156
 methods for diffusing, 149
 optical absorption spectrum, 195
 segregation coefficients, 108
 -silicon phase diagram, 251
- Infrared modulators, 205
 Infrared optical elements, 2, 204
 Infrared transmissivity (*see* Absorption coefficient)
- Iron, activation energy, 169
 diffusion coefficient, 157
 methods for diffusion, 149
 segregation coefficient, 108
 -silicon phase diagram, 252
 solid solubility, 266
- Isomorphous phase system, 236
 Izod test, 224
- Junction depth, 119
- Lapping, 231
 (*See also* Grinding; Polishing)
- Latent heat, of fusion, 2, 40, 213
 of vaporization, 213
- Lattice mobility, 167
 Lead-silicon phase diagram, 253
 Levitation, 22, 62, 77
 Light emission, 200
 Light figures, 99
 Limited source, 122
 Lineage, 102
 Lithium, activation energy, 169
 complex formation, 256
 diffusion coefficient, 157
 methods for diffusing, 144
 segregation coefficient, 108
 -silicon phase diagram, 253
 solid solubility, 266
- Magnesium-silicon phase diagram, 254
 Manganese, activation energy, 169
 methods for diffusing, 149
 -silicon phase diagram, 255
 solid solubility, 266
- Mask failure, 133
 Masking, 76
 Mass, effective, 183
 Mass transport (autodoping), 69
 Mechanical damage, 194, 222, 233
 Melting point, 213

- Mercury-silicon phase diagram, 255
 Miller indices, 84
 Minority carriers (*see* Carriers)
 Misfit ratio, 259
 Mobility, 166
 compensated, 167
 drift, 168
 electron, 177, 179
 Hall, 169
 hole, 177, 179
 impurity, 166, 178
 lattice, 167
 ratio, 177
 ratio of Hall to conductivity, 180
 uncompensated, 167
 variation with electric field, 180
 Modulators, 205
 Modulus, bulk, 213
 of compression, 219
 of rigidity, 220
 of rupture, 213
 shear, 220
 Young's, 213, 218, 221
 Molybdenum, as sheath, 230
 -silicon phase diagram, 256
 Monotectic system, 238
- Nickel-silicon phase diagram, 257
 Niobium-silicon phase diagram, 258
- Open-tube diffusion, 145
 Optical coatings, 205
 Optical coefficients, stress, 203
 Optical elements, 204
 Optical grinding, 210
 Optical orientation, 97
 Optical polishing, 210
 Optical transmissivity (*see* Absorption coefficient)
 Orientation, optical, 97
 rough, 93
 X-ray, 94
 Oxygen, diffusion coefficient, 159
 effect on electrical properties, 256
 optical absorption spectrum, 193–194
 scattering due to, 203
 segregation coefficient, 18
 -silicon complexes, 256
 -silicon phase diagram, 258
 solubility limit, 18
- “Paint-on” source, 145
 Palladium-silicon phase diagram, 259
 Peritectic system, 239
 Peritectoid system, 241
 Phase diagrams, aluminum-silicon, 242
 antimony-silicon, 243
 arsenic-silicon, 244
 beryllium-silicon, 244
 bismuth-silicon, 245
 calcium-silicon, 245
 carbon-silicon, 246
 cerium-silicon, 247
 chromium-silicon, 247
 cobalt-silicon, 248
 copper-silicon, 249
 germanium-silicon, 250
 gold-silicon, 251
 indium-silicon, 251
 iron-silicon, 252
 lead-silicon, 253
 lithium-silicon, 253
 magnesium-silicon, 254
 manganese-silicon, 255
 mercury-silicon, 255
 molybdenum-silicon, 256
 nickel-silicon, 257
 niobium (columbium)-silicon, 258
 oxygen-silicon, 258
 palladium-silicon, 259
 platinum-silicon, 260
 silver-silicon, 261
 sulfur-silicon, 261
 tantalum-silicon, 262
 thallium-silicon, 262
 tin-silicon, 263
 titanium-silicon, 263
 tungsten-silicon, 264
 uranium-silicon, 264
 vanadium-silicon, 265
 zinc-silicon, 265
 zirconium-silicon, 266
 Phosphorus, activation energy, 169
 diffusion coefficient, 155–156
 as getter, 262
 methods for adding to melt, 114
 methods for diffusing, 149
 misfit ratio, 259
 optical absorption spectrum, 196
 precipitates, 259
 segregation coefficient, 108
 solid solubility, 266
 strain produced by, 260
 Photoconductivity, 197
 Physical properties, 213
 Piezoresistance coefficient, 182
 Planes, angle between, 87, 89
 Miller indices of, 84
 reflections from, 96
 spacing of, 86–87, 96
 Plastic deformation, 222
 Plastic flow, 222
 Platinum-silicon phase diagram, 260
 Poisson's ratio, 219, 221
 Polishing, 210
 Polycrystalline growth, 78
 Polymers, 12
 Precipitate, copper, 256, 261
 Pressure, critical, 213
- Rate limitation, 123
 Reflection coefficient, 198
 Reflectivity, 199
 Refractive index, 198–200
 Resistivity, 164
 effect on, of high field, 172
 of pressure, 176, 181
 vs. gold concentration, 171–176
 vs. impurity concentration, 106–107

- Resistivity, vs. silver concentration, 177
vs. temperature, 167–168, 170
- Rheotaxial growth, 78
- Sawing, damage during, 233
effect of feed speed on, 231
electrolytic, 232
with wires, 232
- Segregation coefficient, of carbon, 20
definition of, 50, 108
effect on, of growth rate, 56
of spin, 56
effective, 54
minimizing effect of, 62, 115
from phase diagrams, 242
at silicon-oxide interface, 132–133
table of, 108
- Shear modulus, 220
- SiCl_2 , 14
- SiI_2 , 68
- Silane, 9, 69
- Silicon, amorphous, 2, 5
ferro-, 2, 5
- Silicon carbide, 20
- Silicon monoxide, 207
- Silicon nitride, 21
- Silicon phosphide, 259
- Silicon tetrabromide, 14, 68
- Silicon tetrachloride, 7, 12, 65
- Silicon tetraiodide, 10
- Silver, activation energy, 169
as crucible, 62
diffusion coefficient, 157
effect on resistivity, 177
methods for diffusing, 151
-silicon phase diagram, 261
- Silver cage, 62
- Sintering, 231
- Slip, 261
- Smith function, 123, 144
- Solid solubility limits, 241, 266
- Solubility in silicon, refractory oxides, 20
silicon carbide, 20
- Space-charge region, 174
- Specific heat, 213
- Spike-velocity method, 135
- Spin, 46
- Stacking faults, 75, 136
- Star pattern, 223
- Strain gauges, 224
- Stress, fracture, 214, 222
true, 222
ultimate tensile, 214
- Stress optical coefficients, 203
- Stress relief, 261
- Striations, 59
- Sublimation, heat of, 215
- Sulfur, activation energy, 169
diffusion coefficient, 157
-silicon phase diagram, 261
solid solubility, 266
- Supercooling, 39–40, 59
constitutional, 58
- Surface energy, 229
- Surface tension, 48, 213
- Syntectic system, 239
- Tantalum-silicon phase diagram, 262
- Temperature, critical, 213
Debye, 215
- Thallium, diffusion coefficient, 156
methods for diffusing, 151
-silicon phase diagram, 262
- Thermal conductivity, 213, 219
electronic contribution, 229
- Thermal expansion coefficient, 213, 217, 219, 225
- Thermal shock, 226
- Thermoelectric power, 185
- Tin, misfit ratio, 259
-silicon phase diagram, 263
solid solubility, 266
as solvent, 7, 64
- Titanium-silicon phase diagram, 263
- Transmissivity (*see* Absorption coefficient)
- Triboluminescence, 203
- Trichlorosilane, 12, 68
- True stress, 222
- Tungsten-silicon phase diagram, 264
- Twinning, definition of, 100
detection of, 101
direction of, 100
effect on diffusion, 136
- Tyndall effect, 203
- Ultimate tensile strength, 221
- Ultimate tensile stress, 214
- Uranium-silicon phase diagram, 264
- Vacancies, 153
- Vanadium-silicon phase diagram, 265
- Vapor etching, 72
- Vaporization, heat of, 213
- Whiskers, 30, 32
- X-ray orientation, 94
- Yield point, 221
- Young's modulus, 213, 218, 221
- Zener breakdown, 173
- Zinc, activation energy, 169
diffusion coefficient, 157
methods for diffusion, 151
as reducing agent, 7
segregation coefficient, 108
-silicon phase diagram, 265
solid solubility, 266
- Zirconium oxide, 210
- Zirconium-silicon phase diagram, 266
- Zone axis, 87
- Zone leveling, 35

